



HAL
open science

Exploring the diversity of cyclic electron flow around photosystem I in microalgae species

Suzanne Ferté

► **To cite this version:**

Suzanne Ferté. Exploring the diversity of cyclic electron flow around photosystem I in microalgae species. Biological Physics [physics.bio-ph]. Sorbonne Université, 2019. English. NNT : 2019SORUS615 . tel-03349185

HAL Id: tel-03349185

<https://theses.hal.science/tel-03349185>

Submitted on 20 Sep 2021

HAL is a multi-disciplinary open access archive for the deposit and dissemination of scientific research documents, whether they are published or not. The documents may come from teaching and research institutions in France or abroad, or from public or private research centers.

L'archive ouverte pluridisciplinaire **HAL**, est destinée au dépôt et à la diffusion de documents scientifiques de niveau recherche, publiés ou non, émanant des établissements d'enseignement et de recherche français ou étrangers, des laboratoires publics ou privés.



Biologie du Chloroplaste
et Perception de la Lumière
chez les Micro-algues



PhD Thesis of Sorbonne University

**Prepared in the laboratory of Chloroplast Biology and Light-sensing in Microalgae,
UMR7141, CNRS / Sorbonne University**

Doctoral school: Life Science Complexity, ED 515

Exploring the diversity of cyclic electron flow around photosystem I in microalgae species

Presented by Suzanne FERTE-FOGEL

For the grade of Doctor of Sorbonne University

**Defended on the 13th of December, 2019 at the Institute of Physico-Chemical
Biology in Paris, France.**

PhD jury:

Anja Krieger-Liszkay, CNRS, reviewer

Pierre Cardol, University of Liège, reviewer

David Kramer, Michigan State University, examiner

Assaf Vardi, Weizmann Institute, examiner

Sophie Cribier, UPMC, examiner

Francis-André Wollman, CNRS, supervisor

Benjamin Bailleul, CNRS, supervisor

A mes parents, Catherine et Denis

Pour l'amour et la liberté

A mes frères et sœurs, Colombe, Eloi, Myrtille, Clément et Aurélie

Pour l'amour et la bienveillance

A Benjamin

Pour ce grand voyage

Remerciements

J'ai souvent eu du mal à choisir la voie que j'avais envie de suivre. Mais quelque fois, le chemin s'est tracé naturellement, et c'est de cette manière que je suis arrivée à l'UMR7141 pour commencer ce doctorat sous la direction de Benjamin.

En commençant une thèse, je n'imaginai pas que ce serait une expérience tant humaine que scientifique. Et je tiens à remercier en tout premier lieu Benjamin, mon directeur de thèse et la personne avec qui j'ai entretenu la relation la plus intense de ces trois dernières années. J'ai adoré nos discussions scientifiques et je suis contente d'avoir été encadrée par un aussi bon « mentor ». Ça n'a pas été facile tous les jours mais c'est un beau voyage que nous avons fait. Et j'espère sincèrement que l'on continuera d'entretenir une belle relation par la suite. Je tiens aussi à remercier Francis-André, dont le bureau magique a été pour moi le lieu de confidences et de conseils précieux. Merci d'avoir cru en moi et d'avoir su trouver les mots qui parlent quand j'en avais besoin. En arrivant à l'UMR7141, j'ai aussi trouvé une famille et je tiens à remercier tous les membres du labo, présents et passés pour cet environnement bienveillant que chacun contribue à entretenir. Alexandra, Domitille, je suis contente d'avoir fait ce voyage avec vous !

Je tiens aussi à remercier tous ceux qui ont contribué à mon travail de thèse. Ils sont nombreux, mais j'aimerais remercier en particulier Pascal Campagne, sans qui mon chapitre 3 n'aurait pas fière allure, Kim Thamatrakoln, Kay Bidle et Assaf Vardi qui m'ont permis de participer aux campagnes de terrain en Norvège, Laure Guillou, qui nous a accueilli à Roscoff pour des manip de terrain, Michael Schroda qui m'a invité à étudier le phénotype du mutant *deg1*, Sandrine sans qui mes cultures seraient encore bactériennes, la collection de cultures de Roscoff et en particulier Martin pour leurs efforts administratifs, mon comité de thèse, Laure Guillou, Bénédicte Charrier et Colomban de Vargas et les membres de mon jury, Anja Krieger-Liszkay et Pierre Cardol qui ont relu mon manuscrit en un temps record, et Sophie Cribier, David Kramer et Assaf Vardi qui ont accepté de faire le déplacement.

Et puis il y a ceux qui m'ont soutenu sur la fin difficile. Lorna pour le coaching, les relectures et le soutien. Martin pour les échanges, les relectures et les confidences sur les techniques d'écriture ; et pour les belles discussions sur le lion et le serpent. Fabrice Wallois pour son

coup de pouce secret qui m'a bien aidé ! Florian Pellet, Pierre Crozet et Gauthier Vilmart pour leur écoute, soutien et propositions constructives. Et tous ceux qui m'ont relevé quand j'ai craqué !

Ces trois années ont aussi été marquées par une vie hors labo riche et épanouissante. Et j'ai envie de remercier ici tous ceux qui ont contribué à nourrir et qui nourrissent encore mes besoins de partage, d'amour et de joie. Dans les semaines qui ont suivi mon arrivée à Paris, il y a 5 ans, j'ai rencontré Lorna et Chawee. Depuis, ils sont le socle d'amour de ma vie parisienne et je ressens beaucoup de gratitude pour leur présence dans ma vie. Ces 5 années ont aussi été rythmées par les moments avec le Chaos par UpperCuite, avec qui on est sûrs de ne pas manquer de joie et de partage (parfois plus qu'on aimerait), par les sorties avec la Banda Festayre, les Capellous et la Band'arnac qui ne sont pas les plus fins mais qui ont bien d'autres qualités. Merci à Claude et Alain Trautmann qui m'ont offert un refuge, une présence bienveillante et de beaux moments d'échange pendant ces cinq années parisiennes. Merci à tous les amis, aux cousins, aux oncles et tantes, qui me nourrissent de l'essentiel. Merci à Artur, qui était là pour le début et que j'ai aimé de tout mon cœur.

Ces remerciements sont aussi l'occasion de dire ma reconnaissance à tous ceux qui ont croisé mon chemin, et en particulier ceux qui m'ont ouvert des portes et marqué ma construction intérieure. Ceux qui ont nourri mon goût pour l'abstraction et la connaissance, parmi eux, Christine Palandjian, Eric Mestre, Sophie Paradis. Ceux qui m'ont ouvert les portes de la musique, Cyllette Monginous qui m'a initiée et Gérard Luck qui, par son insistance, m'a fait entrer dans le monde des bandas. Ceux qui m'ont ouvert les portes du sport, Bertrand Diviès pour l'escalade, Jean-Claude Pélissier, pour la course à pied, José Machado pour le rugby. Et enfin, ceux qui ont régulièrement ravivé mon goût pour l'agriculture, Samuel Marguet, Ase et Sigurd Avdem, Marie-Eve et Julien Lasalle et ceux qui m'ont appris le travail du bois dont Even et Cédric Linon.

Je remercie aussi mes 10 cm² de terminaisons nerveuses cutanées, mon ménisque et mon petit bout de couenne du pouce que j'ai perdu en chemin. Votre perte m'aura beaucoup appris sur la nécessité de s'écouter. A Badr et son Ekipe, à Antoine Gerometta qui ont sauvé mon genou (et par là même, ma santé psychologique).

Enfin je voudrais dire merci à ma famille qui est là quoi qu'il arrive. A mes frères et sœurs qui ont enveloppé mon enfance d'un amour bienveillant et de beaucoup de joie. A Colombe, que j'aime depuis le premier jour et qui est un des piliers de ma vie. A Catherine et Denis, mes parents, qui m'ont aimé et qui ont contribué à mon développement par leurs merveilleuses ressources personnelles et en me poussant à chercher plus en dehors du cercle familial.

Table of contents

Table of contents	1
Table of figures	5
List of abbreviations	10
Avant-propos / Foreword	12
Abstract / Résumé (français).....	13
Résumé long (français)	14
Chapter 1: General introduction	20
1. 1. Marine ecosystems, phytoplankton and photosynthesis.....	21
1. 1. 1. Most of the genetic diversity in the Ocean is known	21
1. 1. 2. Phytoplankton plays a crucial role in fluxes of matter and energy in the ocean.....	23
1. 1. 3. Origin and taxonomic diversity of phytoplankton	27
1. 2. Reactions and mechanisms involved in eukaryotic photosynthesis	30
1. 2. 1. Different types of photosynthesis	30
1. 2. 2. The chloroplast: an organelle hosting photosynthesis	31
1. 2. 3. The Calvin-Benson-Bassham cycle synthesizes organic carbon from CO ₂	34
1. 2. 4. The photosynthetic electron transfer chain uses light energy to supply the CBB cycle.....	37
1. 2. 5. From light absorption to energy storage	46
1. 2. 6. Monitoring photosynthesis with chlorophyll fluorescence	52
1. 3. Regulation of the photosynthetic process and acclimation to changing environments.....	57
1. 3. 1. Light stress and photo-inhibition.....	57
1. 3. 2. Protecting photosystem I and II from light stress.....	59
1. 3. 3. Photosynthetic alternative pathways	63
1. 3. 4. CEF, a crucial regulative pathway remaining mysterious	66
1. 4. Thesis outline.....	70
1. 5. Bibliography	72

Chapter 2: Probing PSI activity 84

2.1. How to probe photosystem I with absorption spectroscopy?.....	85
2.1.1. Some reminders about photosystem I	85
2.1.2. Measuring P_{700} redox state to investigate PSI activity	87
2.1.3. Electrochromic Shift: an internal voltmeter	91
2.2. Article: Critical reappraisal of methods to measure photosystem I activity.....	96
2.3. Discussion	125
2.3.1. The P_{700} pulse method underestimates $Y(I)$ because of reduction of PSI acceptors during the multiple turnover pulse	125
2.3.2. Technical considerations regarding P_{700} measurements	129
2.3.3. Generalization to the case of an active photosystem II.....	133
2.3.4. Revisiting the literature based on the P_{700} pulse method	136
2.3.5. Partial conclusions and transition.....	148
2.4. Bibliography	149

Chapter 3: Diversity of cyclic electron flow in microalgae 157

3.1 Introduction: CEF, a still mysterious alternative pathway.....	158
3.1.1. Role of CEF in ATP/NADPH adjustment and photo-protection	158
3.1.2. Regulation of CEF rate	161
3.1.3. Measuring CEF is a methodological challenge.....	163
3.1.4. Chapter outlines	165
3.2 Material and methods	167
3.2.1 Strains, growth and sampling	167
3.2.2 Chemicals.....	168
3.2.3 In vivo spectroscopy	168
3.2.4 ECS spectra and linearity with electric field.....	169
3.2.5 Absorption cross section assessment	170

3.3	Results (I): Exploring CEF diversity	172
3.3.1	DCMU titration reveals CEF behavior	172
3.3.2	Which observables?	174
3.3.3	CEF is not essential to photosynthesis in the dinoflagellate <i>Amphidinium carterae</i>	176
3.3.4	CEF is independent on LEF photosynthesis in the dinoflagellate <i>Symbiodinium sp.</i>	177
3.3.5	<i>Chlamydomonas reinhardtii</i> displays a CEF which is dependent on LEF	179
3.3.6	Partial conclusion on CEF diversity	181
3.4	Results (II): Evaluating CEF and LEF absolute rates as a function of light irradiance in the green alga <i>Chlamydomonas reinhardtii</i>.....	182
3.4.1	ECS-based estimations of the PSI and PSII absorption cross sections	183
3.4.2	Validation of the method for measurement of absorption cross sections.....	186
3.4.3	Evaluating CEF absolute rates from ETR(total) and ETR(II)	191
3.4.4	Calculations of the ATP/NADPH ratio produced by the photosynthetic chain	193
3.5	Discussion and future perspectives.....	196
3.5.1	A simple and robust protocol to investigate CEF diversity highlights three different behaviors	196
3.5.2	Limitations of the DCMU titration method	203
3.5.3	Despite a complex relationship, CEF and LEF remain proportional at all light intensities in <i>Chlamydomonas reinhardtii</i>	206
3.6	Bibliography	210

Chapter 4: Photosynthetic physiology of the coccolithophore

Emiliana huxleyi

Major environmental determinants and signature of viral infection in the field..... 216

4.1	Introduction	217
4.2	Material and methods	219
4.2.1	Mesocosm setup, treatments and sampling	219
4.2.2	Flow cytometry/ qPCR	220
4.2.3	Measurement of environmental (abiotic) parameters.....	221
4.2.4	Photophysiology by Fast Induction and Relaxation fluorometry (FIRe)	222
4.2.5	Statistical analyses	225

4.3	Results	227
4.3.1	A two phases phytoplankton bloom occurred	228
4.3.2	Photosynthetic physiology.....	232
4.3.3	Fluorescence signals were mainly due to <i>Emiliana huxleyi</i> from day 9 to 24th of the experiment	237
4.3.4	Evolution of environmental parameters during the experiment	240
4.3.5	Environmental determinants of <i>E. huxleyi</i> photosynthesis	242
4.3.6	A photosynthetic signature of viral infection?	249
4.4	Conclusion and discussion	252
4.5	Bibliography	255
 Chapter 5: General discussion		260
5. 1.	Methodological overview	261
5. 1. 1.	The importance of cross validations of methods.....	261
5. 1. 2.	Using the flash-induced ECS to estimate the photochemical rate: a good choice?	263
5. 1. 3.	Studying CEF and its abiotic and biotic determinants in the field: an accessible project?	266
5. 2.	Roles of CEF and mechanisms of the regulation of the CEF and LEF	271
5. 2. 1.	ATP:NADPH ratio equilibration	271
5. 2. 2.	A role of CEF when PSII is inhibited?	274
5. 2. 3.	CEF and LEF regulation	275
5. 3.	Three years were too short for	277
5. 3. 1.	Revisiting literature using P ₇₀₀ method.....	277
5. 3. 2.	Exploring cyclic electron flow using our methods	277
5. 3. 3.	Harness all data collected in the field	278
5. 4.	Bibliography	280
 Appendix		284

Table of figures

Figure 1 1: V9 rDNA Operational taxonomy unit rarefaction curves and overall diversity (Shannon index, inset) for each plankton organismal size fraction	22
Figure 1 2: Examples of phytoplankton blooms and microscopic observation of the species involved .	24
Figure 1 3: Bacterial transformation of phytoplankton-derived organic matter.....	26
Figure 1 4: Diversity of eukaryotic phototrophs	28
Figure 1 5: Origins of plastids via A: primary, B: secondary, and C: tertiary endosymbiosis.....	29
Figure 1 6: Diversity of chloroplast structures.....	33
Figure 1 7: Schematic representation of the balanced equation of the Calvin Benson Bassham cycle (CBB cycle).....	35
Figure 1 8: Z-scheme of the electron transfer along photosynthetic chain intermediates.....	39
Figure 1 9: Structure of a dimer of cytochrome <i>b₆f</i>	41
Figure 1 10: The cytochrome <i>b₆f</i> complex drives the Q-cycle	43
Figure 1 11: ATP synthase structure and mechanism involved in the rotation of the CF ₀ domain.....	44
Figure 1 12: A scheme of energetic levels (the so-called Jablonski diagram) of a single molecule showing routes of formation and deactivation of the energetic levels.....	47
Figure 1 13: Structure of plant photosystem II (PSII) and photosystem I (PSI).....	51
Figure 1 14: Schematic representation of the main pathways for excitonic energy dissipation	53
Figure 1 15: The irradiance dependence of chlorophyll fluorescence yields in a marine diatom, <i>P. tricornutum</i>	54
Figure 1 16: Evidence for excitonic connectivity between PSII units	56
Figure 1 17: Efficiency of light absorption and utilization by photosynthetic chain	58
Figure 1 18: A quantitative schematic representation of photosystem and antenna distribution heterogeneity, and of its change during state transitions, in <i>C. reinhardtii</i>	62
Figure 1 19: Schematic representation of the diversity of alternative electron pathways.....	63
Figure 1 20: Electron and plastoquinone transfer within cyt. <i>b₆f</i>	69
Figure 2 1: Structure of the photosystem I.....	87

Figure 2 2: P ₇₀₀ oxidized minus reduced difference spectrum.....	88
Figure 2 3: Principle of the P ₇₀₀ -based methods for the determination of the fraction of open PSI centers, Y(I)	91
Figure 2 4: Electrochromic Shift principle	93
Figure 2 5: <i>Chlamydomonas reinhardtii</i> electrochromic shift spectrum	94
Figure 2 6: Kinetic of the ECS after excitation with a single turnover laser flash	96
Figure 2 7: A representation of the Z-scheme with flared reservoirs, where areas reflect the nernstian redox buffering of the redox components	127
Figure 2 8: Schematic model explaining the error made by the P ₇₀₀ pulse method.....	128
Figure 2 9: P ₇₀₀ oxidation and reduction pathways (blue arrows) and action of the chemicals that are used in our Pm measurement protocol (red crosses or arrows).....	129
Figure 2 10: Maximal P ₇₀₀ absorption change, P _m , measured with the standard protocol or with our improved protocol	131
Figure 2 11: Effects of repetitive shorts pulses treatment on PSI from sunflower leaves in atmospheric conditions (air) or in low oxygen concentration (low O ₂).....	133
Figure 2 12: Comparison of the fraction of open PSI centers in <i>C. reinhardtii</i> estimated with the ECS and P ₇₀₀ methods under different light irradiances.....	136
Figure 2 13: PSI parameters measured by ECS and P ₇₀₀ method during light to dark transition when PSII is inhibited.....	140
Figure 2 14: Comparison of time-dependent changes of reduced P ₇₀₀ (red. P ₇₀₀), Y(I) and Y(II) (here noted Φ I and Φ II, respectively) during a dark-light induction period of a sunflower leaf in air	141
Figure 2 15: Light dependence of PSI parameters, Y(I) (left panel), Y(NA) (middle panel) and Y(ND) (right panel), measured by ECS and P ₇₀₀ method when PSII is inhibited.....	142
Figure 2 16: Light dependence of P ₇₀₀ parameters measured before PSI inactivation treatment (Control) and 2 days after PSI inactivation (Inactivated) on wheat leaves.	143
Figure 2 17: Light irradiance dependency of <i>Arabidopsis thaliana</i> PSI parameters in WT (A and B), WT with antimycin A (C and D) and pgr5 mutant (E and F).	146
Figure 2 18: Evolution of PSI parameters and CEF estimations during sugar maple leaf senescence ..	147
Figure 3 1: Percentage of the publications about cyclic electron flow among the various oxygenic photosynthetic clades.....	165
Figure 3 2: ECS spectrum of <i>Amphidinium carterae</i> (A.) and <i>Symbiodinium sp</i> (B.).....	170

Figure 3 3: Simulation of the change of ETR(II) (blue), ETR(I) (red) and ETR(total) (black) as a function of DCMU concentration in the case of a CEF independent of LEF	173
Figure 3 4: Simulations of the relative changes of ETR(II) (blue) and ETR(total) (black) when titrating LEF by DCMU	174
Figure 3 5: Relative changes of the fraction of open PS, Y(total), and the quantum yield of PSII, Y(II), when titrating LEF by DCMU in the dinoflagellate <i>Amphidinium carterae</i>	177
Figure 3 6: Relative changes of the fraction of open PS, Y(total), and the quantum yield of PSII, Y(II), when titrating LEF by DCMU in the dinoflagellate <i>Symbiodinium sp</i>	178
Figure 3 7: Relative changes of the fraction of open PS, Y(total), and the quantum yield of PSII, Y(II), when titrating LEF by DCMU in the green alga <i>Chlamydomonas reinhardtii</i>	180
Figure 3 8: Estimation of the fraction of light absorbed by all PS and by PSI with an ECS-based method.....	185
Figure 3 9: Kinetics of ECS decrease after light offset at two different light irradiances	186
Figure 3 10: ECS decrease after a single turnover laser flash superimposed to two different light irradiances.....	188
Figure 3 11: Comparison of the total electron transfer rate, ETR(total), estimated by the DIRK method and by the yield method.....	189
Figure 3 12: Estimation of the PSII photon absorption rate by fluorescence and comparison with the ECS-based method	191
Figure 3 13: ETR(total) (black) and ETR(II) (blue) as a function of light irradiance in three biological replicates (shown in panels A, B and C).....	192
Figure 3 14: ETR(total) (black), ETR(II) (blue) and ETR(I) (red) as a function of light irradiance in three biological replicates (shown in panels A, B and C).....	192
Figure 3 15: ETR(total) (black), ETR(II) (blue), ETR(I) (red, open circles) and ETR(I)CEF (red, closed circles) as a function of light irradiance in three biological replicates (shown in panels A, B and C)	193
Figure 3 16: Light dependency of the ratios ETR(I)CEF:ETR(I), CEF:LEF and ATP/NADPH produced by the photosynthetic chain	195
Figure 3 17: Relative changes of Y(total) and Y(II) when titrating LEF by DCMU in (A) <i>Amphidinium carterae</i> (dinoflagellate), (B) <i>Symbiodinium sp.</i> (dinoflagellate) and (C) <i>Chlamydomonas reinhardtii</i> (green alga)	197
Figure 3 18: Relative changes of Y(total) and Y(II) when titrating LEF by DCMU in nitrogen depleted <i>Amphidinium carterae</i> (dinoflagellate).....	199

Figure 3 19: Testing CEF behaviour on a <i>Chaetoceros sp.</i> dominated sample from the field	202
Figure 3 20: Evolution of Y(total) (black) and Y(II) (blue) when temperature is decreasing (phase 1) and increasing (phase 2).	206
Figure 3 21 : Fraction of PSI involved in CEF as a function of light intensity for the three replicates used in section 3.4.3	208
Figure 4 1: Gates used for flow cytometry measurements	221
Figure 4 2: MiniFIRe is a hand luggage transportable device that measures chlorophyll fluorescence	223
Figure 4 3: Three parameters are estimated out of the ETR(II) versus intensity curves	224
Figure 4 4: Location of the experiment and mesocosms setting	228
Figure 4 5: Estimation of the chlorophyll concentration in the mesocosms water along the campaign.....	229
Figure 4 6: Evolution of the concentration of the different groups of phytoplankton from day 0 to day 24 of the campaign	231
Figure 4 7: Measurement of Non Photochemical quenching (NPQ) measured in steady state at 500 $\mu\text{mol photons m}^{-2} \text{s}^{-1}$.(A) and its reversible (q_E , fully reversed in 2-3 minutes) and irreversible (q_I) components (B and C, respectively)	234
Figure 4 8: Evolution of fluorescence parameters indicative of photosynthetic physiology from day 0 to day 23 of the campaign.....	235
Figure 4 9: Between Class Analysis (BCA) on the photosynthetic parameters.....	237
Figure 4 10: Maximal fluorescence, F_m , as a function of the concentration of nanoeukaryotes (A), picoeukaryotes (B) and <i>Synechococcus</i> cells (C)	238
Figure 4 11: Comparison of the water color between day 0 (A) and day 21 of the campaign (B) for the bag 3.	238
Figure 4 12: Electron microscopy observation of a sample harvested in bag 4, day 16 of the campaign.....	239
Figure 4 13: Estimation of the fraction of the fluorescence signal emitted by <i>Emiliana huxleyi</i>	240
Figure 4 14: Evolution of abiotic parameters as a function of time	241
Figure 4 15: Between Class Analysis (BCA) on environmental parameters.....	242
Figure 4 16: Correlation matrix containing photosynthetic variables and abiotic environmental parameters.....	244

Figure 4 17: Contribution of environmental variables to the explanatory model for maximal PSII efficiency, F_v/F_m (A), maximal PSII electron transfer rate, ETR_{max} (B) and non-photochemical quenching, NPQ (C).....	246
Figure 4 18: NPQ at 500 $\mu\text{mol photons m}^{-2} \text{s}^{-1}$ as a function of light intensity	248
Figure 4 19: Estimation of the deviation to the model of the maximal PSII efficiency, F_v/F_m (A, B) and the maximal electron transfer rate, ETR_{max} (C, D).....	250
Figure 4 20: Evolution of the number of mcp gene copies per mL along the experiment in each bag. 251	
Figure 5 1: Importance of considering charge recombinations when measuring the fraction of PS open centers.	263
Figure 5 2: DCMU titration of $Y(\text{total})$, $Y(\text{II})$ and $Y(\text{I})_{P700}$ in <i>Chlamydomonas reinhardtii</i> stt7 mutant. ...	265
Figure 5 3: Example of ECS spectra measured in mono-cultures and in co-culture.	269
Figure 5 4: Expected versus measured ECS signals in 3 mixtures of microalgae.....	270

List of abbreviations

<i>A. carterae</i>	<i>Amphidinium carterae</i>
ATP	Adenosine triphosphate
ADP	Adenosine bisphosphate
<i>C. reinhartii</i>	<i>Chlamydomonas reinhardtii</i>
CBB cycle	Calvin Benson Bassham cycle
CEF	Cyclic electron flow around photosystem I
Cyt. <i>b₆f</i>	Cytochrome <i>b₆f</i>
DBMIB	Dibromo-6-isopropyl-3-methyl-1,4-benzoquinone
DCMU	3-(3,4-dichlorophenyl)-1,1-dimethylurea
<i>E. huxleyi</i>	<i>Emiliana huxleyi</i>
ECS	Electrochromic Shift
EhV	<i>Emiliana huxleyi</i> virus
ETR(I)	Electron transfer rate through photosystem I
ETR(II)	Electron transfer rate through photosystem II
ETR(total)	Electron transfer rate through photosystem I and photosystem II
ETR _{max}	Maximal electron transfer rate through photosystem II
Fd	Ferredoxin
FNR	Ferredoxin: NADP ⁺ reductase
FOC(I)	Fraction of PSI open centers
FOC(II)	Fraction of PSII open centers
Fv	Variable fluorescence
HA	Hydroxylamine
LEF	Linear electron flow
I	Light irradiance
MV	Methyl viologen
NADP	Nicotinamide adenine dinucleotide phosphate
Neuks	Nanoeukaryotes
Neuks HSS	High side scattering nanoeukaryotes
Neuks LSS	Low side scattering nanoeukaryotes
NPQ	Non-photochemical quenching

PC	Plastocyanin
Peuks	Picoeukaryotes
PGR5	Proton gradient regulation 5
PGRL1	Proton gradient regulation like 1
PLS	Partial least square
Pmf	Proton motive force
PS	Photosystem
PSI	Photosystem I
PSII	Photosystem II
Y(I)	PSI yield
Y(I) _{ECS}	PSI yield based on ECS
Y(I) _{P700}	PSI yield based on P ₇₀₀ pulse method;
Y(II)	PSII quantum yield
Y(NA)	PSI acceptor-side limitation
Y(NA) _{P700}	PSI acceptor-side limitation based on P ₇₀₀ pulse method
Y(NA) _{ECS}	PSI acceptor-side limitation based on ECS method
Y(ND)	PSI donor-side limitation
Y(total)	Fraction of PS (PSI+PSII) open centers
DIRK	Dark-interval relaxation kinetics

Avant-propos

Quand je suis arrivé au laboratoire de Biologie du Chloroplaste et Perception de la Lumière chez les micro-algues (à l'époque Physiologie membranaire et moléculaire du chloroplaste), mon sujet de thèse était « Compétition pour les nutriments au sein du phytoplancton ». C'est dire à quel point le cheminement de ma thèse n'a pas été linéaire. Benjamin Bailleul, mon encadrant de thèse a su être à l'écoute de mes centres d'intérêts et de mes envies et ce manuscrit reflète mon cheminement guidé par deux appels principaux : celui du monde marin, une des dernières *terra incognita*, de loin l'écosystème le moins bien compris sur Terre renfermant une diversité photosynthétique très peu étudiée bien que d'importance planétaire, et un intérêt croissant pour le développement méthodologique. Au final, ma thèse peut être vue comme une tentative d'exploration de la diversité photosynthétique chez les micro-algues en utilisant comme objet d'intérêt deux complexes protéiques : les photosystèmes I et II. Après tout, toute la vie marine, l'oxygène, les énergies fossiles, les réseaux trophiques sont dépendants à la base de la conversion de l'énergie lumineuse par ces deux machines moléculaires fascinantes.

Foreword

When I arrived at the laboratory Biologie du Chloroplaste et Perception de la Lumière chez les micro-algues (at that time Physiologie membranaire et moléculaire du chloroplaste), my PhD topic was "Competition for nutrients within phytoplankton". This is to say how much the progression of my thesis was not linear. Benjamin Bailleul, my supervisor, has been able to listen to my interests and my desires and this manuscript reflects my journey guided by two main calls: that of the marine world, one of the last *terra incognita*, by far the least-understood ecosystem on Earth. However, it shelters a photosynthetic diversity who is just beginning to be apprehended although of global importance. And by a growing interest for methodological development. In the end, my thesis can be seen as an attempt to explore photosynthetic diversity in microalgae using as an object of interest two protein complexes: photosystems I and II. After all, all marine life, oxygen, fossil fuels, food webs are dependent on the conversion of light energy by these two fascinating molecular machines.

Abstract

Microalgae supplies virtually all the oceanic trophic chains and participate in almost half of photosynthesis on Earth. Although their genetic diversity is well known, their functional diversity remains little explored. The main route of photosynthesis, the linear flux of electrons from water to CO₂, seems to be well conserved among phylogeny. It involves two photosystems working in series, the photosystem II (PSII) and I (PSI). In plants and green algae, there is a cyclic electron flow that involves only the PSI which would be crucial for photosynthetic regulation. The study of this cyclic electron flow is hampered by the absence of a robust method to measure it. We have shown that the most used method for estimating PSI activity is unreliable. On this basis, we propose an alternative method to detect the presence of cyclic electron flow and to study its dependence on the linear flux. We could show very different behaviors between species of microalgae. Finally, the study of a bloom of the coccolithophore *Emiliana huxleyi* in mesocosm allowed us to highlight a signature of cell infection by a virus which could involve the cyclic electron flow around PSI.

Keywords: phytoplankton, dinoflagellate, coccolithophore, diatom, chlorophyte, photosynthesis, cyclic electron transfer, photosystem, viral infection, mesocosm

Résumé (français)

Les micro-algues sont à l'origine de l'immense majorité des chaînes trophiques océaniques et participent à presque la moitié de la photosynthèse sur Terre. Si leur diversité génétique est aujourd'hui bien connue, leur diversité fonctionnelle reste encore peu explorée. La voie principale de la photosynthèse, le flux linéaire d'électrons depuis l'eau vers le CO₂ semble bien conservé dans la phylogénie. Il fait intervenir deux photosystèmes en série, les photosystèmes II (PSII) et I (PSI). Chez les plantes et les algues vertes, il existe un flux cyclique d'électrons qui ne fait intervenir que le PSI auquel on attribue plusieurs rôles cruciaux dans la régulation de la photosynthèse. L'étude de ce flux cyclique est freinée par l'absence de méthodologie robuste pour le mesurer. Nous avons montré que la méthode la plus utilisée pour estimer l'activité du PSI n'est pas fiable. Sur cette base, nous proposons une méthode alternative pour détecter la présence de ce flux cyclique et pour étudier sa dépendance envers le flux linéaire. Cela a permis de montrer des comportements très différents entre espèces de micro-algues. Enfin, l'étude d'une efflorescence de la coccolithophore *Emiliana huxleyi* en mésocosme nous a permis de mettre en évidence une signature de l'infection des cellules par un virus qui pourrait faire intervenir le flux cyclique autour du PSI.

Mots clés: phytoplancton, dinoflagellé, coccolithophore, diatomée, chlorophycée, photosynthèse, transfert d'électron cyclique, photosystème, infection virale, mésocosme

Résumé long (français)

La quasi-totalité de l'énergie circulant dans la biosphère provient initialement de l'énergie solaire, convertie en énergie chimique par des organismes dits phototrophes. Chez tous ces organismes, la conversion énergétique est permise par une seule et même famille de complexes protéiques : les centres réactionnels. Au cours de l'évolution, un groupe de phototrophes a remporté un succès planétaire : ceux qui pratiquent la photosynthèse oxygénique grâce à deux sous familles de centres réactionnels, les photosystèmes II (PSII) et photosystèmes I (PSI). Les travaux réalisés chez les plantes supérieures et les algues vertes ont permis de montrer que les PSII et PSI peuvent fonctionner en série pour oxyder l'eau et réduire le CO₂, produisant ainsi du dioxygène et des molécules organiques contenant du carbone réduit. Chez les eucaryotes, ces réactions se produisent dans le chloroplaste, plus précisément dans les thylacoïdes qui sont des vésicules aplaties structurées par deux membranes qui délimitent le lumen, compartiment interne, et le stroma, à l'extérieur. Le CO₂ est réduit dans le stroma par le cycle de Calvin-Benson-Bassham qui consomme de l'énergie et du pouvoir réducteur sous la forme d'ATP et de NADPH. Ces composés sont produits par la chaîne photosynthétique du thylacoïde : le PSII oxyde l'eau et réduit des plastoquinones membranaires, les électrons extraits de la molécule d'eau sont ensuite transférés au côté donneur du PSI via un complexe protéique membranaire, le cytochrome *b₆f*, puis via une protéine luménale, la plastocyanine (PC). Le PSI transfère ensuite les électrons depuis les PC vers des ferrédoxines et le NADPH de l'autre côté de la membrane. L'ensemble de ces réactions d'oxydo-réduction correspond à ce que l'on appelle le flux linéaire d'électrons (FLE). Ce flux permet aussi la synthèse d'ATP : en accord avec la théorie chimio-osmotique de Mitchell, le flux d'électrons à travers le *b₆f* est couplé à la translocation de protons depuis le stroma vers le lumen mettant en place un gradient électrochimique utilisé par une ATP synthétase membranaire pour former de l'ATP. Outre le FLE, chez les plantes et les algues vertes, on sait que le PSI peut fonctionner de manière indépendante du PSII : les électrons issus du PSI peuvent être réinjectés dans la chaîne donnant lieu, via le cytochrome *b₆f*, à un flux cyclique d'électrons autour du PSI (FCE). Celui-ci serait essentiel pour ajuster les productions d'ATP et de NADPH aux besoins des voies métaboliques en aval du PSI, notamment le cycle de Calvin, puisqu'il permet la mise en place d'un gradient électrochimique de protons et donc la synthèse d'ATP sans produire de pouvoir réducteur. Le FCE serait aussi impliqué dans les mécanismes de photoprotection en conditions où le cycle de Calvin limite

le flux d'électrons photosynthétique. Bien que proposé dès les années 1950 par Arnon et ses collaborateurs, de nombreuses questions sont restées en suspens concernant le FCE.

Mon travail de thèse a été guidé par une question fondamentale simple : quelle relation fonctionnelle existe-t-il entre l'activité de ces deux photosystèmes ? S'il existe plusieurs méthodes d'étude du PSII qui concordent deux à deux, l'étude de l'activité du PSI reste moins accessible. Il n'existe qu'une méthode couramment utilisée et qui est basée sur des hypothèses fortes jamais testées. Une première partie de mon travail a consisté à tester la fiabilité de cette méthode. C'est l'objet du chapitre 2.

Le chapitre 3 de mon travail propose une approche prudente de l'analyse du FCE, en proposant une méthode de mesure basée sur les observables les plus fiables et permettant de répondre à des questions simples mais fondamentales : le FCE est-il essentiel à la photosynthèse ? Est-il présent chez tous les organismes photosynthétiques ? Quelle est la relation fonctionnelle entre le FCE et le FLE ? Dans quelles conditions le FCE a-t-il lieu ?

Dans le chapitre 4, je présente les résultats d'un travail effectué sur le terrain, sur la coccolithophore *Emiliana huxleyi*. Cette partie ne traite pas directement du FCE car les conditions n'étaient pas réunies pour permettre sa mesure in situ mais propose une exploration des déterminants environnementaux du FLE.

Chapitre 2 : Mesure de l'activité du PSI

Les méthodes les plus couramment utilisées pour étudier les flux d'électrons in vivo consistent en l'analyse de signaux spectroscopiques et ce sont ces méthodes que j'ai utilisées au cours de mon travail de doctorat. La plupart des méthodes estiment les flux électroniques à travers un PS, comme le produit de deux paramètres : le flux de photons parvenant au photosystème considéré, $\sigma \cdot I$ (où σ est la section efficace de capture et I , l'intensité de lumière), et la probabilité qu'un photon absorbé donne lieu à une séparation de charge, c'est à dire le rendement quantique du PS, Y . Dans un premier temps et afin de réduire les sources d'approximations, nous avons travaillé à absorption de lumière constante ($\sigma \cdot I$ constant) sans chercher à estimer ce paramètre. Comment estimer le rendement quantique du PSI, $Y(I)$?

Le photosystème I utilise l'énergie lumineuse pour effectuer un transfert d'électrons depuis une paire spéciale de chlorophylle, P_{700} , vers un accepteur primaire consistant en l'un des centres fer-soufre, le composant et que nous noterons A par la suite. Puisque le rendement quantique maximal du PSI est proche de 1, on peut approximer $Y(I)$ par la fraction de centres ouverts, prêts à faire une séparation de charge (i.e. un transfert d'un électron de P_{700} à A). Lorsqu'un PSI fait une séparation de charge, une première conséquence est l'oxydation de sa

paire spéciale entraînant un changement de son spectre d'absorption et c'est ce signal qu'utilise la méthode de référence, la méthode P_{700} . Le principe de cette méthode est d'estimer la fraction des PSI dont le P_{700} est initialement réduit et peut s'oxyder au cours d'un pulse de lumière saturante, qui est considérée comme la fraction de centres PSI ouverts. Ce pulse est assez long pour permettre plusieurs séparations de charge parce que P_{700} ne peut pas rester oxydé tant qu'il reste un électron dans l'ensemble de la chaîne de ses donneurs d'électrons. L'hypothèse forte de cette méthode est que le transfert de plusieurs électrons ne modifie pas l'état redox des accepteurs PSI. Afin de tester le domaine de validité de cette hypothèse, nous avons proposé une méthode alternative de mesure d' $Y(I)$. Celle-ci est basée sur une deuxième conséquence du transfert d'électrons par le PSI : l'augmentation du champ électrique de part et d'autre du thylacoïde, qui entraîne le changement d'absorption de pigments électro-sensibles. On parle alors d'électro-chromisme (ECS). En conditions de PSII inhibés, seuls les PSI ouverts participent à l'augmentation du champ électrique après un éclair permettant une seule séparation de charge par PS. C'est grâce à ce signal que la méthode ECS estime la fraction de PSI ouverts.

Nous avons pu mettre en évidence que les méthodes P_{700} et ECS divergent lorsque certains P_{700} ne sont pas oxydés par le pulse de lumière saturante. Nous avons montré que cette discordance est liée à un biais de la méthode P_{700} et nous proposons un modèle expliquant ce biais. Lorsque plusieurs séparations de charge ont lieu pendant le pulse utilisé par la méthode P_{700} , alors des accepteurs PSI initialement oxydés se réduisent. Et lorsque le nombre d'accepteurs PSI est plus faible que le nombre de donneurs, certains P_{700} initialement oxydables ne le sont pourtant pas à la fin du pulse parce que leurs accepteurs ont été réduits entre temps. Cette erreur n'est pas négligeable. Dans nos données, la méthode P_{700} sous-estime la fraction de PSI ouverts jusqu'à un facteur 10. Dans la suite de nos travaux, nous avons donc privilégié la méthode ECS pour estimer l'activité des PSI.

La méthode P_{700} peut néanmoins être corrigée. Nous proposons un modèle permettant de prendre en compte la fraction d'accepteurs réduits pendant le pulse qui est soutenu par nos données empiriques. On peut donc proposer une correction des données obtenue avec la méthode P_{700} . Cette correction ouvre la porte à la ré-interprétation des données publiées dans la littérature depuis plus de 25 ans utilisant la méthode P_{700} . Nous avons commencé ce travail et pu montrer par exemple que le phénotype du mutant *pgr5*, potentiellement impliqué dans le FCE, pourrait être en partie dû au biais de la méthode P_{700} .

Chapitre 3 : Diversité du FCE au sein de la phylogénie

Afin d'explorer la diversité du FCE, nous avons proposé une méthode simple, robuste et utilisable dans la plupart groupes photosynthétiques qui permet de mettre en évidence l'existence de FCE chez une espèce et de tester sa relation avec le FLE.

Le principe est de suivre l'évolution du FCE (ou d'une fonction du FCE) lorsque l'on inhibe progressivement et spécifiquement le FLE par un inhibiteur du PSII, le DCMU. On peut modéliser simplement les résultats attendus s'il n'y a pas de CEF ou si le CEF est indépendant du LEF et tester les résultats obtenus chez différentes espèces. Cette méthode présente un avantage majeur : en travaillant avec des organismes pour lesquels la section efficace de capture (σ) est constante, suivre l'évolution des rendements quantiques revient à suivre l'évolution des valeurs absolues de flux. On peut alors éviter la mesure du flux de photons absorbés par les PS, source majeure d'approximations. Nous avons estimé le rendement quantique du PSII par la mesure de sa fluorescence et la fraction de centres (PSI + PSII) ouverts par mesure de signaux ECS (méthode présentée dans la section précédente).

Un premier résultat inattendu est que le FCE n'est pas absolument essentiel à la photosynthèse puisqu'un dinoflagellé, *Amphidinium carterae*, ne présente pas de FCE dans les conditions que nous avons testées. Lorsqu'un FCE a été mis en évidence, nous avons montré deux types de relation fonctionnelle avec le FLE. Il peut se dérouler de manière indépendante du FLE, comme c'est le cas chez le dinoflagellé *Symbiodinium sp.* Dans ce cas, la mesure de FCE est simple : l'activité résiduelle mesurée par ECS lorsque tous les PSII sont inhibés est identique à l'activité cyclique lorsque tous les PS fonctionnent. Dans un troisième cas de figure, nous avons montré que le FCE peut être influencé par les variations de FLE comme c'est le cas chez l'algue verte modèle, *Chlamydomonas reinhardtii*. Ces deux comportements sont-ils le résultat de mécanismes de régulation différents ? De différences d'enzyme(s) impliquée(s) dans le CEF ? Ou simplement d'un état physiologique différent ? Ces questions restent à approfondir.

Dans le cas de *Chlamydomonas reinhardtii*, puisque le FCE est dépendant du FLE, la mesure du FCE nécessite la mesure de valeurs absolues de flux PSII et de flux totaux dans les conditions que l'on souhaite étudier. Pour cela, nous avons commencé un travail de développement et de validation de méthodes de mesure des flux de photons parvenant aux PSII et à tous les PS. Nos résultats sont encourageants même si une incertitude reste quant à l'amplitude des flux à travers le PSII. Nous avons pu montrer que le FCE est proportionnel au FLE quelle que soit l'intensité de lumière, ce qui constitue un argument fort dans le sens d'un rôle du FCE dans l'ajustement des ratios ATP/NADPH produits par la chaîne photosynthétique aux besoins du cycle de Calvin. De plus, en utilisant les valeurs les plus extrêmes de flux à travers le PSII, nous

montrons que le FCE permet de produire suffisamment d'ATP pour subvenir aux besoins du cycle de Calvin...et sûrement plus. Quels mécanismes régulateurs permettent d'assurer une proportionnalité entre les FCE et FLE ? Qu'est-ce qui détermine l'amplitude du CEF ? Certaines conditions entraînent-elles une modification de cette relation ? Ces questions restent des pistes de travail pour la suite de ce projet.

Chapitre 4 : Étude sur le terrain des déterminants environnementaux de la physiologie photosynthétique de l'haptophyte *Emiliana huxleyi*

Une approche plus holistique pour étudier la diversité des mécanismes photosynthétiques est l'étude de populations prélevées sur le terrain. Au printemps 2018, nous avons été invités à participer à une campagne scientifique sur la côte norvégienne dont l'objectif était d'étudier les déterminants environnementaux biotiques et abiotiques qui sont en jeu lors d'une efflorescence de l'haptophyte *Emiliana huxleyi*. En participant à cette campagne, nous avons l'espoir de tester notre méthode de mesure du FCE développée au chapitre 3 sur des échantillons prélevés directement sur le terrain. Cependant, en raison de la faible concentration des microalgues étudiées in situ, les signaux de spectroscopie d'absorption (par exemple les mesures d'ECS et de P_{700} nécessaires pour sonder le FCE) étaient trop faibles pour être exploitables. Les signaux de fluorescence étant plus importants, nous avons pu suivre l'évolution de paramètres liés au PSII et au LEF au cours de la campagne et mettre en évidence l'influence de facteurs environnementaux déterminant la physiologie photosynthétique.

La campagne s'est déroulée à la station marine de Bergen en Norvège et a duré 24 jours. De grands sacs en plastique transparents ont été remplis d'environ 11 m³ d'eau prélevée directement dans le fjord et ont été fixés sur un radeau à quelques dizaines de mètres de la côte. L'ajout de nutriments a permis de provoquer le développement spécifique d'*Emiliana huxleyi* et nous avons pu montrer qu'à partir du jour 9, les signaux de fluorescence mesurés étaient principalement ceux d'*Emiliana huxleyi*. En utilisant une approche de statistique multivariée, nous avons pu étudier les facteurs environnementaux influençant la physiologie photosynthétique d'*Emiliana huxleyi*. Notre modèle statistique permet de prédire les résultats expérimentaux avec une bonne fiabilité et de montrer les principaux facteurs environnementaux déterminant la physiologie photosynthétique. Mais l'intérêt principal de cette approche s'est révélé dans l'étude des jours et des sacs pour lesquels les paramètres photosynthétiques dévient par rapport au modèle. Nous avons ainsi pu identifier une diminution du rendement quantique maximal du PSII de l'ordre de 25 à 30% uniquement certains jours et pour certains réplicats. Même si les résultats sont encore préliminaires, ces

jours semblent parfaitement corrélés à des évènements d'infection intracellulaire d'*Emiliania huxleyi* par son virus spécifique. L'inhibition spécifique du PSII pose une question immédiate : le FCE est-il stimulé pendant l'infection virale, puisqu'il pourrait fournir de l'ATP pour un processus infectieux qui est énergétiquement coûteux ?

Ce travail de thèse est fondé sur deux axes de recherche: l'exploration de la diversité du FCE chez les microalgues et l'étude de la physiologie photosynthétique sur le terrain. La convergence de ces deux axes a seulement été initiée et une perspective générale de ce travail serait d'explorer les déterminants, les rôles et les mécanismes de régulation du FCE in situ. Pour cela, je propose des pistes d'améliorations en vue de la mesure de FCE sur le terrain

Chapter 1: General introduction

Summary

1. 1. Marine ecosystems, phytoplankton and photosynthesis.....	21
1. 1. 1. Most of the genetic diversity in the Ocean is known	21
1. 1. 2. Phytoplankton plays a crucial role in fluxes of matter and energy in the ocean	23
1. 1. 3. Origin and taxonomic diversity of phytoplankton	27
1. 2. Reactions and mechanisms involved in eukaryotic photosynthesis	30
1. 2. 1. Different types of photosynthesis	30
1. 2. 2. The chloroplast: an organelle hosting photosynthesis	31
1. 2. 3. The Calvin-Benson-Bassham cycle synthesizes organic carbon from CO ₂	34
1. 2. 4. The photosynthetic electron transfer chain uses light energy to supply the CBB cycle.....	37
1. 2. 5. From light absorption to energy storage.....	46
1. 2. 6. Monitoring photosynthesis with chlorophyll fluorescence	52
1. 3. Regulation of the photosynthetic process and acclimation to changing environments..	57
1. 3. 1. Light stress and photo-inhibition.....	57
1. 3. 2. Protecting photosystem I and II from light stress	59
1. 3. 3. Photosynthetic alternative pathways.....	63
1. 3. 4. CEF, a crucial regulative pathway remaining mysterious	66
1. 4. Thesis outline.....	70
1. 5. Bibliography.....	72

This introduction attempts to introduce the importance of the study of photosynthesis in the context of the exploration of the marine world, insisting on the concepts necessary for the understanding of chapter III "field measurements". In a second time the photosynthetic process will be presented, emphasizing the two photosystems and their relative functions.

1. 1. Marine ecosystems, phytoplankton and photosynthesis

1. 1. 1. Most of the genetic diversity in the Ocean is known

The ocean is a single, continuous and global entity. It covers 71% of the Earth surface but remains little explored in comparison to land environment. Within the past decades, ocean ecosystems exploration flourished thanks to new technologies and revealed the complexity and particularity of marine ecosystems.

Over many centuries, global expeditions have led to major scientific breakthroughs, notably with the early voyages of the H.M.S. Beagle (1831–1836) and the H.M.S. Challenger (1872–1876). But because microbiology was not yet mature, those expeditions missed most of the ocean diversity. Last century's biology was marked by laboratories studies and molecular scale tools were developed. This enabled a fine understanding of molecular mechanisms of cell division, organization and metabolism. Last decades were also widely influenced by genomics development. And reinforced by those new tools and knowledges, recent global expeditions discovered a new facet of ocean ecosystems: the planktonic world. Recently, the Sorcerer II expeditions (2003–2010) (Rusch et al., 2007) and the Malaspina expedition (2010–2011) (Laursen, 2011) carried out global surveys of prokaryotic metagenomes from the ocean's surface and bathypelagic layer (>1,000 m), respectively. The Tara Oceans expedition (2009–2013) complemented these surveys by collecting a wide variety of planktonic organisms (from viruses to fish larvae) from the ocean's surface (0–200 m) and mesopelagic zone (200–1 000 m) at a global scale. Tara ocean surveyed 210 ecosystems in 20 biogeographic provinces, collecting over 40 000 samples of seawater and plankton (Pesant et al., 2015). And one of the first question that was addressed in the light of this new set of data is: who is living in the ocean? And how diverse are the organisms? The circumglobal Tara ocean expedition collected billions of organisms but is it representative of the whole ocean diversity? To tackle this issue, a commonly used technique is called

rarefaction and estimates the number of new species that would be found by sampling more organisms. From Tara samples, about 500 million of ribosomal DNA were sequenced and grouped in operational taxonomic unit (OTU), i.e. closely related organisms. Figure 1-1 shows rarefaction curves plotting the number of OTU described as a function of the number of sequencing since the beginning. The slope of the curves, representing the number of new OTU per read, decreases to reach really low values meaning that more sequencing would not allow to discover much new species (de Vargas et al., 2015). We now know that more than 95% of the weight of living matter in the ocean is made of microscopic organisms, more than whales and fishes put together, and most of it is plankton.

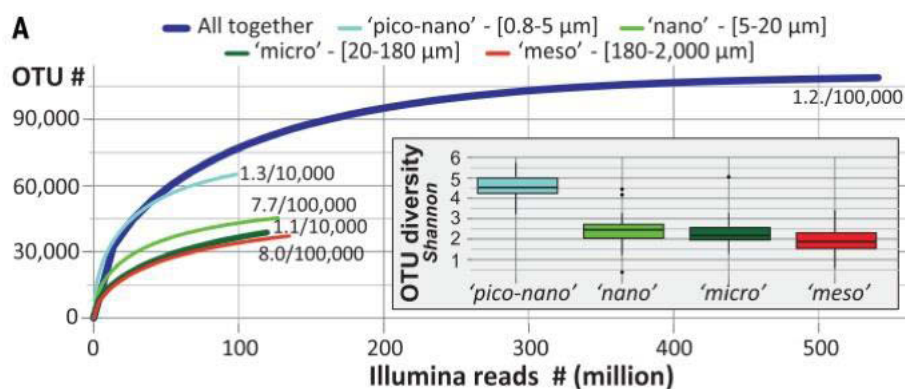


Figure 1-1: V9 rDNA Operational taxonomy unit rarefaction curves and overall diversity (Shannon index, inset) for each plankton organismal size fraction

From de Vargas et al., 2015.

334 plankton samples were collected during the circumglobal Tara Oceans expedition. Hypervariable V9 rDNA was amplified by PCR and sequenced by illumine method in different size fractions of plankton ('pico-nano', [0.8-5μm]; 'nano', [5-20μm]; 'micro', [20-180μm]; 'meso', [180-2,000μm]). Sequences were clustered in operational taxonomy units (OTU). Proximity to saturation is indicated by weak slopes at the end of each rarefaction curve (e.g., 1.2/100,000 means 1.2 novel metabarcodes obtained every 100 000 rDNA reads sequenced). Shannon index has been calculated for each size fraction as an indicator of genetic diversity.

The word "plankton" comes from the Greek *planktos* "errant" and includes diverse organisms based on a common characteristic: their limited ability to move, meaning that they drift with the water current. From the virus of less than one micron to the siphonophore over ten meters long, their size varies greatly but most of them are microscopic. They cannot be detected by naked eye and this is why their importance have long been underestimated. Among the planktonic organisms, phytoplankton are the first link in aquatic food webs.

1. 1. 2. Phytoplankton plays a crucial role in fluxes of matter and energy in the ocean

Defined as autotrophic planktonic organisms (Haeckel, 1890), these organisms account for less than 1% of the global primary biomass of primary producers and are nonetheless responsible for 45% of annual net primary production at the surface of the earth (Falkowski et al., 2004, Field et al., 1998) and more than 75% of primary productivity at the ocean scale. Phytoplankton fix more than a hundred million tons of carbon every day (Behrenfeld et al., 2001; Falkowski et al., 1998). Their primary production is estimated about 50 Pg year⁻¹ (Behrenfeld et al., 2001; Falkowski et al., 1998).

Like terrestrial plants, phytoplankton performs photosynthesis: using solar light energy that is captured with pigments (mainly chlorophylls), it transforms CO₂ and water into carbohydrates while producing oxygen. And this is virtually the only gateway for energy and carbon input in the marine biosphere. Phytoplankton plays therefore a crucial role in feeding the trophic chains, producing half the O₂ that we breathe and storing an important amount of atmospheric CO₂ through the biological pump, playing an important –but still not fully resolved- role of buffer of global climate changes.

Besides the rather regular seasonal patterns at global scale, some species are capable of explosive growth over a few days or weeks reaching high concentrations (up to tens of thousands of cells per milliliter). And although it is microscopic, phytoplankton become visible to the naked eye during those phenomena known as blooms (Figure 1-2). Density becomes so high that phytoplankton pigments and cell wall properties induce changes of the water color. Blooms can occur on a relatively small scale or cover hundreds of square kilometers of the ocean's surface, becoming visible from space. Among the huge diversity of phytoplankton, only few species have the capacities to bloom. One of them is the coccolithophore *Emiliana huxleyi* whose blooms can be visualized from satellites because it possesses microscopic calcite shells that diffuses light and can give water a chalky color (Figure 1-2A). The third chapter of my thesis will focus on the photo-physiology of this species, a model organism for coccolithophores (e.g. Tyrell and Merico, 2004; Wilson et al., 2005; Bidle and Vardi, 2011).



Figure 1-2: Examples of phytoplankton blooms and microscopic observation of the species involved

A. An exceptionally dense bloom of the dinoflagellate *Alexandrium monilatum* in lower Chesapeake Bay along the north shore of the York River between Sarah's Creek and the Perrin River on 8/17/2015. Credit: © W. Vogelbein/VIMS. B. *Alexandrium monilatum* observation through an optic microscope. Source: Center for applied aquatic ecology

C. The Florida "red tide" dinoflagellate *Karenia brevis*, along the Gulf Coast of the United States. Source: National Oceanic and Atmospheric Administration (NOAA). D. *Karenia brevis* observation through an optic microscope. Source: Schrope, Nature 2008

E. South Atlantic Ocean image from space, December 2, 2014. The aquamarine stripes and swirls are likely coccolithophores. The various shades of green are probably a mix of diatoms, dinoflagellates and other species. Source: NASA images by Norman Kuring, NASA's Ocean Color Group, using the Visible Infrared Imaging Radiometer Suite (VIIRS) data from the Suomi National Polar-orbiting Partnership. The coccolithophore *Emiliana huxleyi* (F) and the dinoflagellate *Prorocentrum sp.* (G) were previously observed in the region during ship-based studies. Observation through optic microscope (F) and transmission electronic microscope (G). Source: Roscoff culture collection (RCC 2563 and RCC 1212, respectively).

Historically, and by analogy with land marine food webs, primary consumers were thought to be the zooplankton, serving as a crucial link between primary producers and the rest of the trophic chain including higher consumers such as large fish and ultimately top predators (Figure 1-3). And it is important to note that this concerns directly human survival since in 2015, according to the Food and Agriculture Organization of the United Nations report, 17% of animal proteins consumed in the world came from fish. However, this classical food web view has been challenged by the discovery of abundant heterotrophic prokaryotes. It is now commonly assumed that net zooplankton are not metabolically dominant and that a large proportion of the flux of matter and energy in the marine food web passes through bacteria in the form of dissolved organic matter (DOM), a concept named the microbial loop. The microbial loop is the process by which DOM derived from primary producers such as phytoplankton is foraged and recycled by heterotrophic bacteria that use DOM as a food source (Azam et al., 1983; Hobbie et al., 1972; Pomeroy, 1974). These bacteria are

consumed by zooplankton, and the link to the traditional food web is established (Figure 1-3). Marine bacteria hold a significant influence in this loop, as they allow for an energy pathway that may have otherwise been lost. Viruses, by infecting and lysing marine bacteria and phytoplankton, are also vital players in the fixation and cycling of key elements, such as carbon, nitrogen, and phosphorus (Wilhelm and Suttle, 1999). Through the viral shunt, viral lysis of microbial cells releases dissolved organic matter and particulate organic matter back into the microbial loop. By doing so, viruses drive carbon and nutrients of these cells away from grazers, and redirects it to other microorganisms through the form of DOM (Figure 1-3). It has been estimated that ocean viruses might turn over as much as 150 gigatons of carbon per year (Suttle, 2007).

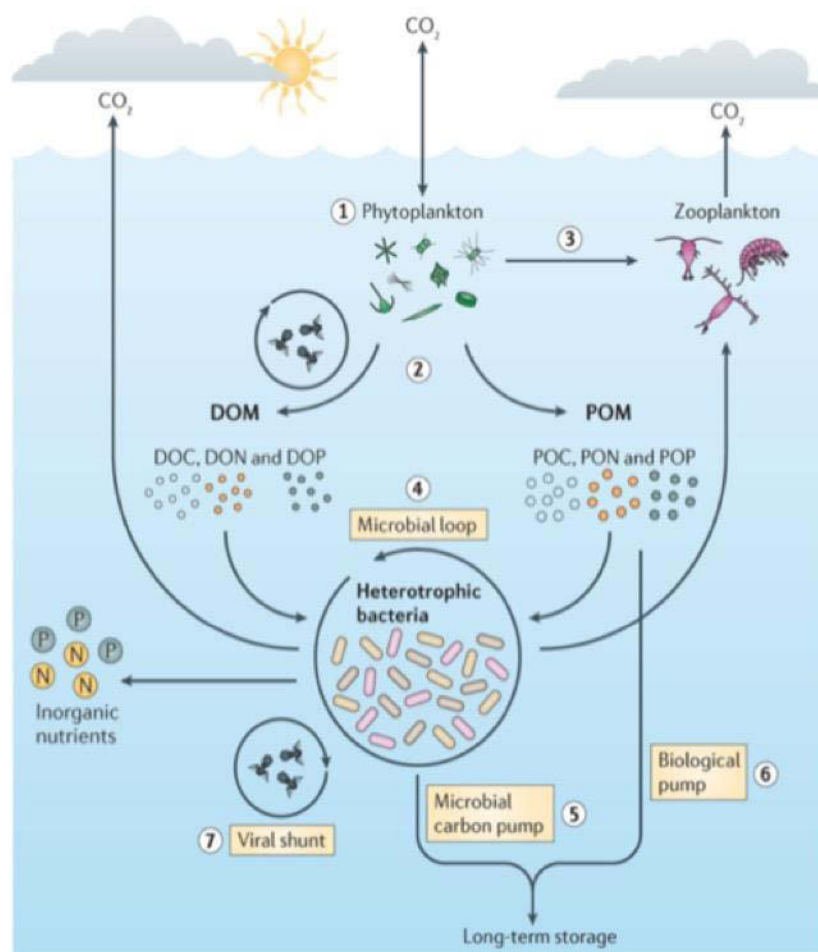


Figure 1-3: Bacterial transformation of phytoplankton-derived organic matter

The marine carbon cycle includes a number of processes, several of which are mediated by microorganisms. Key processes of the marine carbon cycle include the conversion of inorganic carbon (such as CO_2) to organic carbon by photosynthetic phytoplankton species (step 1); the release of both dissolved organic matter (DOM; which includes dissolved organic carbon (DOC), dissolved organic nitrogen (DON) and dissolved organic phosphorous (DOP)) and particulate organic matter (POM; which includes particulate organic carbon (POC), particulate organic nitrogen (PON) and particulate organic phosphorous (POP)) from phytoplankton (step 2); the consumption of phytoplankton biomass by zooplankton grazers (step 3) and the mineralization (that is the release of CO_2 via respiration during the catabolism of organic matter) and recycling of organic matter by diverse heterotrophic bacteria (which is known as the microbial loop; step 4). A fraction of the heterotrophic bacteria is consumed by zooplankton, and the carbon is further transferred up the food web. Heterotrophic bacteria also contribute to the remineralization of organic nutrients, including DON and DOP, to inorganic forms, which are then available for use by phytoplankton. The microbial carbon pump (step 5) refers to the transformation of organic carbon into recalcitrant DOC that resists further degradation and is sequestered in the ocean for thousands of years. The biological pump (step 6) refers to the export of phytoplankton-derived POM from the surface oceans to deeper depths via sinking. Finally, the viral shunt (step 7) describes the contributions of viral-mediated cell lysis to the release of dissolved and particulate matter from both the phytoplankton and the bacterial pool. From Buchan et al., 2014.

1. 1. 3. Origin and taxonomic diversity of phytoplankton

Who are the phytoplankton organisms? Are they part of the same phylogenetic family as terrestrial plants?

Figure 1-4 presents a phylogenetic tree of eukaryotes based on the analysis of the gene encoding the RNA 18s cells. Photosynthetic organisms are indicated on the colored branches. On this tree, we see that terrestrial plants belong to a single monophyletic family belonging to Chlorophyta. Green algae are close relatives of terrestrial plants and also belong to the Chlorophyta clade. On the other hand, marine photosynthetic eukaryotes are distributed in many branches of the phylogenetic tree of eukaryotes such as Glaucophyta and Rhodophyta, which group together with Chlorophyta in the Archaeplastida (Figure 1-4). We also find marine phototrophs within Alveolata, among which we find dinoflagellates (Dinophyceae), Stramenopila which comprises diatoms, Haptophyta which includes coccolithophores, but also Rhizaria, Discoba or Cryptista (Obornik, 2019).

The ability to perform oxygen photosynthesis is also found in some species of bacteria (not shown on this tree), called cyanobacteria. A question that arises with regard to this tree is: how to explain the presence of photosynthetic organisms within such diverse phylogenetic groups? Has the ability to achieve photosynthesis appeared several times during evolution by evolutionary convergence?

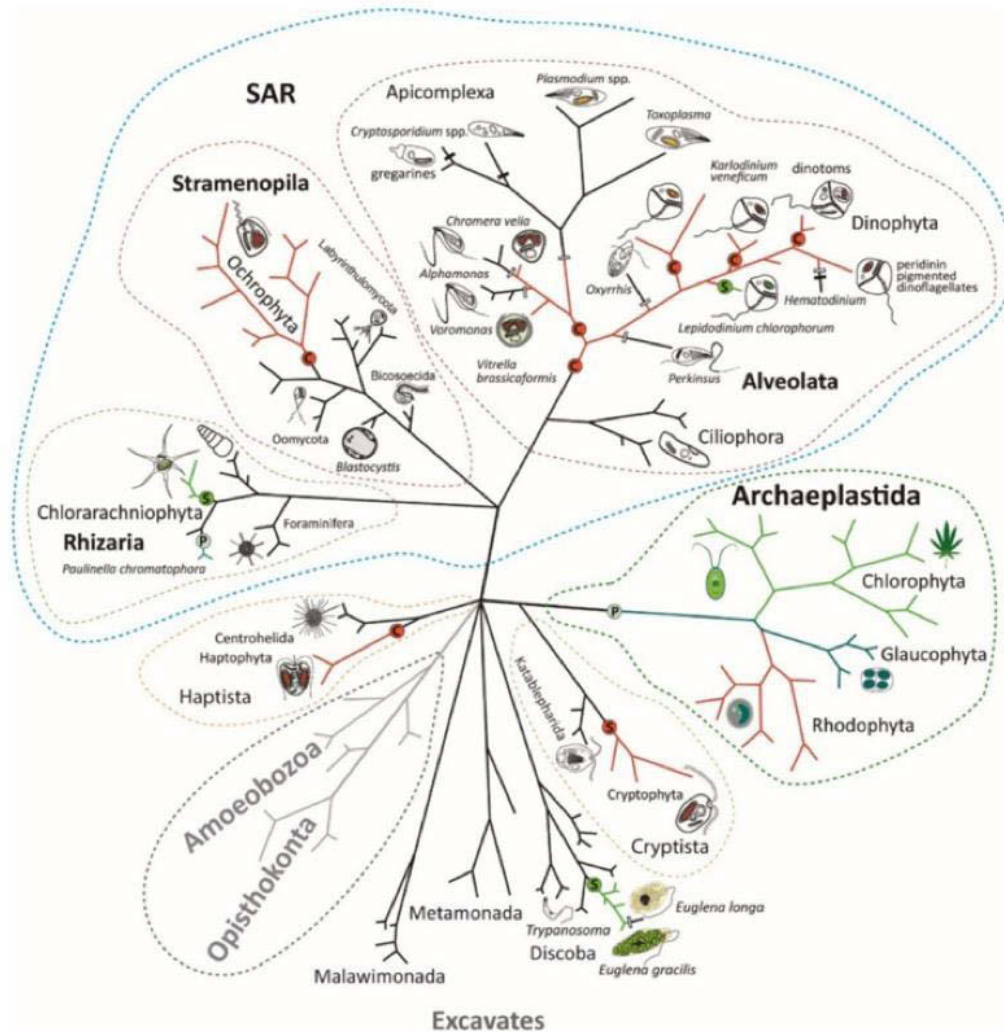


Figure 1-4: Diversity of eukaryotic phototrophs

Endosymbiotic events are shown in the hypothetical tree: P-primary endosymbiosis; C-complex endosymbiosis; S-secondary endosymbiosis. Losses of photosynthetic ability (white rectangles) or losses of the entire plastid (black rectangles) are indicated. SAR: Stramenopila + Alveolata + Rhizaria.

From Obornik, 2019

Several arguments led to propose a chimeric origin of photosynthetic eukaryotes. In 1970, based on morphological arguments (the resemblance between chloroplasts and cyanobacteria), Margulis proposed that the chloroplasts of eukaryotic cells come from the incorporation of a cyanobacterium by a heterotrophic unicellular (Margulis, 1970): this is the endosymbiotic theory. Since then, many arguments have accumulated to support this theory, one of the most robust of which is phylogenetic: chloroplast DNA analyses show the close kinship between all chloroplast and cyanobacteria (Rodríguez-Ezpeleta, 2005). Nowadays, it is well admitted that the photosynthetic organelle of algae and plants (the plastid) traces its origin to a primary endosymbiotic event in which a previously non-photosynthetic protist engulfed and enslaved a cyanobacterium (Figure 1-5). This eukaryote

then gave rise to the red, green and glaucophyte algae (Bhattacharya, Yoon and Hackett, 2004). However, many algal lineages, such as the chlorophyll c-containing stramenopiles, have a more complicated evolutionary history involving a secondary endosymbiotic event, in which a protist engulfed an existing eukaryotic alga, in this case, a red alga; the additional engulfment of a green alga was suggested (Bhattacharya, Yoon and Hackett, 2004; Prihoda et al. 2012, Moustafa et al., 2009). Another algal group, the dinoflagellates, has undergone tertiary (engulfment of a secondary plastid) and even quaternary endosymbiosis (Figure 1-5).

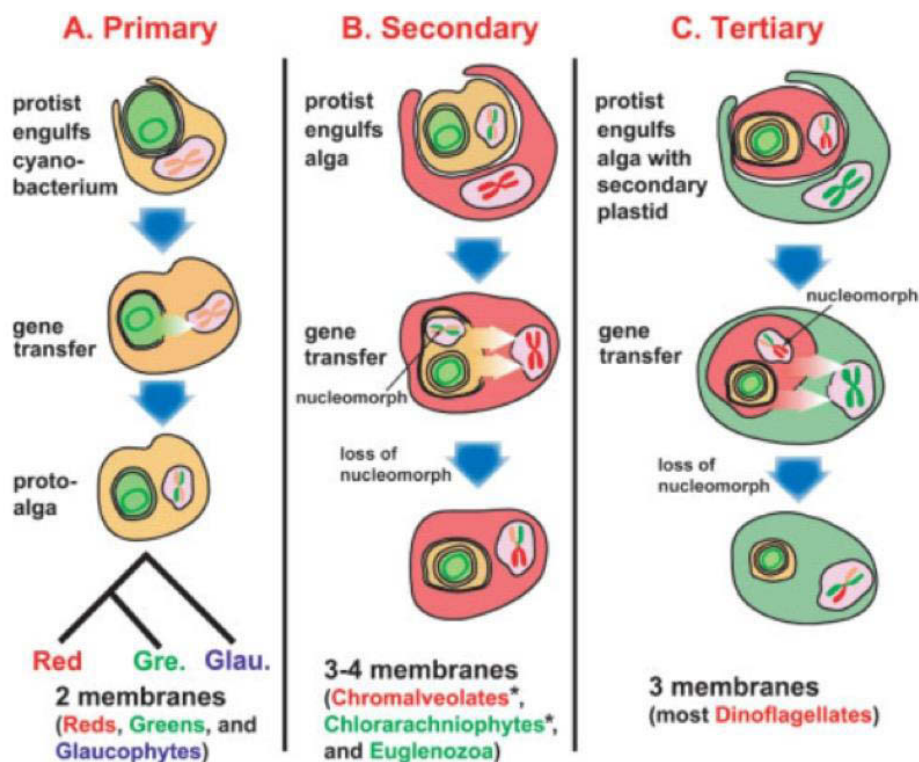


Figure 1-5: Origins of plastids via A: primary, B: secondary, and C: tertiary endosymbiosis.

Gene transfer from the endosymbiont to the host nucleus is shown with the arrows and the colored chromosomes. The mitochondrion has been omitted from these figures. The remnant algal nucleus (nucleomorph) in secondary and tertiary endosymbioses is shown. This genome has been lost in all algae but the cryptophytes (member of the chromalveolates) and chlorarachniophytes (marked with asterisks). From Bhattacharya, Yoon and Hackett, 2004.

Photosynthetic eukaryotes are chimeras. The study of their nuclear genome shows a great phylogenetic diversity whereas the study of the plastid genome shows a close relation of kinship. A question that arises is what about functional diversity? Do photosynthetic eukaryotes have a significant diversity linked to the origin of the host cell that integrated the organelles? Or do they have common mechanisms for using light energy inherited from the common cyanobacterium ancestor?

1.2. Reactions and mechanisms involved in eukaryotic photosynthesis

In this second part of the introduction, after presenting the diversity of photosynthetic types, we will detail the major reaction steps involved in oxygenic photosynthesis as well as the molecular mechanisms allowing the transformation of light energy into chemical energy.

1.2.1. Different types of photosynthesis

Among the three fundamental domains of living organisms, bacteria, archaea and eukaryotes (Woese et al., 1990), we find photosynthetic organisms within bacteria and eukaryotes only. It is to note that another mechanism of conversion of light energy into chemical energy exists which is fundamentally different from the chlorophyll-based photosynthesis. Halophilic archaea possess bacteriorhodopsins, retinal-binding integral membrane proteins, which can use light to pump protons, generate an electrochemical proton gradient and produce adenosine triphosphate (ATP) from adenosine diphosphate (ADP) through this process (Hayashi, Tajkhorshid and Schulten, 2003). Later, metagenomics approaches revealed widespread retinal-binding rhodopsin proteins, called proteorhodopsins in marine bacteria (Beja et al, 2000). It also exists in eukaryotes (Bieszke et al., 1999). These discoveries have challenged the notion that only chlorophyll-based photosynthesis allows the conversion of solar energy into the marine ecosystem (Beja et al, 2000). The importance of proteorhodopsins in the global conversion of light into chemical energy and biomass is still a matter of debate (Fuhrman et al. 2008). Here, we will not consider the light-driven ATP synthesis catalyzed by bacteriorhodopsins and proteorhodopsins, and the term “photosynthesis” will be used in its historical meaning, i.e. for the conversion of light into chemical energy based on chlorophylls or bacteriochlorophylls.

The use of chlorophyll or bacteriochlorophyll also distinguishes two different types of photosynthesis, whose general principles are the same but which depend on different sources of electrons. Oxygenic photosynthesis uses water as a source of electrons, a reaction that results in the release of molecular oxygen, and those electrons can be transferred through two photosystems to reduce carbon dioxide. But some photosynthetic bacteria can

use light to extract electrons from other molecules than water. They use instead inorganic compounds, like H_2 or H_2S , or inorganic compounds like malate. Because they do not evolve O_2 , their photosynthesis is named anoxygenic photosynthesis. Another difference with oxygenic phototrophs is that they possess only one type of reaction center: a pheophytin-quinone (type II) reaction center, or an iron-sulfur (type I) one. Among anoxygenic phototrophs using type-II reaction centers are purple bacteria and green filamentous bacteria. On the contrary, green sulfur bacteria and heliobacteria use type-I reaction center (Blankenship, 1992).

In this work, we will only consider oxygenic photosynthesis, which exists in cyanobacteria and in photosynthetic eukaryotes. A major difference between these two groups of organisms is structural: in photosynthetic eukaryotes, photosynthesis occurs in specialized organelles, the plastids, while cyanobacteria do not possess intracellular organelles. In the latter, photosynthesis occurs in membrane invaginations. The following paragraph therefore only concerns eukaryotes.

1. 2. 2. The chloroplast: an organelle hosting photosynthesis

The site of photosynthesis in eukaryotes is the plastid, a membranous subcellular organelle (Figure 1-6). Chloroplast numbers per cell vary considerably in plants, from 1 to 1000 depending on species, life stage and environment. Microalgae generally possess one or a few chloroplasts delimited by 2, 3 or 4 membranes (Staehelin, 1986; Falkowski and Raven, 2013). The inner membrane encloses the stroma, a concentrated solution of enzymes that also contains the DNA, RNA and ribosomes involved in the synthesis of several chloroplast proteins. Inside the chloroplast, membrane folds form bags called thylakoids which delimit an internal space, the lumen. In higher plants, thylakoids consist of stacks of disk-like sacs named grana which are interconnected by unstacked stroma lamellae whereas in green algae, the grana organization typical of plants is replaced by a mix of stacked and unstacked thylakoid membranes that still allow a lateral heterogeneity in protein content of these membranes (Staehelin, 1986,

Figure 1-6). In secondary phototrophs (photosynthetic species deriving from the second endosymbiosis), the organelle where photosynthesis takes place is not properly speaking a chloroplast, since this term was historically used for chlorophyll *a* and *b* containing plastids.

Secondary endosymbionts contain chlorophyll *a* and *c*, and we use the generic term plastid (Gould, Waller and McFadden, 2008). Electron micrographs show no thylakoid subdomains in secondary plastids, only loose stacks of two, three or four thylakoids (most of the time 3, Pyszniak and Gibbs, 1992) which still lead to a marked difference in protein content between the outer membrane of a stack and its inner membranes.

The main role of chloroplasts/plastids is the photosynthetic metabolism, but it also hosts nitrate and sulfate reduction, as well as synthesis of chlorophylls, carotenoids, haems, amino acids and fatty acids (Jensen and Leister, 2014).

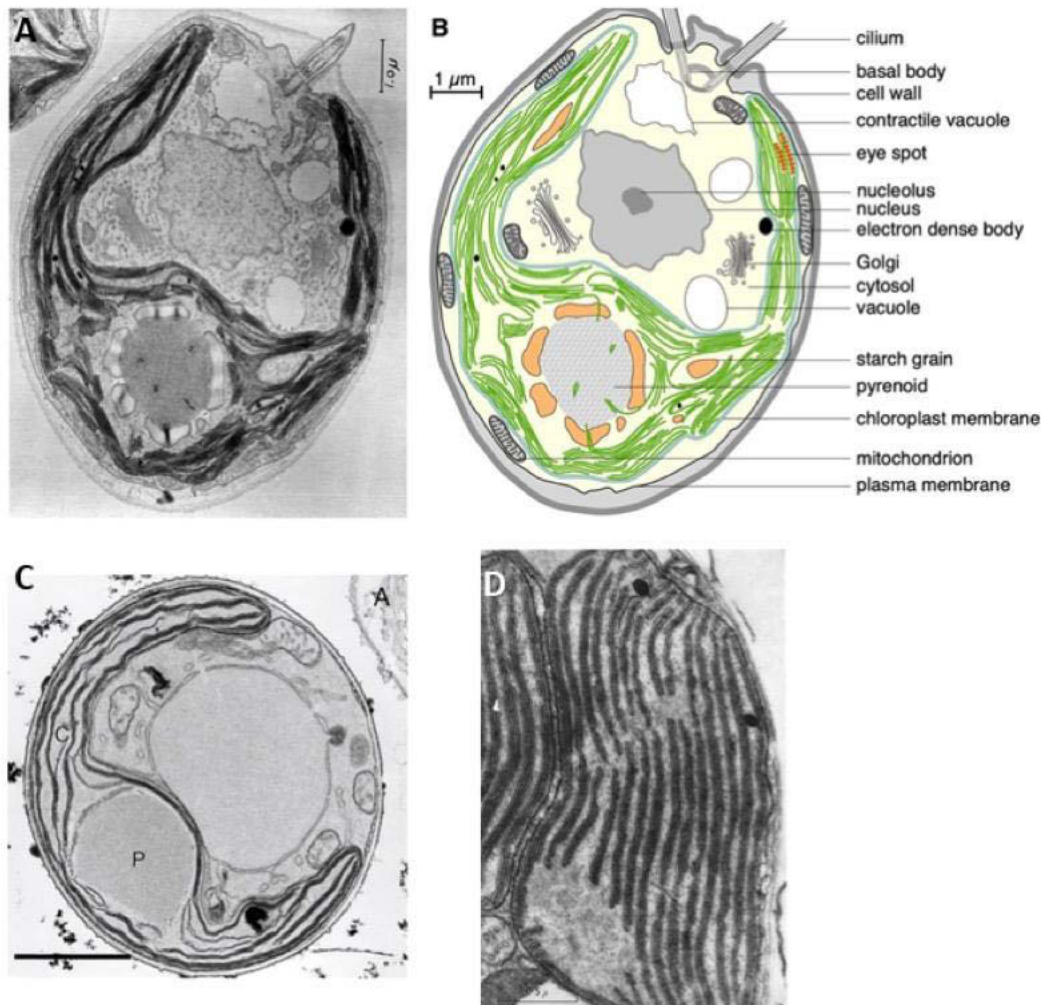


Figure 1-6: Diversity of chloroplast structures

A. Originally published by Ohad et al., 1967). Transmission electron micrograph (TEM) of a *Chlamydomonas reinhardtii* cell.

B. From Salomé and Merchant, 2019. Drawing of a *C. reinhardtii* cell based on the TEM image in (A).

C. From Buma et al., 2000. TEM micrographs cell of *Emiliana huxleyi*. N, nucleus; P, pyrenoid; C, chloroplast. Scale varies; bars represent 1 μm .

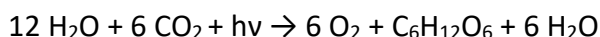
D. From Dodge, 1968. Transmission electronic micrographs of cell of the dinoflagellate *Aureodinium pigmentosum*. A median section through a chloroplast to show the large number of more or less parallel lamellae composed of 2-4 thylakoids, the granular stroma with dark lipid droplets and the thick chloroplast envelope. x 70000.

1. 2. 3. The Calvin-Benson-Bassham cycle synthesizes organic carbon from CO₂

a) Oxygenic photosynthesis, a two-step reaction

In the first decade of the 20th century, it was generally assumed that light, absorbed by photosynthetic pigments, directly reduced CO₂ which in turn combined with water to form carbohydrates. And under this hypothesis, CO₂ was considered as the source of O₂ generated by photosynthesis. But in 1931, based on work on purple sulfur bacteria, Cornelis van Niel proposed that photosynthesis is a two-stage process in which light energy is used to oxidize H₂O into O₂ (van Niel and Muller, 1931). The validity of van Niel's hypothesis was established unequivocally by two experiments. In 1937, Robert Hill discovered that when isolated chloroplasts that lack CO₂ are illuminated in the presence of an artificial electron acceptor, O₂ evolved with concomitant reduction of the acceptor. This Hill reaction demonstrates that CO₂ does not participate directly in the O₂ producing reaction. In 1941, when the oxygen isotope ¹⁸O became available, Samuel Ruben and Martin Kamen directly demonstrated that the source of O₂ in photosynthesis is H₂O.

It is now well understood that photosynthesis is enabled by two steps: the production of reducing power in the form of reduced nicotinamide adenine dinucleotide phosphate (NADPH) and chemical energy in the form of ATP that occurs in the membrane photosynthetic chain thanks to light energy. Carbon fixation then uses products of the photosynthetic chain in the stromal compartment. The result of the "light" phase of photosynthesis is the conversion of light energy into chemical energy, stored in molecules with high energy potential, ATP and NADPH. In the "dark" phase of photosynthesis, ATP and NADPH are used together to catalyze all of the carbon assimilation reactions used to make carbohydrates, called the Benson-Calvin cycle. When the final carbon molecule is glucose, the entire process described so far leads to the following reaction:



In the following two sections, I will describe first the Calvin Benson Bassham cycle where reduction of carbon dioxide occurs (the biosynthetic, or "dark", phase of photosynthesis), and then the photochemical phase which occurs in the thylakoid membranes (also called "light" phase of photosynthesis).

b) Discovery and chemical equation of the CBB cycle

The metabolic pathway by which most of the autotrophs incorporate CO_2 into carbohydrates was elucidated between 1946 and 1953 by Melvin Calvin, James Bassham and Andrew Benson (Bassham, Benson and Calvin, 1953). The basic experimental strategy they used was to expose growing cultures of the green alga *Chlorella* to radioactive labelled $^{14}\text{CO}_2$ for varying times and under different illumination conditions and then to drop the cells into boiling alcohol so as to disrupt them while preserving their labeling pattern. The radioactive products were then separated and identified by a two-dimensional paper chromatography coupled to autoradiography. The overall pathway is presented in Figure 1-7 and shows that the reduction of CO_2 requires an energy supply in the form of adenosine triphosphate (ATP) and an input of reducing power provided by a coenzyme, the reduced form of nicotinamide adenine dinucleotide phosphate (NADPH). These two substrates are used with a ratio of 3 ATP for 2 NADPH. Although other carbon fixation pathways have been found in autotroph bacteria and archae, CBB cycle is the only carbon fixation pathway operating in eukaryotes (Hügler and Sievert, 2011).

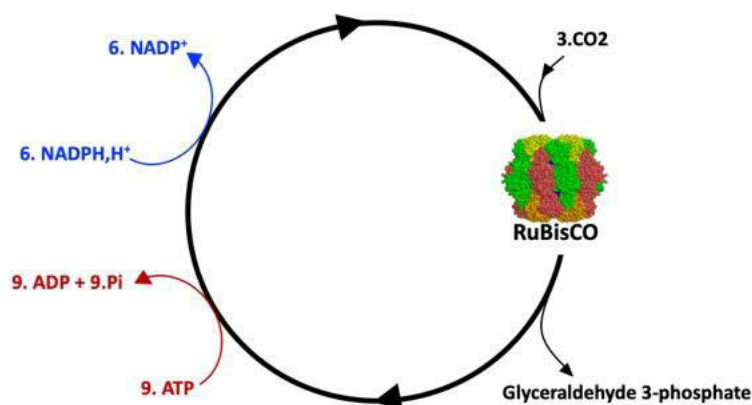


Figure 1-7: Schematic representation of the balanced equation of the Calvin Benson Bassham cycle (CBB cycle)

A form I RuBisCO is represented by a model of its structure. Large subunits are shown in red and green and small subunits are shown in yellow and orange.

c) Carbon concentration mechanisms (CCM) enable high rate of carbon fixation

The first step along the reductive pathway of CO_2 is catalyzed by the Ribulose-1,5-bisphosphate Carboxylase Oxygenase, RuBisCO, a big protein complex. RuBisCO has a low affinity for CO_2 and catalyzes also a reaction of ribulose-1,5-bisphosphate and molecular oxygen (O_2) that is competing with carbon fixation. Carbon fixation rate is thus depending on

the ratio of CO₂ concentration over O₂ concentration in the surrounding environment of RuBisCO (Delgado et al., 1995).

The way to deal with CO₂ is obviously very different for terrestrial organisms (plants) and for aquatic organisms. CO₂ can dissolve into water and its concentration in surface Ocean ranges from 10 to 30 μM (Reinfelder, 2011). Dissolved CO₂ is not the only source of inorganic carbon in aquatic environments. CO_{2(d)} can undergo nucleophilic displacement from a water molecule, leading to the formation of H₂CO₃ that is in chemical equilibrium with bicarbonate and carbonate ions: $\text{CO}_{2(g)} \rightleftharpoons \text{CO}_{2(d)} + \text{H}_2\text{O} \rightleftharpoons \text{H}_2\text{CO}_3 \rightleftharpoons \text{HCO}_3^- + \text{H}^+ \rightleftharpoons \text{CO}_3^{2-} + 2\text{H}^+$

The ionic forms do not contribute to the vapor pressure of the gaseous form, thus the concentration of the sum of all dissolved inorganic carbon can greatly exceed the atmosphere/water equilibrium concentration of gaseous CO₂. In the surface ocean, total dissolved inorganic carbon is approximately 200 times higher than dissolved CO₂ concentration (Falkowski and Raven, 2013). Nevertheless, transient patches of CO₂-depleted surface seawater may persist for several days to weeks (Takahashi, 2009) because CO_{2(d)} diffusion rate and bicarbonate dehydration to CO₂ are low processes regarding potential consumption by photosynthetic reactions (Falkowski and Raven, 2013).

In all marine phytoplankton, the intrinsic Michaelis constant (K_m) of the Rubisco is much higher than the apparent photosynthetic requirement for extracellular dissolved CO₂ ($K_{1/2}$) (Kaplan and Reinhold, 1999). This is attributed to carbon concentration mechanisms, CCM, that increase locally the CO₂ concentration. The biophysics and biochemistry of CCMs vary within and among marine phytoplankton clades such as dinoflagellates, haptophytes and diatoms (Reinfelder, 2011). They may involve the activity of external or intracellular carbonic anhydrase and active HCO₃⁻ transport. CCM have thus a cost of energy and nutrient: for enzymes production and for active transport of bicarbonate. In general, coccolithophores have low-efficiency CCM, and diatoms and the haptophyte genus *Phaeocystis* have high-efficiency CCM while dinoflagellates appear to possess moderately efficient CCM (Takahashi, 2009).

1. 2. 4. The photosynthetic electron transfer chain uses light energy to supply the CBB cycle

Calvin Benson cycle reactions involve consumption of reducing power in the form of NADPH and chemical energy in the form of ATP high energy bond. This is supplied by the photosynthetic electron transfer chain whose mechanistic details have been resolved in the second part of the 20th century. Resolution of the pathway allowing electron transfer from water to NADP⁺ has first been investigated with chemical tools. Thus, the global pattern of the pathways has been resolved before understanding the molecules and protein complexes that were involved.

a) Oxidoreduction reactions involved in the photosynthetic electron transport

▪ *Resolution of the photosynthetic electron transport pathway*

In 1953, the groups of Robert Hill working with isolated chloroplast and the one of Cornelius van Niel working with bacteria could show that light energy was used for endergonic electron transfer and not for photolysis of CO₂ (van Niel et al., 1953). Arnon and collaborators then highlighted that isolated chloroplasts are capable of ATP synthesis (Arnon, Allen and Whatley, 1954). This is suggesting that light driven electron transfer is followed by a downhill exergonic reaction coupled to ATP synthesis. Cyclic electron transfer has first been proposed as the pathway of photophosphorylation. But in 1958, Arnon's group could show that ATP synthesis was coupled to a linear electron pathway inducing a donor oxidation and a final acceptor reduction (Arnon, Whatley and Allen, 1957). This raised a thermodynamic problem: it was difficult to imagine a downhill electron transport that could be coupled to the endergonic ATP synthesis.

Emerson, Chalmers and Cederstrand, revealed the existence of two site of photochemistry, based on the spectral dependence of the photosynthetic process (Emerson, Chalmers and Cederstrand, 1957). Those two sites were called photosystem I and photosystem II. Later, two cytochromes were discovered in the chloroplast, named cytochrome b6 and cytochrome f, and Hill and Bendall proposed that those cytochromes allow the electron transfer between the two photosystems and their operation in series (Hill and Bendall, 1960). In agreement with the redox potentials of the two cytochromes and the two reaction centers, the general Z scheme or diagram of the photosynthetic electron transfer, was elucidated (Hill and Bendall, 1960). In addition to the electron transfer chain between PSII

and PSI, involving cytochromes b6 and f, this included a set of reactions allowing the transfer of electrons from water to the donor side of the PSII, and some electron transfer steps on the acceptor side of PSI, where NADPH is produced before being exported for carbon assimilation. Figure 1-8 shows the Z-scheme completed thanks to the well-established characterization of the cofactors involved in electron transfer and the determination of their redox potential.

- *Electron transfer chain and redox potentials*

Describing the Z-scheme of photosynthesis requires the use of oxidoreduction principles. "Oxidation" and "reduction" reactions, refer to the loss or gain of one or more electrons, respectively. The redox potential is a scale (in volts) that has been developed to predict the tendency of a redox reaction. The molecules with the lowest redox potential will tend to be oxidized by molecules of higher redox potential.

When these considerations are applied to the photosynthetic electron transfer chain, it is clear that linear electron transfer from water to NADP^+ is unfavorable. Two photochemical steps that occur in photosystem II (PSII) and photosystem I (PSI) are crucial: the light catalyzed electron transfer from the high redox potential special pairs P_{680} and P_{700} towards the low redox potential acceptors, Q_A and iron-sulfur centers (F_x , F_A and F_B), respectively (Nelson and Yocum, 2006). Those are highly endergonic (i.e. thermodynamically unfavorable) reactions. Those two steps are put in series thanks to exergonic (i.e. thermodynamically favorable) electron transfer from PSII to PSI via the membrane plastoquinones (PQ), the cytochrome *b₆f* complex (cyt. *b₆f*) and the luminal plastocyanins (PC) that reduce the PSI primary donor, P_{700} . At the donor side of PSII, Oxygen Evolving Complex (OEC), a metallic center $(\text{Mn})_4\text{Ca}$ catalyzes transfer of electrons from water to a tyrosine residue, Y_Z that in turn reduces P_{680}^+ . At the acceptor side of PSI, F_B reduces ferredoxin (Fd) that in turn reduces NADP^+ .

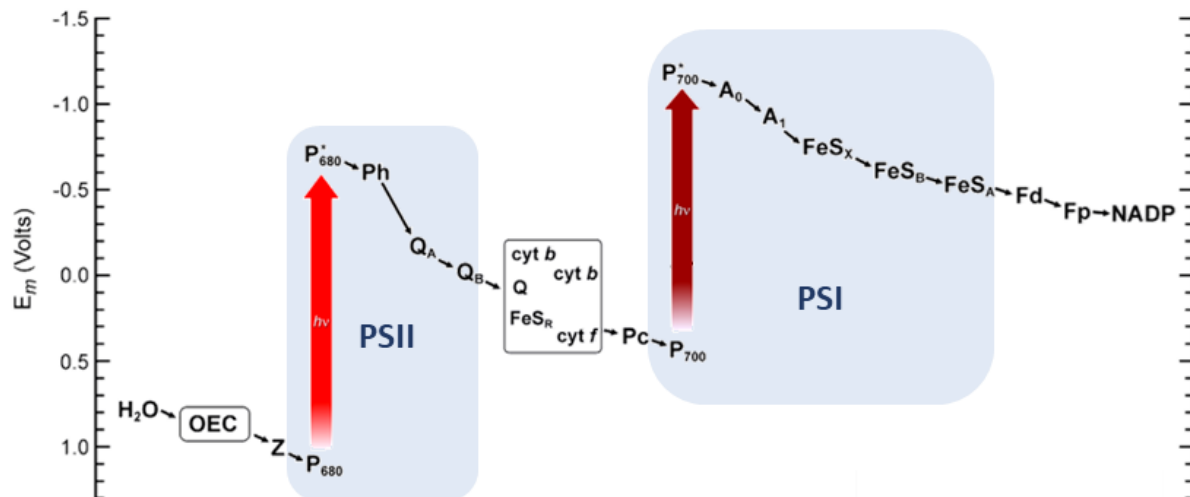


Figure 1-8: Z-scheme of the electron transfer along photosynthetic chain intermediates

Adapted from Govindjee and Björn, 2017.

The redox carriers were placed according to the accepted midpoint redox potentials (pH 7). OEC: oxygen evolving complex, Z: electron donor to photosystem II (PSII), P_{680} : reaction center chlorophyll (Chl) *a* of PSII, Ph: pheophytin, Q: quinone, Cyt: cytochrome, FeS_R : Reiske iron-sulfur protein, Pc: plastocyanin, P_{700} : reaction center Chl *a* of photosystem I (PSI), A_0 and A_1 : primary electron acceptors of PSI, FeS_x , FeS_B , and FeS_A : bound iron-sulfur protein acceptors of PSI, Fd: soluble ferredoxin, Fp: flavoprotein (ferredoxin-NADP reductase). In this diagram, electron transfer through the redox components of plastoquinone pool and Cyt *b*₆f complex is not shown.

From these first discoveries, the development of absorption and fluorescence spectroscopy, Nuclear Magnetic Resonance, Electron Paramagnetic Resonance or X-ray diffraction crystallography has allowed to study the structure and function of each of the photosynthetic protein complexes. These studies allowed the resolution of crystallographic structures of the different photosynthetic complexes and to understand the relation between their structure and function. This deepened the knowledge on photosynthesis, generating more and more precise models, which we will present in the following.

b) Chemiosmotic coupling and ATP production by the photosynthetic electron transport chain

▪ *The chemiosmotic theory*

The principle of the coupling between the exergonic electron transfer from PSII acceptors to PSI donors and ATP production has been proposed by Peter Mitchell in 1968 (Mitchell, 1968). The previous assumption was that ADP was converted into ATP by direct transfer of high-energy phosphoryl groups from some other intermediate, as was known to occur during glycolysis. Thus, it was postulated that high-energy intermediates were produced as a result of electron transfer reactions and that these intermediates then drove ATP synthesis

by phosphoryl group transfer. However, no such intermediates were found and phosphorylation of ADP was rather observed to be closely associated to the membrane and dependent of its integrity. These findings led Peter Mitchell, in 1961, to formulate the chemiosmotic hypothesis in which he postulated that the proton electrochemical gradient across the membrane was the driving force for ATP synthesis (Mitchell 1961). After long and intense debates during the 1960s and 70s, Mitchell's chemiosmotic hypothesis – which became known instead as the chemiosmotic theory – became a paradigm in the intellectual framework of bioenergetics and he won a Chemistry Nobel Prize in 1978.

The electrochemical proton gradient, $\Delta\mu_{\text{H}^+}$, has two components: a chemical one that depend on the pH difference between lumen and stroma, ΔpH , and an electric component that is a function of the electric field across the membrane, $\Delta\Psi$:

$\Delta\mu_{\text{H}^+} = F.\Delta\Psi - 2.3 RT.\Delta\text{pH}$, where F is the Faraday constant, R the gas constant and T, the temperature.

The photosynthetic electron flow builds an electrochemical proton gradient and we will describe the mechanisms coupling proton movements to electron transfer along the thylakoid hereafter, when describing the molecular actors of the electron transfer.

- *Proton liberation and oxygen evolution*

On the PSII donor side, the Oxygen Evolving Complex (OEC), also known as the water-splitting complex plays a crucial role. It contains a metalloenzyme core containing 4 atoms of manganese and one atom of calcium, $(\text{Mn})_4\text{Ca}$. The OEC allows the transfer of electrons liberated by the oxidation of a water molecule, according to $2 \text{H}_2\text{O} \rightarrow 4 \text{H}^+ + 4 \text{e}^- + \text{O}_2$ up to a tyrosine Z residue involved in the reduction of P680^+ . The great works of Joliot and Kok, between 1968 and 1975, based on the observation of oscillations of period 4 in the emission of oxygen upon short saturating flashes demonstrated the role of of the manganese complex in the electron accumulation (Kok, Forbush and McGloin, 1970). The OEC is in its most oxidized form every four photochemical events (the manganese atoms are oxidized) and then reacts with a water molecule to produce molecular oxygen O_2 . This process liberates 4 protons while fueling 4 electrons into the electron transfer chain.

- *Cytochrome b_6f and Q-cycle*

The electron transfer from water to the plastoquinone pool in the thylakoid membrane is made possible thanks to PSII; PSI allows electron transfer from plastocyanin (or cytochrome c_6) to NADPH. The missing piece, which allows the functioning in series of the two

photosystems and involves the two cytochromes discovered by Hill and Bendal is a quinol:plastocyanin (cytochrome c_6) oxidoreductase: the cytochrome b_6f complex. The transfer from water to NADPH permitted by the combined activities of the two photosystems and the cytochrome b_6f is called linear electron flow (LEF). It is found in all organisms performing oxygenic photosynthesis i.e. cyanobacteria and its derivatives from a primary and secondary endosymbiotic event. Four major subunits constitute the heart of the complex: cytochrome b_6 , the subunit IV, the Rieske protein and the cytochrome f (Figure 1-9). The complex forms a homodimer (Huang et al., 1994) as confirmed by electron microscopy and X-ray crystallography (Stroebel et al., 2003). In total seven prosthetic groups are contained within a cytochrome b_6f monomer. Two b haems (b_L and b_H) are axially ligated to the cytochrome b_6 and a haem c_i also is linked to cytochrome b_6 but its function is not clear yet. One c haem is covalently attached to the extramembrane luminal domain of cytochrome f and one Fe_2S_2 cluster is present in the extramembraner luminal domain of the Rieske protein. In addition, one chlorophyll a and one β -carotene are found in the complex, whose roles are still not fully understood (Stroebel et al., 2003).

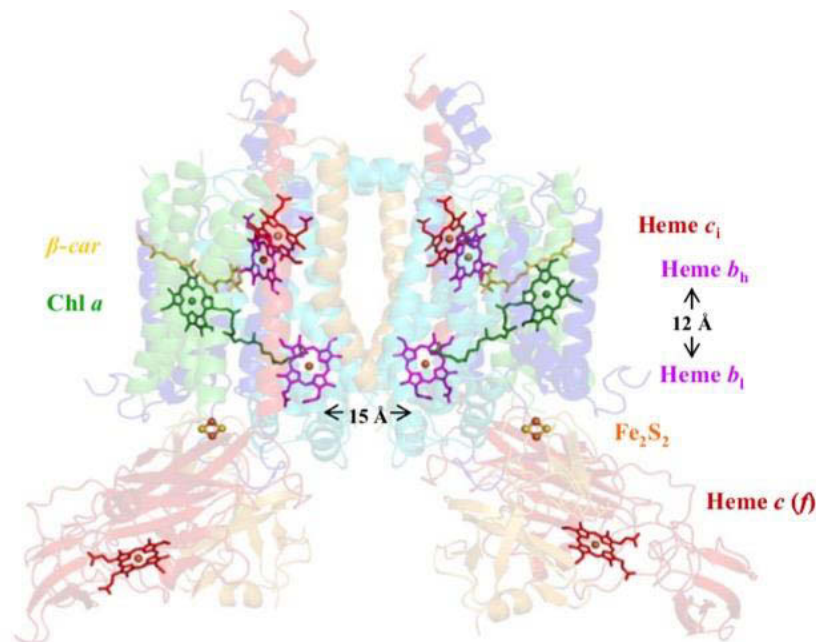


Figure 1-9: Structure of a dimer of cytochrome b_6f

From de Vitry and Kuras 2009.

Helices for cytochrome b_6 are colored in cyan, helices for subunit IV are shown in blue, the Rieske subunit is shown in orange, cytochrome f is shown in red, the PetG, PetL, PetM and PetN subunits are shown in green. Shown as wireframes are the β -carotenes colored in yellow, the chlorophylls colored in green and the hemes colored either in pink (b-type hemes) or in red (c-type hemes). The Fe_2S_2 centers are shown as a ball-and-stick model (yellow and orange).

Electron transfer from plastoquinols to plastocyanins is exergonic and is coupled at the cytochrome *b₆f* site to proton translocation from the stroma to the lumen against the electrochemical proton gradient. Two mechanisms are involved. In the first mechanism, a plastoquinone is reduced by two electrons at the acceptor side of PSII, recruiting two protons from the stroma, and is reoxidized at the luminal Q_o site of cytochrome *b₆f*, thus releasing 2 protons inside the lumen. The second mechanism is called the Q-cycle for “Quinone cycle” and was first described by Mitchell in 1975 (Mitchell, 1975). The two electrons released at the Q_o site follow two different pathways: one is directed to the cytochrome f and will reduce a PC while the other one is transferred via b_L and b_H haems to the stromal Q_i site where a plastoquinone is fixed. Hence, oxidation of two plastoquinols at the Q_o site induce the reduction of one plastoquinone at the Q_i site thanks to two stromal protons (Figure 1-10). All in all, 4 H⁺ are translocated to the lumen every 2 electrons transferred through the cytochrome *b₆f*. After many debates whether the Q-cycle is facultative or not (Berry and Rumberg, 1999), the Q-cycle is now considered to be constitutive (Sacksteder et al., 2000).

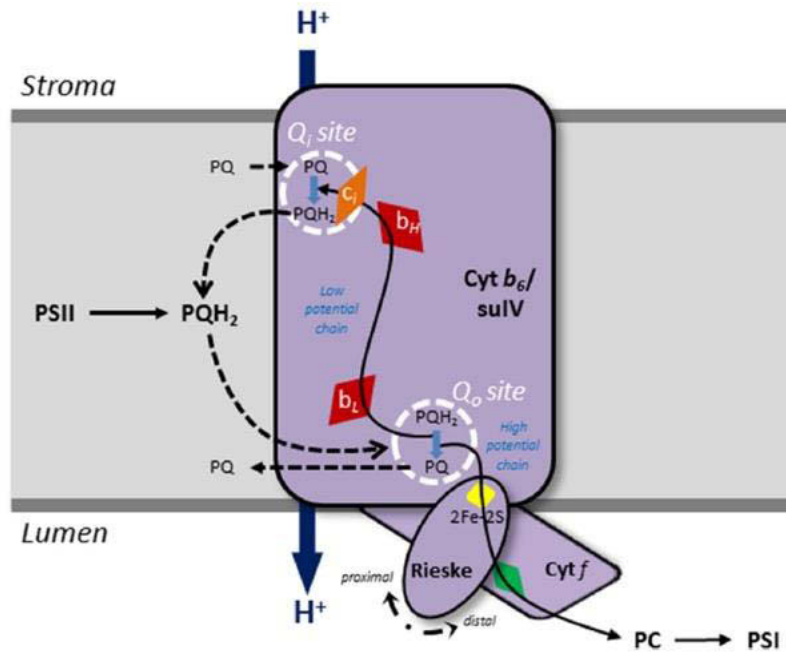


Figure 1-10: The cytochrome b_6f complex drives the Q-cycle

From Dumas et al., 2016.

Electron transfer (solid black arrows) is coupled to proton translocation (blue arrow) across the thylakoid membrane, establishing the $\Delta\mu H^+$. PQH₂ oxidation occurs at the Q_o site and PQ reduction at the Q_i site. Electrons are transferred to the low-potential chain (haems b_L, b_H and c_i) and to the high-potential chain (Fe-S, cyt *f*, PC, PSI) upon PQH₂ oxidation. Movement of the Rieske subunit between proximal and distal positions is necessary for electron transfer from PQH₂ to cyt *f*. Dashed black arrows represent the movement of quinone species between the PQ pool and the two cyt *b₆f* catalytic sites.

c) ATP synthase

As predicted by Mitchell in the chemiosmotic theory, the chloroplast (CF₀-F₁) ATP synthase is located inside the thylakoid membrane, in the non-appressed regions in plants. This large complex is able to use the $\Delta\mu H^+$ to produce ATP from ADP and inorganic phosphate, P_i. The mechanism involved in ATP synthesis has been resolved by John Walker and Paul Boyer who shared a Noble Prize for Chemistry in 1997. As shown in Figure 1-11, the enzyme has two major domains: the three-fold CF₁ catalytic domain that protrudes at the stromal side and that is linked to the membrane domain CF₀ thanks to a peripheral stalk.

The F₁ domain consists of three $\alpha\beta$ heterodimers, which define the catalytic site, and of the central γ and ϵ subunits which are attached to the c-ring (polymer of c subunits arranged in a ring). The F₀ domain, the motor of the enzyme, is composed of three subunits with a stoichiometry a₁b₂c₉₋₁₂. Figure 1-11 presents the model of rotation generation of CF₀ induced by proton translocation from lumen to stroma. This movement induces rotation of the central stalk and causes conformational changes in the $\alpha\beta$ heterodimers, resulting in the synthesis of ATP. According to this mechanism, one c-ring rotation results in three ATP

molecules. Hence, the number of protons needed to synthesize one ATP molecule would not depend on the extent of the $\Delta\mu\text{H}^+$ but only on the number of c subunits composing the c-ring (Hahn et al., 2018). It is of note that the ATP synthase is a reversible enzyme, the sense of the reaction being only determined by thermodynamics, i.e. the electrochemical proton gradient and the ratio ATP over $\text{ADP}+\text{P}_i$.

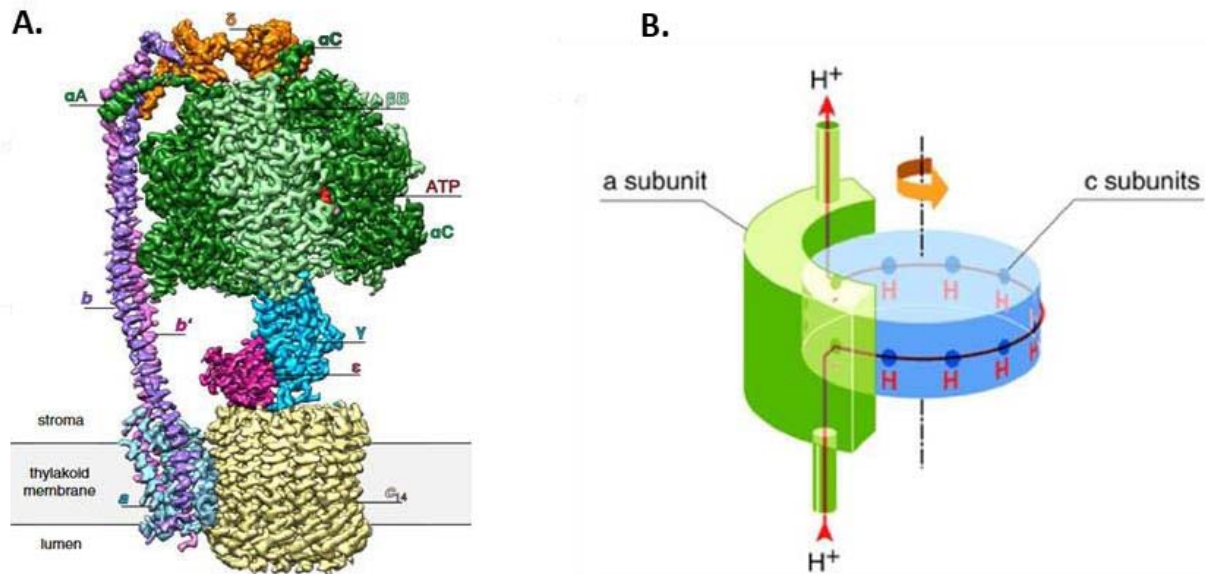


Figure 1-11: ATP synthase structure and mechanism involved in the rotation of the CF_0 domain

A. Adapted from Hahn et al., 2018. High-resolution cryo-EM map of the spinach chloroplast $\text{cF}_1\text{F}_0\text{ATP}$ synthase. Surface representation of the overall structure of the spinach chloroplast $\text{cF}_1\text{F}_0\text{ATP}$ synthase showing α subunits (dark green), β subunits (light green), γ (blue); δ (orange), ϵ (purple), a (light blue), b (violet), b' (pink), c_{14} (pale yellow), ATP (red). cF_0 ($\text{abb}'c_{14}$) is embedded in the thylakoid membrane (grey), whereas cF_1 (a3b3ged) extends into the stroma. B. Adapted from Stock et al., 2000. Model of the generation of rotation by movement of protons through the F_0 domain of ATP synthase. Two half channels across the interface between the a subunit (green) and the c ring (blue) are linked by rotation of the c ring.

d) Electron-proton coupling and ATP/NADPH ratios

As presented above, photosynthetic reactions can be separated into two steps: the photosynthetic chain that produces cell usable energy (ATP) and reducing power (NADPH) and the synthesis pathways, being mainly the CBB cycle which uses ATP and NADPH to produce organic matter. It has long been debated whether ATP/NADPH ratio produced by the linear electron flow (LEF) is equivalent to ATP/NADPH ratio required for CBB cycle and other metabolic process (e.g. Allen, 2003).

- *ATP/ NADPH ratio produced by the LEF*

ATP and NADPH production by the LEF are coupled and, based on the molecular understanding of the mechanisms involved in electron transfer and ATP synthesis, it is

possible to calculate the ratio ATP/NADPH produced by LEF. We presented earlier the sites of proton liberation in the lumen: 1H^+ is transferred per electron at the OEC level and thanks to the Q-cycle, the cytochrome b_6f couples the transfer of one electron to the translocation of two protons. The coupling between electron transfer and H^+ translocation results thus in 6 protons translocation to the lumen every 2 electrons transferred from water to NADP^+ . The number of protons needed for 3 ATP production depends on the number of c-subunits of the ATP synthase CF_0 domain. The group of Kühlbrandt recently obtained structures of the ATP synthase ($\text{CF}_1\text{-F}_0$) from spinach and confirmed that it contains 14 c subunits (Hahn et al., 2018). Hence, 14 H^+ are needed to form 3 ATP. The 6 H^+ translocated by the LEF would thus result in the synthesis of 1.29 ATP.

- *ATP/NADPH ratio required for CO_2 fixation and associated metabolic pathways*

As presented above, it is well admitted that the CBB cycle uses a ratio of 3 ATP per 2 NADPH under atmospheric conditions. But, more generally, the required ATP/NADPH ratio depends on CO_2 partial pressure in the vicinity of the Rubisco (Kramer & Evans, 2011); it can vary from 1,5 to 1,65. As presented previously, microalgae also use carbon concentrating mechanisms (CCM) involving active transport of inorganic carbon inside the chloroplast. CCM thus need ATP and are more active when CO_2 concentration is low. The carbon concentrating mechanisms have an extra cost in terms of ATP, and could in some conditions increase the required ATP/NADPH ratio for carbon concentration and assimilation to 2 ATP per NADPH. All in all, the overall CO_2 reduction pathways need at least 1,5 ATP per NADPH (CBB cycle under atmospheric conditions) but this ratio may increase depending on environmental conditions such as inorganic carbon and nutrient availability.

- *Coupling between CO_2 reduction and LEF leads to an ATP shortfall*

The comparison of the ATP/NADPH ratio produced by the linear electron flow (1.29) and the one required for CO_2 reduction (>1.5) reveals that LEF alone cannot fuel the CBB cycle with enough ATP (Allen, 2003). We have mentioned before that the plastid is not just the site of carbon assimilation, but also the site of nitrate and sulfate reduction and of amino acids and fatty acids synthesis (Jensen and Leister, 2014). All those metabolic pathways require ATP and/or NADPH with varying stoichiometry (Noctor and Foyer, 1998), making the simple comparison of the two above ratios quite naïve. Nevertheless, some level of ATP/NADPH adjustment of the “light phase” of photosynthesis is necessary to respond to varying demands of ATP and NADPH for downstream PSI metabolism (Noctor and Foyer, 1998).

1. 2. 5. From light absorption to energy storage

a) Light absorption and photochemistry

The photosynthetic process of energy conversion begins when a pigment is excited by a quantum of light, a photon, and an electron is moved from one molecular orbital (ground state) to another of higher energy (excited state). Such an excited molecule is unstable (the lifetime of a chlorophyll in water is in the ns range) and tends to return to its original fundamental energy level with one of the following relaxation pathways (Figure 1-12): (1) by converting the energy into heat (non-radiative dissipation) or (2) by re-emitting a photon of lower energy, i.e. at a longer wavelength (fluorescence) (3) by transferring the energy - but not the electron - directly to a nearby pigment molecule by a process called Förster resonance energy transfer (FRET) (Förster, 1948), (4) by transferring the high-energy electron to another nearby molecule, an electron acceptor; this is the photochemical event or charge separation.

In the thylakoid membrane, the supercomplexes formed by the assembly of light harvesting complexes (LHC), involved in the capture of light energy, and of photosystem cores, where the electron transfers occur, enable an efficient photochemistry. The following paragraphs describe the structure of these supercomplexes and the reaction steps of photochemistry.

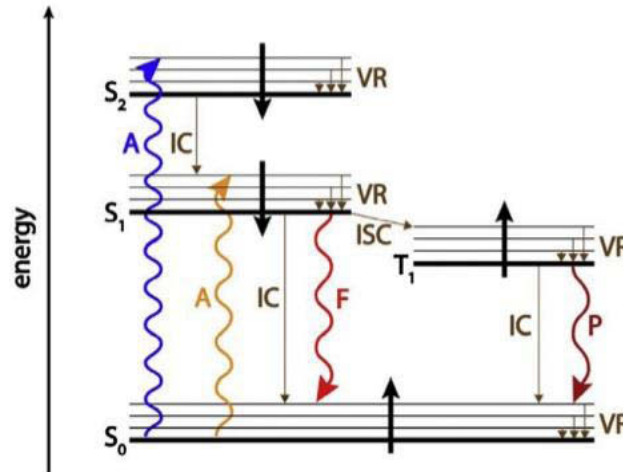


Figure 1-12: A scheme of energetic levels (the so-called Jablonski diagram) of a single molecule showing routes of formation and deactivation of the energetic levels

From Lazar et al., 2015.

The thin horizontal lines show vibrational energy levels which are superimposed on electronic energy levels of the ground state (S_0), excited singlet states (S_1 and S_2) and excited triplet state (T_1) shown by thick horizontal lines. Vertical thick arrows symbolically show orientation of spin; when the arrows in the ground and excited states are in the opposite/same directions, the singlet/triplet excited state is realized. Vertical wavy arrows indicate radiative transitions by means of absorption of light (A) of different wavelengths (shorter wavelength (blue) means higher energy whereas longer wavelength (orange) means lower energy) and by means of emission of light by fluorescence (F; S_1 – S_0 transition) and by phosphorescence (P; T_1 – S_0 transition). Thin vertical or skew arrows indicate non-radiative transitions by means of vibrational relaxation (VR), internal conversion (IC), and inter-system crossing (ISC) which all represent a loss of energy by heat dissipation. For the case of a photosynthetic pigment molecule, additional deactivations of the excited states not shown in the figure can occur: via energy transfer to another molecule and via photochemistry (the primary charge separation).

b) Light harvesting complexes and absorption cross-section of the PS

In the beginning of the 20th century, Willstätter determined the structure of the most abundant green pigment in photosynthetic eukaryotes, the chlorophyll (chl), and he was awarded the Nobel Prize in Chemistry in 1915 for this work. In 1932, Robert Emerson and William Arnold demonstrated that chloroplasts contain much more chlorophyll molecules than reaction centers and suggested that most of the chlorophylls serve as light harvesting pigments (Emerson and Arnold, 1932). Using spectrophotometric titration, they could calculate the concentration of chlorophyll contained in a *Chlorella* sample. They then measured the amount of O_2 production of the sample which had been exposed to saturating brief flash of light. They calculated that each flash of saturating intensity produced only one molecule of O_2 per ~ 2400 molecules of chlorophyll. In hindsight, since we now know that at least eight photons must be sequentially absorbed to liberate one O_2 molecule, these results suggest that the photosynthetic unit contains about 300 chlorophyll molecules forming an antenna. In higher plants and green algae, the antenna system increases the fraction of light

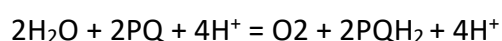
absorbed by more than two orders of magnitude funneling light energy to the photochemical converters (i.e. special pair of chlorophyll) and thereby enhance their absorption cross-section (Croce and van Amerongen, 2014).

We now know that all organisms that perform oxygenic photosynthesis have an antenna system that increases the optical section of photosystems. In plants and green algae, where most of the studies of antenna systems in eukaryotes have been performed, these antennae are made up of pigment-binding complexes integrated into the membrane and referred to as LHC (Light Harvesting Complex, reviewed in Caffarri et al., 2014). Pigment-protein complexes from PSII and PSI are called LHCb and LHCa, respectively.

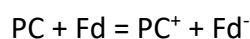
In the case of plant PSII, the core generally forms a dimer surrounded by Lhcb proteins (also called CP24, CP26 and CP29) (Figure 1-13A). The external antenna system is composed of pigment-protein monomer complexes which are in direct contact with the PSII core and of the trimeric LHCII, which are generally less strongly associated with it (Dekker et al., 2005; Caffarri et al., 2009). The organization of the Lhc proteins around the photosystem cores is different between PSII and PSI. According to the crystallographic model and the analysis of single particles, in plant PSI, a single layer of Lhca proteins (also called LHCI) is linked on one side of the central complex from PsaG (Figure 1-13A) and the order of binding is: Lhca1, Lhca4, Lhca2, Lhca3 (Amunts et al., 2010).

c) Structure and function of photosystem II and photosystem I

The two photosystems are the sites of photochemistry. PSII and PSI differ in the reaction they catalyze: the PSII is the site of water oxidation at the luminal side and of the reduction of the membrane soluble plastoquinones next to the stromal site, according to the reaction:



PSI catalyzes the oxidation of luminal PC by stromal ferredoxins (Fd) according to the equation:



What particular structural organizations of the PS enable their catalytic function? Are there structural and functional similarities between PSII and PSI? What are their differences? Hereafter, is presented a brief review of the state of the art on these issues.

- *General structure of the PS*

The PSII core is a multisubunit complex composed of approximately 25-30 subunits (Guskov et al., 2009; Caffarri et al., 2009). Most of the chromophores involved in light harvesting, as well as the electron transfer reactions, are linked to four main subunits, called D1, D2, CP43 and CP47, which are all membrane proteins containing several transmembrane helices. The D1 and D2 subunits are homologous and form a heterodimer whose transmembrane alpha helices are organized in a handshake motif. The D1-D2 complex together with cyt. b_{559} (composed of the PsbE and PsbF subunits) is often called the PSII reaction center (RC) because it binds most of the cofactors involved in the photocatalytic activity of this photosystem. The CP43 and CP47 subunits bind a total of 29 chl a molecules (based on the cyanobacterial structural model) which function as an internal antenna and allow the transfer of excitation energy from the peripheral antenna system to the reaction center. The chl a composing the internal light collection system seem to be organized mainly in two layers parallel to the plane of the membrane and located near the lumenal and stromal sides of the membrane (Figure 1-13A).

The central core complex of PSI is made up of fewer proteins (~ 15 subunits) than PSII (Jensen et al., 2007). The large PsaA and PsaB subunits form a hetero-dimer which binds the vast majority of cofactors for light capture (~ 80 Chls a and ~ 20 - carotenes) as well as the cofactors involved in electron transfer reactions with the exception of the terminal electron acceptors (Fe-S F_A and F_B clusters that will be described below), which are linked by the PsaC subunit (Figure 1-13A and B). As in the case of PSII, the chl a molecules involved in light harvesting are organized in two parallel layers and located near the lumenal and stromal sides of the membrane, respectively, while the cofactors involved in stabilizing the charge separation form two parallel branches, perpendicular to the plane of the membrane. The other subunits are involved in different processes, such as docking of plastocyanin (donor site, PsaF), docking of ferredoxin (PsaC, PsaD, PsaE, acceptor side), stabilization of the LHCI antenna system (PsaK, PsaG) or the formation of the host site for LHCII binding to PSI.

- *Electron transfer chains within photosystems*

In PSII and PSI, the cofactors involved in electron transfer (ET) reactions are organized into two parallel chains (or branches) which are perpendicular to the plane of the membrane (Figure 1-13B). This configuration allows the transfer of electrons through the membrane

and the formation of an electrochemical potential generated by photochemistry (reviewed in Nelson and Yocum, 2006 and Caffarri et al., 2014).

All the structural models of photosynthetic reaction center (RC) with sufficient resolution show a similar pattern in the cofactors involved in electron transfer reactions: they are organized into two chains located at the interface of the two main subunits of the reaction centers. Thus, each monomer of the reaction centers, PsaA and PsaB for PSI, PsbA (D1) and PsbD (D2) for PSII, contains a similar set of cofactors (Figure 1-13B): a group of at least six chlorines, which are the pigments from which the primary charge separation is initiated, and two quinone type molecules, the plastoquinones (PQ) in the PSII and the phylloquinones (PhQ) in the PSI, which act as successive electron acceptors. Other cofactors are specific to each electron transfer chain. In the case of PSI, the 6 chlorines involved in the separation of the initial charges are chl *a* while in PSII four are chl *a* and the others are pheophytins. Of the six chlorine pigments, two molecules of chl *a* form a dimer face to face (each coordinated by one of the two RC subunits). These have been frequently identified as the sites for primary charge separation (primary donor, P), and for this reason are also called "special pairs" and named P₆₈₀ for PSII and P₇₀₀ for PSI (names indicate their maximum absorption change upon photo-oxidation in the red region). The exact charge separation mechanisms in both PSI and PSII are still a subject of debate.

In the case of PSII, only one of the two electron transfer branches is used for photochemistry (branch A, Figure 1-13B, Diner et al., 1996; reviewed in Nelson and Yocum, 2006 and Caffarri et al., 2014) and therefore only one of the two Pheo molecules (linked to the D1 subunit) is photochemically reduced. On the other hand, in PSI, the two electron transfer branches are used after charge separation (branches A and B, Figure 1-13B; Santabarbara et al., 2010).

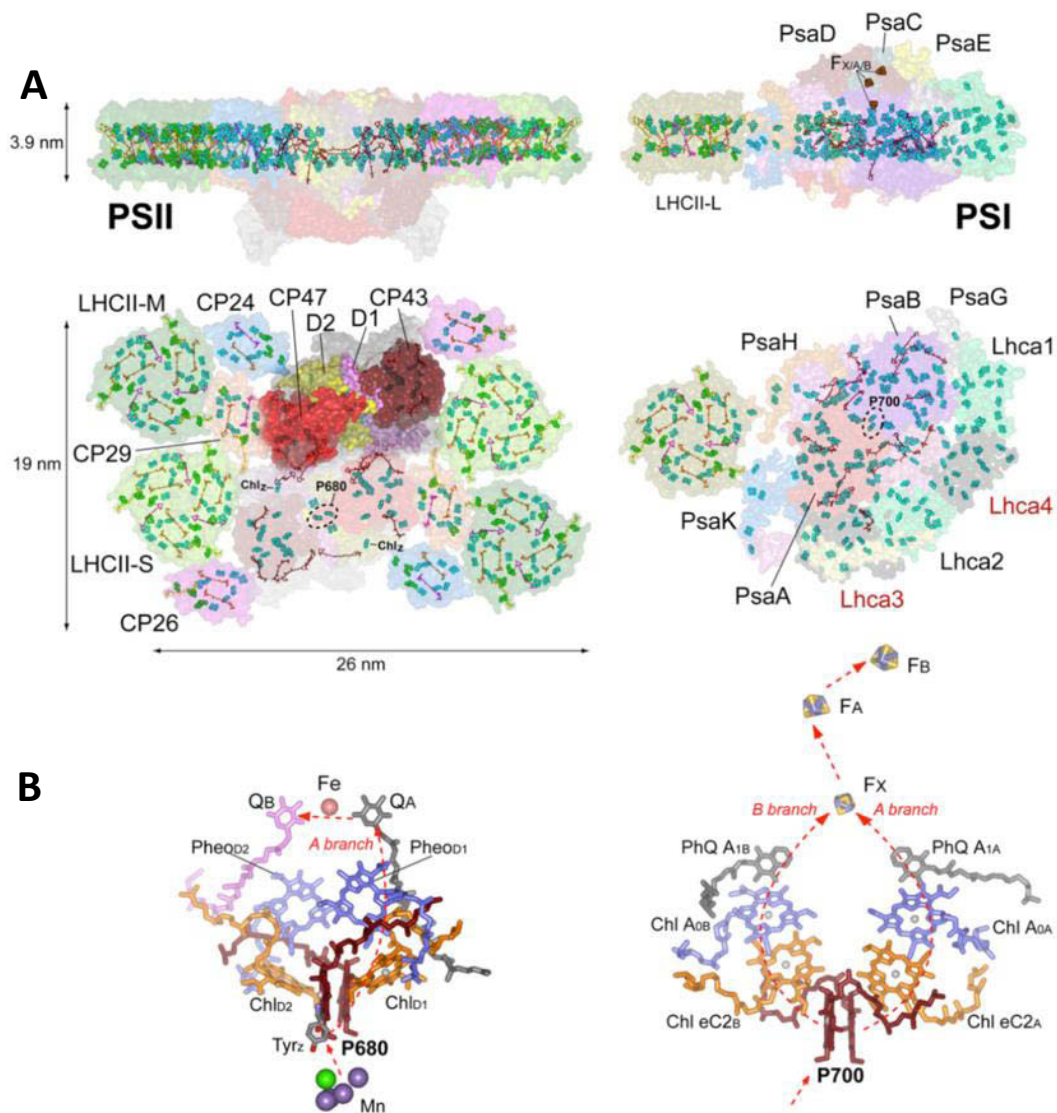


Figure 1-13: Structure of plant photosystem II (PSII) and photosystem I (PSI)

From Caffarri et al., 2014.

A. Lateral (upper diagrams) and luminal (lower diagrams) views of the PSII-LHCII supercomplex and of the PSI-LHCII supercomplex (as found in State II conditions). PSII-LHCII model has been constructed from a crystal structure of the cyanobacterial PSII core, and from the spinach LHC structures. PSI model is based on the structure from pea. In the upper diagram of the two monomers composing the dimeric core of PSII, the D1 and D2 reaction center subunits and the internal antenna proteins of the core complex CP43 and CP47 are indicated in color and other core proteins are shown in transparent grey. Peripheral antenna proteins are also indicated: CP24, CP26 and CP29 are the monomeric minor LHCb proteins and LHCII-S, -M and -L are the trimeric LHCII. In the PSI model the PsaA and PsaB core subunits are indicated, as well as the Lhca antenna complexes and other subunits visible from the luminal surface. The position of Chls and carotenoids is also shown. In the case of the Chls, for simplicity they are represented by only four atoms: the central magnesium and the 4 nitrogen atoms. In PSII and LHCII, Chl_a is indicated in blue and Chl_b in green. For PSI, the low resolution of the crystal structure in the Lhca region, where Chl_b molecules are, does not allow assigning their position and thus all Chls are indicated only in blue. Carotenoids are drawn using the following colors: -carotene, brown; lutein, orange; violaxanthin, violet; neoxanthin, yellow. The special pairs (P₆₈₀ in PSII and P₇₀₀ in PSI) are highlighted with dotted ovals. Chl_z in PSII RC is also indicated. The FeS center acceptors are only shown for the lateral view of PSI.

B. Cofactors involved in electron transfer reactions of PSII (left) and PSI (right). For PSII and PSI, models are extracted from the structure of cyanobacteria and pea, respectively. P680 is the “special pair” of PSII. Electron

extracted from water in the Mn center of the OEC goes through a Tyrosine (Tyrz) to the P_{680} . From excited P_{680}^* , electrons follow the “A branch” by reducing in sequence the ChlD1, the PheoD1 (pheophytin), the Q_A (quinone) and finally the Q_B (which gets double reduced and detaches from PSII when protonated). An iron atom (Fe) is in between the two quinones. P_{700} is the “special pair” of PSI. From excited P_{700}^* , electrons follow both the “A branch” and “B branch” to reduce an accessory Chl $eC2_A/eC2_B$, a second Chl A_{0A}/A_{0B} and then a PhQ $A_{1A}/1B$ (phylloquinone). Electrons from both branches converge on the F_X acceptor and exit from PSI by passing two other 4Fe-4S centers, F_A and F_B . See text for further discussion on ET mechanism and reaction sequence.

1. 2. 6. Monitoring photosynthesis with chlorophyll fluorescence

We saw previously that when a chlorophyll is excited after absorbing a photon, one of the relaxation pathways involves emission of a photon of lower energy (fluorescence). This signal can be used to probe PSII activity and the principle of the method is presented hereafter.

- *Theoretical principle of chl a fluorescence*

Chlorophyll fluorescence is now widely used for physiology and ecophysiology studies. The principle is based on a model for photochemistry in PSII where all excited chlorophyll relaxation pathways compete with each-other (Butler, 1978). When a chlorophyll is excited after absorbing a photon, there are three pathways (see Figure 1-14) that allow its relaxation to its fundamental energy level:

- (1) photochemistry, which corresponds to the transfer of an electron from the special pair of chlorophyll, P_{680} to its primary acceptor, a pheophytin and from there to the first stable acceptor Q_A ,
- (2) the non-radiative relaxation, which consists in the dissipation of energy in the form of heat,
- (3) the radiative relaxation, which is the re-emission of a lower energy photon (i.e. at a longer wavelength).

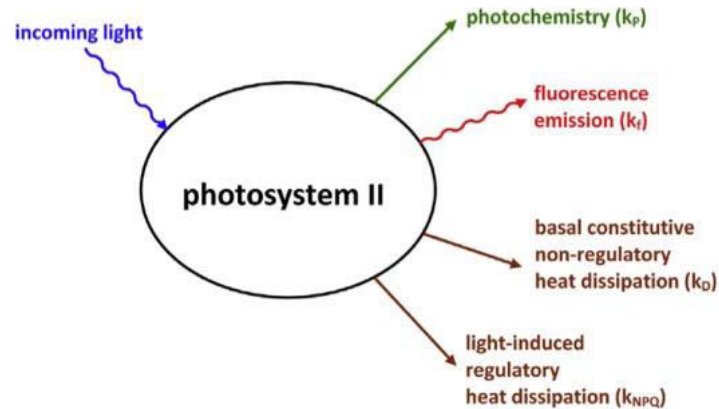


Figure 1-14: Schematic representation of the main pathways for excitonic energy dissipation

From Lazar, 2015.

k_p , k_f , k_D and k_{NPQ} represent degenerate kinetics constant of photochemistry, fluorescence, and basal and regulated heat dissipation, respectively.

As these three de-excitation pathways compete with each other, photochemistry, i.e. the electron transfer from P_{680}^+ to Q_A quenches fluorescence (photochemical quenching), as does an increase in the rate of non-radiative relaxation (heat loss) (non-photochemical quenching).

The accurate measurement of the photochemical yield of PSII therefore requires the measurement of both photochemical and non-photochemical quenching. Two extreme cases can be drawn: in the dark, Q_A is completely oxidized and PSII centers are open: the photochemical yield is maximal and the fluorescence yield is minimal, termed F_0 . At the opposite, when applying a brief saturating pulse of light which reduces all Q_A on a dark-adapted sample, photochemical yield drops to zero and the fluorescence yield is maximal (F_m). A photosynthetic sample exposed to a continuous actinic illumination will have a fluorescence yield (F'), which is intermediate between these two values. If this actinic illumination is strong, the fluorescence yield of this illuminated sample after a brief saturating pulse of light (F_m') can be different from F_m , if light-induced heat dissipation processes (see Figure 1-15) are activated.

Based on these parameters, several systems have been proposed, which vary greatly depending on the model of energetic connection between PSII, i.e. whether a “puddle” model (all PSII are isolated with their own antenna) or a “lake” model (where the exciton is shared by all PSII centers) is used. Some parameters are more robust than others and prove valid in both models. It is the case of the $(F_m - F_0)/F_m$, generally written F_v/F_m , the maximal quantum yield of PSII when it is dark-adapted, or its equivalent in the light, $Y(II) = (F_m' - F')/F_m'$, the quantum efficiency of PSII (Genty, 1989; Lazar, 2015).

Figure 1-15 shows the light dependence of photosynthetic parameters F_0' , F' and F_m' . Under high light, the maximal fluorescence (after the saturating pulse is applied, i.e. when the contribution of photochemistry is almost null) decreases, reflecting the activation of light induced regulatory heat dissipation mechanism (see Figure 1-15). The efficiency of light-induced heat dissipation process can be probed with the parameter $NPQ = (F_m - F_m')/F_m$ (Bilger and Björkman, 1990). The NPQ must be used cautiously: it has two components, the q_E process which is reversible in the minute timescale, and the photoinhibition q_I process which relaxes very slowly, in the tens of minutes to hours timescale. The two processes can therefore be distinguished based on their different relaxation characteristics.

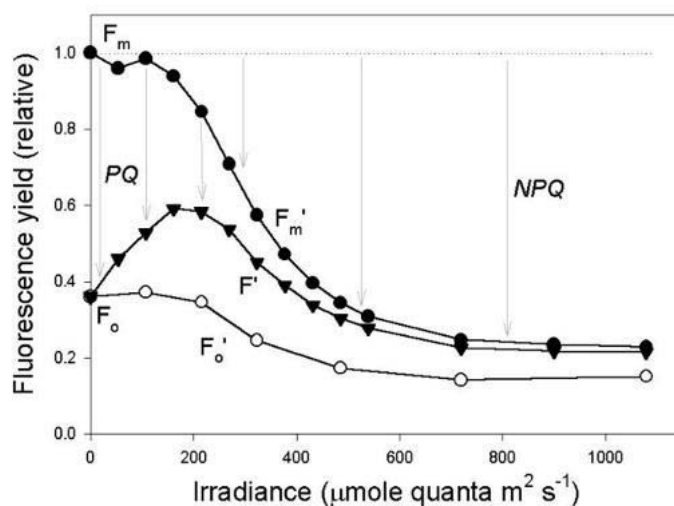


Figure 1-15: The irradiance dependence of chlorophyll fluorescence yields in a marine diatom, *P. tricornutum*
From MiniFIRe guide, Max Gorbunov (DMCS, Rutgers University, NJ, USA).

F_0 and F_m are the minimum (open reaction centers) and maximum (closed centers) fluorescence yields, respectively, measured in dark-adapted cells. F_0' and F_m' are the minimum (open centers) and maximum (closed centers) fluorescence yields, respectively, measured in a light adapted state. F_0' is measured in light-adapted cells following a brief (~ 1 s) exposure to darkness. F' is the actual fluorescence yield measured under ambient light. PQ and NPQ are photochemical quenching and non-photochemical quenching, respectively.

- *Relationship between fluorescence and activity of PSII centers*

Some measurements of PSII parameters require more caution; it is the case for the measurement of the fraction of active PSII centres often called open centers (that will be used in chapter 2 and 3). An open center is defined as a PSII with an oxidized Q_A (capable of doing a charge separation if it receives a photon), so that the fraction of open centers is equivalent to the fraction of oxidized Q_A . In 1964, Joliot and Joliot compared the PSII activity measured as O_2 production to the fraction of open PSII centers, estimated by the amount of

O₂ emitted after a saturating flash, in *Chlorella*. They measured a deviation from the expected linear relationship if the PSII centers were independent from each other and interpreted this result as indicative of a connectivity between PSII centers, ie a possibility of energy transfer between adjacent PSII: an exciton meeting a closed PSII could be transferred to an adjacent open PSII center (Joliot and Joliot, 1964). This behavior was confirmed with fluorescence measurements. When PSII is inhibited by an inhibitor allowing only a single charge separation per PSII, e.g. orthophenantroline, we expect that the kinetics of fluorescence rise follow an exponential law in the case of non-connected PSII. Instead the fluorescence rise showed an initial sigmoidicity confirming that the closure of centers is not followed by an equivalent decrease in photosynthetic activity (Figure 1-16).

In the absence of connectivity, i.e. in the “puddle” model, the fraction of open PSII centers can be calculated with the term q_p which is the ratio of the quantum yield to the maximal quantum yield (when all Q_A are oxidized): $q_p = Y(II)/(F_v'/F_m')$ (Lazar, 2015) where $F_v'/F_m' = (F_m' - F_0')/F_m'$ is the maximal quantum yield measured after a short dark adaptation (typically few tens of seconds) of the illuminated sample.

An extreme case of connectivity is the “lake” model where an exciton can be shared by all PSII. A parameter q_L has been calculated to estimate the fraction of open PSII centers in this extreme case scenario: $q_L = Y(II)/(F_v'/F_m') \cdot F_0'/F'$ (Kramer, 2004).

The amplitude of connectivity has been well studied in plants (Stirbet, 2013) and in some green algae like *Chlorella* (Joliot and Joliot 1964; Lavorel and Joliot, 1972) but not much is known about connectivity in marine microalgae. A conservative approach consists in estimating the fraction of open PSII centers based on the two extreme models, “puddle” and “lake” which provide upper and lower limits to the estimation, respectively.

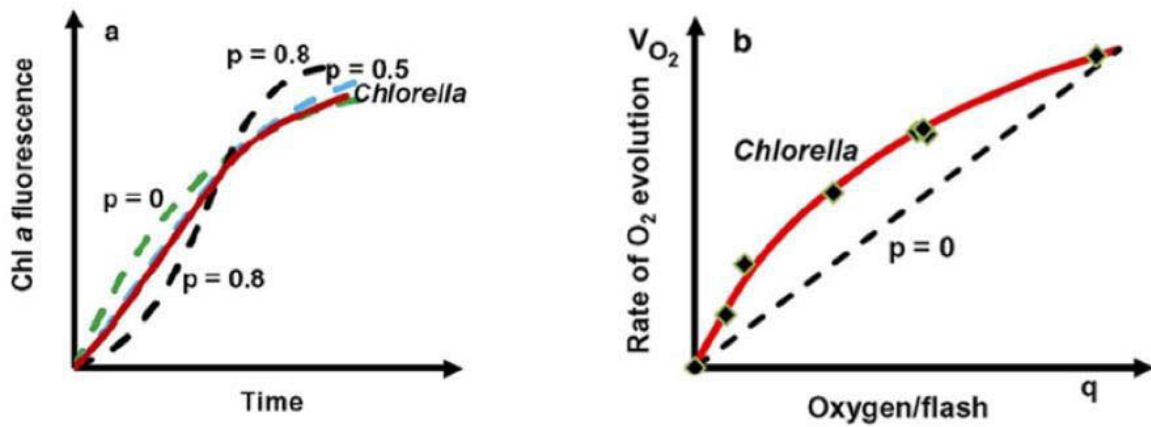


Figure 1-16: Evidence for excitonic connectivity between PSII units

From Stirbet, 2013.

a. Chlorophyll *a* fluorescence induction kinetics: experimental data on *Chlorella* cells (continuous red line) and theoretical transients (dashed lines) for different values of the connectivity constant p . b. Rates of oxygen evolution (diamonds) in *Chlorella* cells as a function of the calculated photochemical complex concentration (i.e., fraction of active photosystem II units, q). The figure was redrawn from the original figures (Figs 2, 3) of Joliot and Joliot (1964).

1. 3. Regulation of the photosynthetic process and acclimation to changing environments

In the previous section, we discussed the stoichiometry of the two products of the “light phase” of photosynthesis, ATP and NADPH, which needs to be adjusted to the metabolic requirements downstream PSI. Another constraint on the photosynthetic physiology concerns the substrates of the photosynthetic electron transfer chain, the light intensity. The photosynthetic process balances the absorption of photons to the capacity of the metabolic pathways after PSI, through a combination of regulatory mechanisms. In this section, I will present the various regulatory mechanisms allowing the photosynthetic chain to adjust electron and proton circuits to the availability of its substrate and the metabolism demand for its products.

1. 3. 1. Light stress and photo-inhibition

The light dependency of photosynthesis usually shows three phases: (i) under low light, photosynthesis is proportional to light intensity – light is limiting photosynthesis, (ii) under high light, the photosynthetic process becomes limited by chemical reactions (cytochrome *b₆f*, CBB cycle) instead of photo-chemical ones (Figure 1-17), and (iii) under very high light, a drop in photosynthetic rate might appear, which reflects the photo-destruction of the photosynthetic machinery (Figure 1-17). Chlorophylls of the photosynthetic antenna absorb light and reach an excited singlet state ($^1\text{Chl}^*$). The exciton can be transferred by Förster resonance energy transfer towards the special pair of chlorophyll performing photochemistry. In a low light regime, most of PSII are open and therefore the photochemical yield is high. But in high light conditions, photosynthesis saturates, indicating that one of the light independent electron transfer reactions becomes the limiting step and that the excitation flux exceeds the assimilation capacity (Figure 1-17) leading to an over-reduction of the PQ pool and Q_A . When Q_A is reduced, the photochemical yield decreases and the yield of other relaxation pathways increase in a complementary way (Figure 1-12). These include also the probability of internal conversion to form triplet state of chlorophylls ($^3\text{Chl}^*$) (Krieger-Liszkay, 2005), which is not one of the main pathways of chlorophyll de-excitation and is not shown in Figure 1-17. However, the formation of triplet states can also be enhanced because of an increased probability that charge separation between P_{680}^+ and

Pheo⁻ recombines (i.e. reverses, the transfer from Pheo⁻ to P₆₈₀⁺ being thermodynamically favorable) when oxidized Q_A is not available to move the electron further (Krieger-Liszkay, 2005). The formation of triplets is dangerous because chlorophylls in a triplet state can react with O₂ to produce singlet oxygen, ¹O^{2*}, a very toxic molecule which can degrade lipids, pigments or proteins at the vicinity of PSII. In particular, singlet oxygen can degrade the D1 protein (Nixon et al., 2010). This leads to photo-inhibition (Figure 1-17), together with other processes like the limitation in electron transfer from the donor-side of PSII (Nixon et al., 2010).

It is not clear yet if the degradation of the D1 protein is a side-damage or if it is an advantageous process, involved in protection of PSII (Nixon et al., 2010, Keren and Krieger-Liszkay, 2011). In any case, there is a PSII-repair mechanism, which appears as a regulation process and operates in three phases: (i) disassembly of the PSII, (ii) the replacement of the damaged subunit specifically by a newly synthesized subunit D1, sometimes D2, (Ohad et al., 1984), and (iii) PSII reassembly (Nixon, 2010). Photo-inhibition occurs when the rate of damage of PSII outcompetes the rate of its repair.

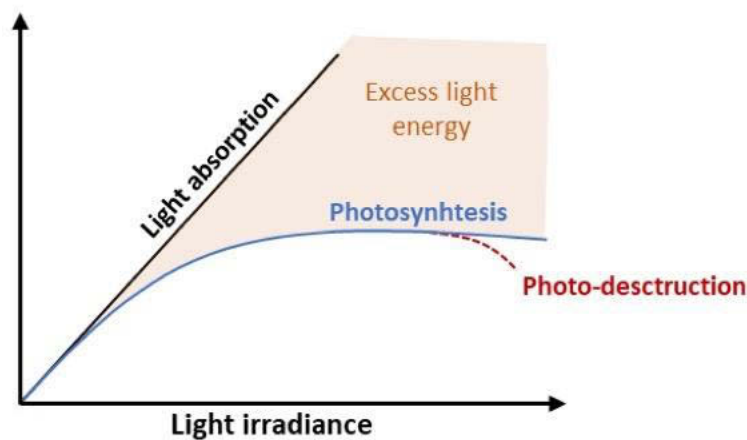


Figure 1-17: Efficiency of light absorption and utilization by photosynthetic chain

In contrast to PSII, PSI is very rarely damaged (Sonoike, 2011; Scheller and Haldrup, 2005) but, when this happens, the photo-inhibition of PSI is very fast and the damage is practically irreversible (Tikkanen et al., 2014). Damage on PSI occurs in conditions of acceptor side limitation (when electrons accumulate after PSI), which favors reduction of O₂ into superoxide anion radicals, hydrogen peroxide and hydroxyl radicals which destroy the iron-sulfur centers involved in the electron transfer (Sonoike et al. 1995). The process is almost irreversible because there is no known repair mechanism for PSI (Sonoike, 2011).

1. 3. 2. Protecting photosystem I and II from light stress

Efficient photosynthesis must meet several criteria - we have listed 3 of them so far: providing enough ATP for the downstream metabolism, protecting PSII from high light stress and protecting PSI from acceptor side limitation. How does the photosynthetic machinery achieve proper function in such a constrained situation? As discussed in this section, a master regulator of the photosynthetic electron transfer chain allows this, which is the electrochemical proton gradient across the thylakoid. Indeed, $\Delta\mu\text{H}^+$ plays the dual role of driving ATP (Mitchell 1966) and regulating photo-protection mechanisms through its osmotic component, the ΔpH (Kramer, 2003).

- *Cytochrome b_6f activity is regulated by the ΔpH across the thylakoid membrane*

When the capacity of reoxidation of PSI acceptors is low, putting PSI at high risk of photo-inhibition, a process called “photosynthetic control” allows to relax the reducing pressure on the iron-sulfur centers of PSI. This is achieved by making *cyt. b_6f* the actual rate-limiting step in photosynthesis (Rumberg and Siggel, 1969; Laisk et al., 2005). In conditions of limitation of photosynthesis downstream PSI, the ATP/ADP ratio and the ΔpH increase, making the H^+ release thermodynamically more difficult during the oxidation of PQH_2 in the cytochrome *b_6f* (Laisk et al., 2005) The consequent slowdown of cytochrome *b_6f* electron transfer results in oxidized cytochrome *f* , PC and P_{700} (Rumberg and Siggel, 1969). The involvement of ΔpH is involved in this regulation as demonstrated by the effect of nigericin, a H^+/K^+ antiporter (Joliot and Johnson, 2011). Nigericin dissipates the ΔpH without significantly affecting the electric field $\Delta\Psi$ and thereby maintaining ATP synthesis. In the presence of nigericin, P_{700} is more reduced and more PSI photoinhibition occurs, indicating that “photosynthetic control” is arrested.

- *pH-dependent -quenching of excited chlorophylls*

The osmotic component of the electrochemical proton gradient, the ΔpH , also regulates PSII photo-protective mechanisms (Demmig-Adams, Gilmore & Adams 1996; Holt, Fleming & Niyogi 2004; Holt, Fleming and Niyogi, 2004) via the q_E process, an energy-dependent quenching of excited chlorophylls in the antenna. This process harmlessly dissipates excess light in the form of heat (Holt, Fleming and Niyogi, 2004) and can be visualized in vivo through the non-photochemical quenching (NPQ) of chlorophyll fluorescence. In saturating light, when photochemistry is low, the heat and fluorescence pathways compete with each other. Therefore, the development of the q_E mechanism is accompanied by a decrease of

the fluorescence. It is to note that photo-inhibition of PSII, sometimes called q_i , also results in a decrease of the fluorescence, but, as mentioned earlier, the two processes can be distinguished based on their relaxation kinetics: q_E relaxes in the timescale of minutes whereas the recovery from q_i is in the timescale of tens of minutes or hours (Holt, Fleming and Niyogi, 2004).

The exact mechanism by which heat dissipation is regulated is still debated, but the molecular actors of the process are known, as well as their dependence upon ΔpH . The q_E mechanism is present in most photosynthetic organisms and involves changes of pigments (the xanthophyll cycle) and/or conformational changes of specific PSII subunits (Goss and Lepetit, 2015).

- *Xanthophyll cycle: role of carotenoids*

In plants and green algae or brown algae, the development of q_E , the rapidly reversible NPQ, is associated to the xanthophyll cycle. It consists in the reversible conversion of a carotenoid pigment, violaxanthine (Vx) into a de-epoxidized form, zeaxanthine (Zx) via the intermediate form antheraxanthin (Yamamoto, Nakayama and Chichester, 1962). Another xanthophyll cycle is found in diatoms, haptophytes and dinoflagellates (Brown et al., 1999; Hager and Stransky, 1970; Stransky and Hager, 1970), which consists in a one-step reaction from diadinoxanthin (DD) to its de-epoxidized form diatoxanthin (DT).

De-epoxidation of Vx (or DD) into Zx (or DT) is catalyzed by the violaxanthin de-epoxidase (VDE) soluble in the lumen and active at low pH (optimum at pH around 5 for the violaxanthin de-epoxidase). The zeaxanthin epoxidase (ZEP) catalyzes the reverse reaction, from Zx (DT) to Vx (DD). The main working model is that under high light, photosynthetic chain is actively translocating protons into the lumen, thus decreasing the luminal pH, activating VDE which increases the concentration of Zx and heat dissipation.

- *PsbS/LHCSR3/LHCX*

PsbS is a PSII subunit that is involved in NPQ mechanism (Li et al., 2000) and that displays several acidic residues in the lumen, playing the role of pH sensors and inducing some conformational changes in PSII favoring heat dissipation processes. In *Chlamydomonas reinhardtii* reversible NPQ is highly affected in mutants lacking LHCSR3, a protein that is part of PSII antennae (Peers et al., 2009). LHCSR proteins are not expressed constitutively but only in specific conditions, e.g. transition from dark to light (Savard, Richard and Guertin,

1996) or sulfur deprivation (Zhang et al., 2004). Like for PsbS, it contains acidic residues that can sense the luminal pH and generate conformational changes and heat dissipation (Bonente et al., 2011). In diatoms, LHCX proteins are part of the L1818/Lhcsr family to whom LHCSR3 belongs (Koziol et al., 2007) and also participate to the modulation of NPQ (Bailleul & Rogato et al., 2010; Zhu and Green, 2010; Buck et al., 2019).

- *Other photosynthetic acclimation mechanisms*

Even though $\Delta\mu\text{H}^+$ plays a major role in the regulation of photosynthesis, other important modes of regulation do not rely on it. Higher plants and green algae are able to adjust light excitation energy between the two photosystems, a process called state transition (Bonaventura and Myers, 1969). The current admitted model is that state transitions are mediated by the reversible displacement of a fraction of the chl b -containing light harvesting proteins LHCII, between PSII and PSI (Figure 1-18). This redistribution of light harvesting between the two photosystems is regulated by the redox state of the PQ pool and cytochrome b6f complex. In a situation where PSII activity exceeds PSI activity, the reduction of these intersystem electron carriers activates the STT7/STN7 kinase which in turn phosphorylates the LHCII leading to their lateral movement towards PSI (Wollman, 2001). The opposite situation -where the intersystem electron carrier would be highly oxidized- leads to the deactivation of the kinase. Then, a phosphatase dephosphorylates the LHCII which re-associate with PSII (Wollman, 2001). In *Chlamydomonas reinhardtii*, this process can modify the absorption cross-section of PSII by up to 40% in (Nawrocki et al., 2016). This process seems to be crucial in response to changing environment. *Stn7 Arabidopsis* mutant growth is impaired under changing light conditions (Bellaflore et al., 2005).

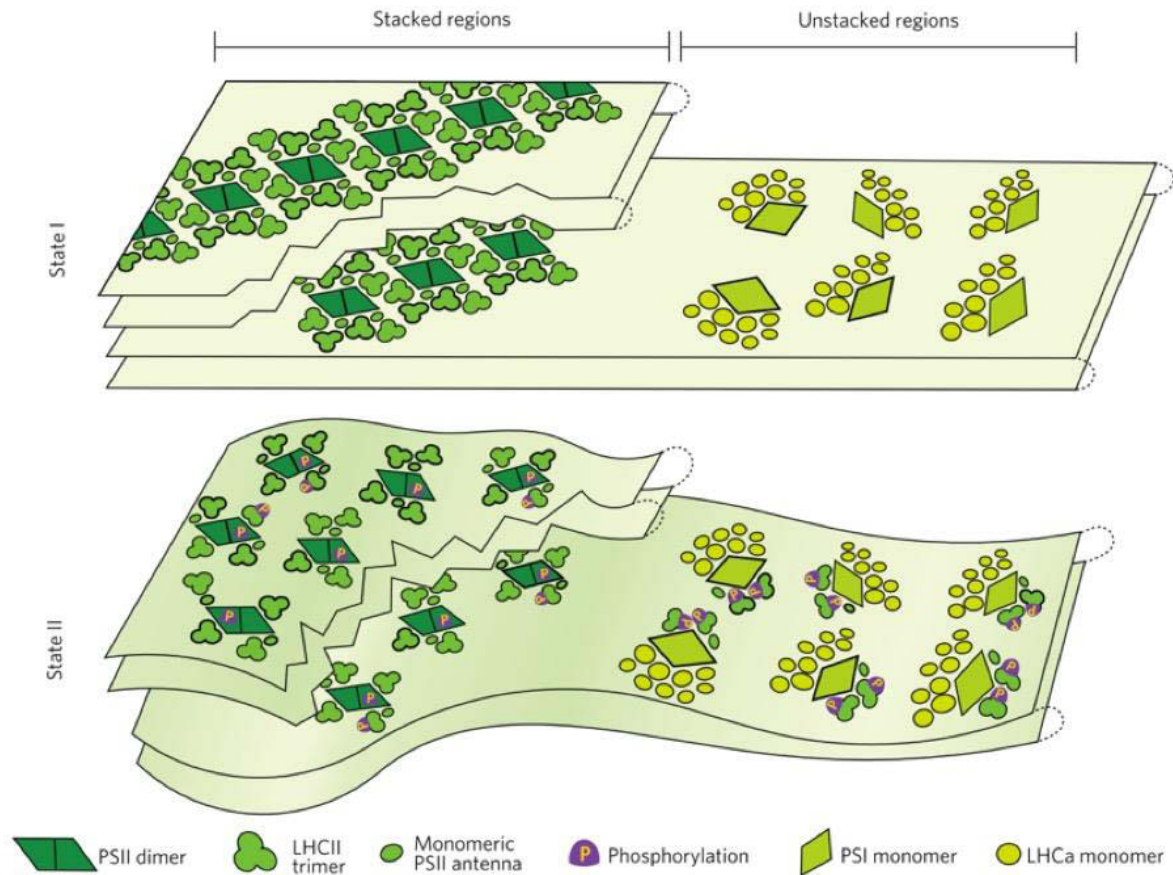


Figure 1-18: A quantitative schematic representation of photosystem and antenna distribution heterogeneity, and of its change during state transitions, in *C. reinhardtii*

From Nawrocki et al., 2016.

In state I, when the intersystem electron carriers are oxidized, PSII-LHCII supercomplexes form group in the stacked regions of the thylakoids, whereas PSI form supercomplexes with nine LHCa proteins mostly in the unstacked regions. Upon reduction of the intersystem electron carriers, phosphorylation of PSII core and antenna occurs, leading to electrostatic repulsion from the stacked regions of the membrane and the antenna migration to the unstacked regions, loosening the overall stacking. In state II, the PSI-LHCa supercomplex further increases its size by about 40% (in Nawrocki et al., 2016) by attaching two LHCII trimers and a monomeric antenna.

1. 3. 3. Photosynthetic alternative pathways

In photosynthetic organisms, besides the linear electron flow from water to CO₂, there are alternative electron transfers, that is to say transfers of electrons along the electron transfer chain, which do not lead to the reduction of CO₂ (Eberhard, Finazzi and Wollman, 2008). These alternative pathways allow the establishment of an electrochemical gradient of protons (and thus the synthesis of ATP) regardless of the activity of the CBB cycle and they allow an increase of the ATP/NADPH ratio produced by the photosynthetic chain.

We mentioned previously that the limitation of the electron flow downstream PSI can have dramatic consequences, causing the photoinhibition of photosystems, and especially PSI. Moreover, we have shown that the protective mechanisms allowing the downregulation of the *cyt. b₆f* activity and the increase in light energy dissipation as heat depend on the implementation of an electrochemical proton gradient. Alternative electron transfers therefore represent a major evolutionary advantage: not only they produce extra ATP but they increase the $\Delta\mu\text{H}^+$ and therefore the protection of both photosystems. Several alternative pathways have been described in the literature, that we will briefly review here. Figure 1-19 summarizes the different alternative electron pathways.

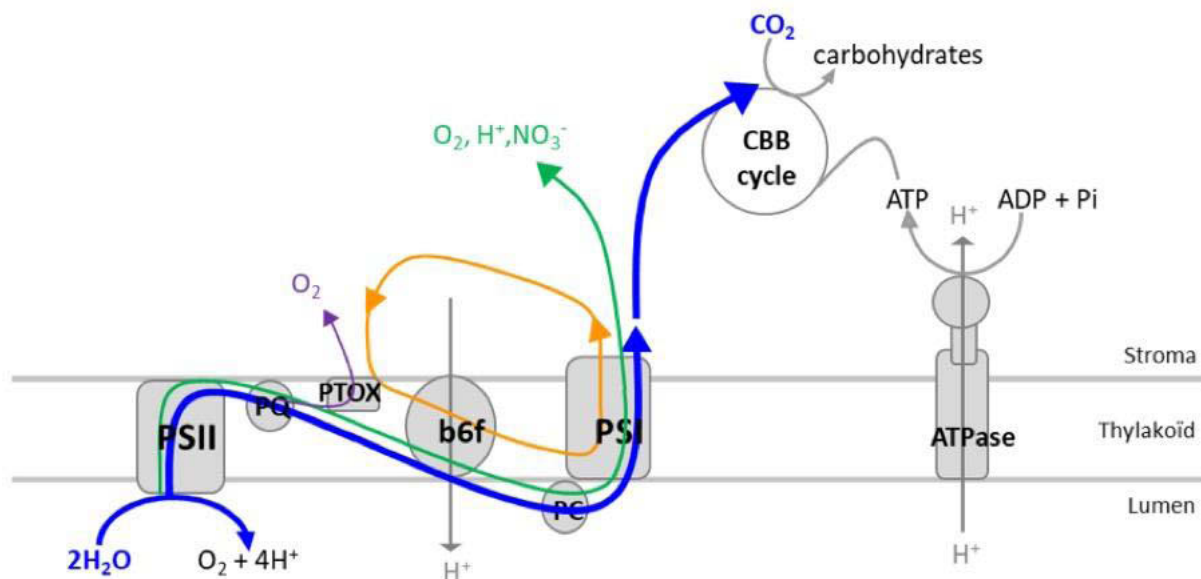


Figure 1-19: Schematic representation of the diversity of alternative electron pathways

Arrows represent linear electron flow from water to CO₂ (blue), the alternative pathways using both PSII and PSI, e.g. Mehler reactions, flavodiiron proteins or hydrogenase pathway (green), the ones using only PSII, PTOX pathway (purple), and the ones using only PSI, the cyclic electron flow around PSI (orange).

Alternative electron flows (AEF) can be classified according to their final electron acceptor. A first type of AEF corresponds to the water to water cycle: the electrons extracted from water at the PSII level are used by oxidases to reduce molecular oxygen and regenerate water. Several oxidases have been identified among which most of them use electrons downstream PSI. We can mention the flavodiiron proteins identified in *Chlamydomonas reinhardtii* (Chaux et al., 2017), in moss (Gerotto et al., 2016) and in cyanobacteria (Zhang et al., 2009) but the gene coding for these proteins is absent in angiosperms (Yamamoto et al., 2016). This alternative pathway would be mainly involved under changing light conditions, as a transitory sink for electrons during the acclimation period (Chaux et al., 2017, Allahverdiyeva et al., 2013).

Another water-to-water route concerns the Mehler reactions, or superoxide dismutase pathway which transfers electrons from the acceptor side of PSI to O₂. The superoxide formed is detoxified by a superoxide dismutase and ascorbate peroxidase, consuming NADPH (Asada et al., 2000). The superoxide dismutase has been identified in plants (Asada et al., 2000), green algae (Chen et al., 1996), cyanobacteria (Asada et al., 1975), diatoms (Wolfe-Simon et al., 2006) and dinoflagellates where it is said to be the main alternative electron flow (Roberty et al., 2014). This reaction occurs in isolated thylakoids (Asada, 1999) but its rate in vivo is not clear yet because of sources of confusion with other water to water cycles, especially the one involving flavodiiron proteins.

Finally, the electrons can be rerouted to the mitochondrial chain after PSI. The existence of such a flow has been shown in green algae (Lemaire, Wollman and Bennoun, 1988), diatoms (Bailleul et al., 2015) or in plants (Scheibe, 2004) and other observations suggest strong energetic exchanges between organelles in the green lineage (Cardol et al., 2010; Cardol et al., 2009). Such a pathway can be considered like a “meta”- water to water cycle. This pathway requires the diffusion of reducing power from the plastid to the mitochondria that is enabled by malate shuttles in plants (Scheibe, 2004) but with potentially slow rates (Scheibe et al., 2005). In diatoms, it would play an important role with about 10% of electrons constitutively rerouted from the chloroplast to the mitochondrion (Bailleul et al., 2015).

A particular water to water pathway is that of the Plastid Terminal oxidase (PTOX) which redirects the electrons from the plastoquinol to molecular oxygen, thus not involving PSI. This pathway has been found in several phylogenetic clades such as plants (Wetzel et al., 1994; Carol et al., 1999) or cyanobacteria (Cardol et al., 2008; Bailey et al., 2008). But under

non-stressed conditions, PTOX is found at low concentrations in plants thylakoids (about 1 PTOX for 100 PSII, Lennon et al., 2003) and should not play a crucial role in photosynthetic regulation (Nawrocki et al, 2016; Nawrocki et al., 2019c). This path seems to play only a role in very specific stress conditions, as in the case of microalgae deprived of iron (Cardol et al., 2008; Bailey et al., 2008) grown at low temperature and high irradiance (Ivanov et al., 2012) or in alpine plants that constitutively express high levels of PTOX (Streb et al., 2005). A model has been proposed to explain the apparently low activities of PTOX in vivo and its high turnover rate in vitro. PTOX would bind to the membrane only in conditions of high light and alkaline stromal pH. It would then play a role of safety valve protecting the PQ pool from over-reduction (Krieger-Liszkay and Feilke, 2016).

Other alternative pathways ultimately reduce other molecules than O₂ and can take place in anoxia. This is the case of the hydrogenase pathway, only expressed after several tens of minutes of anoxia in *Chlamydomonas reinhardtii* (Godaux et al., 2015) in *Chlorella fusca* but not in *Chlorella variabilis* (Winkler et al., 2002) and which uses electrons from the acceptor side of the PSI to reduce protons into dihydrogen.

We can also mention the rerouting of photosynthetic electrons for nitrate reduction followed by nitrite excretion that has been described in some cyanobacteria (Reyes et al., 1993). In cyanobacteria, an artificial alternative pathway was engineered via a sucrose sink (Abramson et al, 2016).

Finally, there is an alternative electron flow that does not have any final product since it reroutes the electrons from acceptor side of the PSI back to the inter-system chain, upstream cytochrome *b₆f*, giving rise to a cyclic electron flow around PSI (CEF). In plant and green algae, cyclic electron flow is considered essential for photosynthesis and would be of crucial importance for photosynthetic response to changing environment. In the following section, we will present the state of the art concerning this pathway, i.e. the proteins involved in the re-introduction of the reducing power from PSI acceptor side back to the chain, and the conditions favoring it.

1. 3. 4. CEF, a crucial regulative pathway remaining mysterious

a) CEF would be crucial under stress conditions

As an alternative electron flow, three main roles have been proposed for CEF. The first one is to participate to the photosynthetic control in conditions where metabolic pathway downstream PSI are limiting the linear electron flow. The second one is to protect PSII by activating pH dependent heat dissipation processes. The last one is to adjust the ATP/NADPH ratio produced by the light phase of photosynthesis to the metabolic pathways requirement. All these roles could be involved in response to changing environment, when CEF has been proposed to play a crucial role.

It would be crucial under several light regimes: under high light in plants (Joliot and Johnson, 2011; Huang and Zhang, 2012; Miyake et al., 2005a; Rumeau, Peltier and Cournac, 2007), under fluctuating light (Suorsa et al., 2012), at light onset (Joliot and Joliot 2002).

But CEF would also be involved in dealing with fluctuating gas availability: its rate would change depending on carbon availability in green algae (Lucker & Kramer, 2013) and in plants (Miyake et al., 2005b) to respond to the higher ATP demand associated to CCMs. It would also be enhanced during anoxia in plants (Kukuczka et al., 2014) and green algae (Alric, 2010) or as a starter at light onset in anoxia (Godaux et al., 2015). CEF could also be involved in coping with high O₂ concentration under high light (Walker et al., 2014). CEF has been proposed to be important in response to changing temperatures in dinoflagellates (Aihara, Takahashi and Minagawa, 2016) and plants (Huang, Zhang and Cao, 2010; Yamori et al, 2011) and its rate would depend on life stages as during leaf senescence in plants (Junker and Ensminger 2016).

Although CEF seems very important in response to environmental factors, CEF remains widely mysterious. One of the first points to emphasize is that there is no clear consensus regarding the enzymes involved in the reinjection step from PSI acceptors, back into the chain, that we will call hereafter the “cycling step”. Three main pathways have been proposed in the literature, none of them excluding the other ones. And I will present them in the next section.

b) Three main CEF pathways are proposed in the literature

▪ *PGRL1-PGR5 dependent pathway*

In 2002, the PGR5 protein has been proposed to catalyze a major pathway for CEF. Munekage et al isolated a *pgr5 Arabidopsis thaliana* mutant that was affected in q_E implementation during high light illumination. Isolated chloroplasts were affected in non-photochemical reduction of the PQ pool (Munekage et al., 2002). Since no redox cofactor has been identified in the PGR5 protein it has been proposed to catalyse CEF. In 2008, DalCorso et al. isolated a PGRL1 mutant presenting the same phenotype as PGR5 mutant and showed that PGRL1 and PGR5 could form heterodimer complexes (DalCorso et al., 2008). PGRL1 is supposed to house a Fe containing cofactor (Hertle et al., 2013) and might be involved in PSI/*b₆f* supercomplexes performing an enclosed cyclic electron flow (Iwai et al., 2010). Nevertheless, the effective implication of PGRL1-PGR5 proteins in CEF is more and more debated. Several studies suggest that the CEF amplitude is not affected in *pgr1* or *pgr5* mutants. In the transition from dark to light the pool of electrons accumulated in the dark allows transitory high CEF in PSII inhibited samples. In these conditions, CEF is easily assessable since linear electron flow is not active. During transition from dark to light, the *Arabidopsis pgr5* mutant and *Chlamydomonas pgr1* mutant have no phenotype and display the same maximal CEF as their respective wild types (Nandha et al., 2007; Nawrocki et al., 2019a).

▪ *NDH / Nda2 pathway*

Cyanobacteria and higher plants express a membrane type I NADPH dehydrogenase complex commonly called NDH (Mastubayashi et al., 1987; Peltier, Aro and Shikanai, 2016). This complex is partly homologous to bacterial and mitochondrial complex I, a NADH:ubiquinone oxidoreductase. By analogy, it has been proposed that the chloroplast NDH is involved in the transfer of electrons from NADPH to the plastoquinone pool, thus enabling CEF. NDH expression is low under non stress conditions (Livingston et al., 2010) but mutants overexpressing NDH1 show a phenotype compatible with an increased CEF compared to the WT (Livingston et al., 2010). Moreover, by analogy with bacterial and mitochondrial complex I, it has been proposed that the chloroplast NDH1 is able to move 2 protons from the stroma to the lumen per electron transferred, thus increasing the ATP production of CEF (Strand et al, 2017). It is to note NDH1 lacks an NADH binding site and most likely uses ferredoxin as a substrate (Yamamoto, Peng, Fukao, & Shikanai, 2011).

Some green algae including *Chlamydomonas reinhardtii* (Maul et al., 2002) and conifers are lacking NDH1 (Wakasugi et al., 1994). But *Chlamydomonas reinhardtii* have another protein performing a similar function, Nda2, which is not a transmembrane protein and does not couple electron transfer to proton translocation (Jans et al, 2008). Nevertheless, its maximal rate is expected to be low by comparison with the linear electron flow (few electrons per second, Nawrocki et al, 2019b).

- *C_i haem from the cytochrome b₆f complex*

Cytochrome *b₆f* houses a haem *c_i* whose role has not been understood yet. Figure 1-20b shows that it is located at the stromal side of the complex, near the Q_i site where PQ is reduced by the b haems. Moreover, Figure 1-20a shows a crystal structures of a cytochrome *b₆f* monomer showing that haem *c_i* also would be accessible for a reduction from a stromal protein (Kurusu, Zhang, Smith, & Cramer, 2003; Stroebel et al., 2003). On Figure 1-20a, we can see that Fd could attach on the stromal side of the cytochrome *b₆f* and its distance to the *c_i* haem would enable an electron transfer (Stroebel et al., 2003). The structure of the cytochrome *b₆f* gave support to an idea originally proposed by Mitchell (Mitchell, 1975): a CEF pathway involving transfer to haem *c_i* through a ferredoxin oxidase enzyme such as ferredoxin:NADP⁺ reductase, FNR, or directly from the ferredoxin (Iwai et al., 2010; Nawrocki et al., 2019b). In such a pathway the concentration of the enzyme involved in the “cycling step” (ie the cyt. *b₆f* itself) is in a stoichiometric concentration with PSI (from 0.5 to 1.25 in plants, Anderson, 1992), which theoretically enables high rates of CEF.

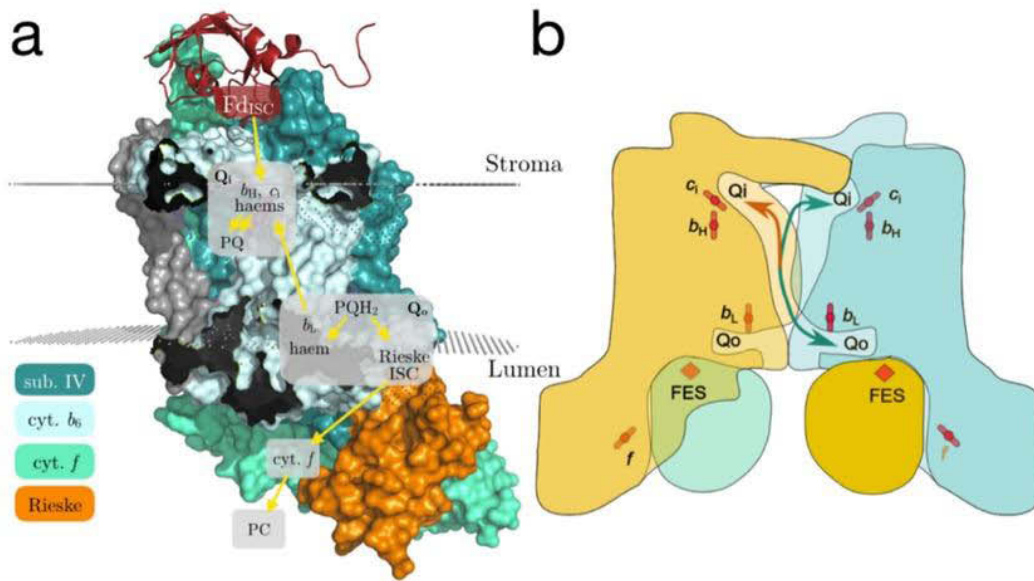


Figure 1-20: Electron and plastoquinone transfer within cyt. b_6f

From Nawrocki et al., 2019b

a. A scheme of possible cyclic electron transfer within cyt. b_6f . A side view of the cyt. b_6f monomer from the dimerization surface perspective. The stromal and luminal surfaces of the thylakoid membrane are depicted in grey. Each subunit of the monomer is colored as indicated on the left side of the figure. The electron transfer pathways are shown as yellow arrows. Ferredoxin in its putative binding mode is shown in a red cartoon form.

b. PQ/PQH₂ transfer within cyt. b_6f dimer. Side view of the complex. One cyt. b_6f monomer is in orange, while the other one is blue. Possible route for the quinone/quinol between the Q_o and Q_i side are represented in green for transfer in the same monomer, which implies crossing the narrow portion of the crevice, or in green/orange for transfer in the opposite monomer, which uses a broader and shorter path.

- *Summarizing our understanding of the CEF pathway*

Investigation of the pathway(s) involved in CEF has mainly been driven by a genetic approach. It is important to note that until now, we do not know of any mutant that would perform no CEF. Neither NDH, nor *pgr1* or *pgr5* mutants show a total absence of CEF. This suggests that either the different pathways compensate each other, or that we have not identified the principal pathway yet or that the total absence of CEF would be lethal.

A main limitation of this strategy is that it is not an “all other things being equal” approach. Indeed, any mutation of an intermediate of the photosynthetic chain would change intermediate redox equilibria and potentially CEF even if it is not directly involved in CEF (Kramer & Evans, 2011). For example, it has been suggested that the lack of q_E phenotype observed in the *pgr5* mutant (Munekage et al., 2002) is related to changes in ATP synthase permeability more than to CEF involvement (Avenson et al., 2005). Thus, it seems crucial to understand the CEF dependence on linear electron flow and on cell physiology to better interpret the phenotype observed in putative CEF mutants.

1. 4. Thesis outline

The recent awareness of the importance of marine photosynthesis to global biogeochemical processes resulted in unprecedented efforts to study phytoplankton. While we now roughly assessed the whole ocean diversity at a genomic level, the main challenge is to understand the ocean diversity at the functional level. Investigating the diversity of cyclic electron flow within photosynthetic organisms is the main objective of my PhD. Our approach was driven by methodological considerations. We first determined the reliable tools that were available to probe CEF and then defined the biological questions we could address with these tools. I hope it will participate to the global effort on understanding the different microalgae assets and strategies to deal with environment constraints.

This thesis is divided in three chapters.

Chapter 2: Since cyclic electron flow is only involving photosystem I, investigating the former requires the accurate measurement of the latter. The first chapter of this manuscript aims at determining the best method to measure PSI quantum yield, and from there the electron flow through PSI. The most commonly used method is based on the absorbance changes of the PSI special pair, P_{700} , depending on its redox state. Proposed 25 years ago, this method is based on a strong assumption that has never been tested. In order to test the domain of validity of this method, we describe an alternative method for measuring the activity of PSI which is based on probing the electric field generated across the thylakoid by PSI photochemistry.

Chapter 3: The second chapter is divided into two parts. First, I propose a simple and robust method based on the outputs of chapter 2 to highlight the presence of CEF, and if so, its relationship with LEF. Applying this method to several microalgae species, I could show three typical and distinct CEF behaviors. When CEF is independent of LEF, the measurement of its amplitude is simple: it is the residual activity when the LEF is inhibited. But when CEF depends on LEF, as it is the case for *Chlamydomonas reinhardtii*, CEF measurement is more complex and requires a more sophisticated approach. Thus, I performed an in depth analysis of LEF and CEF in the latter species using more complicated (and less robust)

measurements. These approaches lead me to discuss the relative amplitude of the CEF and the LEF as well as their modes of regulation.

Chapter 4: The chapter is not immediately connected to the CEF topic. It deals with results obtained in the field during a mesocom study campaign of a bloom of *Emiliana huxleyi*, a haptophyte whose ecological importance we mentioned in the introduction. By participating in this project, my goal was to test the method developed in Chapter 3 on field samples. This part of the project did not succeed because the signals related to PSI activity were far too low. However, thanks to measurements based on PSII fluorescence, I followed the photosynthetic physiology of *Emiliana huxleyi* during the campaign and in collaboration with a statistician of the Pasteur Institute, I developed a model to explain the variation of photosynthetic parameters from environmental data ... and you will see that this approach finally made it possible to address questions related to CEF.

1. 5. Bibliography

Abramson, B. W., Kachel, B., Kramer, D. M., & Ducat, D. C. (2016). Increased photochemical efficiency in cyanobacteria via an engineered sucrose sink. *Plant and Cell Physiology*, *57*(12), 2451-2460.

Aihara, Y., Takahashi, S., & Minagawa, J. (2016). Heat induction of cyclic electron flow around photosystem I in the symbiotic dinoflagellate *Symbiodinium*. *Plant physiology*, *171*(1), 522-529.

Allahverdiyeva, Y., Mustila, H., Ermakova, M., Bersanini, L., Richaud, P., Ajlani, G., ... & Aro, E. M. (2013). Flavodiiron proteins Flv1 and Flv3 enable cyanobacterial growth and photosynthesis under fluctuating light. *Proceedings of the National Academy of Sciences*, *110*(10), 4111-4116.

Allen, J. F. (2003). Cyclic, pseudocyclic and noncyclic photophosphorylation: new links in the chain. *Trends in plant science*, *8*(1), 15-19.

Alric, J. (2010). Cyclic electron flow around photosystem I in unicellular green algae. *Photosynthesis research*, *106*(1-2), 47-56.

Amunts, A., Toporik, H., Borovikova, A., & Nelson, N. (2010). Structure determination and improved model of plant photosystem I. *Journal of Biological Chemistry*, *285*(5), 3478-3486.

Anderson, J. M. (1992). Cytochrome b 6 f complex: dynamic molecular organization, function and acclimation. *Photosynthesis Research*, *34*(3), 341-357.

Arnon, D. I., Allen, M. B., & Whatley, F. R. (1954). Photosynthesis by isolated chloroplasts. *Nature*, *174*(4426), 394-396.

Arnon, D. I., Whatley, F. R., & Allen, M. B. (1957). Triphosphopyridine nucleotide as a catalyst of photosynthetic phosphorylation. *Nature*, *180*(4578), 182-185.

Asada, K. (1999). The water-water cycle in chloroplasts: scavenging of active oxygens and dissipation of excess photons. *Annual review of plant biology*, *50*(1), 601-639.

Asada, K. (2000). The water–water cycle as alternative photon and electron sinks. *Philosophical Transactions of the Royal Society of London. Series B: Biological Sciences*, *355*(1402), 1419-1431.

Asada, K. O. Z. I., Yoshikawa, K., Takahashi, M., Maeda, Y., & Enmanji, K. (1975). Superoxide dismutases from a blue-green alga, *Plectonema boryanum*. *Journal of Biological Chemistry*, *250*(8), 2801-2807.

Avenson, T. J., Cruz, J. A., Kanazawa, A., & Kramer, D. M. (2005). Regulating the proton budget of higher plant photosynthesis. *Proceedings of the National Academy of Sciences*, *102*(27), 9709-9713.

Azam, F., Fenchel, T., Field, J. G., Grey, J. S., Meyer-Reil, L. A., & Thingstad, F. (1983). The ecological role of water-column microbes. *Mar. ecol. Prog. ser.*, *10*, 257-263.

Bailey, S., Melis, A., Mackey, K. R., Cardol, P., Finazzi, G., van Dijken, G., ... & Grossman, A. (2008). Alternative photosynthetic electron flow to oxygen in marine *Synechococcus*. *Biochimica et Biophysica Acta (BBA)-Bioenergetics*, *1777*(3), 269-276.

- Bailleul, B., Berne, N., Murik, O., Petroustos, D., Prihoda, J., Tanaka, A., ... & Krieger-Liszkay, A. (2015). Energetic coupling between plastids and mitochondria drives CO₂ assimilation in diatoms. *Nature*, 524(7565), 366.
- Bailleul, B., Rogato, A., De Martino, A., Coesel, S., Cardol, P., Bowler, C., ... & Finazzi, G. (2010). An atypical member of the light-harvesting complex stress-related protein family modulates diatom responses to light. *Proceedings of the National Academy of Sciences*, 107(42), 18214-18219.
- Bassham, J. A., Benson, A. A., & Calvin, M. (1953). Isotope studies in photosynthesis. *Journal of Chemical Education*, 30(6), 274.
- Behrenfeld, M. J., Randerson, J. T., McClain, C. R., Feldman, G. C., Los, S. O., Tucker, C. J., ... & Kolber, D. D. (2001). Biospheric primary production during an ENSO transition. *Science*, 291(5513), 2594-2597.
- Béja, O., Aravind, L., Koonin, E. V., Suzuki, M. T., Hadd, A., Nguyen, L. P., ... & Spudich, E. N. (2000). Bacterial rhodopsin: evidence for a new type of phototrophy in the sea. *Science*, 289(5486), 1902-1906.
- Bellaïf, S., Barneche, F., Peltier, G., & Rochaix, J. D. (2005). State transitions and light adaptation require chloroplast thylakoid protein kinase STN7. *Nature*, 433(7028), 892.
- Berry, S., & Rumberg, B. (1999). Proton to electron stoichiometry in electron transport of spinach thylakoids. *Biochimica et Biophysica Acta (BBA)-Bioenergetics*, 1410(3), 248-261.
- Bhattacharya, D., Yoon, H. S., & Hackett, J. D. (2004). Photosynthetic eukaryotes unite: endosymbiosis connects the dots. *Bioessays*, 26(1), 50-60.
- Bidle, K. D., & Vardi, A. (2011). A chemical arms race at sea mediates algal host-virus interactions. *Current opinion in microbiology*, 14(4), 449-457.
- Bieszke, J. A., Braun, E. L., Bean, L. E., Kang, S., Natvig, D. O., & Borkovich, K. A. (1999). The nop-1 gene of *Neurospora crassa* encodes a seven transmembrane helix retinal-binding protein homologous to archaeal rhodopsins. *Proceedings of the National Academy of Sciences*, 96(14), 8034-8039.
- Bilger, W., & Björkman, O. (1990). Role of the xanthophyll cycle in photoprotection elucidated by measurements of light-induced absorbance changes, fluorescence and photosynthesis in leaves of *Hedera canariensis*. *Photosynthesis research*, 25(3), 173-185.
- Blankenship, R. E. (1992). Origin and early evolution of photosynthesis. *Photosynthesis research*, 33(2), 91-111.
- Bonaventura, C., & Myers, J. (1969). Fluorescence and oxygen evolution from *Chlorella pyrenoidosa*. *Biochimica et Biophysica Acta (BBA)-Bioenergetics*, 189(3), 366-383.
- Brown, B. E., Ambarsari, I., Warner, M. E., Fitt, W. K., Dunne, R. P., Gibb, S. W., & Cummings, D. G. (1999). Diurnal changes in photochemical efficiency and xanthophyll concentrations in shallow water reef corals: evidence for photoinhibition and photoprotection. *Coral Reefs*, 18(2), 99-105.
- Buchan, A., LeCleir, G. R., Gulvik, C. A., & González, J. M. (2014). Master recyclers: features and functions of bacteria associated with phytoplankton blooms. *Nature Reviews Microbiology*, 12(10), 686-698.

- Buck, J. M., Sherman, J., Bártulos, C. R., Serif, M., Halder, M., Henkel, J., ... & Falkowski, P. G. (2019).** Lhcx proteins provide photoprotection via thermal dissipation of absorbed light in the diatom *Phaeodactylum tricornutum*. *Nature communications*, *10*(1), 1-12.
- Buma, A. G., Van Oijen, T., Van De Poll, W., Veldhuis, M. J., & Gieskes, W. W. (2000).** The sensitivity of *Emiliania huxleyi* (Prymnesiophyceae) to ultraviolet-b radiation. *Journal of Phycology*, *36*(2), 296-303.
- Butler, W. L. (1978).** Energy distribution in the photochemical apparatus of photosynthesis. *Annual Review of Plant Physiology*, *29*(1), 345-378.
- Caffarri, S., Kouřil, R., Kereiče, S., Boekema, E. J., & Croce, R. (2009).** Functional architecture of higher plant photosystem II supercomplexes. *The EMBO journal*, *28*(19), 3052-3063.
- Caffarri, S., Kouřil, R., Kereiče, S., Boekema, E. J., & Croce, R. (2009).** Functional architecture of higher plant photosystem II supercomplexes. *The EMBO journal*, *28*(19), 3052-3063.
- Caffarri, S., Tibiletti, T., C Jennings, R., & Santabarbara, S. (2014).** A comparison between plant photosystem I and photosystem II architecture and functioning. *Current Protein and Peptide Science*, *15*(4), 296-331.
- Cardol, P., Alric, J., Girard-Bascou, J., Franck, F., Wollman, F. A., & Finazzi, G. (2009).** Impaired respiration discloses the physiological significance of state transitions in *Chlamydomonas*. *Proceedings of the National Academy of Sciences*, *106*(37), 15979-15984.
- Cardol, P., Bailleul, B., Rappaport, F., Derelle, E., Béal, D., Breyton, C., ... & Finazzi, G. (2008).** An original adaptation of photosynthesis in the marine green alga *Ostreococcus*. *Proceedings of the National Academy of Sciences*, *105*(22), 7881-7886.
- Cardol, P., De Paepe, R., Franck, F., Forti, G., & Finazzi, G. (2010).** The onset of NPQ and $\Delta\mu\text{H}^+$ upon illumination of tobacco plants studied through the influence of mitochondrial electron transport. *Biochimica et Biophysica Acta (BBA)-Bioenergetics*, *1797*(2), 177-188.
- Carol, P., Stevenson, D., Bisanz, C., Breitenbach, J., Sandmann, G., Mache, R., ... & Kuntz, M. (1999).** Mutations in the Arabidopsis gene IMMUTANS cause a variegated phenotype by inactivating a chloroplast terminal oxidase associated with phytoene desaturation. *The Plant Cell*, *11*(1), 57-68.
- Chaux, F., Burlacot, A., Mekhalfi, M., Auroy, P., Blangy, S., Richaud, P., & Peltier, G. (2017).** Flavodiiron proteins promote fast and transient O_2 photoreduction in *Chlamydomonas*. *Plant physiology*, *174*(3), 1825-1836.
- Chen, H., Romo-Leroux, P. A., & Salin, M. L. (1996).** The iron-containing superoxide dismutase-encoding gene from *Chlamydomonas reinhardtii* obtained by direct and inverse PCR. *Gene*, *168*(1), 113-116.
- Croce, R., & Van Amerongen, H. (2014).** Natural strategies for photosynthetic light harvesting. *Nature chemical biology*, *10*(7), 492.
- DalCorso, G., Pesaresi, P., Masiero, S., Aseeva, E., Schünemann, D., Finazzi, G., ... & Leister, D. (2008).** A complex containing PGRL1 and PGR5 is involved in the switch between linear and cyclic electron flow in Arabidopsis. *Cell*, *132*(2), 273-285.
- De Vargas, C., Audic, S., Henry, N., Decelle, J., Mahé, F., Logares, R., ... & Carmichael, M. (2015).** Eukaryotic plankton diversity in the sunlit ocean. *Science*, *348*(6237), 1261605.

- De Vitry, C., & Kuras, R. (2009).** The cytochrome *b₆f* complex. In *The Chlamydomonas sourcebook* (pp. 603-637). Academic Press.
- Dekker, J. P., & Boekema, E. J. (2005).** Supramolecular organization of thylakoid membrane proteins in green plants. *Biochimica et Biophysica Acta (BBA)-Bioenergetics*, 1706(1-2), 12-39.
- Delgado, E., Medrano, H., Keys, A. J., & Parry, M. A. J. (1995).** Species variation in Rubisco specificity factor. *Journal of Experimental Botany*, 46(11), 1775-1777.
- Diner, B. A., & Babcock, G. T. (1996).** Structure, dynamics, and energy conversion efficiency in photosystem II. In *Oxygenic photosynthesis: the light reactions* (pp. 213-247). Springer, Dordrecht.
- Dodge, J. D. (1968).** The fine structure of chloroplasts and pyrenoids in some marine dinoflagellates. *Journal of cell science*, 3(1), 41-47.
- Eberhard, S., Finazzi, G., & Wollman, F. A. (2008).** The dynamics of photosynthesis. *Annual review of genetics*, 42, 463-515
- Emerson, R., & Arnold, W. (1932).** The photochemical reaction in photosynthesis. *The Journal of general physiology*, 16(2), 191-205.
- Emerson, R., Chalmers, R., & Cederstrand, C. (1957).** Some factors influencing the long-wave limit of photosynthesis. *Proceedings of the National Academy of Sciences of the United States of America*, 43(1), 133.
- Engelmann, T. W. (1882).** Über sauerstoffausscheidung von pflanzenzellen im mikrospektrum. *Pflügers Archiv European Journal of Physiology*, 27(1), 485-489.
- Falkowski, P. G., & Raven, J. A. (2013).** *Aquatic photosynthesis*. Princeton University Press.
- Falkowski, P. G., Barber, R. T., & Smetacek, V. (1998).** Biogeochemical controls and feedbacks on ocean primary production. *Science*, 281(5374), 200-206.
- Falkowski, P. G., Katz, M. E., Knoll, A. H., Quigg, A., Raven, J. A., Schofield, O., & Taylor, F. J. R. (2004).** The evolution of modern eukaryotic phytoplankton. *Science*, 305(5682), 354-360.
- Field, C. B., Behrenfeld, M. J., Randerson, J. T., & Falkowski, P. (1998).** Primary production of the biosphere: integrating terrestrial and oceanic components. *Science*, 281(5374), 237-240.
- Förster, T. (1948).** Zwischenmolekulare energiewanderung und fluoreszenz. *Annalen der physik*, 437(1-2), 55-75.
- Fuhrman, J. A., Schwalbach, M. S., & Stingl, U. (2008).** Proteorhodopsins: an array of physiological roles? *Nature Reviews Microbiology*, 6(6), 488.
- Genty, B., Briantais, J. M., & Baker, N. R. (1989).** The relationship between the quantum yield of photosynthetic electron transport and quenching of chlorophyll fluorescence. *Biochimica et Biophysica Acta (BBA)-General Subjects*, 990(1), 87-92.
- Gerotto, C., Alboresi, A., Meneghesso, A., Jokel, M., Suorsa, M., Aro, E. M., & Morosinotto, T. (2016).** Flavodiiron proteins act as safety valve for electrons in *Physcomitrella patens*. *Proceedings of the National Academy of Sciences*, 113(43), 12322-12327.
- Godaux, D., Bailleul, B., Berne, N., & Cardol, P. (2015).** Induction of photosynthetic carbon fixation in anoxia relies on hydrogenase activity and Proton-Gradient Regulation-Like1-mediated cyclic electron flow in *Chlamydomonas reinhardtii*. *Plant physiology*, 168(2), 648-658.

- Goss, R., & Lepetit, B. (2015).** Biodiversity of NPQ. *Journal of plant physiology*, 172, 13-32.
- Gould, S. B., Waller, R. F., & McFadden, G. I. (2008).** Plastid evolution. *Annu. Rev. Plant Biol.*, 59, 491-517.
- Govindjee, S. D., & Björn, L. O. (2017).** Evolution of the Z-scheme of photosynthesis: a perspective. *Photosynth. Res*, 133, 5-15.
- Grennan, A. K., & Ort, D. R. (2007).** Cool temperatures interfere with D1 synthesis in tomato by causing ribosomal pausing. *Photosynthesis research*, 94(2-3), 375-385.
- Guskov, A., Kern, J., Gabdulkhakov, A., Broser, M., Zouni, A., & Saenger, W. (2009).** Cyanobacterial photosystem II at 2.9-Å resolution and the role of quinones, lipids, channels and chloride. *Nature structural & molecular biology*, 16(3), 334.
- Haeckel, E. (1890).** Plankton-studien
- Hager, A. T., & Stransky, H. (1970).** Das Carotinoidmuster und die Verbreitung des lichtinduzierten Xanthophyllcyclus in verschiedenen Algenklassen. *Archiv für Mikrobiologie*, 71(2), 132-163.
- Hahn, A., Vonck, J., Mills, D. J., Meier, T., & Kühlbrandt, W. (2018).** Structure, mechanism, and regulation of the chloroplast ATP synthase. *Science*, 360(6389), eaat4318.
- Hayashi, S., Tajkhorshid, E., & Schulten, K. (2003).** Molecular dynamics simulation of bacteriorhodopsin's photoisomerization using ab initio forces for the excited chromophore. *Biophysical journal*, 85(3), 1440-1449.
- Hertle, A. P., Blunder, T., Wunder, T., Pesaresi, P., Pribil, M., Armbruster, U., & Leister, D. (2013).** PGRL1 is the elusive ferredoxin-plastoquinone reductase in photosynthetic cyclic electron flow. *Molecular cell*, 49(3), 511-523.
- Hill, R., & Bendall, F. A. Y. (1960).** Function of the two cytochrome components in chloroplasts: a working hypothesis. *Nature*, 186(4719), 136.
- Hobbie, J. E., Holm-Hansen, O., Packard, T. T., Pomeroy, L. R., Sheldon, R. W., Thomas, J. P., & Wiebe, W. J. (1972).** A study of the distribution and activity of microorganisms in ocean water 1. *Limnology and oceanography*, 17(4), 544-555.
- Holt, N. E., Fleming, G. R., & Niyogi, K. K. (2004).** Toward an understanding of the mechanism of nonphotochemical quenching in green plants. *Biochemistry*, 43(26), 8281-8289.
- Huang, D., Everly, R. M., Cheng, R. H., Heymann, J. B., Schagger, H., Sled, V., ... & Cramer, W. A. (1994).** Characterization of the chloroplast cytochrome b6f complex as a structural and functional dimer. *Biochemistry*, 33(14), 4401-4409.
- Huang, W., Yang, S. J., Zhang, S. B., Zhang, J. L., & Cao, K. F. (2012).** Cyclic electron flow plays an important role in photoprotection for the resurrection plant *Paraboea rufescens* under drought stress. *Planta*, 235(4), 819-828.
- Huang, W., Zhang, S. B., & Cao, K. F. (2010).** Stimulation of cyclic electron flow during recovery after chilling-induced photoinhibition of PSII. *Plant and cell physiology*, 51(11), 1922-1928.
- Hügler, M., & Sievert, S. M. (2011).** Beyond the Calvin cycle: autotrophic carbon fixation in the ocean. *Annual review of marine science*, 3, 261-289.

- Ivanov, A. G., Rosso, D., Savitch, L. V., Stachula, P., Rosembert, M., Oquist, G., ... & Hüner, N. P. A. (2012). Implications of alternative electron sinks in increased resistance of PSII and PSI photochemistry to high light stress in cold-acclimated *Arabidopsis thaliana*. *Photosynthesis research*, 113(1-3), 191-206.
- Iwai, M., Takizawa, K., Tokutsu, R., Okamuro, A., Takahashi, Y., & Minagawa, J. (2010). Isolation of the elusive supercomplex that drives cyclic electron flow in photosynthesis. *Nature*, 464(7292), 1210
- Jans, F., Mignolet, E., Houyoux, P. A., Cardol, P., Ghysels, B., Cuiné, S., ... & Franck, F. (2008). A type II NAD (P) H dehydrogenase mediates light-independent plastoquinone reduction in the chloroplast of *Chlamydomonas*. *Proceedings of the National Academy of Sciences*, 105(51), 20546-20551.
- Jensen, P. E., & Leister, D. (2014). Chloroplast evolution, structure and functions. *F1000prime reports*, 6.
- Jensen, P. E., Bassi, R., Boekema, E. J., Dekker, J. P., Jansson, S., Leister, D., ... & Scheller, H. V. (2007). Structure, function and regulation of plant photosystem I. *Biochimica et Biophysica Acta (BBA)-Bioenergetics*, 1767(5), 335-352.
- Joliot, P. (1964). Etude cinétique de la réaction photochimique libérant l'oxygène au cours de la photosynthèse. *CR Acad. Sci.*, 258, 4622-4625.
- Joliot, P., & Johnson, G. N. (2011). Regulation of cyclic and linear electron flow in higher plants. *Proceedings of the National Academy of Sciences*, 108(32), 13317-13322.
- Joliot, P., & Joliot, A. (2002). Cyclic electron transfer in plant leaf. *Proceedings of the National Academy of Sciences*, 99(15), 10209-10214.
- Junker, L. V., & Ensminger, I. (2016). Relationship between leaf optical properties, chlorophyll fluorescence and pigment changes in senescing *Acer saccharum* leaves. *Tree physiology*, 36(6), 694-711
- Kaplan, A., & Reinhold, L. (1999). CO₂ concentrating mechanisms in photosynthetic microorganisms. *Annual review of plant biology*, 50(1), 539-570.
- Keren, N., & Krieger-Liszkay, A. (2011). Photoinhibition: molecular mechanisms and physiological significance. *Physiologia Plantarum*, 142(1), 1-5.
- Kok, B., Forbush, B., & McGloin, M. (1970). Cooperation of charges in photosynthetic O₂ evolution—I. A linear four step mechanism. *Photochemistry and Photobiology*, 11(6), 457-475.
- Kramer, D. M., & Evans, J. R. (2011). The importance of energy balance in improving photosynthetic productivity. *Plant Physiology*, 155(1), 70-78.
- Kramer, D. M., Johnson, G., Kiirats, O., & Edwards, G. E. (2004). New fluorescence parameters for the determination of Q A redox state and excitation energy fluxes. *Photosynthesis research*, 79(2), 209.
- Krause, G. H., & Weis, E. (1991). Chlorophyll fluorescence and photosynthesis: the basics. *Annual review of plant biology*, 42(1), 313-349.
- Krieger-Liszkay, A. (2005). Singlet oxygen production in photosynthesis. *Journal of experimental botany*, 56(411), 337-346.

- Krieger-Liszkay, A., & Feilke, K. (2016).** The dual role of the plastid terminal oxidase PTOX: between a protective and a pro-oxidant function. *Frontiers in plant science*, *6*, 1147.
- Kukuczka, B., Magneschi, L., Petroustos, D., Steinbeck, J., Bald, T., Powikrowska, M., ... & Hippler, M. (2014).** Proton gradient regulation5-like1-mediated cyclic electron flow is crucial for acclimation to anoxia and complementary to nonphotochemical quenching in stress adaptation. *Plant physiology*, *165*(4), 1604-1617.
- Laisk, A., Eichelmann, H., Oja, V., & Peterson, R. B. (2005).** Control of cytochrome *b₆f* at low and high light intensity and cyclic electron transport in leaves. *Biochimica et Biophysica Acta (BBA)-Bioenergetics*, *1708*(1), 79-90.
- Laursen, L. (2011).** *Spain's ship come in. Nature* *475*:16–17
- Lavorel, J., & Joliot, P. (1972).** A connected model of the photosynthetic unit. *Biophysical journal*, *12*(7), 815-831.
- Lazár, D. (2015).** Parameters of photosynthetic energy partitioning. *Journal of Plant Physiology*, *175*, 131-147.
- Lemaire, C., Wollman, F. A., & Bennoun, P. (1988).** Restoration of phototrophic growth in a mutant of *Chlamydomonas reinhardtii* in which the chloroplast *atpB* gene of the ATP synthase has a deletion: an example of mitochondria-dependent photosynthesis. *Proceedings of the National Academy of Sciences*, *85*(5), 1344-1348.
- Lennon, A. M., Prommeenate, P., & Nixon, P. J. (2003).** Location, expression and orientation of the putative chlororespiratory enzymes, Ndh and IMMUTANS, in higher-plant plastids. *Planta*, *218*(2), 254-260.
- Li, X. P., BjoÈrkman, O., Shih, C., Grossman, A. R., Rosenquist, M., Jansson, S., & Niyogi, K. K. (2000).** A pigment-binding protein essential for regulation of photosynthetic light harvesting. *Nature*, *403*(6768), 391.
- Lucker, B., & Kramer, D. M. (2013).** Regulation of cyclic electron flow in *Chlamydomonas reinhardtii* under fluctuating carbon availability. *Photosynthesis research*, *117*(1-3), 449-459.
- Margulis, L. (1970).** Origin of eukaryotic cells: evidence and research implications for a theory of the origin and evolution of microbial, plant, and animal cells on the Precambrian earth (p. 349). *New Haven: Yale University Press*.
- Merritt, J. E., & Loening, K. L. (1979).** Nomenclature of tetrapyrroles. *Pure and Applied Chem*, *51*, 2251.
- Meyer, M., & Griffiths, H. (2013).** Origins and diversity of eukaryotic CO₂-concentrating mechanisms: lessons for the future. *Journal of experimental botany*, *64*(3), 769-786.
- Mitchell, P. (1961).** Coupling of phosphorylation to electron and hydrogen transfer by a chemi-osmotic type of mechanism. *Nature*, *191*(4784), 144-148.
- Mitchell, P. (1966).** Chemiosmotic coupling in oxidative and photosynthetic phosphorylation. *Biological Reviews*, *41*(3), 445-501.
- Mitchell, P. (1975).** The protonmotive Q cycle: a general formulation. *FEBS letters*, *59*(2), 137-139.
- Mitchell, P. D. (1968).** Chemiosmotic coupling and energy transduction. *Glynn Research*.

- Miyake, C., Horiguchi, S., Makino, A., Shinzaki, Y., Yamamoto, H., & Tomizawa, K. I. (2005a).** Effects of light intensity on cyclic electron flow around PSI and its relationship to non-photochemical quenching of Chl fluorescence in tobacco leaves. *Plant and cell physiology*, 46(11), 1819-1830.
- Miyake, C., Miyata, M., Shinzaki, Y., & Tomizawa, K. I. (2005b).** CO₂ response of cyclic electron flow around PSI (CEF-PSI) in tobacco leaves—relative electron fluxes through PSI and PSII determine the magnitude of non-photochemical quenching (NPQ) of Chl fluorescence. *Plant and Cell Physiology*, 46(4), 629-637.
- Moustafa, A., Beszteri, B., Maier, U. G., Bowler, C., Valentin, K., & Bhattacharya, D. (2009).** Genomic footprints of a cryptic plastid endosymbiosis in diatoms. *Science*, 324(5935), 1724-1726.
- Munekage, Y., Hojo, M., Meurer, J., Endo, T., Tasaka, M., & Shikanai, T. (2002).** PGR5 is involved in cyclic electron flow around photosystem I and is essential for photoprotection in Arabidopsis. *Cell*, 110(3), 361-371
- Nandha, B., Finazzi, G., Joliot, P., Hald, S., & Johnson, G. N. (2007).** The role of PGR5 in the redox poisoning of photosynthetic electron transport. *Biochimica et Biophysica Acta (BBA)-Bioenergetics*, 1767(10), 1252-1259.
- Nawrocki, W. J., Bailleul, B., Cardol, P., Rappaport, F., Wollman, F. A., & Joliot, P. (2019a).** Maximal cyclic electron flow rate is independent of PGRL1 in *Chlamydomonas*. *Biochimica et Biophysica Acta (BBA)-Bioenergetics*, 1860(5), 425-432.
- Nawrocki, W. J., Bailleul, B., Picot, D., Cardol, P., Rappaport, F., Wollman, F. A., & Joliot, P. (2019b).** The mechanism of cyclic electron flow. *Biochimica et Biophysica Acta (BBA)-Bioenergetics*.
- Nawrocki, W. J., Buchert, F., Joliot, P., Rappaport, F., Bailleul, B., & Wollman, F. A. (2019c).** Chlororespiration controls growth under intermittent light. *Plant physiology*, 179(2), 630-639.
- Nawrocki, W. J., Santabarbara, S., Mosebach, L., Wollman, F. A., & Rappaport, F. (2016).** State transitions redistribute rather than dissipate energy between the two photosystems in *Chlamydomonas*. *Nature plants*, 2(4), 16031
- Neilson, J. A., & Durnford, D. G. (2010).** Structural and functional diversification of the light-harvesting complexes in photosynthetic eukaryotes. *Photosynthesis research*, 106(1-2), 57-71.
- Nelson, N., & Yocum, C. F. (2006).** Structure and function of photosystems I and II. *Annu. Rev. Plant Biol.*, 57, 521-565.
- Nixon, P. J., Michoux, F., Yu, J., Boehm, M., & Komenda, J. (2010).** Recent advances in understanding the assembly and repair of photosystem II. *Annals of botany*, 106(1), 1-16.
- Noctor, G., & Foyer, C. H. (1998).** A re-evaluation of the ATP: NADPH budget during C3 photosynthesis: a contribution from nitrate assimilation and its associated respiratory activity? *Journal of Experimental Botany*, 49(329), 1895-1908
- Oborník, M. (2019).** Endosymbiotic Evolution of Algae, Secondary Heterotrophy and Parasitism. *Biomolecules*, 9(7), 266.
- Ohad, I., Kyle, D. J., & Arntzen, C. J. (1984).** Membrane protein damage and repair: removal and replacement of inactivated 32-kilodalton polypeptides in chloroplast membranes. *The Journal of Cell Biology*, 99(2), 481-485.

- Ohad, I., Siekevitz, P., & Palade, G. E. (1967).** BIOGENESIS OF CHLOROPLAST MEMBRANES: I. Plastid Dedifferentiation in a Dark-Grown Algal Mutant (*Chlamydomonas reinhardtii*). *The Journal of cell biology*, 35(3), 521-552.
- Peers, G., Truong, T. B., Ostendorf, E., Busch, A., Elrad, D., Grossman, A. R., ... & Niyogi, K. K. (2009).** An ancient light-harvesting protein is critical for the regulation of algal photosynthesis. *Nature*, 462(7272), 518.
- Peltier, G., Aro, E. M., & Shikanai, T. (2016).** NDH-1 and NDH-2 plastoquinone reductases in oxygenic photosynthesis. *Annual review of plant biology*, 67, 55-80.
- Pesant, S., Not, F., Picheral, M., Kandels-Lewis, S., Le Bescot, N., Gorsky, G., ... & Dimier, C. (2015).** Open science resources for the discovery and analysis of Tara Oceans data. *Scientific data*, 2, 150023.
- Pomeroy, L. R. (1974).** The ocean's food web, a changing paradigm. *Bioscience*, 24(9), 499-504.
- Prihoda, J., Tanaka, A., de Paula, W. B., Allen, J. F., Tirichine, L., & Bowler, C. (2012).** Chloroplast-mitochondria cross-talk in diatoms. *Journal of experimental botany*, 63(4), 1543-1557.
- Pysznik, A. M., & Gibbs, S. P. (1992).** Immunocytochemical localization of photosystem I and the fucoxanthin-chlorophyll *a/c* light-harvesting complex in the diatom *Phaeodactylum tricornutum*. *Protoplasma*, 166(3-4), 208-217.
- Reinfelder, J. R. (2011).** Carbon concentrating mechanisms in eukaryotic marine phytoplankton. *Annual review of marine science*, 3, 291-315.
- Reyes, J. C., Chávez, S., Muro-Pastor, M. I., Candau, P., & Florencio, F. J. (1993).** Effect of glucose utilization on nitrite excretion by the unicellular cyanobacterium *Synechocystis sp.* strain PCC 6803. *Appl. Environ. Microbiol.*, 59(9), 3161-3163.
- Roberty, S., Bailleul, B., Berne, N., Franck, F., & Cardol, P. (2014).** PSI Mehler reaction is the main alternative photosynthetic electron pathway in *Symbiodinium sp.*, symbiotic dinoflagellates of cnidarians. *New Phytologist*, 204(1), 81-91.
- Rodríguez-Ezpeleta, N., Brinkmann, H., Burey, S. C., Roure, B., Burger, G., Löffelhardt, W., ... & Lang, B. F. (2005).** Monophyly of primary photosynthetic eukaryotes: green plants, red algae, and glaucophytes. *Current biology*, 15(14), 1325-1330.
- Rumberg, B., & Siggel, U. (1969).** pH changes in the inner phase of the thylakoids during photosynthesis. *Naturwissenschaften*, 56(3), 130-132.
- Rumeau, D., Peltier, G., & Cournac, L. (2007).** Chlororespiration and cyclic electron flow around PSI during photosynthesis and plant stress response. *Plant, cell & environment*, 30(9), 1041-1051.
- Rusch, D. B., Halpern, A. L., Sutton, G., Heidelberg, K. B., Williamson, S., Yooseph, S., ... & Beeson, K. (2007).** The Sorcerer II global ocean sampling expedition: northwest Atlantic through eastern tropical Pacific. *PLoS biology*, 5(3), e77
- Sacksteder, C. A., Kanazawa, A., Jacoby, M. E., & Kramer, D. M. (2000).** The proton to electron stoichiometry of steady-state photosynthesis in living plants: a proton-pumping Q cycle is continuously engaged. *Proceedings of the National Academy of Sciences*, 97(26), 14283-14288.
- Salomé, P. A., & Merchant, S. S. (2019).** A series of fortunate events: Introducing *Chlamydomonas* as a reference organism. *The Plant Cell*, 31(8), 1682-1707.

- Santabarbara, S., Galuppini, L., & Casazza, A. P. (2010).** Bidirectional electron transfer in the reaction centre of photosystem I. *Journal of integrative plant biology*, 52(8), 735-749.
- Santabarbara, S., Heathcote, P., & Evans, M. C. (2005).** Modelling of the electron transfer reactions in Photosystem I by electron tunnelling theory: the phyloquinones bound to the PsaA and the PsaB reaction centre subunits of PS I are almost isoenergetic to the iron-sulfur cluster FX. *Biochimica et Biophysica Acta (BBA)-Bioenergetics*, 1708(3), 283-310.
- Savard, F., Richard, C., & Guertin, M. (1996).** The *Chlamydomonas reinhardtii* LI818 gene represents a distant relative of the cabI/II genes that is regulated during the cell cycle and in response to illumination. *Plant molecular biology*, 32(3), 461-473.
- Scheibe, R. (2004).** Malate valves to balance cellular energy supply. *Physiologia plantarum*, 120(1), 21-26.
- Scheibe, R., Backhausen, J. E., Emmerlich, V., & Holtgreffe, S. (2005).** Strategies to maintain redox homeostasis during photosynthesis under changing conditions. *Journal of experimental botany*, 56(416), 1481-1489.
- Scheller, H. V., & Haldrup, A. (2005).** Photoinhibition of photosystem I. *Planta*, 221(1), 5-8.
- Schrope, M. (2008).** Oceanography: Red tide rising. *Nature News*, 452(7183), 24-26.
- Sonoike, K. (2011).** Photoinhibition of photosystem I. *Physiologia Plantarum*, 142(1), 56-64
- Sonoike, K., Terashima, I., Iwaki, M., & Itoh, S. (1995).** Destruction of photosystem I iron-sulfur centers in leaves of *Cucumis sativus* L. by weak illumination at chilling temperatures. *FEBS letters*, 362(2), 235-238.
- Staehelein, L. A. (1986).** Chloroplast structure and supramolecular organization of photosynthetic membranes. In *Photosynthesis III* (pp. 1-84). Springer, Berlin, Heidelberg.
- Stirbet, A. (2013).** Excitonic connectivity between photosystem II units: what is it, and how to measure it? *Photosynthesis research*, 116(2-3), 189-214.
- Stock, D., Gibbons, C., Arechaga, I., Leslie, A. G., & Walker, J. E. (2000).** The rotary mechanism of ATP synthase. *Current opinion in structural biology*, 10(6), 672-679.
- Strand, D. D., Fisher, N., & Kramer, D. M. (2017).** The higher plant plastid NAD (P) H dehydrogenase-like complex (NDH) is a high efficiency proton pump that increases ATP production by cyclic electron flow. *Journal of Biological Chemistry*, 292(28), 11850-11860.
- Stransky, H. T., & Hager, A. (1970).** Das Carotinoidmuster und die Verbreitung des lichtinduzierten Xanthophyllcyclus in verschiedenen Algenklassen. *Archiv für Mikrobiologie*, 71(2), 164-190.
- Streb, P., Josse, E. M., Gallouet, E., Baptist, F., Kuntz, M., & Cornic, G. (2005).** Evidence for alternative electron sinks to photosynthetic carbon assimilation in the high mountain plant species *Ranunculus glacialis*. *Plant, Cell & Environment*, 28(9), 1123-1135.
- Stroebel, D., Choquet, Y., Popot, J. L., & Picot, D. (2003).** An atypical haem in the cytochrome *b₆f* complex. *Nature*, 426(6965), 413.
- Suorsa, M., Järvi, S., Grieco, M., Nurmi, M., Pietrzykowska, M., Rantala, M., ... & Aro, E. M. (2012).** Proton gradient regulation 5 is essential for proper acclimation of Arabidopsis photosystem I to naturally and artificially fluctuating light conditions. *The Plant Cell*, 24(7), 2934-2948.

- Suttle, C. A. (2007).** Marine viruses—major players in the global ecosystem. *Nature Reviews Microbiology*, 5(10), 801.
- Takahashi, T., Sutherland, S. C., Wanninkhof, R., Sweeney, C., Feely, R. A., Chipman, D. W., ... & Watson, A. (2009).** Climatological mean and decadal change in surface ocean pCO₂, and net sea–air CO₂ flux over the global oceans. *Deep Sea Research Part II: Topical Studies in Oceanography*, 56(8-10), 554-577.
- Tikkanen, M., Mekala, N. R., & Aro, E. M. (2014).** Photosystem II photoinhibition-repair cycle protects Photosystem I from irreversible damage. *Biochimica et Biophysica Acta (BBA)-Bioenergetics*, 1837(1), 210-215.
- Tyrrell, T., & Merico, A. (2004).** *Emiliania huxleyi*: bloom observations and the conditions that induce them. In *Coccolithophores* (pp. 75-97). Springer, Berlin, Heidelberg.
- Van Niel, C. B., & Muller, F. M. (1931).** On the purple bacteria and their significance for the study of photosynthesis. *Recueil des travaux botaniques néerlandais*, 28(3/4), 245-274.
- Van Niel, C. B., Allen, M. B., & Wright, B. E. (1953).** On the photochemical reduction of nitrate by algae. *Biochimica et biophysica acta*, 12(1-2), 67-74.
- Walker, B. J., Strand, D. D., Kramer, D. M., & Cousins, A. B. (2014).** The response of cyclic electron flow around photosystem I to changes in photorespiration and nitrate assimilation. *Plant physiology*, 165(1), 453-462.
- Wetzel, C. M., Jiang, C. Z., Meehan, L. J., Voytas, D. F., & Rodermel, S. R. (1994).** Nuclear—organelle interactions: the immutans variegation mutant of *Arabidopsis* is plastid autonomous and impaired in carotenoid biosynthesis. *The Plant Journal*, 6(2), 161-175.
- Wilhelm, S. W., & Suttle, C. A. (1999).** Viruses and nutrient cycles in the sea: viruses play critical roles in the structure and function of aquatic food webs. *Bioscience*, 49(10), 781-788.
- Wilson, W. H., Schroeder, D. C., Allen, M. J., Holden, M. T., Parkhill, J., Barrell, B. G., ... & Quail, M. A. (2005).** Complete genome sequence and lytic phase transcription profile of a Coccolithovirus. *Science*, 309(5737), 1090-1092.
- Winkler, M., Heil, B., Heil, B., & Happe, T. (2002).** Isolation and molecular characterization of the [Fe]-hydrogenase from the unicellular green alga *Chlorella fusca*. *Biochimica et Biophysica Acta (BBA)-Gene Structure and Expression*, 1576(3), 330-334.
- Woese, C. R., Kandler, O., & Wheelis, M. L. (1990).** Towards a natural system of organisms: proposal for the domains Archaea, Bacteria, and Eucarya. *Proceedings of the National Academy of Sciences*, 87(12), 4576-4579.
- Wolfe-Simon, F., Starovoytov, V., Reinfelder, J. R., Schofield, O., & Falkowski, P. G. (2006).** Localization and role of manganese superoxide dismutase in a marine diatom. *Plant physiology*, 142(4), 1701-1709.
- Wollman, F. A. (2001).** State transitions reveal the dynamics and flexibility of the photosynthetic apparatus. *The EMBO journal*, 20(14), 3623-3630.
- Yamamoto, H. Y., Nakayama, T., & Chichester, C. O. (1962).** Studies on the light and dark interconversions of leaf xanthophylls. *Archives of Biochemistry and Biophysics*, 97(1), 168-173.

- Yamamoto, H., Peng, L., Fukao, Y., & Shikanai, T. (2011).** An Src homology 3 domain-like fold protein forms a ferredoxin binding site for the chloroplast NADH dehydrogenase-like complex in *Arabidopsis*. *The Plant Cell*, 23(4), 1480-1493.
- Yamamoto, H., Takahashi, S., Badger, M. R., & Shikanai, T. (2016).** Artificial remodelling of alternative electron flow by flavodiiron proteins in *Arabidopsis*. *Nature plants*, 2(3), 16012.
- Yamori, W., Sakata, N., Suzuki, Y., Shikanai, T., & Makino, A. (2011).** Cyclic electron flow around photosystem I via chloroplast NAD (P) H dehydrogenase (NDH) complex performs a significant physiological role during photosynthesis and plant growth at low temperature in rice. *The Plant Journal*, 68(6), 966-976.
- Zhang, P., Allahverdiyeva, Y., Eisenhut, M., & Aro, E. M. (2009).** Flavodiiron proteins in oxygenic photosynthetic organisms: photoprotection of photosystem II by Flv2 and Flv4 in *Synechocystis sp.* PCC 6803. *PLoS One*, 4(4), e5331.
- Zhang, Z., Shrager, J., Jain, M., Chang, C. W., Vallon, O., & Grossman, A. R. (2004).** Insights into the survival of *Chlamydomonas reinhardtii* during sulfur starvation based on microarray analysis of gene expression. *Eukaryotic cell*, 3(5), 1331-1348.
- Zhu, S. H., & Green, B. R. (2010).** Photoprotection in the diatom *Thalassiosira pseudonana*: role of LI818-like proteins in response to high light stress. *Biochimica et Biophysica Acta (BBA)-Bioenergetics*, 1797(8), 1449-1457.

Chapter 2: Probing PSI activity

Summary

2.1. How to probe photosystem I with absorption spectroscopy?.....	85
2.1.1. Some reminders about photosystem I	85
2.1.2. Measuring P_{700} redox state to investigate PSI activity.....	87
2.1.3. Electrochromic Shift: an internal voltmeter	91
2.2. Article: Critical reappraisal of methods to measure photosystem I activity.....	96
2.3. Discussion	125
2.3.1. The P_{700} pulse method underestimates $Y(I)$ because of reduction of PSI acceptors during the multiple turnover pulse	125
2.3.2. Technical considerations regarding P_{700} measurements	129
2.3.3. Generalization to the case of an active photosystem II	133
2.3.4. Revisiting the literature based on the P_{700} pulse method	136
2.3.5. Partial conclusions and transition	148
2.4. Bibliography.....	149

2.1. How to probe photosystem I with absorption spectroscopy?

To investigate Cyclic Electron Flow around PSI *in vivo* in microalgae, the most powerful approach consists in comparing the activities of photosystem II, which participates in linear electron flow only, and photosystem I, involved in both linear and cyclic electron flows (Fan et al., 2016). It is also important to have robust measurement of the state of PSI to visualize the accumulation of stromal reductants downstream PSI or to get insights into PSI photoinhibition. In this first chapter, I will present the methodological work I have done to determine the best way to investigate PSI state and activity, through absorption difference spectroscopy.

Photosynthetic organisms absorb sunlight with an absorption spectrum that depends on the pigments that compose them. This absorption spectrum is slightly modified when it is transferred from darkness to light, i.e. whether photosynthetic activity is taking place or not. These light-induced absorption changes are mostly due to the oxidation/reduction of some photosynthetic electron carriers and/or to the trans-thylakoidal electric field generated by photosynthesis, and can be used to our advantage for probing the photosynthetic process.

In this section, I will compare two methods based on absorption difference spectroscopy to measure the PSI conversion efficiency, or quantum yield. Since the maximal quantum yield of photosystem I is close to 1 (Nelson 2009), measuring the quantum yield of PSI is equivalent to measuring the fraction of PSI open centers. The aim is to determine the most accurate and robust approach to investigate PSI yield before we perform comparisons of PSII and PSI activities in chapter 3.

2.1.1. Some reminders about photosystem I

Photosystem I (PSI) operates at the end of the electron transfer chain and is a plastocyanin-ferredoxin oxydo-reductase: it uses the light energy to catalyze the endergonic reduction of the ferredoxins by the plastocyanins (Nelson and Yocum 2006; Scheller 1996). PSI reaction center is a multiple subunit complex (Figure 2-1A) that contains non-proteic electron carriers: P₇₀₀, A₀, A₁, F_x, F_A and F_B (Figure 2-1A and B) that were first identified spectroscopically during the last half-century (Brettel 1997). Light energy enables photochemistry, which consists in the oxidation of P₇₀₀, a pair of chlorophyll *a* called “special pair” (whose redox potential $E'm =$

+430 mV; Kok, 1961; Sétif and Mathis, 1980), and the reduction of A_0 , a chlorophyll *a* monomer. Alternative models propose that P_{700} is not involved in the charge separation directly but instead in its stabilization (Holtzwarth et al., 2006; Li et al., 2006). The electron is then transferred to A_1 , a phylloquinone in most organisms, F_x an interpolypeptide iron-sulfur center (4Fe-4S) ($E'_m \sim -705$ mV; Golbeck and Bryant, 1991), and finally to F_A ($E'_m - 520$ mV; Golbeck, 1993) and F_B ($E'_m - 580$ mV; Golbeck, 1993), which are (4Fe-4S) clusters bound to PsaC, an extrinsic PSI subunit. Oxidized ferredoxin can dock at the stromal side of PSI and get an electron from F_B , thus stabilizing the charge separation.

Hence, a turnover of PSI results in three main consequences: the oxidation of P_{700} , the reduction of iron-sulfur proteins and the transfer of a net positive charge from the stroma to the lumen. These changes, occurring after a photochemical event in PSI, also determine the signals potentially available to study the activity of this photosystem.

The reduction of iron-sulfur proteins and especially of the soluble ferredoxin could therefore be used to probe PSI activity but the absorption changes related to ferredoxin oxidation/reduction occurs in the near infra-red region, where they are difficult to deconvolute from other signals, mainly iron-sulfur clusters F_A , F_B and F_x , plastocyanin and P_{700} contributions (Klughammer and Schreiber, 1991). Thanks to recent advances in the deconvolution of those signals (Schreiber 2017), *in vivo* measurements of ferredoxin redox state might be soon possible, but the methodology is not yet completely mature.

The other two available signals have been routinely used for decades and will be exploited in this chapter: (i) the oxidation of P_{700} can be assessed by measuring absorption changes in the near far red region and (ii) the electric field generated across the thylakoid membrane by PSI turnovers can be probed through Electrochromic Shift (ECS) signals. Those two methods are described in more detail below.

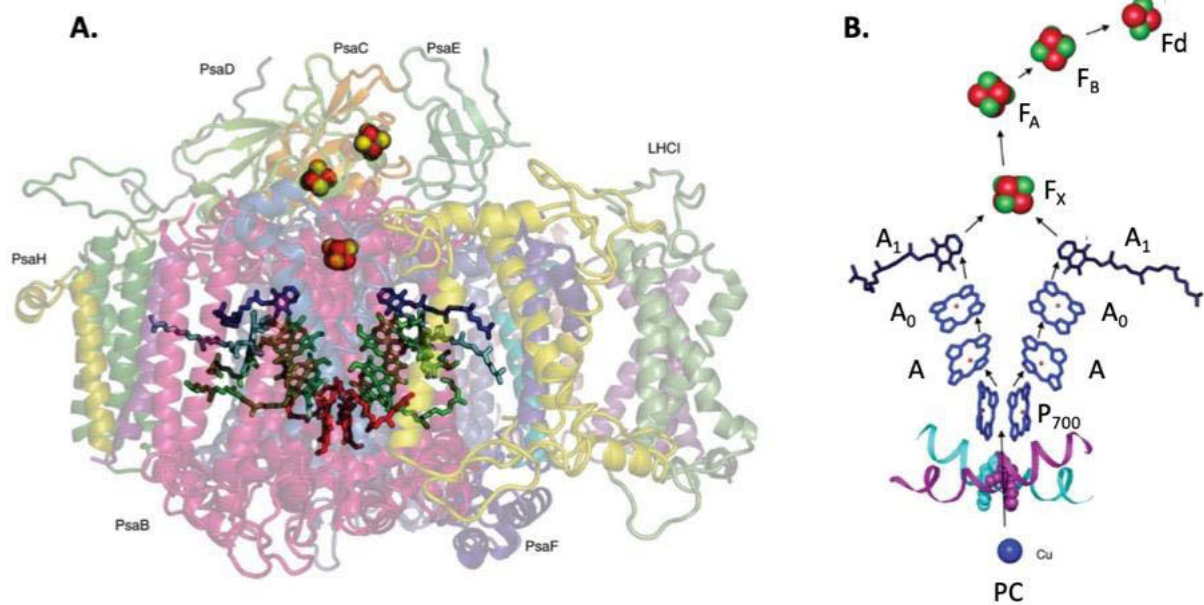


Figure 2-1: Structure of the photosystem I

From (Nelson and Yocum 2006).

A. side view of the structure of plant photosystem I. The cofactors involved in light-induced electron transport, i.e., P_{700} , A_0 , A_1 , F_X , F_A , and F_B , are shown along with the backbones of the 16 subunits. The positions of the proteic subunits, PsaB, PsaC, PsaD, PsaE, and PsaF are shown. In the electron transport chain, the P_{700} Chl (red) and the other Chl (green) are indicated. The quinones (blue) and, in the iron-sulfur clusters, the iron (red) and the sulfur (yellow) are also indicated.

B. Structural model of the pathway for light-induced electron transport from plastocyanin (PC) to ferredoxin (Fd) in photosystem I. Chlorophylls (blue), phylloquinones (black), the copper atom of PC (blue), and the iron (red balls) and sulfur (green balls) of the three Fe_4-S_4 clusters and the Fd Fe_2-S_2 are depicted. Two tryptophan residues (light-blue and light-pink space-filling structures) that might be involved in electron transport from PC to P_{700} are also shown in the context of their secondary structural environment.

2.1.2. Measuring P_{700} redox state to investigate PSI activity

a) Source of the signal

Photosynthesis consists in electron transfers that involve several redox cofactors. Some of these cofactors absorb in the visible light and do not display the same absorption spectrum depending on whether they are in their oxidized or reduced form. The measurement of absorption changes will specifically inform on the changes of the redox state of those electron carriers. For example, light-induced PSI photochemistry induces a main absorption band bleaching (in the Q_y region) with a maximum at ~ 695 nm. This absorption change comes from the oxidation of P_{700} (Ke 2001). The difference absorption spectrum of P_{700} (P_{700}^+ minus P_{700}) is presented in Figure 2-2 and shows a bleaching region around 680-710 nm in the green alga *Chlamydomonas reinhardtii* (Webber et al. 1996).

PSI core complex proteins are highly conserved among cyanobacteria and photosynthetic eukaryotes (Mix et al. 2005). Moreover, in cyanobacteria, plants and green algae, P_{700} absorption change spectra is conserved (Drop et al. 2014; Hiyama and Ke 1972; Webber et al. 1996).

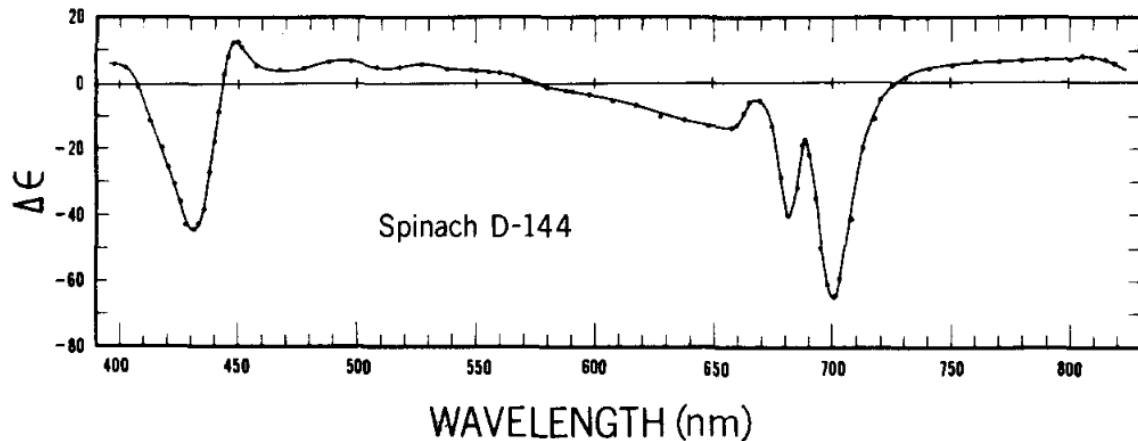


Figure 2-2: P_{700} oxidized minus reduced difference spectrum

From Hiyama and Ke, 1972.

A short flash (20 μ s duration) was applied on a reaction mixture containing: D-144 particles (i.e. a fraction of lysed chloroplasts enriched in PSI, see Anderson and Boardman, 1966 for protocol details). All $\Delta\epsilon$ values were calculated from ΔA based on $\Delta\epsilon_{701\text{nm}} = 64 \text{ mequiv}^{-1}\cdot\text{cm}^{-1}$.

b) Signal deconvolution

We should note that the absorption difference signals in the near infrared region are not only due to P_{700} absorption changes. They also contain contributions from plastocyanin oxidation (which has a relatively flat spectrum), some local electric field indicating changes, ferredoxin reduction as well as iron-sulfur centers (Klughammer and Schreiber 1991). On top of that, an important fluorescence of chlorophylls can be artefactually measured in the near infra-red. For this reason, obtaining the sole contribution related to P_{700} redox changes requires some deconvolution step. Two procedures are commonly used to deconvolute the P_{700} contribution from others.

- the first one is favored in plants and measures the difference between the absorption changes at 820 and 870 nm (e.g. Joliot and Joliot 2006; Klughammer and Schreiber, 1994). This is the procedure used in the Walz systems, like the Dual-PAM-100 measuring system (Walz, Germany).

- the second one is used in microalgae and measures the difference of absorbance changes at 705 and at 735/740 nm (e.g. Godaux et al. 2015; Nawrocki et al. 2019). This is the procedure used by default in the Joliot-type spectrometers JTS-10 or JTS-100 (Bio-Logic, Grenoble, France).

It is to note that the first procedure gives smaller signals but also minimizes the artefactual contribution of chlorophyll fluorescence. In this chapter, I always worked in conditions of fully inhibited PSII; the variable fluorescence from PSII is abolished and this is why I used 705-735 nm instead (Alric et al. 2010b).

c) Probing P₇₀₀ redox state

Regardless of the combination of wavelengths used to determine the absorption changes related to P₇₀₀ oxidation/reduction, the determination of its absolute redox state also requires two absorption references: the absorption level when P₇₀₀ is fully reduced and the absorption level when P₇₀₀ is fully oxidized.

The maximum absorbance, when P₇₀₀ is completely reduced, is obtained in the dark, when all the photosynthetic intermediates are in thermodynamic equilibrium with the ambient redox potential of the cell (P₇₀₀ being a very strong oxidant, it is virtually fully reduced). At the opposite, reaching the situation where 100% of P₇₀₀ are in the oxidized state is a lot more difficult, because this situation is way off equilibrium. This situation is usually attained when two requirements are met, (i) P₇₀₀ oxidation rate is very high, under high light illumination and (ii) the electron transfer towards PSI is slowed-down, making P₇₀₀ reduction as slow as possible. This is usually obtained by inhibiting PSII with DCMU or by using specific PSI excitation (far red in plants). As mentioned in the manuscript and in the discussion of this chapter, the measurement of the absorption references corresponding to fully oxidized P₇₀₀ is a difficult task.

d) PSI yield and P₇₀₀ redox state

Since the 1980s, changes in P₇₀₀ absorption, reflecting its redox state, have been used to study the quantum yield of PSI and the most recent method has been proposed by Klughammer and Schreiber in 1994. Let's first explain the link between the redox state of P₇₀₀ and the yield of PSI, i.e. the fraction of open PSI centers. By definition, an open center will perform a charge separation if it receives a photon. In the beginning of the 1990s, Harbinson and Foyer used P₇₀₀ absorption changes to differentiate two types of PSI centers:

- $[P_{700}^+]$ centers that are closed because their primary donor is oxidized. Those centers are called donor side limited because PSI donor does not have any electron to transfer. The fraction of $[P_{700}^+]$ centers is noted $Y(ND)$ hereafter.
- $[P_{700}]$ centers with a reduced primary donor, described as open centers (i.e. ready to transfer an electron).

The PSI yield, which is the fraction of absorbed photons converted into stable charge separation, was calculated as the fraction of open PSI, $[P_{700}]$ as shown in Figure 2-3 (Foyer et al. 1992; Harbinson and Foyer 1991).

In 1994, Klughammer and Schreiber suggested that in some conditions, $[P_{700}]$ centers can be closed because their acceptor, called A hereafter and corresponding to all the PSI iron-sulfur proteins (Malkin and Bearden, 1971; Oh-Oka et al., 1991), is reduced (Klughammer and Schreiber 1994). These $[P_{700} A^-]$ centers are called acceptor side limited centers because the acceptor cannot accept any electron. The fraction of $[P_{700} A^-]$ and of $[P_{700} A]$ centers are noted $Y(NA)$ and $Y(I)$, respectively. Klughammer and Schreiber proposed a method to discriminate between open PSI centers, $[P_{700} A]$ and acceptor side limited centers, $[P_{700} A^-]$. This method is based on the fact that among $[P_{700}]$ centers, only P_{700} from open centers are oxidizable if they receive enough light.

The most straightforward method would be to use a single turnover laser flash, i.e. a flash of light high enough so that all PSI receive at least a photon and short enough so that all PSI cannot perform more than one charge separation. But because P_{700} reduction by plastocyanin (PC) is fast (compared to the time resolution of commercial devices) and falls in the same kinetics as charge recombination, the use of a single turnover laser flash to probe the fraction of open PSI is not possible. Indeed, the electron transfer from PC to P_{700} can occur with half-times of $\sim 5\mu s$ or $\sim 200\mu s$ following P_{700} oxidation, if the plastocyanin is docked to PSI or needs to diffuse in the lumen, respectively (Hippler et al. 1997). This falls in the same timerange as the charge recombination between P_{700}^+ and A_1^- (Warren et al. 1990). It is thus intrinsically impossible to discriminate between $[P_{700} A]$ and $[P_{700} A^-]$ by the sole measurement of P_{700} absorption changes after a single turnover laser flash stimulation.

Klughammer and Schreiber suggested to use a few milliseconds saturating pulse of light instead (Klughammer and Schreiber, 1994). This pulse, whose intensity must be high enough to allow oxidation of all PSI secondary donors before a b_6f turnover, is supposed to oxidize all P_{700} from $[P_{700} A]$ centers (Figure 2-3). But this method is assuming a strong hypothesis: that

it is possible to transfer several negative charges to the stromal side without modifying the fraction of $[P_{700} A^-]$ centers. In this chapter, I tested the reliability of this hypothesis.

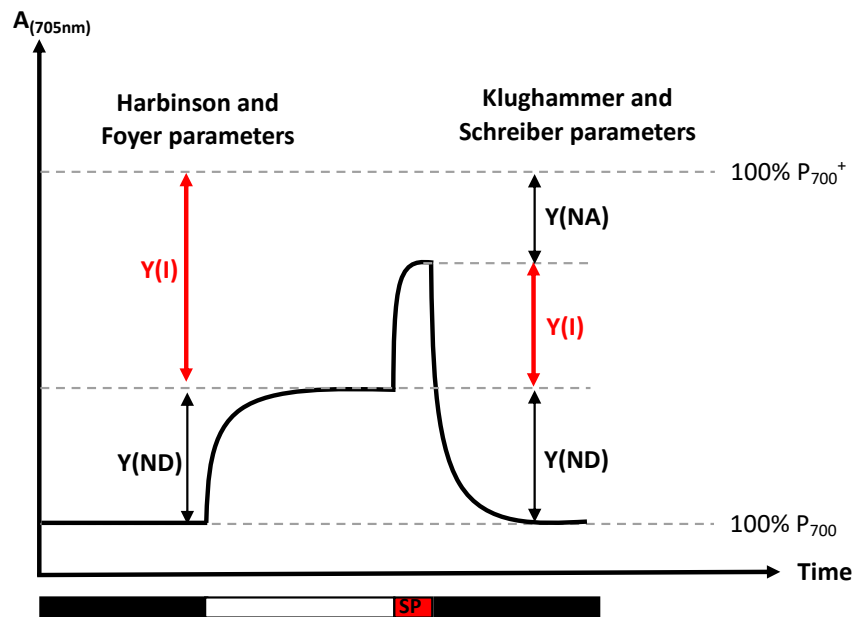


Figure 2-3: Principle of the P_{700} -based methods for the determination of the fraction of open PSI centers, $Y(I)$
 In both Habinson & Foyer and Klughammer & Schreiber methods, the fraction of donor side limited centers, $Y(ND)$ is estimated as the fraction of P_{700} that is oxidized under the given light conditions. Harbinson & Foyer method consider $Y(I)$ as the fraction of reduced P_{700} while Klughammer & Schreiber method estimates $Y(I)$ as the fraction of P_{700} that can be oxidized during a multiple turnover saturating light pulse (SP). Black, white and red horizontal bars correspond to darkness, light and multiple turnover saturating light pulse, respectively.

2.1.3. Electrochromic Shift: an internal voltmeter

As discussed before, the photochemistry of PSI generates an electric field across the thylakoid membrane because an electron is transferred from the luminal side (P_{700} / plastocyanin) to the stromal side (iron-sulfur centers / ferredoxin). Therefore, measuring the electric field across the thylakoid could, in principle, probe the activity of PSI. Such a measurement of the trans-thylakoid electric field exists and is based on the Stark effect on photosynthetic pigments. It is commonly called Electrochromic Shift (ECS) signal (Witt 1979). The principle of the method based on this signal is presented hereafter.

a) Source of the ECS signal

When the photosynthetic chain is at work, photosystems transfer electrons from the lumen to the stroma and the electron transfer from water to NADPH is coupled to a translocation of protons from the stroma to the lumen. This results in a proton motive force which includes an electric field, $\Delta\Psi$, between the inside and the outside of the thylakoid.

Some photosynthetic pigments embedded in the membrane are sensitive to this electric field. As shown in the Figure 2-4A, in the presence of an electric field, the energy levels of the fundamental and excited states of a pigment can be modified. As a result, the energy of the photon which can be absorbed (whose energy is equal to the difference between excited and fundamental energy levels) by the pigment will be modified and the absorption spectrum of the latter will be shifted. This phenomenon is known as the Stark effect (Stark 1913). The spectrum of the “field indicating absorption change” corresponds to the difference between the absorption of the pigment in the presence of the electric field and the one in its absence, and typically displays a "double-wave" spectrum (Figure 2-4B). Such “field indicating absorption changes” were first reported in photosynthetic systems by Junge and Witt (Junge and Witt 1968) and give information about the electric field across photosynthetic membranes (Witt 1979).

The electrochromic shift can depend on the electric field in two different manners: it can increase linearly with the electric field (this is the case for a pigment with a permanent dipolar moment) or quadratically with the electric field (this is basically the case for a pigment with no permanent dipolar moment but a polarizability, i.e. its dipolar moment will be induced by the electric field itself). Such a quadratic electric field has been described in mutants of green algae (Joliot and Joliot 1989), in diatoms (Bailleul et al., 2015) and other stramenopiles (Berne et al., 2018). In *Chlamydomonas reinhardtii*, the species used in this chapter, the electrochromic signal increases linearly with the electric field generated across the photosynthetic membrane (Joliot and Joliot, 1989). The amplitude of this signal will therefore directly measure the amplitude of the electric field created by the photosynthetic activity.

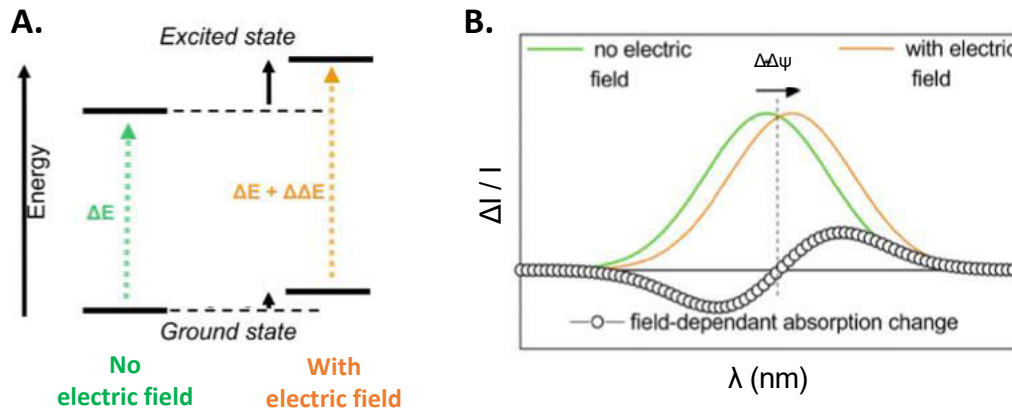


Figure 2-4: Electrochromic Shift principle

A: Modification of the energy levels of the pigment in the presence of an electric field. B: Shift of the absorption spectrum (orange versus green) of the pigment and the resulting absorption difference (open black circles) spectrum. From Bailleul et al. 2010.

Most photosynthetic eukaryotes possess ECS signals, and this is also true for cyanobacteria even though the signals are very small in the latter (Viola et al., 2019). However, the ECS spectra differ depending on the phylogenetic clade, indicating that the pigments sensitive to the electric field are different (Bailleul et al., 2010). The presence of ECS signals in most eukaryotic photosynthetic organisms make the approach followed in this chapter applicable to other species, as we will see in Chapter 3.

b) ECS signal deconvolution

The ECS spectrum of *Chlamydomonas reinhardtii* is presented in Figure 2-5. ECS signal shows a maximum in the green region and we should note that ECS signal is not the only one contribution to light-induced absorption changes in this spectral region. There is also the oxidation/reduction of c-type cytochromes (like cytochrome f or cytochrome c6). Practically, in green algae like *Chlamydomonas reinhardtii*, as well as in plants, the ECS signal is measured as the difference between the absorption change at 520 nm and the one at 546 nm (e.g. Bujaldon et al., 2017; Buchert et al., 2017).

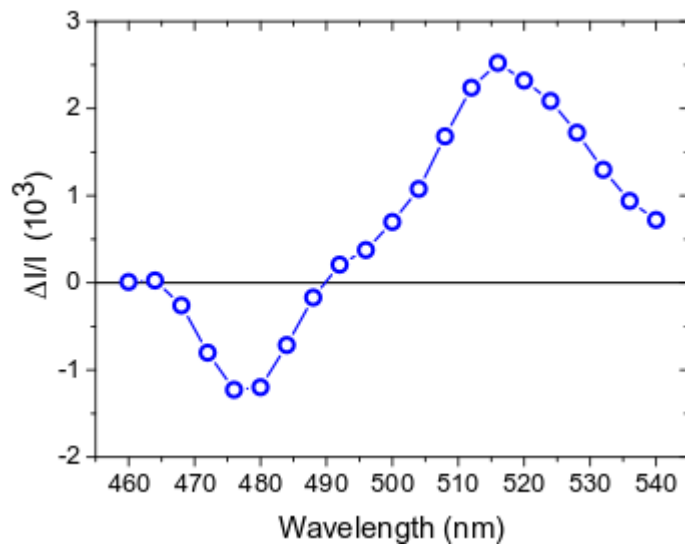


Figure 2-5: *Chlamydomonas reinhardtii* electrochromic shift spectrum

Absorption change was measured 100 μ s after a single turnover saturating laser flash in the *Chlamydomonas reinhardtii* T222⁺ wild type. Cultures were centrifugated, resuspended at the concentration of 10^7 cells.mL⁻¹ in minimum medium and dark-adapted for 20 min while vigorously stirred.

Adapted from Bujaldon et al., 2017

c) Studying photosynthetic complexes activity with ECS

The electrochromic signal allows many applications for the study of photosynthesis (reviewed in Bailleul et al., 2010). In this chapter, I will mostly focus on the flash-induced ECS signals, i.e. the measurement of the ECS signal after a single turnover laser flash. The first observations of ECS signals were performed with single turnover flashes (Junge and Witt, 1968) and the ECS kinetics following the flash was thoroughly investigated first in green algae (Joliot and Delosme, 1974). Let's underline the role of the photosynthetic complexes in the implementation and dissipation of the electric field. The chloroplastic F1-F0 ATP synthase (CF1-F0) is the only photosynthetic complex which dissipates the electric field by transferring protons from the stroma to the lumen. The three other photosynthetic complexes, involved in the transfer of electrons from water to NADPH, set up the electric field with a yield of one positive charge transferred to the lumen per turnover:

- the activity of the photosystem II leads to the oxidation of water molecules and the release of a proton in the lumen per electron transferred (and the uptake of a proton on the stromal side to reduce a plastoquinone into plastoquinol);
- the photosystem I transfers one electron from the luminal plastocyanins to the stromal ferredoxins;

- the cytochrome b_6f translocates two protons in the lumen per electron transferred, assuming the Q cycle is always operating (Sacksteder et al., 2000). His net contribution is therefore one positive charge transferred to the lumen per turnover.

The photosystems are the sites of photochemistry and their activities are immediately modified by light perturbations whereas the activities of cytochrome b_6f and ATP synthase, that are biochemical steps, are modified later after the light disturbance. Hence, after a single turnover flash on a dark-adapted sample, following the kinetics of ECS is a very powerful way to obtain a lot of information on the photosynthetic complexes (Joliot and Delosme, 1974). The open PS will perform a charge separation right after the flash, giving rise to a first increase of the ECS called “a phase” (Figure 2-6B). At the end of this “a phase”, a PSI donor has been oxidized and an electron has been transferred to the plastoquinol pool. This out-of-equilibrium situation is followed by the turnover of the cytochrome b_6f , which transfers an electron from a plastoquinol to PSI donors and pumps protons concomitantly. This b_6f contribution induces a second ECS rise known as “b phase”. Finally, the electric field generated by those two phases is dissipated by ATP synthase until dark adapted state is reached again, and this third phase is known as “c phase”.

In this chapter, I will use this method to measure the fraction of open PSI centers. By definition, an open center is a center that will perform a charge separation if it receives a photon. After a single turnover flash, only open centers will perform a charge separation and generate an electric field: the amplitude of the a phase is proportional to the number of open centers. By normalizing this signal by the amplitude of the a phase when all the centers are open, i.e. in the same sample once dark-adapted, we can calculate a fraction of open centers.

$$Y(\text{total}) = \frac{\text{a phase (conditions of interest)}}{\text{a phase (dark-adapted)}}$$

Given the aim of this chapter, we need to distinguish between the contributions of PSII and PSI. PSII can be inhibited by the addition of two inhibitors. The first one is 3-(3,4-dichlorophenyl)-1,1-dimethylurea (DCMU) which competes with PQ for the Q_B pocket of PSII and inhibits electron transfer from Q_A to the plastoquinone pool. In the presence of DCMU, one charge separation can still occur in PSII (from P_{680} to Q_A) and this is why we add hydroxylamine, an effective P_{680} electron donor that blocks irreversibly PSII in a $[P_{680} Q_A^-]$ state, unable to perform any charge separation. This can be easily checked by using chlorophyll fluorescence: there should not be any variable fluorescence left once PSII is fully

inhibited with DCMU and HA. In these conditions, only PSI participates to the generation of electric field and the fraction of open PSI centers can be calculated as discussed before.

The “a phase” can also be used to calculate the ratio between the functional PSII and PSI and the principle is schematized in Figure 2-6B. In a dark-adapted sample, the amplitude of the a phase is proportional to the number of total photosystem. By comparing the amplitude when all the centers are functional and the one when only the PSI are active (in the presence of DCMU and HA) we can calculate the PSII to PSI ratio. And given n_2 and n_1 the fractions of photosystems being PSII and PSI, respectively:

$$n_1 = \frac{a \text{ phase (dark, DCMU+HA)}}{a \text{ phase (dark-adapted)}}$$

$$n_2 = \frac{a \text{ phase (dark-adapted)} - a \text{ phase (dark-adapted, DCMU+HA)}}{a \text{ phase (dark-adapted)}} = 1 - n_1$$

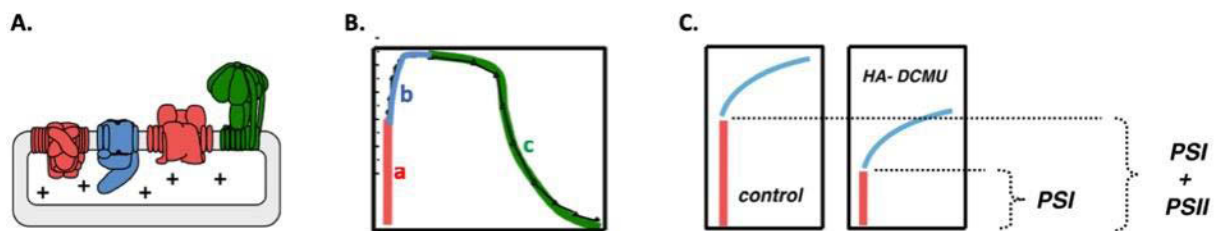


Figure 2-6: Kinetic of the ECS after excitation with a single turnover laser flash

From (Bailleul et al. 2010).

Schematic representation of the thylakoid complexes involved in the electric field implementation and dissipation: the photosystems (in red), the cytochrome b_6f (blue) and ATP synthase (green).

Schematic kinetics of the ECS signal after excitation with a single turnover (STO) laser flash showing typical phase a, b and c attributed to PS (red), cytochrome b_6f (blue) and ATP synthase (green) activities, respectively.

Schematic representation of the ECS signal after a STO laser flash in the absence and presence of PSII inhibitor (3-(3,4-dichlorophenyl)-1,1-dimethylurea, DCMU, and hydroxylamine, HA).

2.2. Article: Critical reappraisal of methods to measure photosystem I activity

Critical reappraisal of methods to measure photosystem I activity

Suzanne Ferté¹, Marc Romero Arderiu¹, Ginga Shimakawa², Benjamin Bailleul¹

¹Institut de Biologie Physico-Chimique, Laboratory of Chloroplast Biology and Light Sensing in Microalgae, UMR7141 Centre National de la Recherche Scientifique (CNRS), Sorbonne Université, Paris, France.

²Institute for Integrative Biology of the Cell (I2BC), CEA, CNRS, Université Paris-Sud, Université Paris-Saclay, 91198 Gif sur Yvette, France

Corresponding author: Benjamin Bailleul, bailleul@ibpc.fr, +33(0) 1 58 41 51 01.

Abstract

Photosystem I (PSI) works in series with photosystem II to convert light into chemical energy in oxygenic photosynthesis. The most widely used, but non-validated, method to measure PSI activity is based on the absorption changes that occur with the oxidation-reduction of P_{700} , the special pair of PSI reaction centre. PSI yield is calculated as the fraction of P_{700} that is reduced but is photo-oxidizable given a multiple turnover light pulse. Here we compare estimates from this method with results obtained by measuring the electro-chromic shift of photosynthetic pigments in the green alga *C. reinhardtii*. We show that the P_{700} -based method systematically underestimates PSI yield by as much as tenfold in our dataset, because the multiple turnover pulse itself generates an artefactual over-reduction of the PSI acceptor side. We propose a correction formula to be used to reassess published data and to give a more robust view of light phase regulation.

Abbreviations list

ATP, adenosine triphosphate; CEF, cyclic electron flow around PSI; cyt b_6f , cytochrome b_6f ; DBMIB, dibromo-6-isopropyl-3-methyl-1,4-benzoquinone; DCMU, 3-(3,4-dichlorophenyl)-1,1-dimethylurea; ECS, electro-chromic shift; HA, hydroxylamine; LEF, linear electron flow; MV, methylviologen; NADPH, nicotinamide adenine dinucleotide phosphate; pmf, proton motive force; PSI, photosystem I; PSII, photosystem II; $Y(I)$, PSI yield; $Y(I)_{ECS}$, PSI yield based on ECS; $Y(I)_{P_{700}}$, PSI yield based on P_{700} pulse method; $Y(NA)$, PSI acceptor-side limitation; $Y(NA)_{P_{700}}$, PSI acceptor-side limitation based on P_{700} pulse method; $Y(ND)$, PSI donor-side limitation.

Introduction

In oxygenic photosynthesis, the photosynthetic electron transfer chain comprises two photosystems. Photosystem II (PSII) and photosystem I (PSI) work in series to allow linear transfer of electrons generated from the oxidation of water in PSII to reduce NADP⁺ into nicotinamide adenine dinucleotide phosphate (NADPH) downstream of PSI. The electron transfer from PSII to PSI involves the plastoquinone pool diffusing in the thylakoid membrane, the lumen-soluble plastocyanins (or cytochrome *c*₆) and a plastoquinol-plastocyanin oxidoreductase called cytochrome *b*₆*f* (*cyt b*₆*f*). The electron transfer is coupled to the translocation of protons across the thylakoid membrane, giving rise to an electrochemical proton gradient or proton motive force (pmf). The pmf comprises both an electric ($\Delta\psi$) and an osmotic (ΔpH) component and fuels the synthesis of adenosine triphosphate (ATP) by the CF₁-F₀ ATP synthase. The methods used to measure the linear electron flow from water to NADPH mostly rely on measurements of PSII because it is the most convenient photosynthetic complex to probe. The PSII chlorophyll fluorescence yield is high enough to allow the energy conversion in PSII to be calculated (Kautsky et al., 1960; Duysens, 1963; reviewed in Baker, 2008). The oxidation of water, the final electron donor, occurs in the oxygen evolving complex of PSII so it is also possible to measure O₂ evolution as a powerful alternative assay. Fluorescence and oxygen-based methodologies have been cross-validated (Genty et al., 1992) and are now well established and widely used by the community of photosynthesis researchers. However, measuring PSII activity alone is not sufficient to view the complexity of photosynthetic function and regulatory flexibility. For instance, in addition to the linear electron flow involving the two photosystems, several modes of alternative electron flow can play an important role in providing some flexibility in terms of ATP/NADPH ratios (Eberhard et al., 2008). In cyanobacteria, terrestrial plants and green algae, it has been shown that electron transfer from reduced PSI acceptors back to the inter-photosystem chain at the plastoquinone pool or at the *b*₆*f* level can occur, allowing PSI to operate independently from PSII (Arnon et al., 1958; reviewed thoroughly in Bendall and Manasse, 1995, and in Shikanai, 2007). This gives rise to a cyclic electron flow (CEF) around PSI, which is thought to play a crucial role in photosynthetic regulation by increasing the ATP/NADPH balance (Allen, 2002). Since CEF does not produce any quantifiable net product, the most accurate way to measure CEF in physiological conditions is to compare PSII and PSI activities (Fan et al., 2016). The CEF participates, together with other alternative electron flows, in the protection of both photosystems under excess light by regulating *cyt b*₆*f* and PSII activities (Endo and Asada, 2008;

Chaux et al., 2015). The over-reduction of PSI acceptors when the Calvin-Benson-Bassham cycle performs poorly (as in conditions like chilling or low CO₂ availability) results in severe photo-inhibition of PSI (Havaux and Davaud, 1994; Terashima et al., 1994; reviewed in Sonoike, 2011 and in Scheller and Haldrup, 2005) through the oxidative destruction of the iron-sulfur clusters (Sonoike et al., 1995). Photosynthetic organisms can respond to this harmful situation by slowing down cyt *b₆f* activity, through “photosynthetic control” (Rumberg and Siggel, 1969; Foyer et al, 2012; Joliot and Johnson, 2011). To fully understand the complexity of photosynthetic regulation by investigating this important process requires measurements of the PSI energy conversion efficiency, and of its acceptor-side and donor-side limitations, i.e. the loss of PSI efficiency due to lack of PSI acceptors or donors, respectively. However, measurements of PSI activity are not as straightforward as for PSII.

Measuring PSI yield with pulse-induced P₇₀₀ absorption changes

PSI is a protein complex embedded in the thylakoid membrane which catalyzes the electron transfer from the special pair P₇₀₀ to the iron-sulfur [4Fe-4S] centers and to the stromal soluble electron carrier [2Fe-2S] ferredoxin (Golbeck, 2007). In 1972, Hiyama and Ke showed *in vitro* that the absorption spectrum of P₇₀₀ changes depending on its redox state (Hiyama and Ke, 1972). The same is true *in vivo* and absorption variation at 705 and 820 nm are mainly due to P₇₀₀ redox state changes (Harbinson and Woodward, 1987). Historically, this property has been used to differentiate between the fractions of PSI with a reduced or oxidized P₇₀₀ that were originally considered as open and closed centers, respectively (Harbinson et al., 1989; Harbinson and Foyer, 1991). Because of the high maximal quantum yield of PSI, close to 1 (Nelson, 2009), the fraction of open PSI centers can be considered as the quantum yield of PSI. In 1994, Klughammer and Schreiber suggested that in some conditions, PSI centers may be closed even though they have a reduced P₇₀₀, because of over-reduction of the PSI acceptor. In these conditions, the fraction of open PSI measured with the Harbinson and Foyer method was overestimated. An advanced method was thus proposed based on P₇₀₀ absorption changes in response to a multiple turnover light pulse (Klughammer and Schreiber, 1994). The rationale behind this method is based on the fact that PSI can be found in three different redox states. Two PSI cofactors are involved in the first stable charge separation: P₇₀₀ and the first stable acceptor, called A hereafter, which corresponds to the PSI iron-sulfur proteins (Malkin and Bearden, 1971; Oh-Oka et al., 1991). To perform a stable charge separation, defined here as transferring an electron from P₇₀₀ to A, a PSI center needs P₇₀₀ to

be reduced and A to be oxidized. These $[P_{700} A]$ PSI centers are thus considered to be open as they are ready to perform a charge separation as soon as the next photon is absorbed. Accordingly, centers in which both P_{700} and A are oxidized, denoted $[P_{700}^+ A]$, or in which both P_{700} and A are reduced, $[P_{700} A^-]$, are considered to be closed, as they will not be able to perform a charge separation. $[P_{700}^+ A]$ centers are called donor-side limited centers because the oxidation of P_{700} in the light reflects a bottleneck in the electron transfer upstream of PSI (on the donor side).

Under a given light irradiance, the donor-side limited fraction can be measured straightforwardly with absorption difference spectroscopy as the fraction of oxidized P_{700} , called Y(ND). It should be noted that the centers in which P_{700} is oxidized and A is reduced, $[P_{700}^+ A^-]$ would also be considered to be donor-side limited. The difficulty stems from the distinction between the fraction of open centers, called Y(I) or Φ I, and the fraction of $[P_{700} A^-]$ centers, called Y(NA), because both have a reduced P_{700} . The latter are called acceptor-side limited centers because the reduction of both cofactors in the light reflects a bottleneck in the electron transfer downstream of PSI (on the acceptor side). To avoid confusion, we will use $Y(I)_{P_{700}}$ and $Y(NA)_{P_{700}}$ hereafter when referring to estimations of the PSI yield and acceptor-side limitation with the P_{700} pulse method, while reserving the notation Y(I) and Y(NA) for the true values of the PSI yield and acceptor-side limitation, respectively. Klughammer and Schreiber reasoned that the acceptor-side limited centers cannot perform charge separation whatever the light intensity and therefore calculated $Y(NA)_{P_{700}}$ as the fraction of centers whose P_{700} is not photo-oxidizable by a multiple turnover pulse of very intense light. By deduction, open centers are therefore defined as centers with reduced but photo-oxidizable P_{700} , i.e. $Y(I)_{P_{700}} = 1 - Y(NA)_{P_{700}} - Y(ND)$.

An internal contradiction in the P_{700} pulse method

For all photo-oxidizable P_{700} to be oxidized despite being rapidly reduced by plastocyanin or other secondary donors like cytochrome c_6 ($t_{1/2} \approx 5 \mu\text{s}$ if the secondary donor is already fixed, otherwise $t_{1/2} \approx 200 \mu\text{s}$, Hippler et al., 1997), according to Klughammer and Schreiber “the light pulses must be sufficiently long to allow several PSI turnovers, such that the immediate donor pool is emptied during a pulse”. When all secondary donors are oxidized, the P_{700} reduction rate does indeed become limited by the rate of electron transfer through cyt b_6f ($t_{1/2} \approx 10 \text{ ms}$), slowing down the re-reduction of P_{700} by 2 to 3 orders of magnitude. A sufficiently strong light pulse would therefore allow all photo-oxidizable P_{700} to be probed.

However, an explicit assumption of this method is that “at least during the early phase of a saturation pulse, the oxidation of the donor side is more pronounced than the reduction at the acceptor side. For this reason, it appears unlikely that a reaction center in the state $P_{700} A$ is converted into the state $P_{700} A^-$ during the first milliseconds of a saturating light pulse”. These two hypotheses are clearly contradictory. PSI photochemistry and charge conservation dictate that electrons extracted on the donor side are transferred to the acceptor side. If several photochemical events are allowed to oxidize several secondary donors, then several electrons will be transferred through PSI, modifying the redox state of the acceptors. For this reason, we are concerned that the pulse-method could overestimate the acceptor-side limitation, $Y(NA)_{P700} > Y(NA)$, and underestimate the fraction of open PSI centers $Y(I)_{P700} < Y(I)$, when the pool of PSI donors is large.

Electro-chromic shift as an alternative method to measure PSI yield

Why not use a single turnover flash instead of a multiple turnover pulse? The single turnover flash, which can be produced with a laser, is routinely favored in photophysiology studies (e.g. Junesch and Graber, 1987; Joliot and Delosme, 1974). It would have the advantage of allowing all open PSI to perform one - and only one - charge separation without perturbing the state of the acceptor side. Unfortunately, the charge recombination between P_{700}^+ and A^- , when A (the pool of iron sulfur clusters) is reduced, has the same kinetics as the electron transfer from a secondary donor to P_{700}^+ (Warren et al., 1990). Both processes will give the same output in terms of the amplitude of the flash-induced P_{700} oxidation and/or its relaxation kinetics, making P_{700} unsuited as a variable for distinguishing between open centers and acceptor-side limited centers after a single turnover flash. However, there is at least one clear difference between a charge separation stabilized by the electron transfer from secondary donors to P_{700} and a charge separation followed by a charge recombination: in the first case, a positive charge remains in the lumen, but in the second case the charge is cancelled. The electric field across the thylakoid can be probed *in vivo* by monitoring the electro-chromic shift (ECS) of the photosynthetic pigments (Witt, 1979; Bailleul et al., 2010). This phenomenon which is a special case of the Stark effect (Stark, 1914) stems from the shift in the absorption spectrum of some of the photosynthetic pigments embedded in the thylakoid membrane when photosynthetic activity generates an electric field (a component of the pmf) across the thylakoid. ECS could in principle indicate the proportion of PSI centers that are open by quantifying the stable electric field generated by a saturating single turnover flash.

Despite the inherent contradiction mentioned earlier, the P_{700} pulse method has been widely used to investigate many aspects of photosynthesis, e.g. PSI photo-inhibition (e.g. Brestic et al., 2015; Zivcak et al., 2015), photosynthetic control (e.g. Weis et al., 1987), ferredoxin oxidation pathways (e.g. Voss et al., 2008), responses to cold temperatures (e.g. Suzuki et al., 2011; Wang et al., 2013) or cyclic electron flow (e.g. Laisk et al., 2010; Talts et al., 2007; DalCorso et al., 2008; Kono et al., 2014; Kou et al., 2015). Commercial measurement devices have been developed on this basis, like the Dual-Pam distributed by Walz (Germany) and the P_{700} pulse method has become the standard methodology to probe PSI activity. The authors of the original paper acknowledged that since “an alternative, proven method for ΦI determination is lacking, only indirect evidence for the correctness and general applicability of the proposed approach can presently be given” (Klughammer and Schreiber, 1994). We believe that measuring the stable electric field (stabilized charge separation) induced by a single turnover flash with ECS is such an alternative method to probe the fraction of open centers. It has the advantage of clearly distinguishing charge recombination events occurring in acceptor-side limited centers (the electric field relaxes in hundreds of μs) and stabilized charge separation in open centers (the electric field remains stable). In this work, we have compared estimates of the fraction of PSI open centers by measuring P_{700} oxidation after a multiple turnover pulse and ECS generated by a single turnover flash. We observed that whenever a significant $Y(NA)_{P_{700}}$ is measured at the end of the pulse, the P_{700} pulse method overestimates the acceptor-side limitation and therefore underestimates the fraction of PSI open centers by up to ten-fold in our dataset. We show that the overestimation is proportional to $(1-Y(NA)_{P_{700}})$ as expected based on theoretical calculations, and a simple formula can therefore be applied to the P_{700} pulse method to correct measurements of $Y(I)$. We propose that potentially erroneous literature on photosynthetic regulation is reappraised and corrected.

Material and methods

Strains, growth and sampling. *Chlamydomonas reinhardtii* wild type laboratory strain T222 and the $pc3.1^+$ mutant strain were obtained from the Chlamystation (<http://chlamystation.free.fr/>). *Arabidopsis thaliana* Col-0 was a kind gift from Dr Fredy Barneche and Menuu Singla (Ecole Normale Supérieure, Paris, France). The dinoflagellate *Amphidinium carterae* (RCC1522) was obtained from the Roscoff Culture Collection (<http://roscoff-culture-collection.org/>). *Chlamydomonas* cells were grown in Tris-acetate-

phosphate (TAP) medium (Harris, 2009) at 25°C under continuous light provided by white LEDs and were harvested when the cell density was between 2 and 6 million cells per mL. The light irradiance was 30 $\mu\text{mol photons m}^{-2} \text{s}^{-1}$ for the wild type and 10 $\mu\text{mol photons m}^{-2} \text{s}^{-1}$ for the light-sensitive *pc3.1*⁺. *A. thaliana* was grown at 22°C with an 8-hr light/16-hr dark photoperiod at a light intensity of 100 $\mu\text{mol photons m}^{-2} \text{s}^{-1}$. Leaves were harvested at the rosette stage (5 weeks after germination). *Am. carterae* was grown in enriched seawater/artificial water (Berges, Franklin, and Harrison 2001) at 19°C under a 12-hr photoperiod at a light intensity of 30 $\mu\text{E m}^{-2} \text{s}^{-1}$ using fluorescent tubes. Cells were harvested in the exponential growth phase when the cell density was between 80 000 and 200 000 cells per mL.

For photosynthetic measurements, liquid cultures of *C. reinhardtii* or *Am. carterae* were concentrated by centrifugation (4 min at 3500 rpm) and resuspended in their supernatant to a density of $\sim 10^7$ or 10^6 cells mL^{-1} , respectively. Ficoll® was added at 5 to 10 % (volume-to-volume) to prevent drifts in the absorption measurements due to sedimentation of the cells. Concentrated samples were then stirred at 350 rpm under 10 $\mu\text{E m}^{-2} \text{s}^{-1}$ white light for at least 30 min before starting measurements.

Inhibitors/chemicals. Hydroxylamine (HA), (3,4-dichlorophenyl)-1,1-dimethylurea (DCMU), methylviologen (MV), dibromo-6-isopropyl-3-methyl-1,4-benzoquinone (DBMIB), glucose and glucose oxidase were obtained from Sigma Aldrich. DCMU and DBMIB were diluted in ethanol. HA, MV, glucose and glucose oxidase were diluted in distilled water. PSII was inhibited with 10 μM DCMU and 100 to 500 μM HA (for each experiment, the minimal concentration to reach maximal fluorescence in the dark was determined and used). When necessary, anoxic conditions were induced by addition of 20 mM glucose and glucose oxidase ($\sim 280 \text{ U mL}^{-1}$) in brimful, tightly closed cuvettes. MV at a concentration of 4 mM was added to the microalgae sample or infiltrated into leaves 4 min before measurements to allow it to fully infiltrate the stroma. To compare leaf samples with and without MV, we used two pieces of the same leaf, sampled symmetrically across the leaf axis. MV did not seem to release acceptor-side limitation in the dinoflagellate *Am. carterae*.

In vivo spectroscopy. All spectroscopic measurements were performed using a Joliot Type Spectrophotometer (JTS10, Biologic, Grenoble, France) so fluorescence and absorption difference were measured on the same sample. The actinic continuous light and the saturating pulse (5000 $\mu\text{mol photons m}^{-2} \text{s}^{-1}$, corresponding to ~ 2200 photons per PSI per second) were

provided by orange LEDs (630 nm) and the saturating laser flash was provided by a dye laser (690 nm) pumped with a Nd:YAG laser (6 ns duration, 532 nm).

For fluorescence, detection pulses were provided by a white LED with a blue filter (470 nm). Reference and measuring photodiodes were protected from actinic light with a BG39 Schott filter (Mainz, Germany) and an LPF650+RG665 Schott filter, respectively. PSII maximal quantum yield was calculated as $F_v/F_m = (F_m - F_0)/F_m$, where F_0 is the fluorescence level in the dark-adapted (for 1 min) sample and F_m is the maximal fluorescence levels obtained after a saturating light pulse in dark-adapted sample. These measurements were performed to verify that after DCMU and HA treatment, all PSII centers were closed, i.e. $F_v/F_m = 0$.

To correct for artefacts, all data shown for absorption change measurements (both P_{700} and ECS) are the differences between the measurement in the presence of the actinic light (laser flash, background actinic light or saturating pulse) and the measurement in the absence of actinic light. P_{700} redox changes were measured as the difference in the absorbance changes at 705 and 735 nm to correct for contributions from scattering and plastocyanin absorption changes. Usually, the 810-870 nm region is preferred for probing P_{700} to minimize artefacts due to changes in the fluorescence yields. This was not the case for the protocol used here as we used DCMU and HA to fully close all PSII centers. In these conditions, we found that 705-735 nm and 810-870 nm gave similar results (not shown) but we chose the near far-red region because the signal-to-noise ratios are better. The light-detecting diodes were protected from scattered actinic light with an RG695 Schott filter (Mainz, Germany). We calculated $Y(I)_{P_{700}}$, $Y(NA)_{P_{700}}$ and $Y(ND)$ as described in Klughammer and Schreiber (1994). To normalize the output, we realized that the maximal absorption change corresponding to the oxidation of 100% of P_{700} was not reached with common protocols described in the literature (i.e. using far-red light or a saturating DCMU concentration). The absorption change corresponding to 100% P_{700} oxidation was reached by adding a saturating laser flash to a few ms of a saturating pulse in the presence of the cyt b_6f inhibitor DBMIB (1 μ M) and the PSI electron acceptor MV. Electro-chromic shift (ECS) signals were measured as the difference in the absorbance changes at 520 and 546 nm for *C. reinhardtii* and *A. thaliana* or at 563 nm for *Am. carterae*. These wavelengths were chosen to eliminate absorption changes related to c-type cytochromes. The detection wavelengths were provided by a white LED with appropriate interferential filters (10 nm full width at half-maximum, Edmund Optics). The measuring and reference photodiodes were protected from scattered and transmitted actinic light by a BG39 Schott filter (Mainz, Germany). All ECS data were normalized to the ECS increase produced by a

single-turnover saturating flash in the presence of DCMU and HA in dark-adapted cells, and results are therefore expressed as charge separation per PSI. The fraction of open PSI centers, $Y(I)_{ECS}$, was calculated as the ratio between the ECS increase induced by the saturating flash in the condition of interest and that in dark-adapted samples.

Results

We aimed to test the validity of the P_{700} pulse method by comparing it to an alternative ECS-based method. The principles by which the two methods can be used to estimate the fraction of open PSI centers are presented in Fig. 1A (see also Methods). For initial validation studies, we decided to use the green alga *Chlamydomonas reinhardtii* instead of higher plant leaves, because it is easier to use chemicals with liquid cell cultures as samples are more homogeneous and results readily reproducible. In all experiments, (3,4-dichlorophenyl)-1,1-dimethylurea (DCMU) and hydroxylamine (HA) were added to the cells in order to fully inhibit PSII. In these conditions the flash-induced ECS only reflects the contribution from PSI. We first varied the fraction of open PSI centers, or PSI yield, by modulating the light intensity. In these conditions, the PSI yield is determined by the rate of photon absorption by PSI and the rate of the CEF around PSI. After photosynthesis reached its steady-state rate, we measured the PSI yield with the ECS-based method, $Y(I)_{ECS}$, and with the P_{700} pulse method, $Y(I)_{P700}$. As expected, the PSI yield measured with both methods (see Methods) decreased with increasing light irradiance, reflecting the fact that CEF saturates under relatively low irradiance, but not in the first two irradiance conditions for $Y(I)_{P700}$ (Fig. 1 B-C).

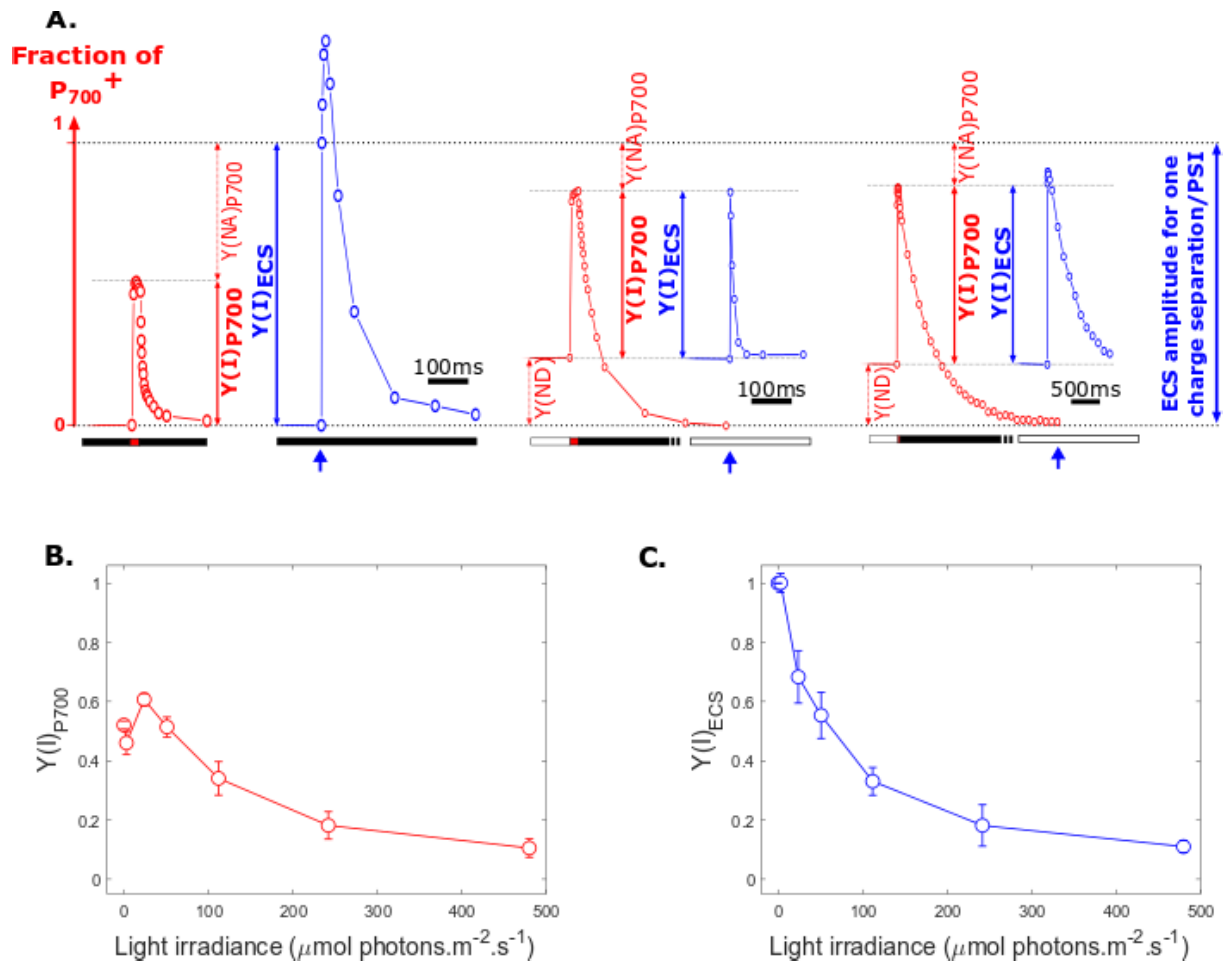


Figure 1 Light dependency of the fraction of open PSI centers in *C. reinhardtii* estimated with ECS (blue) and P_{700} (red) methods

Experiments were carried out in oxic conditions and PSII was inhibited with DCMU (10 μM) and HA (saturating concentrations, see Material and methods). (A) Examples of ECS (blue) and P_{700} (red) kinetics. Experiments were carried out in the dark or on top of a background light. A single turnover laser flash (for ECS) or a multiple turnover saturating pulse of light (for P_{700}) was applied after steady state was reached and the flash-induced absorption change (ECS) or the maximal absorption change during the pulse (P_{700}) was used to estimate the fraction of open PSI centers ($Y(I)_{ECS}$ or $Y(I)_{P_{700}}$). Blue arrows represent the single turnover laser flash. White, black and red bars represent light, dark and multiple turnover saturating pulse of light, respectively. The acceptor and donor side limitation, $Y(NA)$ and $Y(ND)$, are calculated as in (Klughammer and Schreiber, 1994) and shown on the panels. Left: in dark-adapted cells, without MV. Middle: under a 26 $\mu\text{mol photons m}^{-2} \text{s}^{-1}$ background light without MV. Right: in the presence of MV (4 mM), under a 3 $\mu\text{mol photons m}^{-2} \text{s}^{-1}$ background light. (B and C) Light dependency of $Y(I)_{P_{700}}$ (B) and $Y(I)_{ECS}$ (C) under steady-state illumination. Data of B and C are the average (\pm SD) of 3 biological replicates.

Discrepancy between ECS and P_{700} based measurements of PSI yield

Results from the two methods were plotted against each other (Figure 2A). In most light conditions, the two methods produce the same results. The notable exceptions are the first two irradiance conditions, i.e. in the dark (see also Figure 1A right) and at 3 $\mu\text{mol photons m}^{-2} \text{s}^{-1}$, the lowest irradiance tested which corresponds to ~ 2 photons per PSI per second (see Methods). In these two conditions, the PSI yield based on ECS, $Y(I)_{ECS}$, is close to 1 which is

equivalent to ~100% PSI centers being open. The $Y(I)_{P700}$ is ~0.5 in these two conditions, meaning that the P_{700} pulse method measures only 50% of PSI centers as being open. At light intensities of $26 \mu\text{mol photons m}^{-2} \text{s}^{-1}$ and higher, no discrepancy was measured once a steady state was achieved, i.e. after at least 3 minutes of illumination (Figure 2A). However, even under light intensities for which the two methods produce similar results in the steady state, a discrepancy was observed at the dark-to-light transition. Figure 2C shows how $Y(I)_{\text{ECS}}$ and $Y(I)_{P700}$, initially as in the dark-adapted situation as described above, change at the onset of irradiance at $800 \mu\text{mol photons m}^{-2} \text{s}^{-1}$. During the transition from dark to light, the PSI yield measured by P_{700} is always lower than the one measured with ECS (Figure 2C).

The discrepancy increases with the level of reduction of PSI acceptors at the end of the pulse

In the absence of acceptor-side limited centers, a situation which can be reached by using the artificial PSI acceptor methylviologen (MV), all reduced P_{700} are photo-oxidizable. In these conditions, $Y(I)$ should be equal to the fraction of reduced P_{700} and should be correctly assessed with the P_{700} pulse method. As expected, in the presence of MV the two methods give the same results (Figure 1A and Figure 2B). In the presence of MV, since electrons are efficiently rerouted towards O_2 on the acceptor side of PSI (Izawa, 1980), CEF is significantly slowed down (Fan et al., 2007). This results in a similar PSI yield for a light intensity 10 times lower (compare middle and right panels in Figure 1A). The agreement between P_{700} and ECS estimations of PSI yield in the absence of acceptor-side limitation was also observed recently in cyanobacteria using phenazine methosulfate as a PSI electron acceptor (Figure 3 in Viola et al., 2019). This consistency between results strongly suggests that there is no intrinsic error or artefact in the methods used, and that the discrepancy in dark and low light or during dark to light transitions is related to the presence of reduced PSI acceptors.

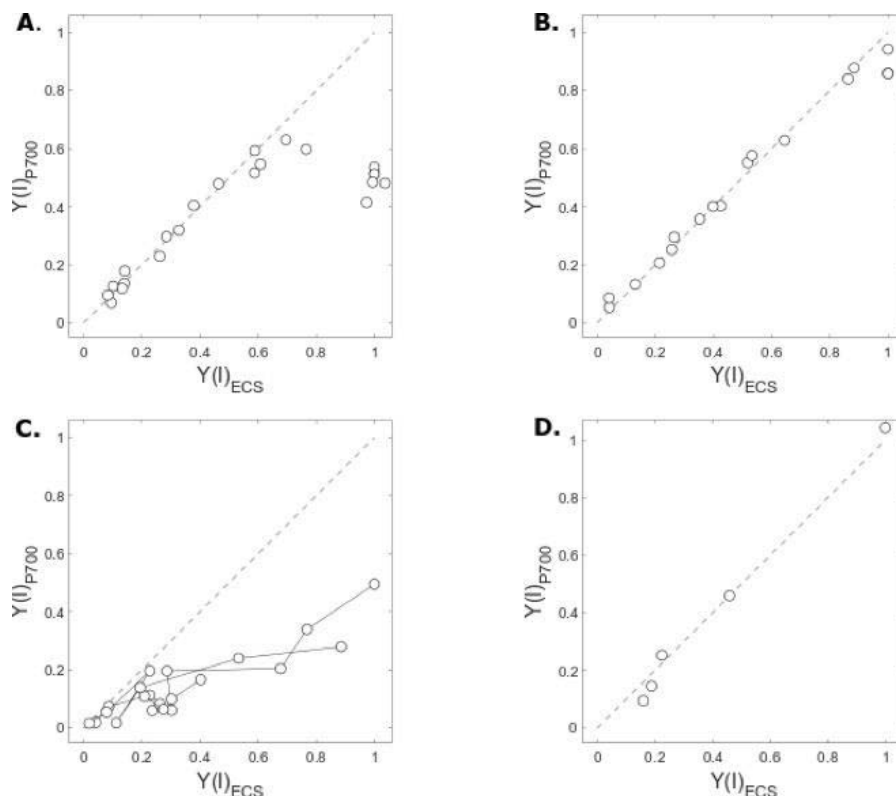


Figure 2 Comparison of the fractions of PSI open centers estimated with ECS and P₇₀₀ methods in *C. reinhardtii* in oxic conditions

PSII were inhibited with DCMU (10 μ M) and HA (saturating concentration, see Material and methods). Experiments were carried out in the absence (A and C) or presence (B and D) of MV (4 mM). (A and B) $Y(I)_{P700}$ plotted as a function of $Y(I)_{ECS}$ at steady state of light for different light intensities. Data points correspond to those shown in Figure 1B and 1C. (C and D) $Y(I)_{P700}$ plotted as a function of $Y(I)_{ECS}$ during the dark-to-light transition at the onset of a 800 μ mol photons $m^{-2} s^{-1}$ light irradiance. Datapoints correspond to measurements at different times during the 700 ms following light onset. Data corresponds to the average (\pm SD) of 3 biological replicates (one for panel D).

To further confirm the causal link between the discrepancy and the level of reduced PSI acceptors, we took the opposite approach by creating conditions in which the acceptor-side limitation is known to be especially high. In anoxic conditions, the reductants produced by glycolysis and the Krebs cycle cannot be re-oxidized by the mitochondrial respiration chain. This reducing power diffuses in the cell via membrane shuttles and results in a reducing pressure in the chloroplast stroma (Hoefnagel et al., 1998). What is more, chloroplast oxidases, like plastid terminal oxidase (Bennoun, 1983; Houilles-Verne et al., 2011; Nawroki et al., 2019) or flavodirion proteins (Chaux et al., 2017), cannot deal with this reducing pressure in the absence of their substrate O_2 . Consequently, anoxia leads to enhanced reducing pressure on PSI acceptors. In dark-adapted anoxic cells, the discrepancy was even higher than in oxic conditions as the $Y(I)_{ECS}$ remained equal to 1 (Figure 3A and C) but the $Y(I)_{P700}$ decreased to a value of ~ 0.3 (Fig 3A and 3D). Again, we compared $Y(I)_{ECS}$ and $Y(I)_{P700}$ in

transitory situations at different times after the onset of different light irradiances. For both methods, the estimated fraction of open PSI centers was very low in the first seconds after the onset of light but increased to reach steady-state values in 1 or 2 minutes. In the steady state the two values were the same but during the transitory phase, $Y(I)_{ECS}$ was systematically higher than $Y(I)_{P700}$ (Figure 3B). The discrepancy at the very onset of light was very strong with initial values of $Y(I)_{ECS} \sim 0.3-0.4$ whereas $Y(I)_{P700}$ was very close to 0 (Figure 3B). It should be noted that assays with MV cannot be done in anoxic conditions, because O_2 is the final electron acceptor in the MV-mediated electron transfer from PSI.

The P₇₀₀ pulse method underestimates PSI yield

With these results, it is clear that one of the estimations of the PSI yield is wrong. Either $Y(I)_{P700}$ underestimates the fraction of open PSI centers or $Y(I)_{ECS}$ overestimates it. As reasoned in the introduction, the discrepancy could arise from an underestimation of $Y(I)_{P700}$ due to the use of a multiple turnover pulse. However, at this stage, we need to demonstrate that $Y(I)_{P700}$ underestimates the fraction of open PSI centers. Looking more closely at the data obtained in dark-adapted anoxic conditions, the two methods give strikingly different results. Is the fraction of open PSI centers 0.3 as given by the P₇₀₀ pulse method, or 1 as ECS indicates? We can answer this question using positive apalogy, or *reductio ad absurdum*. Imagine that the correct value is the one given by $Y(I)_{P700}$ and that ECS method overestimates the PSI yield due to an artefact (e.g. charge recombination not being finished at the time of detection). In that case, after a saturating laser flash, only 30% of PSI will perform a stable charge separation, which will in turn oxidize 0.3 PSI donors (plastocyanin or cytochrome f). After the charge separation is complete, the subsequent turnover of cyt *b₆f* will reduce the PSI donors, giving rise to a second ECS rise, the *b* phase (Joliot and Delosme, 1974; Bailleul et al., 2010). As cyt *b₆f* cannot transfer more electrons than the number of oxidized luminal carriers (i.e. 0.3 electrons), the *b* phase cannot exceed the ECS increase induced by PSI photochemistry. Figure 3C shows the flash-induced ECS kinetics in *C. reinhardtii*, with the characteristic *a* phase (PSI photochemistry here), *b* phase (cyt *b₆f* contribution) and decay phase (due to pmf consumption by CF1FO ATP synthase). The value of the ECS at the end of the *b* phase is 2 ± 0.1 charge separations per PSI, very far from the expected value (~ 0.6) if only 30% of PSI were open. So this scenario is incompatible with our initial hypothesis. If the initial hypothesis is wrong, we conclude that the P₇₀₀ based method does not give a good estimate of the PSI yield. Moreover, an amplitude of 1 for the *b* phase is exactly what is expected if all PSI are open and

perform a stable charge separation after a saturating laser flash as indicated by the ECS-based method. It is to note that such a 1:1 ratio between a and b phases is met in anoxic conditions because (i) the reducing pressure in the chloroplast ensures that the plastoquinone pool is almost fully reduced (Nawrocki et al., 2015) providing enough substrate for $\text{cyt } b_6f$, and (ii) the activity of the CF1F0 ATPase is slowed down sufficiently to ensure that the b phase is not covered by the CF1F0 related ECS decay (Buchert et al., 2017). Finally, the b phase was suppressed in the presence of the $\text{cyt } b_6f$ inhibitor DBMIB, confirming that this second rise in ECS does indeed correspond to the b_6f -catalyzed pumping of protons. We conclude that it is not the $Y(I)_{\text{ECS}}$ which over-estimates the fraction of open PSI centers, but that $Y(I)_{\text{P700}}$ underestimates it.

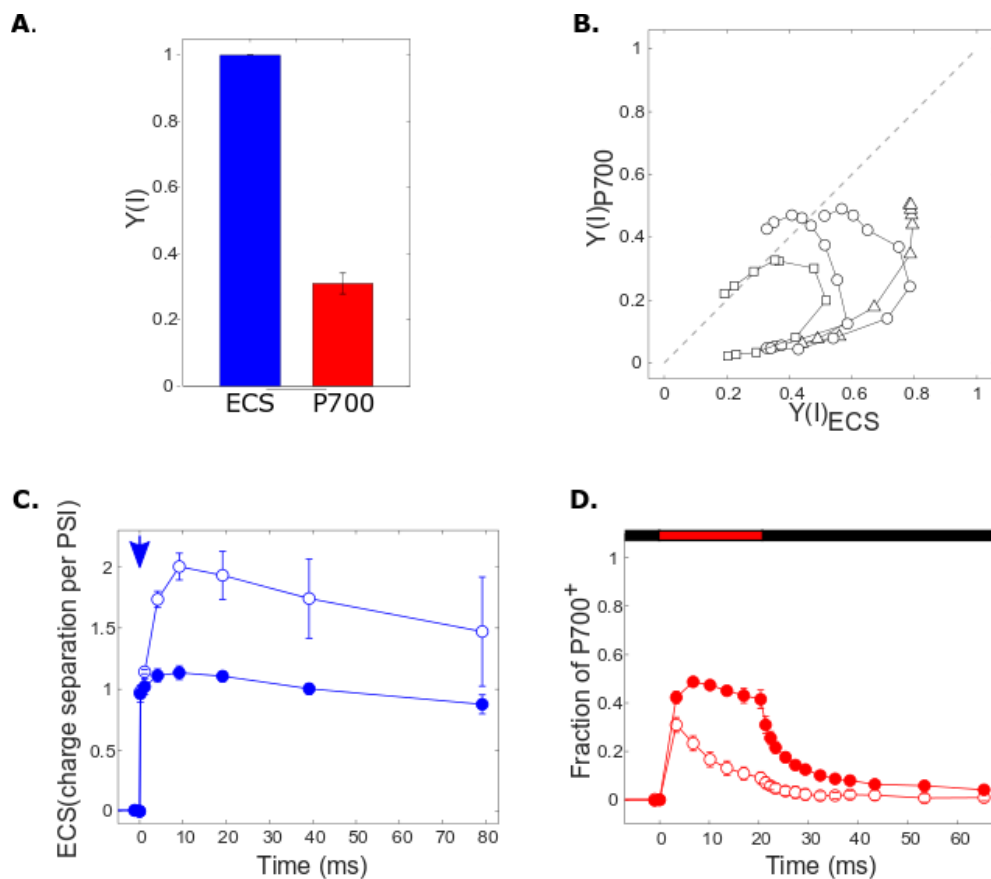


Figure 3 Comparison of the fractions of open PSI centers estimated with ECS and P_{700} methods in *C. reinhardtii* in anoxic conditions

Anoxia was induced by adding glucose (20 mM) and glucose oxidase (280 U.mL⁻¹) (see Material and methods). PSII were inhibited with DCMU (10 μM) and HA (saturating concentration, see material and methods). (A) PSI yield was measured with the two methods in dark-adapted anoxic conditions (B) $Y(I)_{\text{P700}}$ as a function of $Y(I)_{\text{ECS}}$ during the dark-to-light transition in anoxic conditions at different times during the first 3 minutes following the onset of light corresponding to 26 (diamonds), 56 (circles) or 135 (squares) $\mu\text{mol photons m}^{-2} \text{s}^{-1}$. (C) Flash-induced ECS kinetics was measured from dark adapted anoxic conditions in the absence (open circles) or presence (closed circles) of DBMIB (5 μM), a $\text{cyt } b_6f$ inhibitor. Blue arrow corresponds to the single turnover laser flash. (D) Kinetics of P_{700} redox changes (open circles). In this panel, oxic conditions (closed circles) are shown as a control. Black and red horizontal bars correspond to darkness and multiple turnover saturating pulse of light, respectively. For all panels, data corresponds to the average (\pm SD) of 3 biological replicates.

The underestimation by the P_{700} pulse method stems from the use of the multiple turnover pulse

The P_{700} pulse method underestimates PSI yield at the expense of $Y(\text{NA})_{P_{700}}$ which indicates that the open [P_{700} A] and acceptor-side limited [P_{700} A⁻] centers are not distinguished. As postulated in the Introduction, this might be the result of using a multiple turnover pulse. If several charge separations are necessary before reaching the maximal oxidation of P_{700} , then several electrons will be transferred to the PSI acceptor side. The fraction of closed PSI centers due to reduction of the acceptor, [P_{700} A⁻], at the end of the pulse will be overestimated compared to before the pulse. Therefore, the measured $Y(\text{I})_{P_{700}}$ will be lower than the actual PSI yield, $Y(\text{I})$. The number of charge separations can be measured by monitoring the electric field or ECS generated during the multiple turnover pulse and comparing it to the one generated by one saturating laser flash. In dark-adapted oxic *Chlamydomonas*, 4 PSI turnovers occur during the pulse before maximal P_{700} oxidation is reached (Figure 4B) which corresponds to 50% of P_{700} (Figure 4A and B). The 4 electrons transferred might have reduced the acceptor side of PSI and generated some [P_{700} A⁻] centers, preventing the full oxidation of P_{700} . When tested in the presence of MV, one more charge separation can occur (Figure 4C) and this allows almost all P_{700} to be oxidized during the pulse (Figure 4A and B). As a control, we used a plastocyanin mutant which can only perform one charge separation because its P_{700} cannot be reduced. In this case, the pulse-induced ECS increase confirms that only one charge separation occurs (Figure 4C), that all P_{700} is oxidized during the pulse (Figure 4A and B), and that the ECS and P_{700} methods give the same result (Figure 4A). This demonstrates that the P_{700} pulse bias comes from the use of a multiple turnover pulse, which makes the fraction of [P_{700} A⁻] at the end of the pulse higher than that before the pulse.

We investigated whether the discrepancy measured in *C. reinhardtii* is also observed in other photosynthetic species. In the dark, the fraction of open PSI centers should not depend on the activity of other photosynthetic complexes, so we could compare different strains and species, independently modifying the donor and acceptor pool size by adding chemicals. We measured $Y(\text{I})_{\text{ECS}}$ and $Y(\text{I})_{P_{700}}$ in dark-adapted leaves of *Arabidopsis thaliana* and in the dinoflagellate *Amphidinium carterae*. In both cases, we observed the same trend: $Y(\text{I})_{\text{ECS}}$ was higher than $Y(\text{I})_{P_{700}}$. Like in *C. reinhardtii*, there was no discrepancy in *A. thaliana* in the presence of MV (Figure 4). Equivalent data with MV in the dinoflagellate *Am. carterae* was not obtained because we did not detect any effect of MV in this species.

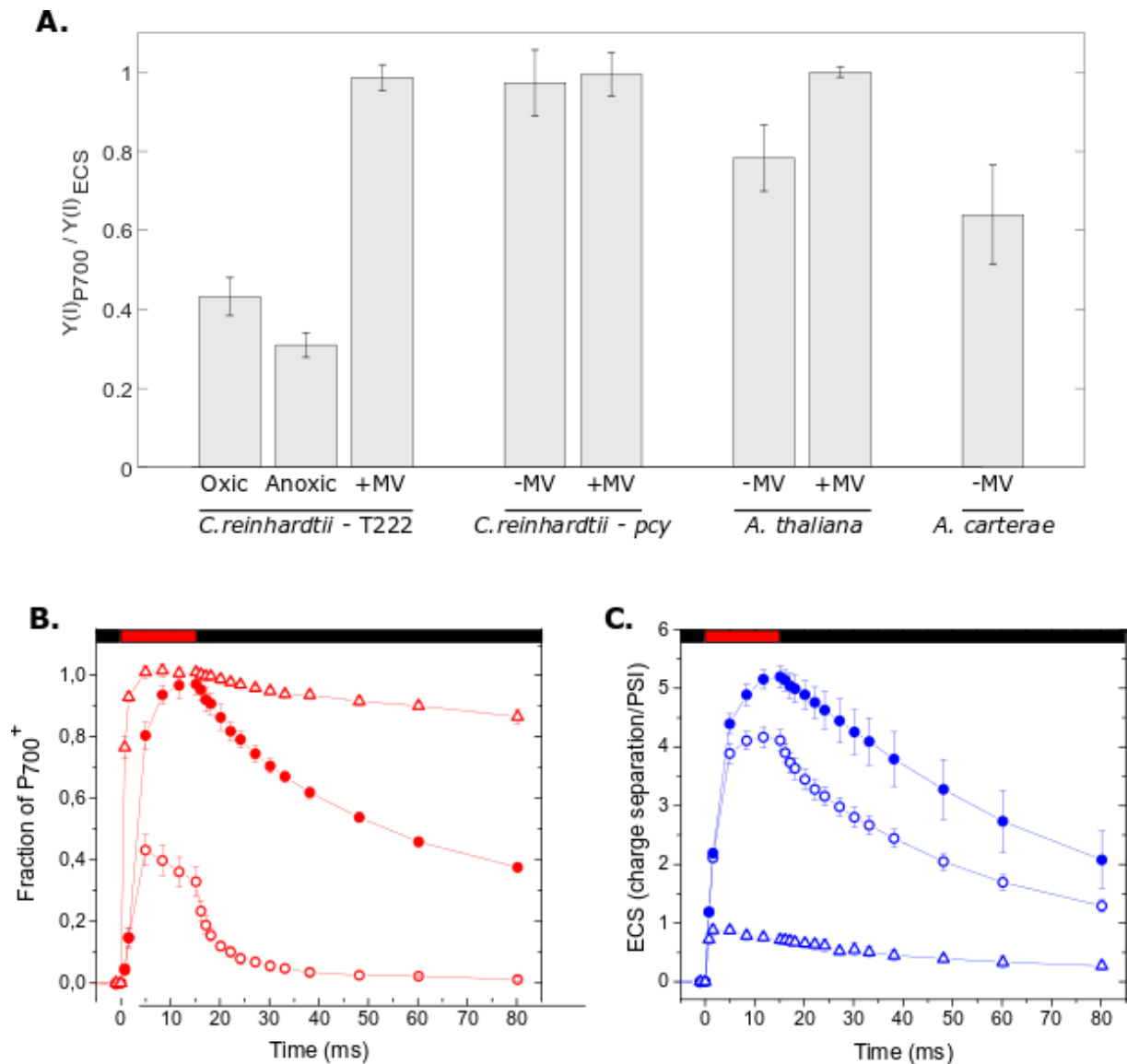


Figure 4 Comparison of the fractions of open PSI centers estimated with ECS and P_{700} methods in dark-adapted conditions in different photosynthetic organisms

PSII were inhibited with DCMU (10 μ M) and HA (saturating concentration, see Material and methods). When needed, anoxia was induced by adding glucose (20 mM) and glucose oxidase (280 U. mL^{-1}) (see Material and methods). (A) ECS and P_{700} based PSI yield in the green alga *Chlamydomonas reinhardtii*, the higher plant *Arabidopsis thaliana* and the dinoflagellate *Amphidinium carterae*. T222, wild type; *pcy*, plastocyanin mutant; +MV (4 mM), methylviologen. (B and C) Kinetics of P_{700} (B) and ECS (C) during and after the multiple turnover saturating light pulse in *C. reinhardtii* wild-type, with (closed circles) and without (open circles) MV (4 mM) and in the plastocyanin mutant without MV (triangles). Black and red horizontal bars correspond to darkness and multiple saturating light pulses, respectively. For all panels, data corresponds to the average (\pm SD) of 3 biological replicates.

Figure 5A sums up all the data presented in Figures 1, 2 and 3 where the ECS and P_{700} methods were compared. We used a color code based on the $Y(\text{NA})_{P700}$ parameter from the Klughammer and Schreiber (K&S) method, which in their original work was intended to measure the acceptor-side limited centers. In all the situations where the $Y(\text{NA})_{P700}$ is low

there is a good agreement between the two methods (darker blue points), whereas all the situations with a discrepancy between the two methods correspond to high $Y(\text{NA})_{P700}$ (darker red points). This is true for the measurements in aerobic steady-state illumination (Supplementary Figure 1A), where only the dark and $3 \mu\text{mol photons m}^{-2} \text{ s}^{-1}$ points show a significant $Y(\text{NA})_{P700}$ and a discrepancy between the two methods. When light is switched on, both in oxic and anoxic conditions, the discrepancy decreases with time concomitant with a decrease of $Y(\text{NA})_{P700}$ (Supplementary Figure 2A and 3). This strongly supports our initial concern that the multiple turnover pulse over-reduces PSI acceptors during the pulse, leading to an overestimation of the acceptor-side limitation at the expense of the PSI yield. In agreement with this, both the $Y(\text{NA})_{P700}$ and the discrepancy are annulled with the addition of MV (Supplementary Fig 1B and 2B).

Rationalizing the PSI yield underestimation by the P_{700} pulse method

Can we rationalize the degree by which PSI yield is underestimated when a multiple turnover pulse is used in the P_{700} method and hence correct for the inherent bias? For this, it is necessary to return to the internal contradiction enounced in the Introduction. In the original description of the K&S method, the authors state that a multiple turnover pulse is necessary to oxidize all PSI secondary donors and P_{700} (Klughammer and Schreiber, 1994). What happens during the pulse? The hypothesis was that all initially open centers become donor-side limited during the pulse, i.e. no PSI are closed on the acceptor side during the pulse. This is very unlikely in conditions where the activity of PSI is strongly limited by a downhill step, i.e. when the initial pool of acceptors is small and/or the initial pool of PSI donors is large. As demonstrated before, this assumption proves wrong. Another extreme case scenario is to consider that the pulse generates only acceptor-side limited centers, i.e. the amount of donor-side limited centers is unchanged. This would be extremely unlikely in conditions where the activity of PSI is strongly limited by an uphill step, i.e. the donor-side limitation [$P_{700}^+ \text{ A}$] is high. So what kind of reasonable assumption can one make regarding the amount of acceptor-side and donor-side limited centers that the pulse will generate? We propose that the most parsimonious hypothesis is to consider that the ratio of acceptor-side to donor-side limited centers at the end of the pulse will be equal to the ratio preceding the pulse. From there, one can calculate the true $Y(\text{I})$ from the P_{700} pulse measurements and estimate the degree of underestimation due to the assumption that all open PSI centers become donor-side limited during the pulse (see Appendix 1 for calculations). If our simple assumption holds true, then

$Y(I)_{P700}$ should underestimate the true PSI yield proportionally to $Y(NA)_{P700}$. We obtain the following equation: $Y(I)_{P700}/Y(I) = 1 - Y(NA)_{P700}$ (equation 4 in Appendix 1). This is exactly the relationship that we obtained experimentally by plotting the ratio between the PSI yield measured by the two methods, i.e. $Y(I)_{P700}/Y(I)_{ECS}$, as a function of the $Y(NA)_{P700}$ (Fig 5B). This validates our hypothesis that the error made by the P_{700} pulse method originates from the erroneous hypothesis that the pulse only generates donor-side limited centers, regardless of the physiological conditions before the pulse.

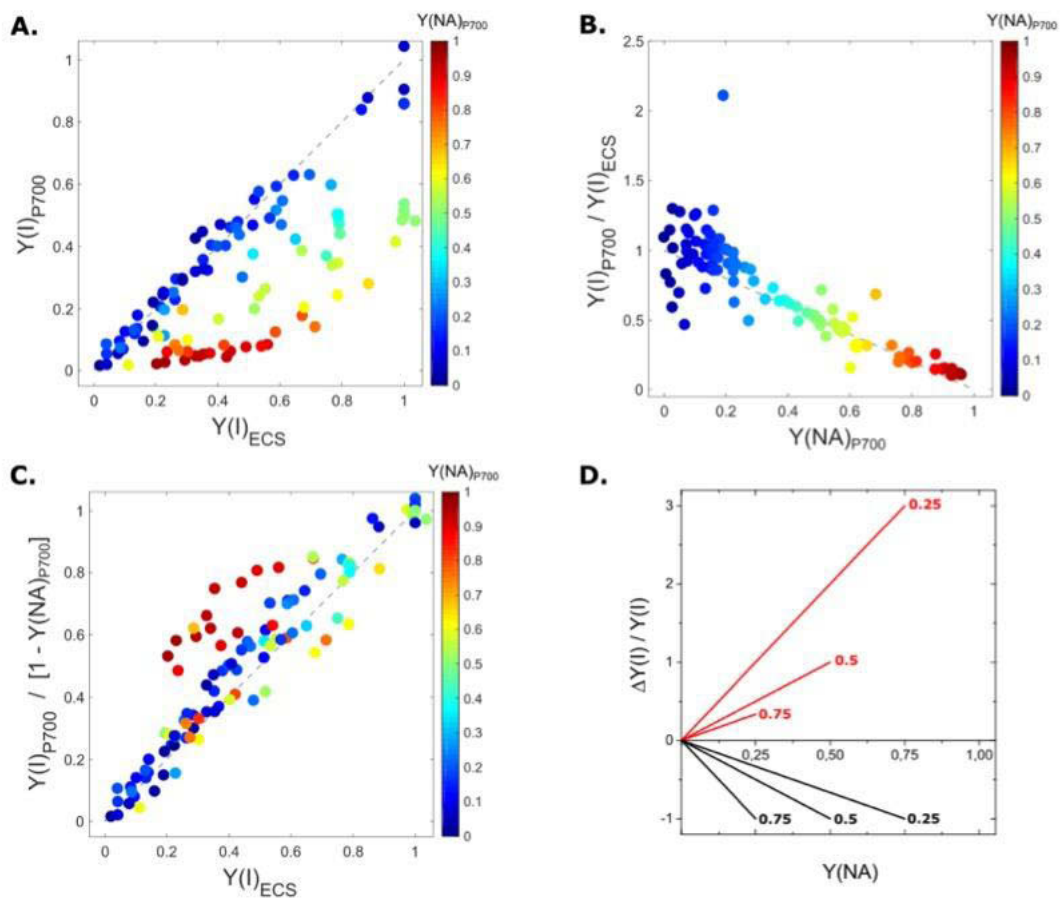


Figure 5 Comparison of the fractions of open PSI centers estimated with ECS and P_{700} methods in *C. reinhardtii*
 For (A), (B) and (C), data from Figures 1, 2 and 3 were used. The color scale on the right represents $Y(NA)_{P700}$ values (i.e. the fraction of P_{700} that are not oxidized during the multiple turnover saturating light pulse). (A) $Y(I)_{P700}$ is plotted as a function of $Y(I)_{ECS}$, (B) The ratio between $Y(I)_{P700}$ and $Y(I)_{ECS}$ is plotted as a function of $Y(NA)_{P700}$. The dashed grey line corresponds to $Y(I)_{P700}/Y(I)_{ECS} = [1 - Y(NA)_{P700}]$. Color scale as in A. (C) The corrected PSI yield $Y(I)_{P700} = Y(I)_{P700} / [1 - Y(NA)_{P700}]$ is plotted as a function of $Y(I)_{ECS}$. The color scale on the right represents $Y(NA)_{P700}$ values (D) Expected relative error of the $Y(I)$ based on the P_{700} pulse method (black) and the Harbinson and Foyer method (red) as a function of the real acceptor side limitation, $Y(NA)$. In each case the expected relationships for $Y(I)$ values of 0.25, 0.5 and 0.75 are shown (see text and Appendix 1).

Discussion

Comparing the PSI parameters estimated based on the P_{700} pulse method with an alternative approach based on ECS allowed us to demonstrate that the P_{700} pulse method underestimates the PSI yield when a significant $Y(\text{NA})_{P_{700}}$ is measured, i.e. when there is an acceptor-side limitation at the end of the pulse. The underestimation went as high as a factor 10 in our dataset (Figure 5B). When a multiple turnover pulse is used and the initial pool of PSI donors is large, several electrons will be transferred to the PSI acceptors during the pulse. The amount by which the PSI yield is underestimated is proportional to $Y(\text{NA})_{P_{700}}$, a dependency that we were able to predict with the following simple assumption. The multiple turnover pulse generates both acceptor-side and donor-side limited PSI centers at a ratio which remains the same as before the pulse. This assumption simply means that the “capacity” for oxidation of PSI acceptors and the “capacity” for reduction of PSI donors do not change within the few ms of the pulse.

Early approaches to assessing PSI yield based on P_{700} measurements considered that all PSI with reduced P_{700} were open (Harbinson and Foyer, 1991). The P_{700} pulse method was developed as an improvement on those approaches, allowing open and acceptor-side limited PSI centers to be distinguished. In conditions where all P_{700} are photo-oxidizable, i.e. $Y(\text{NA})$ is 0, both approaches prove right. As soon as there is a fraction of acceptor-side limited centers, both methods prove wrong and the K&S method cannot be considered as an improvement on the Harbinson and Foyer (H&F) method. This can be clearly visualized in Figure 5D, which displays the relative error of $Y(\text{I})$ estimated by the P_{700} pulse method and by the H&F method, as a function of the true acceptor-side limitation, i.e. the fraction of $[P_{700} \text{ A}^-]$ centers or $Y(\text{NA})$. In both cases, the relative error is proportional to the acceptor-side limitation, but the H&F method naturally overestimates $Y(\text{I})$ whereas the K&S method underestimates it. The slope depends on the (true) PSI yield. For a $Y(\text{I})$ of 0.5, the relative errors made by the H&F and K&S methods mirror each other. However, a major difference is that the dependency between the error and the acceptor-side limitation increases with $Y(\text{I})$ in the case of K&S method (the slope is $(1-Y(\text{I}))^{-1}$, see Appendix 1), but decreases with $Y(\text{I})$ in the case of H&F method (the slope is $Y(\text{I})^{-1}$, see Appendix 1).

The good news is that as the underestimation of the PSI yield with the P_{700} pulse method is proportional to the $Y(\text{NA})_{P_{700}}$ a correction can be made. The correct value for $Y(\text{I})$ can be calculated from the parameters derived from the P_{700} pulse method: $Y(\text{I}) = Y(\text{I})_{P_{700}} / (1 - Y(\text{NA})_{P_{700}})$. When such correction is done, the comparison between the corrected PSI yield

and $Y(I)_{ECS}$ are in very close agreement (Fig 5C), i.e. the ratio becomes 1 as expected (Sup Fig 4), except for the data points for which the $Y(NA)_{P700}$ is higher than 0.8. For those data points, the correction is very prone to small errors as both $Y(I)_{P700}$ and $(1-Y(NA)_{P700})$ are small numbers.

Revisiting 25 years of research base on the P_{700} pulse method, covering many aspects of photosynthesis, will be a challenge. The values of PSI yield measured in dark-adapted photosynthetic samples are good examples of the errors that have been recorded and propagated in the literature. It is clear that given the ambient redox potential in a dark-adapted chloroplast, P_{700} should be fully reduced (the redox potential of P_{700} being 430 mV, Kok, 1961; Sétif and Mathis, 1980) and A should be fully oxidized (the redox potential of iron-sulfur centers being in the -520 to -705 mV range, (Golbeck and Bryant, 1991; Golbeck, 1993). Therefore the PSI yield in the dark should be equal to 1. This is not what the P_{700} pulse method shows. We obtained $Y(I)_{P700}$ values of ~ 0.8 in *A. thaliana* leaves, ~ 0.5 in *C. reinhardtii* and ~ 0.6 in *Am. carterae*. In the literature, $Y(I)_{P700}$ is 0.8 in dark-adapted *A. thaliana* leaves (Kono et al., 2018), 0.8-0.9 in sunflower leaves (Klughammer and Schreiber, 1994; Sejima et al., 2014), 0.7 in barley leaves (Pfündel et al., 2008), 0.5 in pea leaves (Schansker et al., 2003), 0.8 in wheat leaves (Brestic et al., 2015; Zivcak et al., 2015), 0.3-0.42 in *Jatropha curcas* L (Ranjan et al. 2014), 0.65 in *Microsorium punctatum* and 0.55 in *Paraleptochillus decurrens* (Wang et al. 2013). Similar low values of $Y(I)_{P700}$ in dark-adapted photosynthetic organisms have been documented in the angiosperm *Ipomoea nil* and in the cyanobacterium *Synechococcus elongatus* PCC 7942 (Shimakawa et al., 2019).

The literature regarding CEF, and especially the deduced role of the *A. thaliana* proton gradient regulator 5 (PGR5) and proton gradient regulator-like 1 (PGRL1) proteins in this process, might have also been strongly affected by the errors inherent in the P_{700} pulse method. Indeed, one of the main arguments in favor of a role of these proteins in CEF comes from the measurement of a lower $Y(I)_{P700}$ and a higher $Y(NA)_{P700}$ in the *pgrl1* and *pgr5* mutants compared to the wild type (e.g. DalCorso et al., 2008; Kono et al., 2014; Kou et al., 2015). These observations have been interpreted as the signature of a lower CEF rate, leading to acceptor-side limitation. The limitations of the K&S method demonstrated here invalidate this conclusion. It would be wise to reappraise the literature on CEF in a timely way and correct any relevant data as we propose here. Going forward this would increase the robustness and precision of experimental data and give a more accurate view of how the light phase of photosynthesis is regulated in all its diversity.

Acknowledgements

We would like to thank Fredy Barnèche and Meenu Singla for their technical help growing *Arabidopsis thaliana*. We would also like to thank Stefano Santabarbara, Helmut Kirchhoff, Anja Krieger-Liszky and Pierre Sétif for fruitful discussions and Anja Krieger-Liszky for access to the Dual-PAM. B.B. and S.F. acknowledge financial support from the European Research Council (ERC) under the European Union Horizon 2020 research and innovation program (grant agreement no. 715579). We also thank the Roscoff culture collection for providing the strain of *Am. carterae*.

References

- Allen, J. F.** (2002). Photosynthesis of ATP—electrons, proton pumps, rotors, and poise. *Cell*, *110*(3), 273-276.
- Arnon, D. L., Whatley, F. R., & Allen, M. B.** (1958). Assimilatory power in photosynthesis. *Science*, *127*(3305), 1026-1034.
- Bailleul, B., Cardol, P., Breyton, C., & Finazzi, G.** (2010). Electrochromism: a useful probe to study algal photosynthesis. *Photosynthesis research*, *106*(1-2), 179.
- Baker, N. R.** (2008). Chlorophyll fluorescence: a probe of photosynthesis in vivo. *Annu. Rev. Plant Biol.*, *59*, 89-113.
- Bendall, D. S., & Manasse, R. S.** (1995). Cyclic photophosphorylation and electron transport. *Biochimica et Biophysica Acta (BBA)-Bioenergetics*, *1229*(1), 23-38.
- Bennoun, P.** (1983). Effects of mutations and of ionophore on chlororespiration in *Chlamydomonas reinhardtii*. *FEBS Letters*, *156*(2), 363-365.
- Berges, J. A., Franklin, D. J., & Harrison, P. J.** (2001). Evolution of an artificial seawater medium: improvements in enriched seawater, artificial water over the last two decades. *Journal of phycology*, *37*(6), 1138-1145.
- Brestic, M., Zivcak, M., Kunderlikova, K., Sytar, O., Shao, H., Kalaji, H. M., & Allakhverdiev, S. I.** (2015). Low PSI content limits the photoprotection of PSI and PSII in early growth stages of chlorophyll b-deficient wheat mutant lines. *Photosynthesis research*, *125*(1-2), 151-166.
- Buchert, F., Bailleul, B., Hisabori, T.** (2017). A γ -subunit point mutation in *Chlamydomonas reinhardtii* chloroplast F1Fo-ATP synthase confers tolerance to reactive oxygen species. *Biochimica et Biophysica Acta (BBA)-Bioenergetics*, *1858*(12), 966-974.
- Chaux, F., Peltier, G., Johnson, X.** (2015). A security network in PSI photoprotection: regulation of photosynthetic control, NPQ and O₂ photoreduction by cyclic electron flow. *Frontiers in plant science*, *6*, 875.
- Chaux, F., Burlacot, A., Mekhalfi, M., Auroy, P., Blangy, S., Richaud, P., Peltier, G.** (2017). Flavodiiron proteins promote fast and transient O₂ photoreduction in *Chlamydomonas*. *Plant physiology*, *174*(3), 1825-1836.
- DalCorso, G., Pesaresi, P., Masiero, S., Aseeva, E., Schünemann, D., Finazzi, G., ... & Leister, D.** (2008). A complex containing PGRL1 and PGR5 is involved in the switch between linear and cyclic electron flow in *Arabidopsis*. *Cell*, *132*(2), 273-285.
- Delosme, R., Béal, D., Joliot, P.** (1994). Photoacoustic detection of flash-induced charge separation in photosynthetic systems. Spectral dependence of the quantum yield. *Biochimica et Biophysica Acta (BBA)-Bioenergetics*, *1185*(1), 56-64.
- Duysens, L. N. M.** (1963). Mechanism of the two photochemical reactions in algae as studied by means of fluorescence. *Studies on microalgae and photosynthetic bacteria*, 353-372.
- Eberhard, S., Finazzi, G., Wollman, F. A.** (2008). The dynamics of photosynthesis. *Annual review of genetics*, *42*, 463-515.
- Endo, T., Asada, K.** (2008). Photosystem I and photoprotection: cyclic electron flow and water-water cycle. In *Photoprotection, Photoinhibition, Gene Regulation, and Environment* (pp. 205-221). Springer, Dordrecht.
- Fan, D. Y., Nie, Q., Hope, A. B., Hillier, W., Pogson, B. J., Chow, W. S.** (2007). Quantification of cyclic electron flow around Photosystem I in spinach leaves during photosynthetic induction. *Photosynthesis Research*, *94*(2-3), 347.
- Fan, D. Y., Fitzpatrick, D., Oguchi, R., Ma, W., Kou, J., Chow, W. S.** (2016). Obstacles in the quantification of the cyclic electron flux around Photosystem I in leaves of C₃ plants. *Photosynthesis research*, *129*(3), 239-251.
- Foyer, C. H., Neukermans, J., Queval, G., Noctor, G., Harbinson, J.** (2012). Photosynthetic control of electron transport and the regulation of gene expression. *Journal of Experimental Botany*, *63*(4), 1637-1661.

- Genty B, Goulas Y, Dimon B, Peltier JM, Moya I.** 1992. Modulation of efficiency of primary conversion in leaves, mechanisms involved at PSII. In *Research in Photosynthesis, Volume 4*, ed. N Murata, pp. 603–10. Dordrecht: Kluwer Academic Publishers.
- Golbeck, J. H., & Bryant, D. A.** (1991). Current topics in bioenergetics. In *Light-Driven Reactions in Bioenergetics* (Vol. 16).
- Golbeck, J. H.** (1993). The structure of photosystem I: Current Opinion in Structural Biology 1993, 3: 508–514. *Current Opinion in Structural Biology*, 3(4), 508-514.
- Golbeck, J. H.** (Ed.). (2007). *Photosystem I: the light-driven plastocyanin: ferredoxin oxidoreductase* (Vol. 24). Springer Science & Business Media.
- Harbinson, J., Woodward, F. I.** (1987). The use of light-induced absorbance changes at 820 nm to monitor the oxidation state of P-700 in leaves. *Plant, Cell & Environment*, 10(2), 131-140.
- Harbinson, J., Genty, B., Baker, N. R.** (1989). Relationship between the quantum efficiencies of photosystems I and II in pea leaves. *Plant Physiology*, 90(3), 1029-1034.
- Harbinson, J., Foyer, C. H.** (1991). Relationships between the efficiencies of photosystems I and II and stromal redox state in CO₂-free air: evidence for cyclic electron flow in vivo. *Plant physiology*, 97(1), 41-49.
- Harris, E. H.** (2009). *The chlamydomonas sourcebook* (Vol. 1, pp. 119-157). D. B. Stern, & G. B. Witman (Eds.). San Diego, CA: Elsevier.
- Havaux, M., Davaud, A.** (1994). Photoinhibition of photosynthesis in chilled potato leaves is not correlated with a loss of photosystem-II activity. *Photosynthesis research*, 40(1), 75-92
- Hipler, M., Drepper, F., Farah, J., Rochaix, J. D.** (1997). Fast electron transfer from cytochrome c 6 and plastocyanin to photosystem I of *Chlamydomonas reinhardtii* requires PsaF. *Biochemistry*, 36(21), 6343-6349.
- Hiyama, T., Ke, B.** (1972). Difference spectra and extinction coefficients of P700. *Biochimica et Biophysica Acta (BBA)-Bioenergetics*, 267(1), 160-171.
- Hoefnagel, M. H., Atkin, O. K., Wiskich, J. T.** (1998). Interdependence between chloroplasts and mitochondria in the light and the dark. *Biochimica et Biophysica Acta (BBA)-Bioenergetics*, 1366(3), 235-255.
- Houille-Vernes, L., Rappaport, F., Wollman, F. A., Alric, J., Johnson, X.** (2011). Plastid terminal oxidase 2 (PTOX2) is the major oxidase involved in chlororespiration in *Chlamydomonas*. *Proceedings of the National Academy of Sciences*, 108(51), 20820-20825.
- Izawa, S.** (1980). Acceptors and donors and chloroplast electron transport. In *Methods in Enzymology* (Vol. 69, pp. 413-434). Academic Press
- Joliot, P., Johnson, G. N.** (2011). Regulation of cyclic and linear electron flow in higher plants. *Proceedings of the National Academy of Sciences*, 108(32), 13317-13322.
- Joliot, P., Delosme, R.** (1974). Flash-induced 519 nm absorption change in green algae. *Biochimica et Biophysica Acta (BBA)-Bioenergetics*, 357(2), 267-284.
- Junesch, U., Gräber, P.** (1987). Influence of the redox state and the activation of the chloroplast ATP synthase on proton-transport-coupled ATP synthesis/hydrolysis. *Biochimica et Biophysica Acta (BBA)-Bioenergetics*, 893(2), 275-288.
- Kautsky H, Appel W, Amann H** (1960) Die Fluoreszenzkurve und die Photochemie der Pflanze. *Biochem Z* 332:277–292
- Ke, B.** (2001). The primary electron donor of photosystem I—P700. *Photosynthesis: Photobiochemistry and Photobiophysics*, 463-478.
- Klughammer, C., & Schreiber, U.** (2016). Deconvolution of ferredoxin, plastocyanin, and P700 transmittance changes in intact leaves with a new type of kinetic LED array spectrophotometer. *Photosynthesis research*, 128(2), 195-214.
- Klughammer, C., Schreiber, U.** (1994). An improved method, using saturating light pulses, for the determination of photosystem I quantum yield via P700+ absorbance changes at 830 nm. *Planta*, 192(2), 261-268.

- Kono, M., Noguchi, K., Terashima, I.** (2014). Roles of the cyclic electron flow around PSI (CEF-PSI) and O₂-dependent alternative pathways in regulation of the photosynthetic electron flow in short-term fluctuating light in *Arabidopsis thaliana*. *Plant and Cell Physiology*, 55(5), 990-1004.
- Kou, J., Takahashi, S., Fan, D. Y., Badger, M. R., Chow, W. S.** (2015). Partially dissecting the steady-state electron fluxes in Photosystem I in wild-type and *pgr5* and *ndh* mutants of *Arabidopsis*. *Frontiers in plant science*, 6, 758.
- Laisk, A., Talts, E., Oja, V., Eichelmann, H., Peterson, R. B.** (2010). Fast cyclic electron transport around photosystem I in leaves under far-red light: a proton-uncoupled pathway? *Photosynthesis Research*, 103(2), 79-95.
- Malkin, R., Bearden, A. J.** (1971). Primary reactions of photosynthesis: photoreduction of a bound chloroplast ferredoxin at low temperature as detected by EPR spectroscopy. *Proceedings of the National Academy of Sciences*, 68(1), 16-19.
- Nawrocki, W. J., Tourasse, N. J., Taly, A., Rappaport, F., Wollman, F. A.** (2015). The plastid terminal oxidase: its elusive function points to multiple contributions to plastid physiology. *Annual review of plant biology*, 66, 49-74.
- Nelson, N.** (2009). Plant photosystem I—the most efficient nano-photochemical machine. *Journal of nanoscience and nanotechnology*, 9(3), 1709-1713.
- Oh-Oka, H., Itoh, S., Saeki, K., Takahashi, Y., Matsubara, H.** (1991). FA/FB protein from the spinach photosystem I complex: Isolation in a native state and some properties of the iron-sulfur clusters. *Plant and cell physiology*, 32(1), 11-17.
- Rumberg, B., Siggel, U.** (1969). pH changes in the inner phase of the thylakoids during photosynthesis. *Naturwissenschaften*, 56(3), 130-132.
- Scheller, H. V., Haldrup, A.** (2005). Photoinhibition of photosystem I. *Planta*, 221(1), 5-8.
- Shikanai, T.** (2007). Cyclic electron transport around photosystem I: genetic approaches. *Annu. Rev. Plant Biol.*, 58, 199-217.
- Sonoike, K.** (2011). Photoinhibition of photosystem I. *Physiologia Plantarum*, 142(1), 56-64.
- Sonoike, K., Terashima, I., Iwaki, M., Itoh, S.** (1995). Destruction of photosystem I iron-sulfur centers in leaves of *Cucumis sativus* L. by weak illumination at chilling temperatures. *FEBS letters*, 362(2), 235-238.
- Stark, J.** (1914). Beobachtungen über den Effekt des elektrischen Feldes auf Spektrallinien. I. Quereffekt. *Annalen der Physik*, 348(7), 965-982.
- Suzuki, K., Ohmori, Y., Ratel, E.** (2011). High root temperature blocks both linear and cyclic electron transport in the dark during chilling of the leaves of rice seedlings. *Plant and Cell Physiology*, 52(9), 1697-1707.
- Talts, E., Oja, V., Rämme, H., Rasulov, B., Anijalg, A., Laisk, A.** (2007). Dark inactivation of ferredoxin-NADP reductase and cyclic electron flow under far-red light in sunflower leaves. *Photosynthesis research*, 94(1), 109-120.
- Terashima, I., Funayama, S., Sonoike, K.** (1994). The site of photoinhibition in leaves of *Cucumis sativus* L. at low temperatures is photosystem I, not photosystem II. *Planta*, 193(2), 300-306.
- Voss, I., Koelmann, M., Wojtera, J., Holtgreffe, S., Kitzmann, C., Backhausen, J. E., Scheibe, R.** (2008). Knockout of major leaf ferredoxin reveals new redox-regulatory adaptations in *Arabidopsis thaliana*. *Physiologia plantarum*, 133(3), 584-598.
- Wang, J. H., Li, S. C., Sun, M., Huang, W., Cao, H., Xu, F., ... & Zhang, S. B.** (2013). Differences in the stimulation of cyclic electron flow in two tropical ferns under water stress are related to leaf anatomy. *Physiologia plantarum*, 147(3), 283-295.
- Warren, P. V., Parrett, K. G., Warden, J. T., Golbeck, J. H.** (1990). Characterization of a photosystem I core containing P700 and intermediate electron acceptor A1. *Biochemistry*, 29(28), 6545-6550.
- Weis, E., Ball, J. T., Berry, J.** (1987). Photosynthetic control of electron transport in leaves of *Phaseolus vulgaris*: evidence for regulation of photosystem 2 by the proton gradient. In *Progress in photosynthesis research* (pp. 553-556). Springer, Dordrecht.

Witt, H. T. (1979). Energy conversion in the functional membrane of photosynthesis. Analysis by light pulse and electric pulse methods: The central role of the electric field. *Biochimica et Biophysica Acta (BBA)-Reviews on Bioenergetics*, 505(3-4), 355-427.

Zivcak, M., Brestic, M., Kunderlikova, K., Sytar, O., Allakhverdiev, S. I. (2015). Repetitive light pulse-induced photoinhibition of photosystem I severely affects CO₂ assimilation and photoprotection in wheat leaves. *Photosynthesis research*, 126(2-3), 449-463.

Appendix 1: Theoretical calculation of the error made estimating $Y(I)$ with the P700 pulse method.

Let us consider a situation where the “true” fractions of donor-side limited and acceptor-side limited centers open before the pulse are $[P_{700} A]$, $[P_{700}^+ A]$ and $[P_{700} A^-]$ respectively. By convention, $Y(I) = [P_{700} A]$, $Y(ND) = [P_{700}^+ A]$ and $Y(NA) = [P_{700} A^-]$, and :

$$Y(I) + Y(ND) + Y(NA) = 1 \quad (\text{Equation 1})$$

Let us call $[P_{700} A]_p$, $[P_{700}^+ A]_p$ and $[P_{700} A^-]_p$ respectively the fractions of donor-side and acceptor-side limited centers open at the end of the pulse. The amount of acceptor-side limited centers at the end of the pulse is by definition equal to $Y(NA)_{P700}$, i.e. $[P_{700} A^-]_p = Y(NA)_{P700}$. The amount of donor-side limited centers at the end of the pulse is the sum of the donor-side limited centers before the pulse, $Y(ND)$, and the centers whose P_{700} is oxidized during the pulse, i.e. $[P_{700}^+ A]_p = Y(ND) + Y(I)_{P700}$. All PSI centers are supposed to be closed at the end of the pulse, i.e. $[P_{700} A]_p$ or $[P_{700}^+ A]_p + [P_{700} A^-]_p = 1$, which gives:

$$Y(I)_{P700} + Y(ND) + Y(NA)_{P700} = 1 \quad (\text{Equation 2})$$

What is the relationship between the true $Y(I)$ and $Y(NA)$ and the values calculated with the P_{700} method? We propose a parsimonious hypothesis in which the ratio of acceptor-side limited to donor-side limited centers at the end of the pulse is equal to the ratio before the pulse, i.e. $[P_{700} A^-]_p / [P_{700}^+ A]_p = [P_{700} A^-] / [P_{700}^+ A]$, which gives:

$$Y(NA)_{P700} / (Y(ND) + Y(I)_{P700}) = Y(NA) / (Y(ND) + Y(I)) \quad (\text{Equation 3})$$

Combining equations (1), (2) and (3), we can express $Y(I)_{P700}$ and $Y(NA)_{P700}$ as a function of the true $Y(I)$ and $Y(NA)$:

$$Y(I)_{P700} = Y(I) * Y(ND) / (Y(ND) + Y(NA))$$

$$Y(NA)_{P700} = Y(NA) / (Y(ND) + Y(NA)) = Y(NA) / (1 - Y(I))$$

Inversely, we can express the true $Y(I)$ and $Y(NA)$ as a function of $Y(I)_{P700}$ and $Y(NA)_{P700}$:

$$Y(I) = Y(I)_{P700} / (1 - Y(NA)_{P700}) \text{ or } Y(I)_{P700} / Y(I) = (1 - Y(NA)_{P700}) \quad (\text{Equation 4})$$

$$Y(NA) = Y(NA)_{P700} * Y(ND) / (1 - Y(NA)_{P700})$$

The relative error of the P_{700} pulse method can be calculated as :

$$\Delta Y(I) / Y(I) = (Y(I)_{P700} - Y(I)) / Y(I) = -Y(NA)_{P700} = -Y(NA) / (1 - Y(I))$$

The relative error of the Harbinson & Foyer method for the calculation of the PSI yield is

$$\Delta Y(I) / Y(I) = Y(NA) / (Y(I)) \text{ because } Y(NA) \text{ is considered to be part of } Y(I).$$

Supplemental figures

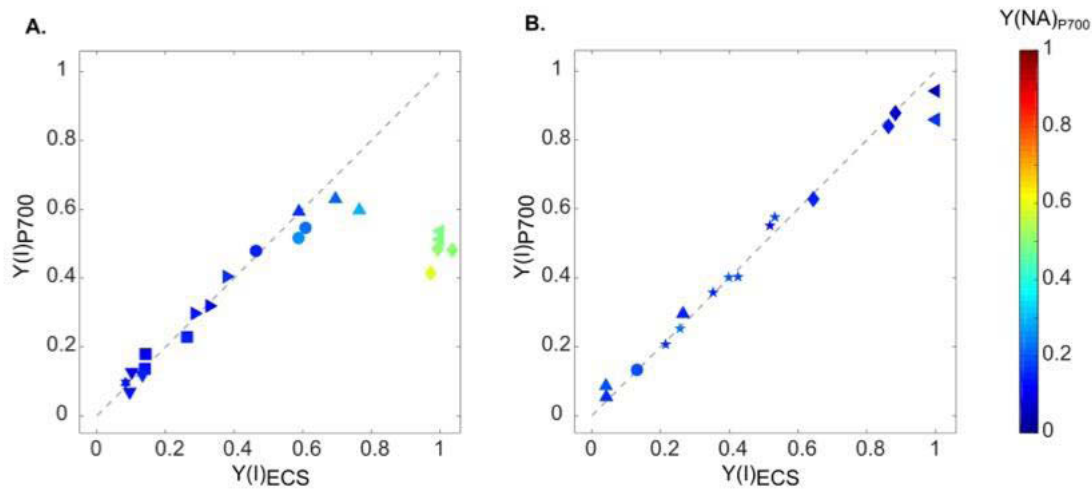


Figure S1: Comparison of the fractions of PSI open centers estimated with ECS and P_{700} methods in *C. reinhardtii* in oxic conditions.

PSII were inhibited with DCMU (10 μM) and HA (saturating concentrations, see Material and methods). $Y(I)_{P700}$ is plotted as a function of $Y(I)_{ECS}$. Values were determined in the absence (A) or presence (B) of MV (4 mM) at steady-state of light for different light intensities. Data points correspond to those shown in Figure 2A and 2B and color code stands for $Y(NA)_{P700}$ values (i.e. the fraction of P_{700} that are not oxidized during a multiple turnover saturating light pulse).

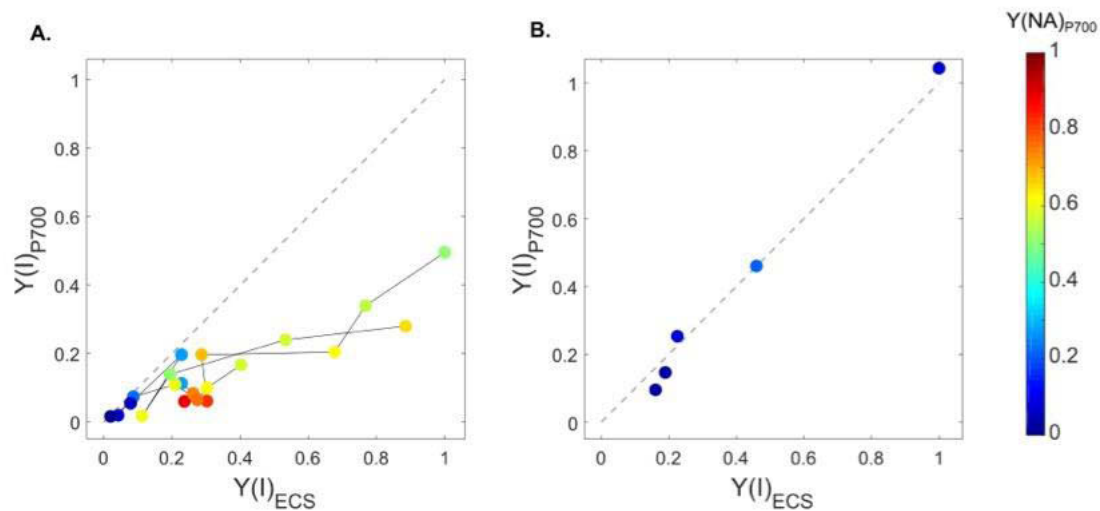


Figure S2: Comparison of the fractions of PSI open centers estimated with ECS and P_{700} methods in *C. reinhardtii* in oxic conditions.

PSII were inhibited with DCMU (10 μM) and HA (saturating concentrations, see Material and methods). $Y(I)_{P700}$ is plotted as a function of $Y(I)_{ECS}$. Values were determined in the absence (A) or presence (B) of MV (4 mM) during the dark-to-light transition at the onset of a 800 $\mu\text{mol photons m}^{-2} \text{s}^{-1}$ light irradiance. Data points correspond to those shown in Figure 2C and 2D and color code stands for $Y(NA)_{P700}$ values (i.e. the fraction of P_{700} that are not oxidized during a multiple turnover saturating light pulse).

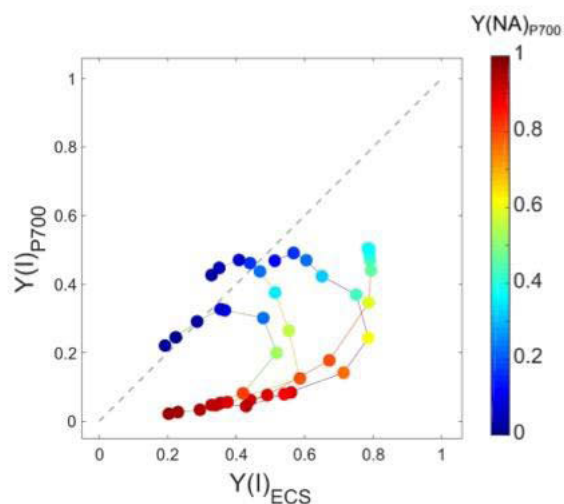


Figure S3: Comparison of the fractions of PSI open centers estimated with ECS and P₇₀₀ methods in *C. reinhardtii* in oxic conditions

PSII were inhibited with DCMU (10 μ M) and HA (saturating concentrations, see Material and methods) while glucose (20 mM) and glucose oxidase (280 U.mL⁻¹) were used to produce anoxia (see Methods). $Y(I)_{P700}$ and $Y(I)_{ECS}$ were measured at different times after the onset of light (26, 56 or 135 μ mol photons m⁻² s⁻¹). Data points correspond to those shown in Figure 3B and color code stands for $Y(NA)_{P700}$ values (i.e. the fraction of P₇₀₀ that are not oxidized during a multiple turnover saturating light pulse).

2.3. Discussion

In the manuscript presented above, we have shown evidences that the P_{700} pulse method developed by Klughammer and Schreiber 25 years ago is not valid, and we proposed an alternative calculation for PSI parameters using the same experimental parameters.

Here, I would like first to summarize our findings, add some important points that were not addressed because of space limitation and give supplementary support to our conclusions.

Second, I would like to discuss the difficult technical aspects of the P_{700} method. Indeed, assuming that the correction we propose is valid and gives correct estimates of PSI parameters, it is nevertheless necessary to have good measurements of the experimental parameters related to PSI state. I will come back to some important methodological aspects.

Third, all the data shown in this manuscript were obtained in conditions of PSII inhibition for the simple reason that it was convenient to measure an ECS signal which depends only on PSI. One could wonder if this induces a bias; it is important to show that the correction we propose still holds when PSII is active because it is the case in most of the publications using the P_{700} pulse method in the literature.

This will naturally lead us to discuss the consequences of the error in the P_{700} method in the literature of the last 25 years in photosynthesis. Using data presented in the manuscript and some chosen representative publications using the P_{700} pulse method, I will try to establish to what extent and in which conditions can the P_{700} method be at the origin of wrong interpretations.

2.3.1. The P_{700} pulse method underestimates $Y(I)$ because of reduction of PSI acceptors during the multiple turnover pulse

a) All PSI centers are open in the dark

One of the strong arguments to demonstrate that the P_{700} pulse method underestimates the fraction of open PSI centers comes from the results in dark adapted samples.

In the article presented above, we demonstrated that in *Chlamydomonas reinhardtii*, in dark and anoxic conditions, the ECS generated by a single turnover is equal to the one measured in oxic conditions in the presence of MV, when all PSI are open according to both methods. This means that all PSI centers are able to perform a stable charge separation if receiving a photon (Article, Figure 3C). In these conditions however, the P_{700} pulse method measures that only

30% of PSI centers are open. Moreover, in oxic dark conditions, all PSI can perform 4 charge separations (Article, Figure 4C), meaning that they have at least, in average, 4 oxidized acceptors. This is hard to reconcile with the conclusion based on P_{700} pulse method, which gives only 50% of PSI centers open.

In addition to those experimental evidences, there is also a thermodynamical argument in dark-adapted samples. In dark conditions, all photosynthetic intermediates are at the thermodynamic equilibrium with the ambient redox potential. In dark-adapted *Chlamydomonas reinhardtii* cells, the ambient redox potential is not far from the redox potential of the plastoquinol/plastoquinone couple, i.e. in the -100 to +100 mV range. It has been shown that the plastoquinone pool is ~70% oxidized in oxic conditions and fully reduced in anoxic conditions (Houille-Vernes et al., 2011). In anoxia, it becomes closer to the redox potential of Q_A/Q_A^- , i.e. -140mV to -145mV in *Chlamydomonas reinhardtii* (Shibamoto et al., 2009; Brinkert et al., 2016). Figure 2-7 shows a scheme where the pool of each intermediates is represented as a flared reservoir and where areas reflect their nernstian redox buffering. Under these conditions and at thermodynamic equilibrium, P_{700} should be completely reduced (its redox potential is $E'_m = +430$ mV, Kok, 1961; Sétif and Mathis, 1980) and the iron-sulfur proteins should be completely oxidized (the redox potential of iron-sulfur centers being in the -520 to -705 mV range, Golbeck and Bryant, 1991; Golbeck, 1993). As a consequence, virtually all PSI should be fully open.

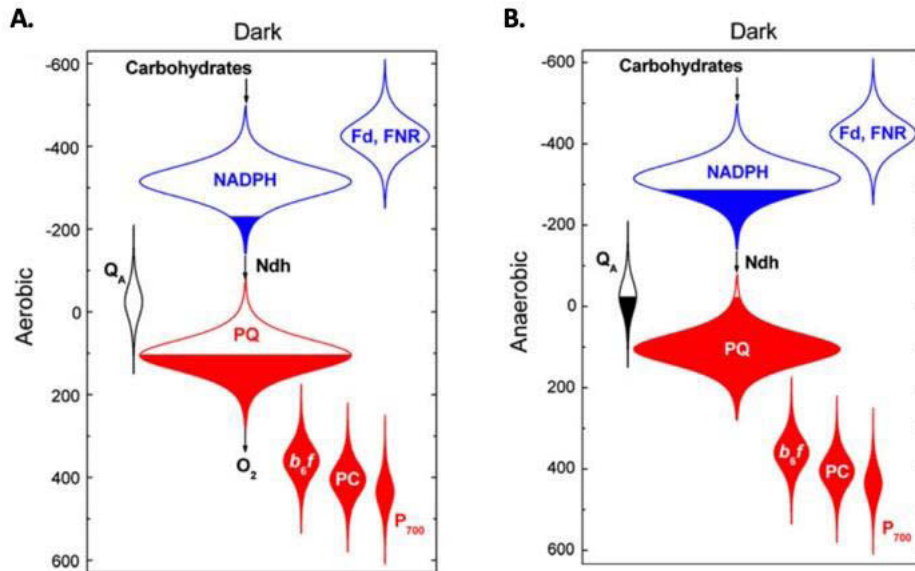


Figure 2-7: A representation of the Z-scheme with flared reservoirs, where areas reflect the nernstian redox buffering of the redox components

From Alric 2010a.

Ordinate axes correspond to the standard redox potential of the intermediates (mV). The overall areas of Q_A and P₇₀₀ correspond to one electron. The author considered that the photosynthetic unit contain 1 PSII, 1 PSI and approximately the same number of electron carriers at the donor and acceptor side of PSI: PSI secondary electron donors (2 plastocyanins; 1 cytochrome f, 1 Rieske; about 6 quinones representing about 12 electrons), and PSI secondary electron acceptors (5 electrons on ferredoxin and ferredoxin NADP-reductase; and 12 on NADP⁺/NADPH). A. and B. represent the redox state of the photosynthetic chain intermediates in the dark, in oxic and anoxic conditions, respectively.

Note that the midpoint potential of Q_A is incorrect: it is indicated as -20 mV instead of -140 to -145 mV (Shibamoto et al., 2009; Brinkert et al., 2016).

Inversely, the measurement of the “b phase” of the flash-induced ECS kinetics demonstrates that the “a phase” of ECS accurately estimates the fraction of open centers. It is important here to discuss the limit of validity of the measurement of PSI yield with ECS. Indeed, in situation of effective acceptor side limitation and high light, ECS can overestimate $Y(I)$ by counting charge separations before they recombine (Alric 2014), a bias which can be taken into account. These aspects will be further discussed in the chapter 3; in particular I will demonstrate that the photochemical rates based on calculations of ECS-based photosystem yields to the photochemical rates based on dark interval ECS relaxation kinetic (Joliot and Joliot 2002; Sacksteder and Kramer 2001) show a perfect match, which is a strong argument for the reliability of $Y(I)_{\text{ECS}}$.

b) Schematic model explaining the error made by the P_{700} pulse method

In the manuscript, we proposed that P_{700} method underestimates $Y(I)$ yield because (i) the multiple turnover pulse allows several charge separations to occur and (ii) the transfer of several electrons on the acceptor side of PSI will change the redox state of PSI acceptors. In order to better visualize this, we propose a scheme (Figure 2.8) representing what happens during a multiple turnover in a dark-adapted sample for an open PSI center. Two situations are considered: in the first one (top), P_{700} is reduced but plastocyanins are oxidized, as well as two PSI acceptors, i.e. the pool of PSI acceptors (2) is larger than the pool of PSI donors (1). In this situation, both ECS and P_{700} based methods will give a correct result.

In the second one (bottom), P_{700} and one plastocyanin are reduced and only one PSI acceptor is oxidized before the measurement, i.e. the pool of PSI donors (2) is larger than the pool of PSI acceptors (1). In this situation, the ECS method will rightly measure that this PSI center is open. The multiple turnover pulse will reduce all PSI acceptors before oxidizing all PSI donors and therefore the P_{700} pulse method will wrongly consider that this PSI center was initially closed.

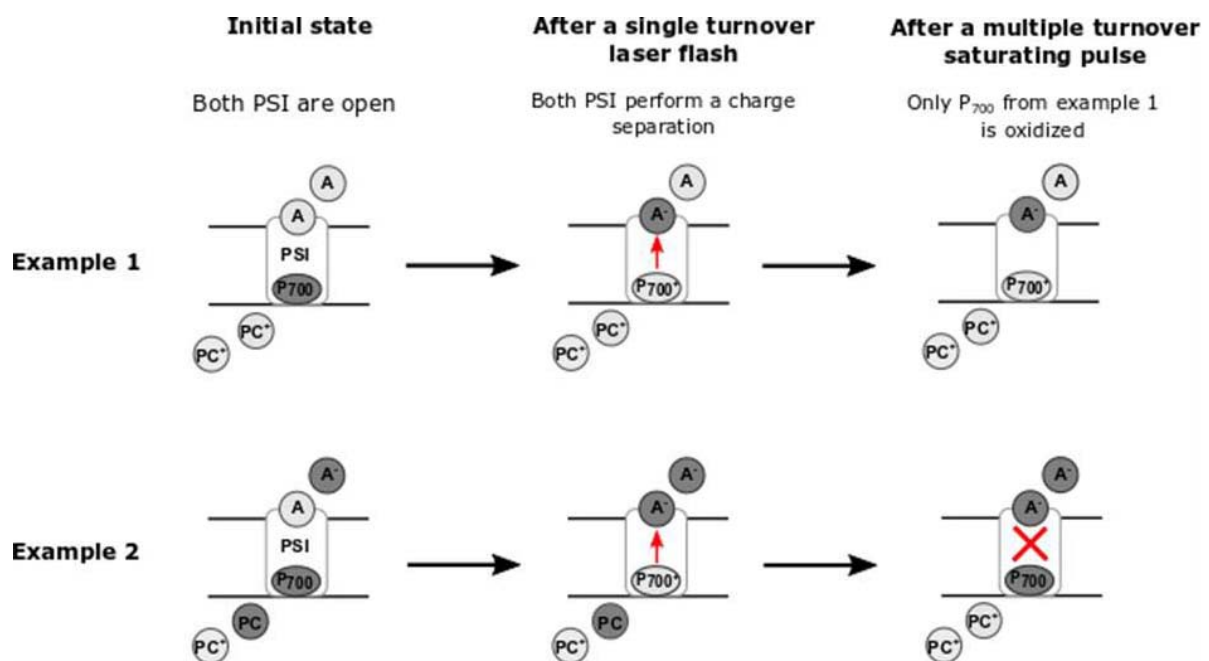


Figure 2-8: Schematic model explaining the error made by the P_{700} pulse method

The figure presents the behavior of two open PSI during a multiple turnover saturating light pulse. P_{700} represents the PSI primary donor, the special pair of chlorophyll; PC refers to plastocyanin, the PSI secondary donor (PC and PC^+ being its reduced and oxidized form, respectively); A represents PSI primary acceptor (A and A^- being its oxidized and reduced form, respectively). In example 1, the number of PSI donors (1 P_{700}) is higher than the number of PSI acceptors (2). In example 2, PSI has two donors (1 PC and 1 P_{700}) and only one acceptor.

2.3.2. Technical considerations regarding P_{700} measurements

The P_{700} pulse method remains an easy measurement, provided that correct estimations of P_{700} parameters are used:

- P_0 , the P_{700} absorption when all P_{700} are reduced
- P_{stat} , the P_{700} absorption under conditions of interest
- $P_{m'}$, the P_{700} absorption after a saturating light pulse
- P_m , the P_{700} absorption when all P_{700} are oxidized

It does not require the use of a laser flash (an expensive setup) and is provided by several commercial instruments. However, even with the correction we provide in the manuscript, we became aware of some technical problems in the practical application of the P_{700} method. I feel it is important to discuss them here.

An important aspect of the P_{700} method is the normalization, i.e. the measurement of the absorption difference corresponding to the change from 100% reduced (P_0) to 100% oxidized (P_m) P_{700} . Obviously, the redox state of P_{700} depends on the ratio of the oxidation and reduction rates of P_{700} . Figure 2-9 shows the main P_{700} oxidation and reduction pathways as well as the action of the chemicals used in the following part.

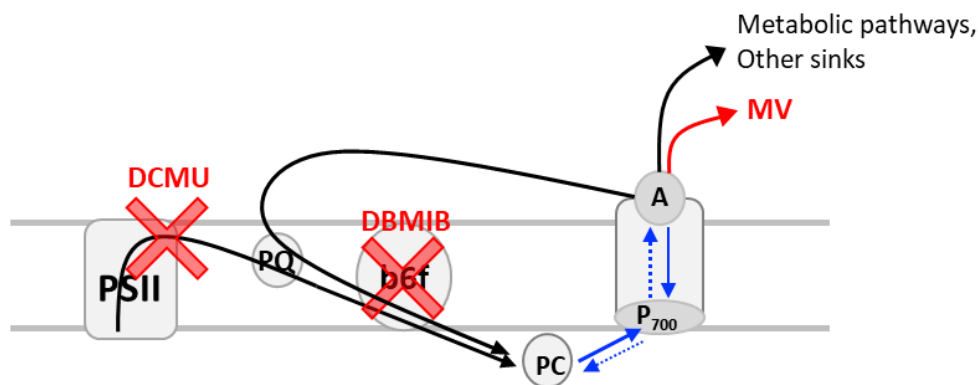


Figure 2-9: P_{700} oxidation and reduction pathways (dashed and solid blue arrows, respectively) and action of the chemicals that are used in our P_m measurement protocol (red crosses or arrows)

Black arrows represent photosynthetic electron flows upstream and downstream PSI. DCMU, DBMIB, MV stand for 3-(3,4-dichlorophenyl)-1,1-dimethylurea, dibromo-6-isopropyl-3-methyl-1,4-benzoquinone and methylviologen, respectively.

a) Reaching the “P₇₀₀ fully oxidized” reference P_m

The full oxidation of P₇₀₀ is a particularly difficult situation to achieve. Indeed, its redox potential is the highest of the inter-system chain. Hence, from a thermodynamic point of view, it is the last intermediate of the chain to be oxidized. In order to oxidize all P₇₀₀, the principle is to: (i) increase the rate of oxidation of P₇₀₀ by using a saturating light, and (ii) decrease the reduction rate of P₇₀₀ and it is this point that we will discuss hereafter.

In the literature, two methods are commonly used to decrease the reduction rate of P₇₀₀. The first one, commonly used in microalgae, is the inhibition of PSII by using a specific inhibitor (DCMU) suppressing the linear flow of electrons. The second one, used in plants, takes advantage of the different absorption spectra between PSII and PSI. When shining far red light, thanks to low energy chlorophylls, PSI is much more excited than PSII which causes oxidation of carriers between PSII and PSI (Gobets and van Grondelle, 2001). In both cases, the oxidation of the inter-system chain would be complete if there was no alternative electron input in the chain (Figure 2-9). As presented in the introduction, there is at least one electron input pathway in the interchain which is the one used by cyclic electron flow (Nda2 or PGRL1/PGR5 pathway). For this reason, we could show that the DCMU treatment could not fully oxidize P₇₀₀. In the presence of DBMIB, a cytochrome *b₆f* inhibitor, both the linear and the cyclic electron flow are arrested (Figure 2-9). We could show that the reduction of P₇₀₀ by the CEF is not negligible since the addition of DBMIB increases the measured P_m by about 10%. Even in the presence of DBMIB, the additional use of the artificial PSI electrons acceptor methylviologen (MV) increased slightly (by 2 to 5 %) the measured P_m, which probably reflects the fact that DBMIB is a leaky inhibitor. If the acceptor side of PSI becomes reduced during the pulse, then even weak electron fluxes from DBMIB-treated cytochrome *b₆f* could be enough to keep some P₇₀₀ reduced. For these reasons, the protocol we used to reach the full oxidation of P₇₀₀ was to superimpose a strong pulse of light (about 2000 photons s⁻¹ PSI⁻¹) and a saturating laser flash, in the presence of 1 μM DBMIB and 4 mM MV (incubated for at least 4 min).

b) Reaching the “P₇₀₀ fully reduced” reference P₀

P₇₀₀ being a high oxidant (E_m ~ 0.430 Volts, Kok, 1961; Sétif and Mathis, 1980), it is thus fully reduced in dark conditions, when all photosynthetic intermediates are at the thermodynamic equilibrium with the ambient redox potential. Measuring the absorption level when all P₇₀₀ are reduced seems straightforward: in the absence of actinic light, 100% of P₇₀₀ should be

reduced. However, even this simple measurement requires some precautions. Indeed, the absorbance in the dark is probed by small pulses of light (detecting light). Although they are short and weak, these pulses lead to the oxidation of a small fraction of P_{700} . This actinic effect of the detecting pulses is small and can be neglected in most conditions. But in the conditions mentioned above (i.e. DBMIB and MV) leading to a very slow re-reduction of P_{700} , if the frequency and/or intensity of the detectors is too high, then the cumulative effect causes a significant oxidation of P_{700} . For this reason, the sequence we used starts in the dark and performs only one detection per second to measure the absorbance in the dark.

c) Potential errors on normalization values ($P_m - P_0$)

To illustrate the error that can be made on the absorption changes corresponding to the oxidation of all P_{700} , we compared the values obtained with the protocol we used in the manuscript and the ones obtained by classical method used in the literature, i.e. adding the sole inhibitor DCMU and detecting every 100ms in dark conditions. In average, the $P_m - P_0$ value obtained with the standard protocol is about 25% lower than the one measured with our protocol (Figure 2-10). Of course, a 25% error on the normalization results in a 25% error on the values of $Y(I)$ and $Y(ND)$ but has even more important consequences on the estimate of $Y(NA)_{P_{700}}$.

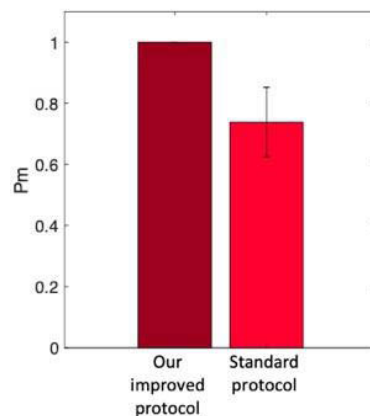


Figure 2-10: Maximal P_{700} absorption change, P_m , measured with the standard protocol or with our improved protocol

P_m was measured as the difference between absorbance in the dark and after a multiple turnover saturating pulse of light (12ms duration). In the standard protocol (light red), only PSII were inhibited by saturating concentration of DCMU and the light sequence provided detection pulses every 100ms in the dark. In our improved protocol (dark red), cytochrome b_6f was inhibited by saturating concentrations of DBMIB ($1\mu\text{M}$) and methylviologen (4mM incubated for at least 4 minutes), a PSI exogenic acceptor, was added in saturating concentrations. Moreover, the sequence provided detection pulses every seconds in dark conditions. Data with both protocols were normalized to the value obtained with the improved protocol and represent the average of three biological samples of *Chlamydomonas reinhardtii* in oxic conditions ($\pm\text{SD}$)

Another possible source of error comes from changes in the number of functional PSI through the course of an experiment, since absorption change depends on the concentration of the absorbing molecule (here P_{700}). Such change can originate from neo-synthesis of PSI in the sample or from PSI photoinhibition which is the destruction of PSI proteins at the stromal side of PSI and the degradation of P_{700} which occurs almost concomitantly (Terashima et al, 1994; Sonoike and Terashima, 1994; Sonoike, 1996). In the case of photoinhibition, one should therefore be cautious when interpreting the decrease in P_m' measurement, i.e. the absorption change after the saturating pulse: it can be due to an accumulation of electrons on the acceptor side of PSI, or it can be due to the destruction of some P_{700} through photoinhibition. We will illustrate this issue with an example from the literature (Sejima et al., 2014). In this work, the authors incubated sunflower leaves in the dark and subjected them to repetitive short pulses of saturating light. They compared the physiological responses under atmospheric conditions or low CO_2 concentration.

At the end of the treatment and under atmospheric conditions, the P_m decreased by 90% (Figure 2-11B). This means that 90% of the PSI centers are photoinhibited. If this is the case, then the increase in $Y(NA)$ (that is the proportion of the PSI centers of which P_{700} cannot be oxidized) up to 0.9 does not mean that the chain is reduced downstream of the PSI, as suggested by the authors, but simply that 90% of PSI centers are inactive/absent (degraded or irreversibly blocked at the iron-sulfur centers). Here, the decrease in P_m is used by the authors both as a measure of the number of photoinhibited PSI and as a measure of the physiological state downstream of the PSI. This leads them to propose that the accumulation of electrons downstream of the PSI leads to PSI photoinhibition, which is not supported by the data. To obtain information on the physiology downstream of the PSI, it is necessary to measure the $Y(NA)$ after normalization on all the active PSI at the time of the measurement, therefore recalculate the P_m at the time of the measurement.

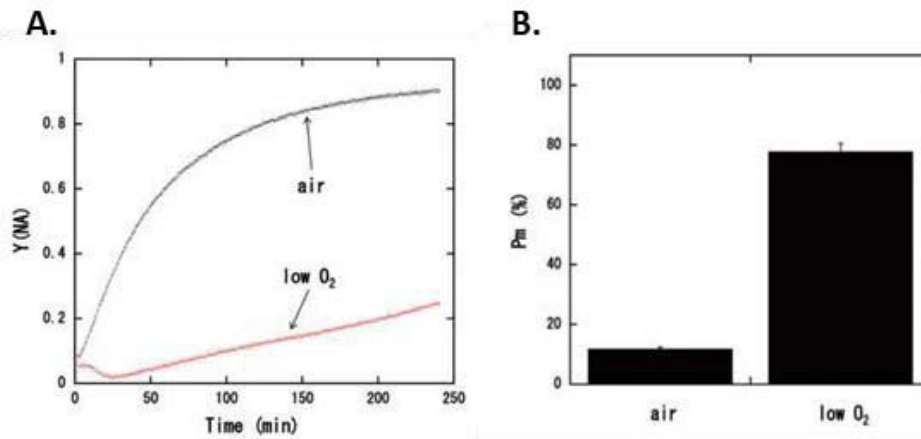


Figure 2-11: Effects of repetitive short pulses treatment on PSI from sunflower leaves in atmospheric conditions (air) or in low oxygen concentration (low O₂)

From Sejima et al. 2014.

Sunflower leaves were submitted to 300ms pulses of 20,000 $\mu\text{mol photons m}^{-2} \text{s}^{-1}$ applied every 10s in dark conditions. (A) The fraction of acceptor side limited centers, Y(NA) was measured after different time of the treatment. (B) The maximal P₇₀₀ absorbance change, P_m, was measured at the end of the experiment (240 min after the beginning of the treatment) and is expressed as a percentage of the initial P_m. In both graphs, results obtained in atmospheric conditions or in low O₂ concentration are shown.

2.3.3. Generalization to the case of an active photosystem II

All the article data were obtained in PSII inhibited samples. From a theoretical point of view, the inhibition of the PSII does not change the conclusions that we drew from our experiments. The P₇₀₀ method error originates from the fact that the multiple turnover pulse potentially induces a modification of the redox state of the PSI acceptors. Because of the short pulse duration and its high intensity, no electron transfer through the cytochrome *b₆f* should occur: the changes induced by the pulse involve only luminal PSI donors after cytochrome *b₆f* and PSII activity is not involved. However, one may wonder if the conclusions drawn remain true when the PSII is functioning, and we decided to address this question experimentally.

When PSII is not inhibited, the calculation of the fraction of PSI open centers with ECS needs an additional step. Indeed, the ECS method gives the fraction of PS (PSI + PSII) open centers that we call Y(total) hereafter. Y(total) is the weighted average of the fraction of open PSI and PSII, FOC(I) and FOC(II), respectively:

$$(1) : Y(\text{total}) = n_1 * \text{FOC(I)} + n_2 * \text{FOC(II)}$$

where n_1 and n_2 are the fraction of PSI and PSII, respectively, which can be estimated as presented in the introduction.

Because the maximal quantum yield of PSI is about 1, we will consider that $Y(I)=FOC(I)$. Therefore, we can use equation (1) to estimate $Y(I)$ from $Y(\text{total})$, measured by ECS, and $FOC(II)$, provided that we can estimate accurately the value of the latter. Fluorescence analysis upon saturation pulse can be used to derive several useful photosynthetic parameters. Among them, q_P is a good estimation of the fraction of PSII open centers, when a pure ‘puddle’ antenna model is considered. In such a model, each PSII center possesses its own independent antenna system.

$$q_P = \frac{\Phi_{II}}{F_v/F_m} = \frac{F_m' - F'}{F_m - F_0}$$

However, it has been shown that closed PSII centers can transfer their exciton to an adjacent open center, a process known as connectivity (Joliot and Joliot, 1964). More realistic models are therefore preferred to the “puddle” model where PSII reaction centers are connected by shared antenna, and are called ‘lake’ model or ‘connected units’ model. Kramer and coworkers (Kramer et al., 2004) proposed another estimation of the fraction of open PSII centers: the parameter q_L , which is more appropriate to species (like terrestrial plants) with a high connectivity of PSII units.

$$q_L = \frac{F_m' - F'}{F_m - F_0} * \frac{F_0}{F'}$$

Finally, the connectivity between PSII centers can vary between species and can also depend on physiological conditions. That’s the reason why we considered a conservative approach where the fraction of open PSII centers is intermediate between the values obtained with the two extreme models: puddle and lake.

$$\frac{F_m' - F'}{F_m - F_0} * \frac{F_0}{F'} \leq FOC(II) \leq \frac{F_m' - F'}{F_m - F_0}$$

By subtracting those two extreme estimations of the fraction of open PSII from the $Y(\text{total})$, we could calculate a minimal and maximal value for $Y(I)_{ECS}$. Figure 2-12A shows comparison of $Y(I)_{P700}$ and $Y(I)_{ECS}$ measured under several light intensities in the absence of PSII inhibitors. $Y(I)_{ECS}$ was shown as a bar whose extremities correspond to its estimations using the puddle or lake model (lower and higher estimations, respectively). In these conditions, $Y(NA)_{P700}$ is high and, as expected, $Y(I)_{P700}$ underestimates the fraction of open PSI regardless of the model we used for $Y(II)$ estimation. In the presence of MV, like in PSII treated samples, the $Y(NA)_{P700}$ is suppressed and the P_{700} and ECS methods concord (Figure 2-12C).

Moreover, the correction of the P_{700} data that we proposed in the manuscript allows better concordance between ECS and P_{700} estimations (Figure 2-12B). As expected, the correction does not modify the results obtained in the presence of MV, since no significant $Y(NA)_{P_{700}}$ was measured in those conditions.

These results confirm that the conclusions of the article remain true in the presence of functional PSII: the ECS and P_{700} methods concord when $Y(NA)_{P_{700}}$ is negligible, i.e. when MV is added. In the other cases, the proposed correction on P_{700} method holds true.

It is to note here that results in MV are compatible with an intermediate PSII connectivity between the puddle and the lake model. Indeed, in these conditions both $Y(I)_{P_{700}}$ and $Y(I)_{ECS}$ are supposed to be correct, and the concordance line ($Y(I)_{P_{700}} = Y(I)_{P_{700}}$) is right in between the values obtained with the two extreme models.

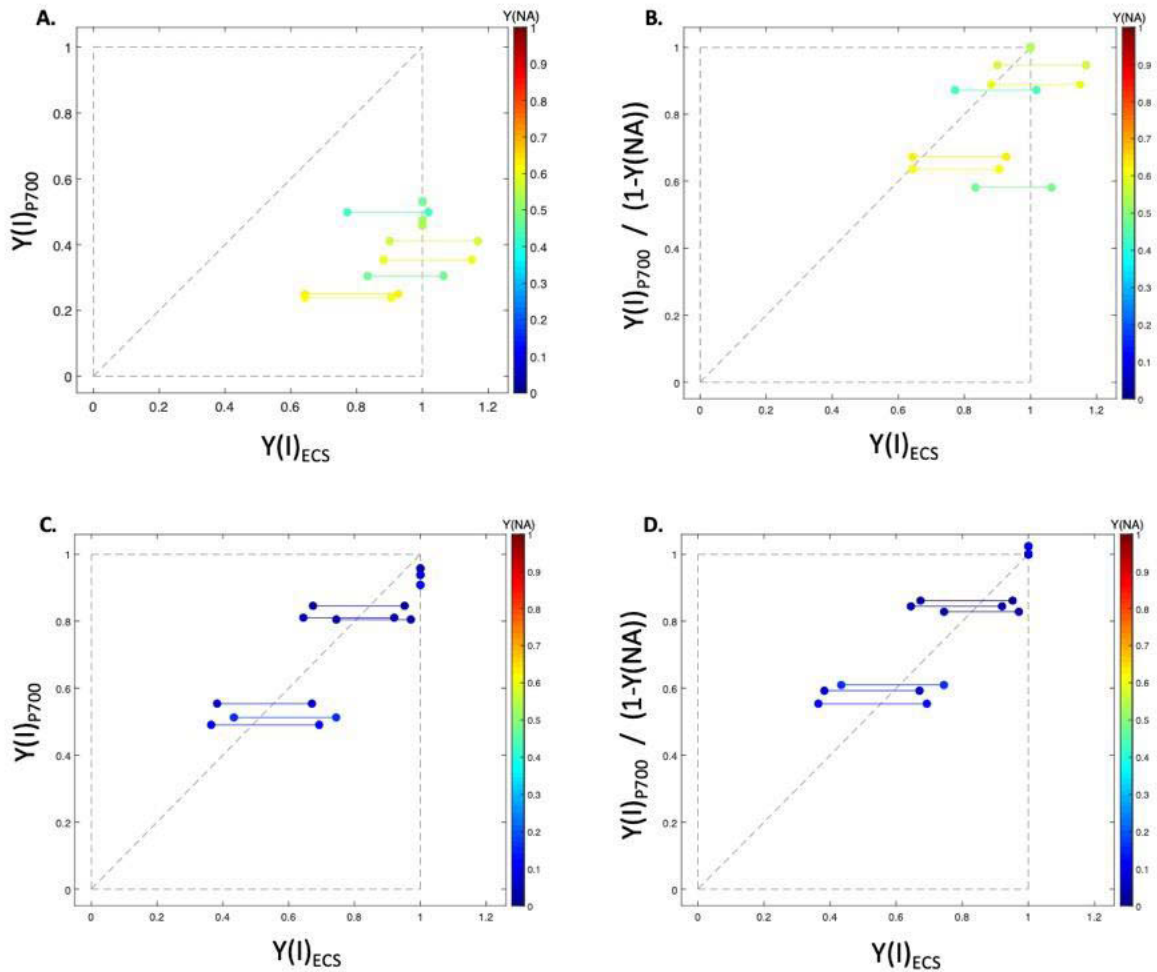


Figure 2-12: Comparison of the fraction of open PSI centers in *C. reinhardtii* estimated with the ECS and P₇₀₀ methods under different light irradiances

The fraction of open PSI centers was estimated with the ECS and P₇₀₀ methods ($Y(I)_{P700}$ and $Y(I)_{ECS}$, respectively). The right and left extremity for $Y(I)_{ECS}$ correspond to $Y(\text{total}) - q_L$ and $Y(\text{total}) - q_P$ respectively. Experiments were carried out in oxic conditions at 0, 56 and 340 $\mu\text{mol photons m}^{-2} \text{s}^{-1}$ in the absence (A) or presence (C) of MV. Panels B and D show the same raw data as panels A and C, respectively, but the value on the ordinate axis is the corrected value $Y(I)_{P700} / (1 - Y(NA))$.

Data correspond to the average (\pm S.D.) of 3 independent biological samples.

2.3.4. Revisiting the literature based on the P₇₀₀ pulse method

In the article presented above, we demonstrated that when P₇₀₀ method measures some reduced PSI acceptors at the end of the pulse ($Y(NA)_{P700}$ is different from 0), it always overestimates the real acceptor side limitation. This leads in turn to an underestimation of the yield of PSI. The questions that automatically rise are:

- In what environmental and physiological conditions is P₇₀₀ method underestimating the PSI yield?

- What are the erroneous conclusions which have been drawn in the past? And the consequences regarding our understanding of the photosynthetic physiology, especially the importance of Cyclic Electron Flow around PSI?

In order to answer those questions, we propose to re-interpret the data shown in figure 2A, 2C and 3B of the article with a more physiological point of view and to highlight the misunderstanding induced by P_{700} bias. We also provide a short review of the literature using P_{700} method using to our advantage the correction to the P_{700} pulse method that we propose, which allows us to recalculate the PSI parameters from the erroneous ones.

In this part, we use the P_{700} data correction proposed in the article (discussion part) to reassess PSI parameters. The corrected PSI yield, $Y(I)_{P700,corr}$, and the acceptor side limitation, $Y(NA)_{P700,corr}$, were calculated as:

$$Y(I)_{P700,corr} = \frac{Y(I)_{P700}}{1 - Y(NA)_{P700}}$$

$$Y(NA)_{P700,corr} = 1 - Y(I)_{P700,corr} - Y(ND) = Y(NA)_{P700} * Y(ND) / (1 - Y(NA)_{P700})$$

We will consider in the following that the correct values for the PSI yield and acceptor side limitation are the ones estimated with ECS estimation of the fraction of open centers and P_{700} estimation of the donor-side limited centers, $Y(ND)$.

In the following, we will discuss the consequences of the bias of the P_{700} pulse method, both during dark-to-light transition and during steady state photosynthesis. The P_{700} pulse method was first developed -and is still mostly used- for investigations of the cyclic electron flow around PSI through the comparison of PSII and PSI yields. Most of the discussion in the following will focus on how the P_{700} pulse method may have drawn erroneous conclusions regarding CEF. This part is not meant to be an exhaustive review of the literature using the P_{700} pulse method, but presents some conditions in which the P_{700} pulse method can lead to misunderstand the photosynthetic physiology.

a) Dark to light transition

During dark to light transition, stromal reactions and photosynthetic chain reactions adjust to each other and reach an equilibrium. In the literature, several works use P₇₀₀ pulse method to evaluate the dynamic of activation of the different stromal pathways, e.g. CBB cycle, CEF or Mehler reactions. In this part, we show that (i) since this process is characterized by transient accumulation of reduced PSI acceptors, the P₇₀₀ method generates important errors, and (ii) these errors led to underestimate the role of CEF during the transition from dark to light.

In this section, I will first come back to the dark-to-light transitions we used in the article manuscript (figure 2C and 3B) and then show an example from the literature.

In Figure 2-13, data from figures 2C and 3B of the manuscript are plotted as a function of time after light onset (one of the three replicates is shown). It compares: the P₇₀₀ parameters ($Y(I)_{P700}$ and $Y(NA)_{P700}$, red curves), the same estimations after correction ($Y(I)_{P700,corr}$ and $Y(NA)_{P700,corr}$, green curves), as well as their estimations by the ECS method ($Y(I)_{ECS}$ and $Y(NA)_{ECS}$, blue curves). As stated in the manuscript, PSII were inhibited and samples were placed in oxic conditions at 800 $\mu\text{mol photons m}^{-2} \text{s}^{-1}$ (left panels: A, B, C) or in anoxic conditions at 135 $\mu\text{mol photons m}^{-2} \text{s}^{-1}$ (right panels: D, E, F).

When steady state is reached (~ 450 ms and ~ 60 s for oxic and anoxic conditions, respectively), all methods provide similar estimation of PSI parameters. However, during the transition period, P₇₀₀ method underestimates the fraction of open PSI centers: $Y(I)_{P700}$ is always lower than $Y(I)_{ECS}$, by a factor up to 4 in oxic conditions and up to 10 in anoxic conditions. It is to note that for all data, when $Y(NA)_{P700}$ is lower than 0.8, the P₇₀₀ correction is reliable: corrected P₇₀₀-based and ECS-based parameters are very close. At the contrary, when $Y(NA)$ is higher than 0.8 (e.g. during the first 10 ms after light onset in oxic conditions, Figure 2-13F), the P₇₀₀ correction is not reliable (as established already in the discussion of the article).

We could estimate the number of PSI stable charge separation occurring during the transitory phase and approximate the ones effected through CEF. An integration of the PSI electron transfer rate, $ETR(I)$, over time until the steady-state is achieved yields the number of stable charge separations performed by PSI, hereafter noted N (Nawrocki et al., 2019). We estimated $ETR(I)$ as:

$$ETR(I) = Y(I) \cdot \sigma_1 \cdot I$$

where $\sigma_1 \cdot I$ is the rate of photon absorption by PSI at the light irradiance I.

We estimated σ_1 through the initial slope of the ECS increase at the onset of light in conditions where PSII is inhibited (see chapter 3 for more details) and we assumed that it was constant over time. PSI was absorbing 118 ± 17 photons s^{-1} and 509 ± 43 photons s^{-1} at $135 \mu\text{mol photons m}^{-2} s^{-1}$ and $800 \mu\text{mol photons m}^{-2} s^{-1}$, respectively.

Figure 2-13C and F present the number of stable PSI charge separations performed before steady state is reached in oxic high light and anoxic medium light conditions, respectively. In both conditions, the P_{700} bias induces an underestimation by a factor ~ 2 of the number of PSI stable charge separations.

Can we go further and determine the PSI charge separations through CEF pathway? In this data, PSII is inhibited. Then, the number of electrons transferred through PSI is the sum of two processes: (i) the oxidation of the initial pool of electrons in the photosynthetic chain in the dark, which represents approximately 10 electrons (Nawrocki et al., 2019) and (ii) the cyclic electron transfer around PSI that reinjects reducing power from the PSI acceptors into the inter-system chain. We calculated the number of charge separation through CEF as $N-10$ and estimated an average CEF during transitory phase. ECS and corrected P_{700} data gave an average CEF of ~ 75 electrons $\text{PSI}^{-1} s^{-1}$ and ~ 50 electrons $\text{PSI}^{-1} s^{-1}$ for the oxic and anoxic conditions, respectively, close to the recent estimation of the maximal cyclic electron flow in *Chlamydomonas reinhardtii*, i.e. ~ 60 electrons $\text{PSI}^{-1} s^{-1}$ (Nawrocki et al., 2019). But P_{700} data largely underestimated the CEF during the transition phase with ~ 25 electrons $\text{PSI}^{-1} s^{-1}$ and ~ 20 electrons $\text{PSI}^{-1} s^{-1}$ for the oxic and anoxic conditions, respectively.

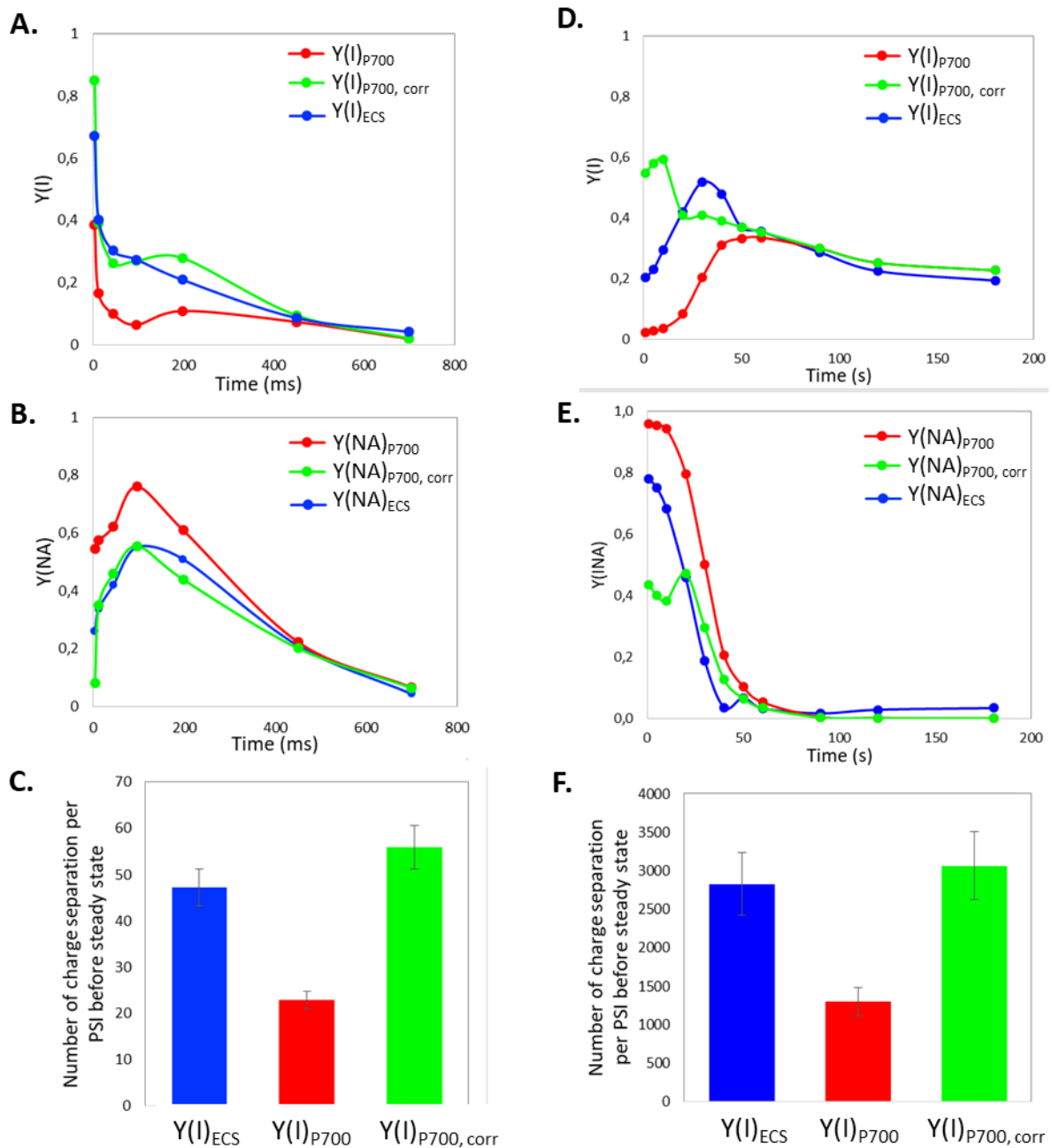


Figure 2-13: PSI parameters measured by ECS and P_{700} method during light to dark transition when PSII is inhibited

The fraction of open PSI centers ($Y(I)$, A/D), and acceptor side limited centers ($Y(NA)$, B/E) were measured at different times after light onset of at $800 \mu\text{mol photons}\cdot\text{m}^{-2}\cdot\text{s}^{-1}$ in oxic conditions (A and B, respectively) and under $135 \mu\text{mol photons}\cdot\text{m}^{-2}\cdot\text{s}^{-1}$ in anoxic conditions (E and F, respectively). PSII was inhibited by saturating concentrations of DCMU ($10\mu\text{M}$) and hydroxylamine (saturating concentration, see material and methods from article) and anoxia was induced by glucose (20mM) and glucose oxidase ($280\text{U}\cdot\text{mL}^{-1}$) addition. Data were obtained from P_{700} method (red), ECS method (blue) or correction of the P_{700} method (green) (see introduction of section 2.3.4 for calculation details). The number of charge separation during the oxic (C) and anoxic (F) transition from dark to light were calculated as the integrated electron transfer rate over time until the steady state is reached. The first 450 ms and first 60 s were considered for oxic and anoxic conditions, respectively. Data corresponds to one representative sample of *Chlamydomonas reinhardtii* wild type T222⁺.

In the literature, measurements of PSI activity through the P_{700} pulse method at the onset of light often show a transiently very high acceptor side limitation. Figure 2-14 is taken from a publication on sunflower leaves (Klughammer and Schreiber, 1994). When light is turned on, quantum yields of PSI (here noted Φ_I) and PSII (here noted Φ_{II}) are very low and later increase concomitantly with time, what is often interpreted as a lag phase before CBB cycle pathway activation (e.g. Schansker et al., 2005; Schansker et al., 2006). Most importantly, Φ_I and Φ_{II} are equal throughout the kinetics, which was interpreted by the authors as an evidence for a pure linear electron flow.

In the light of what we have learnt from the critical analysis of the P_{700} pulse method, it is reasonable to question this conclusion. In these data, “red. P_{700} ” represents the fraction of reduced P_{700} and $Y(NA)_{P700}$ is easily calculated as $Y(NA) = \text{red. } P_{700} - \Phi_I$. At the light onset, $Y(NA)_{P700}$ decreases from 0.9 initially to 0.1 after 3 minutes of illumination. According to our correction, during those 3 first minutes, Φ_I is therefore largely underestimated (by the factor $1 - Y(NA)_{P700}$). This suggests that a transient CEF probably occurs during the first minutes after light onset, which could not be apprehended with the P_{700} pulse method.

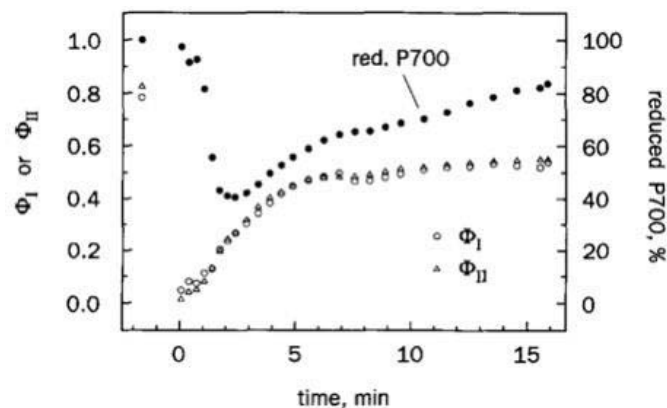


Figure 2-14: Comparison of time-dependent changes of reduced P_{700} (red. P_{700}), $Y(I)$ and $Y(II)$ (here noted Φ_I and Φ_{II} , respectively) during a dark-light induction period of a sunflower leaf in air

From Klughammer and Schreiber 1994.

Fluorescence parameters and P_{700} absorption changes were recorded simultaneously. Actinic light ($800 \mu\text{mol photon m}^{-2} \text{s}^{-1}$) was turned on at time 0.

CEF has often been proposed to be a crucial starter for photosynthesis: when stromal sinks are not yet activated in the dark, CEF would build some ATP and a pmf (Joliot and Joliot, 2006) which helps protecting both photosystems (Endo and Asada, 2008; Chaux et al., 2015). The considerations above illustrate how much the error made by the P_{700} pulse method can lead

to wrong conclusions: it overestimates the acceptor side limitation at the onset of light and largely underestimates the efficiency of the transitory CEF. It is especially true in anoxic conditions where it wrongly measures no CEF during the first seconds following the onset of light.

b) Under steady state low light, PSI yield is underestimated

In this section and in the following ones, we will focus on steady-state situations.

- *When PSII is inhibited, P₇₀₀ method leads to misunderstanding of PSI activity regulation under low light*

Figure 2-15 shows data already presented in the article (Figure 2A) but here, PSI parameters are presented as a function of light irradiance. We represented data obtained with P₇₀₀ method (red), with computation of ECS and fluorescence data (blue) and correcting P₇₀₀ method (green). PSII were inhibited and, as previously discussed, P₇₀₀, corrected-P₇₀₀ and ECS methods concord on data from moderate to high light (> 26 $\mu\text{mol photons m}^{-2} \text{s}^{-1}$). But under low light, $Y(I)_{P700}$ is much lower than $Y(I)_{ECS}$ and $Y(I)_{P700,corr}$, up to a factor 2. This leads to underestimating the electron transfer rate through PSI under low light.

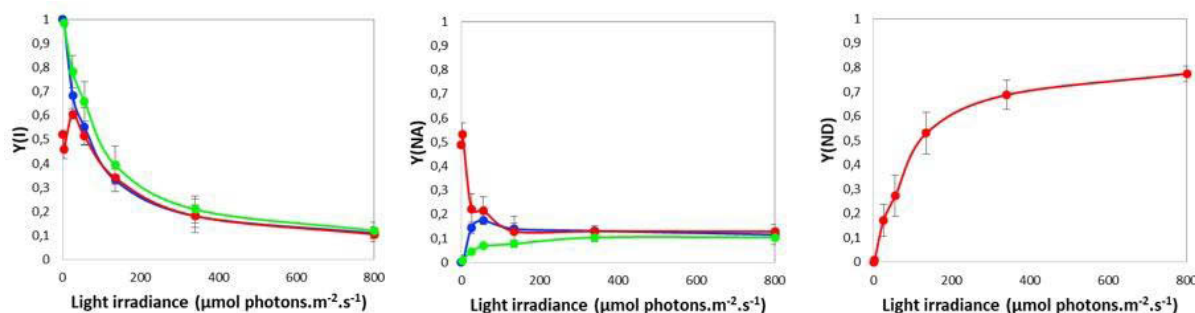


Figure 2-15: Light dependence of PSI parameters, $Y(I)$ (left panel), $Y(NA)$ (middle panel) and $Y(ND)$ (right panel), measured by ECS and P₇₀₀ method when PSII is inhibited.

PSI parameters were measured under steady state light (after a minimum of 2 minutes acclimation) and in oxic conditions. PSII was inhibited by saturating concentrations of DCMU (10 μM) and hydroxylamine (saturating concentration, see material and methods of the manuscript). Data were obtained from P₇₀₀ method (red), ECS method (blue) or correction of P₇₀₀ method (green) (see introduction of section 2.3.4 for calculation details). Data are the average of three independent biological samples ($\pm\text{SD}$) of the *Chlamydomonas reinhardtii* wild type T222⁺ and correspond to data presented in Figure 1 B/C of the manuscript.

- *When PSII is active, P₇₀₀ method underestimates PSI activity under low light*

I believe that such underestimation of PSI activity under low light is common in the literature.

Figure 2-16 shows results from a study on the effect of short pulses in the dark to

photoinhibition of PSI (Zivcak et al., 2015) in wheat leaves. They show that under low light ($<500 \mu\text{mol m}^{-2} \text{s}^{-1}$), $Y(\text{NA})_{\text{P700}}$ is high and PSI yield shows a local drop. This kind of drop of PSI yield under low light is common in the literature and can be found for example in wheat again (Brestic et al., 2015), and for 2 species of fern, *Microsorium punctatum* and *Paraleptochillus decurrens* (Wang et al., 2013). It is reasonable, in the light of our results, to question the meaning of this drop under low light. Because this drop of PSI yield corresponds to a significant increase of $Y(\text{NA})_{\text{P700}}$, I propose that this is a bias due to the overestimation of the acceptor side limitation at the end of the multiple turnover pulse.

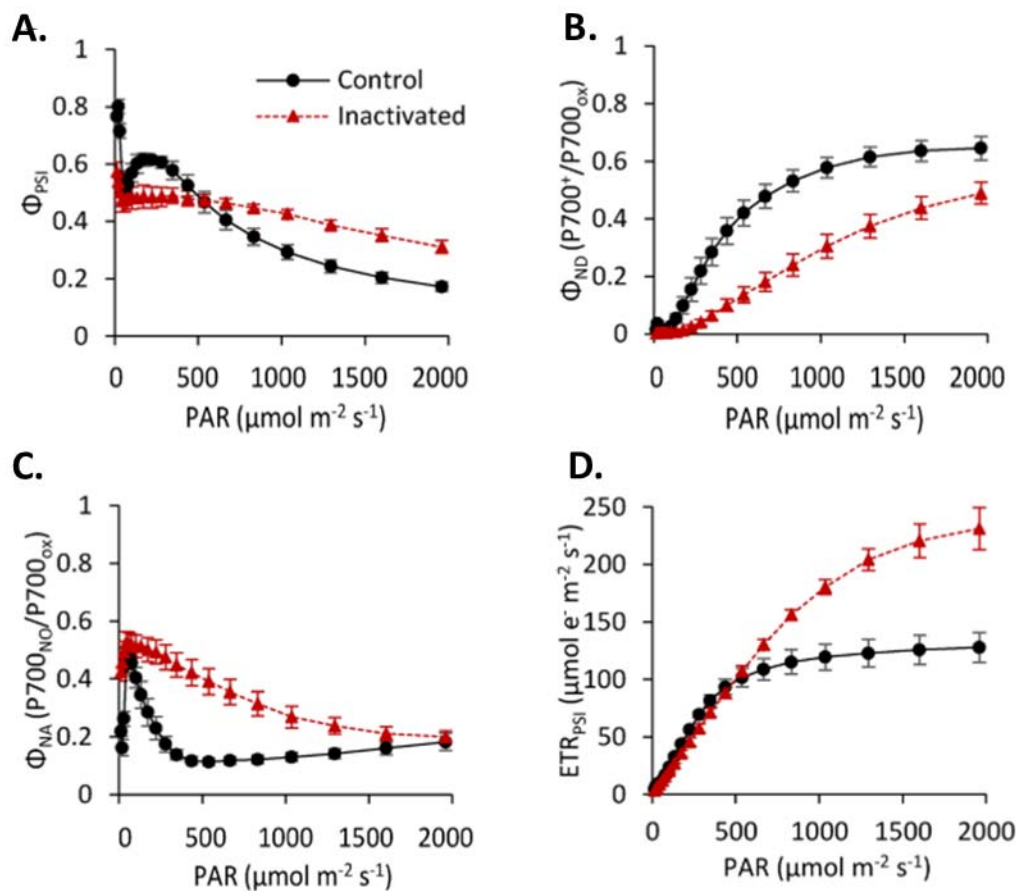


Figure 2-16: Light dependence of P_{700} parameters measured before PSI inactivation treatment (Control) and 2 days after PSI inactivation treatment (Inactivated) on wheat leaves.

From Zivcak et al., 2015.

The fraction of open PSI, here noted Φ_{PSI} (A), the fraction of donor side limited centers, here noted $\Phi(\text{ND})$ (B), and the fraction of acceptor side limited centers, here noted $\Phi(\text{NA})$ (C) were estimated using the P_{700} method under different light intensities. The apparent electron transport rate in PSI (ETR_{PSI}) was estimated based on Φ_{PSI} values calculated using initial Pm. The rapid light curves were obtained after previous acclimation to moderate light (light intensities 14, 21, 30, 45, 61, 78, 103, 134, 174, 224, 281, 347, 438, 539, 668, 833, 1036, 1295, 1602, and $1930 \mu\text{mol photons m}^{-2} \text{s}^{-1}$); the duration of each interval with a given light intensity was 30s.

Data corresponds to the average values from six plants (\pm SD).

c) Role of Antimycin A and PGR5 in CEF

Antimycin A is proposed to be an inhibitor of one of the cyclic electron flow pathways, the PGR5-PGRL1 route (Tagawa et al., 1963). Here we would like to suggest that the bias of P_{700} method could sometimes lead to misunderstanding the role of antimycin A in CEF. We will discuss this based on one example.

Figure 2-17 shows data from an article which is about dissecting electron flows in *Arabidopsis thaliana* (Kou et al., 2015). Figure 2-17A and B show PSI parameters measured in *Arabidopsis thaliana* wild type in the absence (A) and presence (D) of antimycin A. $Y(I)_{P700}$ is always lower in the presence of antimycin A because of higher $Y(NA)_{P700}$. Authors then use $Y(I)_{P700}$ to calculate an electron flow through PSI that they compare to the electron flow through PSII, LEF_{O_2} in order to calculate a Δ flux indicating the amplitude of CEF (Figure 2-17C). Based on this observation, the authors concluded that the CEF is reduced in the presence of Antimycin A.

After we shared with the authors our questions regarding the P_{700} pulse method, the authors kindly sent us the raw data regarding PSI parameters so we could apply the P_{700} correction we propose in the paper. After correction, conclusions are reversed: $Y(I)_{P700,corr}$ appears higher in antimycin A treated samples. This would result in a higher $ETR(I)$. $ETR(II)$ being similar between treated and non-treated (see data in Kou et al., 2015), Δ flux would be higher in antimycin A treated samples than on control leaves, indicating a higher CEF! If this increase of CEF is true (and not due to an artifact related to protocols of normalization for example, i.e. an underestimated P_m leading to a correction bias) we can suggest that this phenotype is due to an inhibition of the respiratory chain, a well-known effect of antimycin A (first proposed by Ahmad et al., 1950, reviewed in Slater et al., 1973). Indeed, it has been shown that inhibition of the respiration chain results in modification of the photosynthetic activity (e.g. Larosa et al., 2018, Cardol et al., 2003). Moreover, we can hypothesize that the lack of ATP production by respiration results in an enhancement of CEF as it has been proposed in the literature (e.g. Alric et al., 2010b; Fisher et al., 2019).

PGR5 is a thylakoid enzyme that have been proposed to be involved (Munekage et al, 2002) together with PGRL1 (Hertle et al. 2013), in cyclic electron flow by reinjecting electrons from acceptor side of PSI into the chain. Here we show that the bias of P_{700} method might also lead to misunderstanding the *pgr5* mutant phenotype.

Figure 2-17G shows PSI parameters measured in *Arabidopsis thaliana pgr5* mutant (Kou et al., 2015). $Y(I)_{P700}$ is always lower in *pgr5* mutant than in the WT (Figure 2-17A and G) because of a higher $Y(NA)_{P700}$ and it exhibits a similar trend as antimycin A treated samples. As presented

above, authors calculated a Δflux much lower in *pgr5* mutant than in the WT, thus concluding in a lower CEF occurrence and proposing PGR5 as an important pathway for CEF (Figure 2-17I). As previously, we calculated PSI parameters with the correction proposed in the article. $Y(I)_{P700,corr}$ appears much higher in *pgr5* mutant than in the WT. This would result in a higher ETR(I). ETR(II) being similar between WT and *pgr5* mutant (see data in Kou et al., 2015), Δflux should be much higher in *pgr5* mutant than in the WT, indicating a much higher CEF! It is to note that our correction gives a $Y(I)$ evolution with light intensity that is not expected: it remains rather stable, meaning that PSI activity does not saturate, even under high light. We have no clear explanation. It might be because under high light (higher than $580 \mu\text{mol photons m}^{-2} \text{ s}^{-1}$) $Y(\text{NA})$ is higher than 0.7 and the correction might be biased in the sense of overestimate of $Y(I)$. But it could also be because of a low PSI/PSII stoichiometry in the PGR5 mutant, as mentioned several times (e.g. Munekage et al., 2002).. If there are much less PSI than PSII in the *pgr1* mutant compared to the wild type, then, a higher ETR per PSI does not mean that the flow through all PSI is higher than the flow through all PSII. And Δflux would not reflect the amplitude of CEF.

But still, here, *pgr5* mutant would not show a lower CEF than in WT And it is to note that similar data were obtained in *Arabidopsis thaliana pgr5* mutant in another work (Huang and Zhang, 2012). In the recent literature, the mechanistic role of the PGR5-PGRL1 heterodimer has been questioned, and a regulatory role is now proposed instead. Indeed, the maximal CEF measured in *Chlamydomonas reinhardtii* was the same, $\sim 60 \text{ electrons PSI}^{-1} \text{ s}^{-1}$, in the wild type and in the *pgr1* mutant (Nawrocki et al., 2019).

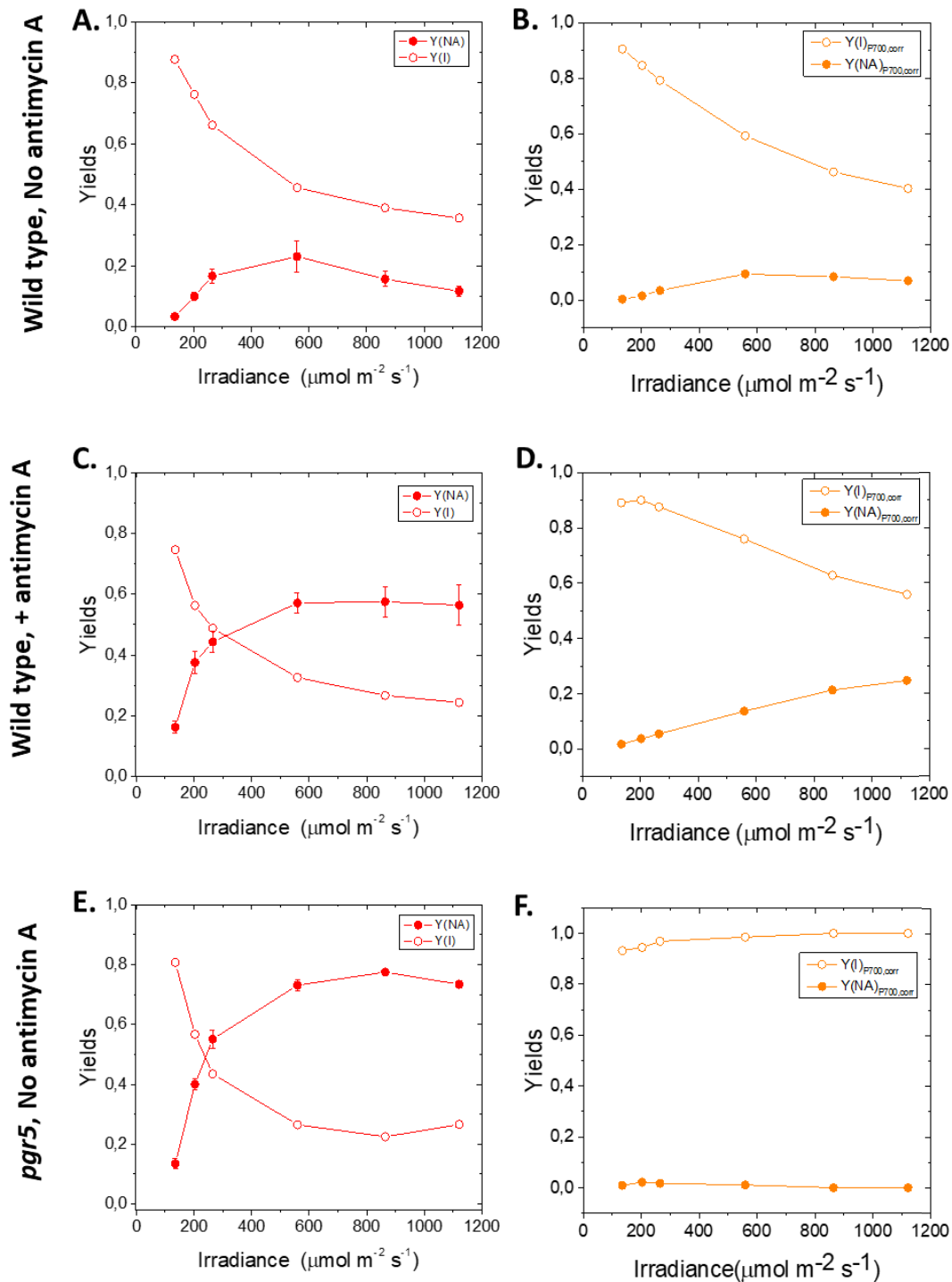


Figure 2-17: Light irradiance dependency of *Arabidopsis thaliana* PSI parameters in WT (A and B), WT with antimycin A (C and D) and *pgr5* mutant (E and F).

Raw data from Kou et al. 2015 was kindly sent by the authors.

Fraction of open PSI, $Y(\text{I})$ and fraction of acceptor side limited PSI, $Y(\text{NA})$, were estimated with the P_{700} method (left panels, A, C and E) and with the correction proposed in our article (right panels, B, D and F). Each leaf disk was exposed to increasing light irradiance steps using white halogen light filtered through neutral density filters. The leaf disk was maintained under each irradiance for about 10 min to reach steady-state photosynthesis. Measurements were performed at 25 °C under air conditions.

Values are means of 8, ND, and 16 leaf disks for A-B, C-D, and E-F, respectively.

d) CEF estimation during leaf senescence

Figure 2-18 shows results from an article on sugar maple leaves physiology during senescence (Junker and Ensminger 2016). From green summer to green autumn, yellow, orange and red leaves, the quantum yield of PSI, $Y(I)_{P700}$ (here referred as Φ_{PSI}) shows a rather stable trend compared to Φ_{PSII} which decreases a lot more. The authors then estimate the evolution of cyclic electron flow during leaf senescence. In this purpose, they estimate the electron flow through photosystem II (J_{PSII}), and through photosystem I (J_{PSI}) and propose that the J_{PSI}/J_{PSII} ratio is an indicator of CEF (Figure 2-18B).

But do we get the same results if we consider the error induced by the P_{700} method? From green summer leaf to red leaf, $Y(NA)_{P700}$ goes from 0.1 to 0.7. Thus, the underestimation of $Y(I)$ by the P_{700} method (calculated as $1/(1-Y(NA)_{P700})$) goes from a factor 1.1 in the green summer leaves to a factor 3.3 in the red leaves. This means that the evolution of the CEF, if correctly estimated by J_{PSI}/J_{PSII} ratio, during leaf senescence is underestimated by a factor 3: instead of increasing by a factor ~ 4 , it might actually increase by a factor ~ 12 .

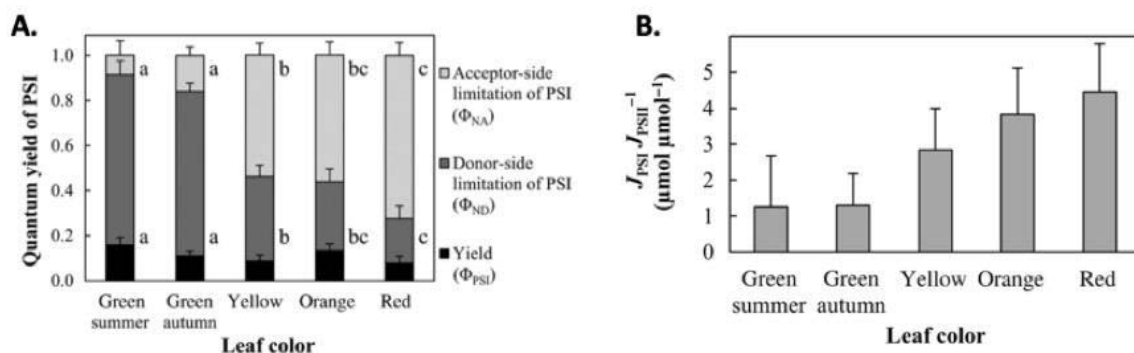


Figure 2-18: Evolution of PSI parameters and CEF estimations during sugar maple leaf senescence

From Junker and Ensminger 2016.

A. PSI parameters were measured using P_{700} method in green sugar maple leaves sampled in summer, and in green, yellow, orange and red leaves sampled in autumn. Φ_{PSI} , Φ_{ND} and Φ_{NA} stands for the fraction of open, acceptor side limited and donor side limited centers, respectively. B. The ratio of electron transport at PSI to electron transport at PSII, J_{PSI}/J_{PSII} was used as an indicator for cyclic electron transport.

Data represents the average five to six leaves sampled from three trees in two consecutive years (\pm SD) taken at a light intensity of $1200 \mu\text{mol photons m}^{-2} \text{s}^{-1}$. Significant differences ($p < 0.05$ using linear-mixed-effect modeling followed by Tukey's multiple comparison, see article for more details) are indicated by different letters.

2.3.5. Partial conclusions and transition

Measuring the quantum efficiency of PSI is very important and P_{700} measurement is probably the easiest and the most accessible way to do so. Indeed, such measurement does not require an expensive laser, the signal over noise is very satisfactory and in organisms with weak ECS signals (e.g. cyanobacteria), it is the only simple way to assess the PSI activity.

However, we have shown that the method proposed by Klughammer and Schreiber and based on P_{700} measurements present a bias: it systematically underestimates the PSI yield proportionally to the acceptor side limitation at the end of the pulse, i.e. the parameter $Y(NA)_{P_{700}}$. We propose a correction of the data allowing to correctly estimate the quantum yield of PSI with the same set of parameters: the correction does not need any additional measurement. By this mean, already produced data can be revisited. Through a short literature review, we could show that, in many physiological conditions, P_{700} method lead to misunderstanding the physiology and in particular, CEF amplitude and variations. A more careful and exhaustive reinterpretation of the literature data might enable advances in the understanding of the pathways and mechanisms of regulation of the CEF.

Nevertheless, for the moment, the correction we propose is not fully satisfying: when $Y(ND)$ is very small and/or $Y(NA)$ very large, the correction fails, considering the ECS measurement as a reference. I think it would be very useful to continue using cross test between ECS and P_{700} methods and to try to find a better correction giving an agreement between the two measurements in all conditions. A third alternative to measure PSI yield could come from photoacoustic measurements, and this could be a powerful way to decide what is the most robust and accurate measurement of PSI yield based on P_{700} measurements.

For the moment, we think that the most reliable method is the ECS. This is why I will favor its use in future chapters.

2.4. Bibliography

- Ahmad, K., Schneider, H. G., & Strong, F. M.** (1950). Studies on the biological action of antimycin A. *Archives of biochemistry*, 28(2), 281.
- Allen, J. F.** (2002). Photosynthesis of ATP—electrons, proton pumps, rotors, and poise. *Cell*, 110(3), 273-276.
- Alric, J.** (2010a). Cyclic electron flow around photosystem I in unicellular green algae. *Photosynthesis research*, 106(1-2), 47-56.
- Alric, J., Lavergne, J., & Rappaport, F.** (2010b). Redox and ATP control of photosynthetic cyclic electron flow in *Chlamydomonas reinhardtii* (I) aerobic conditions. *Biochimica et Biophysica Acta (BBA)-Bioenergetics*, 1797(1), 44-51.
- Alric, J.** (2014). Redox and ATP control of photosynthetic cyclic electron flow in *Chlamydomonas reinhardtii*:(II) Involvement of the PGR5–PGR1 pathway under anaerobic conditions. *Biochimica et Biophysica Acta (BBA)-Bioenergetics*, 1837(6), 825-834.
- Anderson, J. M., & Boardman, N.** (1966). Fractionation of the photochemical systems of photosynthesis I. Chlorophyll contents and photochemical activities of particles isolated from spinach chloroplasts. *Biochimica et Biophysica Acta (BBA)-Biophysics including Photosynthesis*, 112(3), 403-421.
- Bailleul, B., Berne, N., Murik, O., Petroustos, D., Prihoda, J., Tanaka, A., ... Bowler, C. & Finazzi, G.** (2015). Energetic coupling between plastids and mitochondria drives CO₂ assimilation in diatoms. *Nature*, 524(7565), 366.
- Bailleul, B., Cardol, P., Breyton, C., & Finazzi, G.** (2010). Electrochromism: a useful probe to study algal photosynthesis. *Photosynthesis research*, 106(1-2), 179.
- Baker, N. R.** (2008). Chlorophyll fluorescence: a probe of photosynthesis in vivo. *Annu. Rev. Plant Biol.*, 59, 89-113.
- Bendall, D. S., & Manasse, R. S.** (1995). Cyclic photophosphorylation and electron transport. *Biochimica et Biophysica Acta (BBA)-Bioenergetics*, 1229(1), 23-38.
- Bennoun, P.** (1983). Effects of mutations and of ionophore on chlororespiration in *Chlamydomonas reinhardtii*. *FEBS Letters*, 156(2), 363-365.
- Berges, J. A., Franklin, D. J., & Harrison, P. J.** (2001). Evolution of an artificial seawater medium: improvements in enriched seawater, artificial water over the last two decades. *Journal of phycology*, 37(6), 1138-1145.
- Berne, N., Fabryova, T., Istaz, B., Cardol, P., & Bailleul, B.** (2018). The peculiar NPQ regulation in the stramenopile *Phaeomonas sp.* challenges the xanthophyll cycle dogma. *Biochimica et Biophysica Acta (BBA)-Bioenergetics*, 1859(7), 491-500
- Brestic, M., Zivcak, M., Kunderlikova, K., Sytar, O., Shao, H., Kalaji, H. M., & Allakhverdiev, S. I.** (2015). Low PSI content limits the photoprotection of PSI and PSII in early growth stages of chlorophyll b-deficient wheat mutant lines. *Photosynthesis research*, 125(1-2), 151-166.

- Brettel, K.** (1997). Electron transfer and arrangement of the redox cofactors in photosystem I. *Biochimica et Biophysica Acta (BBA)-Bioenergetics*, 1318(3), 322-373.
- Buchert, F., Bailleul, B., Hisabori, T.** (2017). A γ -subunit point mutation in *Chlamydomonas reinhardtii* chloroplast F_1F_0 -ATP synthase confers tolerance to reactive oxygen species. *Biochimica et Biophysica Acta (BBA)-Bioenergetics*, 1858(12), 966-974.
- Bujaldon, S., Kodama, N., Rappaport, F., Subramanyam, R., de Vitry, C., Takahashi, Y., & Wollman, F. A.** (2017). Functional accumulation of antenna proteins in chlorophyll b-less mutants of *Chlamydomonas reinhardtii*. *Molecular plant*, 10(1), 115-130.
- Cardol, P., Gloire, G., Havaux, M., Remacle, C., Matagne, R., & Franck, F.** (2003). Photosynthesis and state transitions in mitochondrial mutants of *Chlamydomonas reinhardtii* affected in respiration. *Plant physiology*, 133(4), 2010-2020
- Chaux, F., Peltier, G., Johnson, X.** (2015). A security network in PSI photoprotection: regulation of photosynthetic control, NPQ and O_2 photoreduction by cyclic electron flow. *Frontiers in plant science*, 6, 875.
- Chaux, F., Burlacot, A., Mekhalfi, M., Auroy, P., Blangy, S., Richaud, P., Peltier, G.** (2017). Flavodiiron proteins promote fast and transient O_2 photoreduction in *Chlamydomonas*. *Plant physiology*, 174(3), 1825-1836.
- DalCorso, G., Pesaresi, P., Masiero, S., Aseeva, E., Schünemann, D., Finazzi, G., ... & Leister, D.** (2008). A complex containing PGRL1 and PGR5 is involved in the switch between linear and cyclic electron flow in *Arabidopsis*. *Cell*, 132(2), 273-285.
- Delosme, R., Béal, D., Joliot, P.** (1994). Photoacoustic detection of flash-induced charge separation in photosynthetic systems. Spectral dependence of the quantum yield. *Biochimica et Biophysica Acta (BBA)-Bioenergetics*, 1185(1), 56-64.
- Drop, B., Webber-Birungi, M., Yadav, S. K., Filipowicz-Szymanska, A., Fusetti, F., Boekema, E. J., & Croce, R.** (2014). Light-harvesting complex II (LHCII) and its supramolecular organization in *Chlamydomonas reinhardtii*. *Biochimica et Biophysica Acta (BBA)-Bioenergetics*, 1837(1), 63-72.
- Duysens, L. N. M.** (1963). Mechanism of the two photochemical reactions in algae as studied by means of fluorescence. Studies on microalgae and photosynthetic bacteria, 353-372.
- Eberhard, S., Finazzi, G., Wollman, F. A.** (2008). The dynamics of photosynthesis. *Annual review of genetics*, 42, 463-515.
- Endo, T., Asada, K.** (2008). Photosystem I and photoprotection: cyclic electron flow and water-water cycle. In *Photoprotection, Photoinhibition, Gene Regulation, and Environment* (pp. 205-221). Springer, Dordrecht.
- Fan, D. Y., Nie, Q., Hope, A. B., Hillier, W., Pogson, B. J., Chow, W. S.** (2007). Quantification of cyclic electron flow around Photosystem I in spinach leaves during photosynthetic induction. *Photosynthesis Research*, 94(2-3), 347.
- Fan, D. Y., Fitzpatrick, D., Oguchi, R., Ma, W., Kou, J., Chow, W. S.** (2016). Obstacles in the quantification of the cyclic electron flux around Photosystem I in leaves of C3 plants. *Photosynthesis research*, 129(3), 239-251.

- Fisher, N., Bricker, T. M., & Kramer, D. M.** (2019). Regulation of photosynthetic cyclic electron flow pathways by adenylate status in higher plant chloroplasts. *Biochimica et Biophysica Acta (BBA)-Bioenergetics*, 1860(11), 148081
- Foyer, C. H., Neukermans, J., Queval, G., Noctor, G., Harbinson, J.** (2012). Photosynthetic control of electron transport and the regulation of gene expression. *Journal of Experimental Botany*, 63(4), 1637-1661.
- Genty B, Goulas Y, Dimon B, Peltier JM, Moya I.** (1992). Modulation of efficiency of primary conversion in leaves, mechanisms involved at PSII. In *Research in Photosynthesis*, Volume 4, ed. N Murata, pp. 603–10. Dordrecht: Kluwer Academic Publishers.
- Gobets, B., & van Grondelle, R.** (2001). Energy transfer and trapping in photosystem I. *Biochimica et Biophysica Acta (BBA)-Bioenergetics*, 1507(1-3), 80-99.
- Godaux, D., Bailleul, B., Berne, N., & Cardol, P.** (2015). Induction of photosynthetic carbon fixation in anoxia relies on hydrogenase activity and Proton-Gradient Regulation-Like1-mediated cyclic electron flow in *Chlamydomonas reinhardtii*. *Plant physiology*, 168(2), 648-658.
- Golbeck, J. H., & Bryant, D. A.** (1991). *Current topics in bioenergetics*. In *Light-Driven Reactions in Bioenergetics* (Vol. 16).
- Golbeck, J. H.** (1993). The structure of photosystem I: Current Opinion in Structural Biology 1993, 3: 508–514. *Current Opinion in Structural Biology*, 3(4), 508-514.
- Harbinson, J., Woodward, F. I.** (1987). The use of light-induced absorbance changes at 820 nm to monitor the oxidation state of P-700 in leaves. *Plant, Cell & Environment*, 10(2), 131-140.
- Harbinson, J., Genty, B., Baker, N. R.** (1989). Relationship between the quantum efficiencies of photosystems I and II in pea leaves. *Plant Physiology*, 90(3), 1029-1034.
- Harbinson, J., Foyer, C. H.** (1991). Relationships between the efficiencies of photosystems I and II and stromal redox state in CO₂-free air: evidence for cyclic electron flow in vivo. *Plant physiology*, 97(1), 41-49.
- Harris, E. H.** (2009). *The chlamydomonas sourcebook* (Vol. 1, pp. 119-157). D. B. Stern, & G. B. Witman (Eds.). San Diego, CA: Elsevier.
- Havaux, M., Davaud, A.** (1994). Photoinhibition of photosynthesis in chilled potato leaves is not correlated with a loss of photosystem-II activity. *Photosynthesis research*, 40(1), 75-92
- Hertle, A. P., Blunder, T., Wunder, T., Pesaresi, P., Pribil, M., Armbruster, U., & Leister, D.** (2013). PGRL1 is the elusive ferredoxin-plastoquinone reductase in photosynthetic cyclic electron flow. *Molecular cell*, 49(3), 511-523.
- Hippler, M., Drepper, F., Farah, J., Rochaix, J. D.** (1997). Fast electron transfer from cytochrome c 6 and plastocyanin to photosystem I of *Chlamydomonas reinhardtii* requires PsaF. *Biochemistry*, 36(21), 6343-6349.
- Hiyama, T., Ke, B.** (1972). Difference spectra and extinction coefficients of P700. *Biochimica et Biophysica Acta (BBA)-Bioenergetics*, 267(1), 160-171.
- Hoefnagel, M. H., Atkin, O. K., Wiskich, J. T.** (1998). Interdependence between chloroplasts and mitochondria in the light and the dark. *Biochimica et Biophysica Acta (BBA)-Bioenergetics*, 1366(3), 235-255.

- Holzwarth, A. R., Müller, M. G., Niklas, J., & Lubitz, W.** (2006). Ultrafast transient absorption studies on photosystem I reaction centers from *Chlamydomonas reinhardtii*. 2: mutations near the P₇₀₀ reaction center chlorophylls provide new insight into the nature of the primary electron donor. *Biophysical journal*, 90(2), 552-565.
- Houille-Vernes, L., Rappaport, F., Wollman, F. A., Alric, J., Johnson, X.** (2011). Plastid terminal oxidase 2 (PTOX2) is the major oxidase involved in chlororespiration in *Chlamydomonas*. *Proceedings of the National Academy of Sciences*, 108(51), 20820-20825.
- Huang, W., Yang, S. J., Zhang, S. B., Zhang, J. L., & Cao, K. F.** (2012). Cyclic electron flow plays an important role in photoprotection for the resurrection plant *Paraboea rufescens* under drought stress. *Planta*, 235(4), 819-828.
- Izawa, S.** (1980). Acceptors and donors and chloroplast electron transport. In *Methods in Enzymology* (Vol. 69, pp. 413-434). *Academic Press*
- Joliot, P. & Joliot, A.** (1964). Etude cinétique de la réaction photochimique libérant l'oxygène au cours de la photosynthèse. *CR Acad. Sci.*, 258, 4622-4625.
- Joliot, P., Delosme, R.** (1974). Flash-induced 519 nm absorption change in green algae. *Biochimica et Biophysica Acta (BBA)-Bioenergetics*, 357(2), 267-284.
- Joliot, P. & Joliot, A.** (1989). Characterization of linear and quadratic electrochromic probes in *Chlorella sorokiniana* and *Chlamydomonas reinhardtii*. *Biochimica et Biophysica Acta (BBA)-Bioenergetics*, 975(3), 355-360.
- Joliot, P., & Joliot, A.** (2002). Cyclic electron transfer in plant leaf. *Proceedings of the National Academy of Sciences*, 99(15), 10209-10214..
- Joliot, P., & Joliot, A.** (2006). Cyclic electron flow in C3 plants. *Biochimica et Biophysica Acta (BBA)-Bioenergetics*, 1757(5-6), 362-368.
- Joliot, P., Johnson, G. N.** (2011). Regulation of cyclic and linear electron flow in higher plants. *Proceedings of the National Academy of Sciences*, 108(32), 13317-13322.
- Junesch, U., Gräber, P.** (1987). Influence of the redox state and the activation of the chloroplast ATP synthase on proton-transport-coupled ATP synthesis/hydrolysis. *Biochimica et Biophysica Acta (BBA)-Bioenergetics*, 893(2), 275-288.
- Junge, W., & Witt, H. T.** (1968). On the ion transport system of photosynthesis—Investigations on a molecular level—. *Zeitschrift für Naturforschung B*, 23(2), 244-254.
- Junker, L. V., & Ensminger, I.** (2016). Relationship between leaf optical properties, chlorophyll fluorescence and pigment changes in senescing *Acer saccharum* leaves. *Tree physiology*, 36(6), 694-711
- Kautsky H, Appel W, Amann H** (1960) Die Fluoreszenzkurve und die Photochemie der Pflanze. *Biochem Z* 332:277–292
- Kautsky, H., & Franck, U.** (1948). Fluoreszenzanalyse des Lichtenergiewechsels der grünen Pflanze. *Naturwissenschaften*, 35(2), 43-51.
- Ke, B.** (2001). The primary electron donor of photosystem I—P700. *Photosynthesis: Photobiochemistry and Photobiophysics*, 463-478.

- Klughammer, C., Schreiber, U.** (1991). Analysis of light-induced absorbance changes in the near-infrared spectral region I. Characterization of various components in isolated chloroplasts. *Zeitschrift für Naturforschung C*, 46(3-4), 233-244.
- Klughammer, C., Schreiber, U.** (1994). An improved method, using saturating light pulses, for the determination of photosystem I quantum yield via P_{700}^+ -absorbance changes at 830 nm. *Planta*, 192(2), 261-268.
- Klughammer, C., & Schreiber, U.** (2016). Deconvolution of ferredoxin, plastocyanin, and P_{700} transmittance changes in intact leaves with a new type of kinetic LED array spectrophotometer. *Photosynthesis research*, 128(2), 195-214.
- Kobayashi, K., Sasaki, D., Noguchi, K., Fujinuma, D., Komatsu, H., Kobayashi, M., Sato, M., Toyooka, K., Sugimoto, K. Wada, H., Matsuda, T.** (2013). Photosynthesis of root chloroplasts developed in *Arabidopsis* lines overexpressing GOLDEN2-LIKE transcription factors. *Plant and cell physiology*, 54(8), 1365-1377.
- Kono, M., Noguchi, K., Terashima, I.** (2014). Roles of the cyclic electron flow around PSI (CEF-PSI) and O₂-dependent alternative pathways in regulation of the photosynthetic electron flow in short-term fluctuating light in *Arabidopsis thaliana*. *Plant and Cell Physiology*, 55(5), 990-1004.
- Kok, B.** (1961). Partial purification and determination of oxidation reduction potential of the photosynthetic chlorophyll complex absorbing at 700 m μ . *Biochimica et biophysica acta*, 48(3), 527-533.
- Kou, J., Takahashi, S., Fan, D. Y., Badger, M. R., Chow, W. S.** (2015). Partially dissecting the steady-state electron fluxes in Photosystem I in wild-type and *pgr5* and *ndh* mutants of *Arabidopsis*. *Frontiers in plant science*, 6, 758.
- Kramer, D. M., Johnson, G., Kiirats, O., & Edwards, G. E.** (2004). New fluorescence parameters for the determination of Q_A redox state and excitation energy fluxes. *Photosynthesis research*, 79(2), 209.
- Laisk, A., Talts, E., Oja, V., Eichelmann, H., Peterson, R. B.** (2010). Fast cyclic electron transport around photosystem I in leaves under far-red light: a proton-uncoupled pathway?. *Photosynthesis Research*, 103(2), 79-95.
- Larosa, V., Meneghesso, A., La Rocca, N., Steinbeck, J., Hippler, M., Szabo, I., & Morosinotto, T.** (2018). Mitochondria affect photosynthetic electron transport and photosensitivity in a green alga. *Plant physiology*, 176(3), 2305-2314.
- Li, Y., Van Der Est, A., Lucas, M. G., Ramesh, V. M., Gu, F., Petrenko, A., ... & Redding, K.** (2006). Directing electron transfer within Photosystem I by breaking H-bonds in the cofactor branches. *Proceedings of the National Academy of Sciences*, 103(7), 2144-2149.
- Malkin, R., Bearden, A. J.** (1971). Primary reactions of photosynthesis: photoreduction of a bound chloroplast ferredoxin at low temperature as detected by EPR spectroscopy. *Proceedings of the National Academy of Sciences*, 68(1), 16-19.
- Mix, L. J., Haig, D., & Cavanaugh, C. M.** (2005). Phylogenetic Analyses of the Core Antenna Domain: Investigating the Origin of Photosystem I. *Journal of molecular evolution*, 60(2), 153-163.
- Munekage, Y., Hojo, M., Meurer, J., Endo, T., Tasaka, M., & Shikanai, T.** (2002). PGR5 is involved in cyclic electron flow around photosystem I and is essential for photoprotection in *Arabidopsis*. *Cell*, 110(3), 361-371.

- Foyer, C. H., Lelandais, M., & Harbinson, J.** (1992). Control of the quantum efficiencies of photosystems I and II, electron flow, and enzyme activation following dark-to-light transitions in pea leaves: relationship between NADP/NADPH ratios and NADP-malate dehydrogenase activation state. *Plant Physiology*, *99*(3), 979-986
- Nawrocki, W. J., Bailleul, B., Cardol, P., Rappaport, F., Wollman, F. A., & Joliot, P.** (2019). Maximal cyclic electron flow rate is independent of PGRL1 in *Chlamydomonas*. *Biochimica et Biophysica Acta (BBA)-Bioenergetics*, *1860*(5), 425-432.
- Nelson, N.** (2009). Plant photosystem I—the most efficient nano-photochemical machine. *Journal of nanoscience and nanotechnology*, *9*(3), 1709-1713.
- Nelson, N., & Yocum, C. F.** (2006). Structure and function of photosystems I and II. *Annu. Rev. Plant Biol.*, *57*, 521-565.
- Oh-Oka, H., Itoh, S., Saeki, K., Takahashi, Y., Matsubara, H.** (1991). F_A/F_B protein from the spinach photosystem I complex: Isolation in a native state and some properties of the iron-sulfur clusters. *Plant and cell physiology*, *32*(1), 11-17.
- Pfündel, E., Klughammer, C., & Schreiber, U.** (2008). Monitoring the effects of reduced PS II antenna size on quantum yields of photosystems I and II using the Dual-PAM-100 measuring system. *PAM Application Notes*, *1*, 21-24.
- Ranjan, S., Singh, R., Singh, M., Pathre, U. V., & Shirke, P. A.** (2014). Characterizing photoinhibition and photosynthesis in juvenile-red versus mature-green leaves of *Jatropha curcas* L. *Plant Physiology and Biochemistry*, *79*, 48-59.
- Rumberg, B., Siggel, U.** (1969). pH changes in the inner phase of the thylakoids during photosynthesis. *Naturwissenschaften*, *56*(3), 130-132.
- Sacksteder, C. A., Kanazawa, A., Jacoby, M. E., & Kramer, D. M.** (2000). The proton to electron stoichiometry of steady-state photosynthesis in living plants: a proton-pumping Q cycle is continuously engaged. *Proceedings of the National Academy of Sciences*, *97*(26), 14283-14288.
- Sacksteder, C. A., & Kramer, D. M.** (2000). Dark-interval relaxation kinetics (DIRK) of absorbance changes as a quantitative probe of steady-state electron transfer. *Photosynthesis Research*, *66*(1-2), 145.
- Schansker, G., Srivastava, A., & Strasser, R. J.** (2003). Characterization of the 820nm transmission signal paralleling the chlorophyll a fluorescence rise (OJIP) in pea leaves. *Functional Plant Biology*, *30*(7), 785-796.
- Schansker, G., Tóth, S. Z., & Strasser, R. J.** (2005). Methylviologen and dibromothymoquinone treatments of pea leaves reveal the role of photosystem I in the Chl a fluorescence rise OJIP. *Biochimica et Biophysica Acta (BBA)-Bioenergetics*, *1706*(3), 250-261.
- Schansker, G., Tóth, S. Z., & Strasser, R. J.** (2006). Dark recovery of the Chl a fluorescence transient (OJIP) after light adaptation: the qT-component of non-photochemical quenching is related to an activated photosystem I acceptor side. *Biochimica et Biophysica Acta (BBA)-Bioenergetics*, *1757*(7), 787-797.
- Scheller, H. V.** (1996). In vitro cyclic electron transport in barley thylakoids follows two independent pathways. *Plant Physiology*, *110*(1), 187-194.

- Schreiber, U.** (2017). Redox changes of ferredoxin, P₇₀₀, and plastocyanin measured simultaneously in intact leaves. *Photosynthesis research*, 134(3), 343-360.
- Sejima, T., Takagi, D., Fukayama, H., Makino, A., & Miyake, C.** (2014). Repetitive short-pulse light mainly inactivates photosystem I in sunflower leaves. *Plant and Cell Physiology*, 55(6), 1184-1193.
- Setif, P., & Mathis, P.** (1980). The oxidation-reduction potential of P₇₀₀ in chloroplast lamellae and subchloroplast particles. *Archives of biochemistry and biophysics*, 204(2), 477-485.
- Shikanai, T.** (2007). Cyclic electron transport around photosystem I: genetic approaches. *Annu. Rev. Plant Biol.*, 58, 199-217.
- Slater, E. C.** (1973). The mechanism of action of the respiratory inhibitor, antimycin. *Biochimica et Biophysica Acta (BBA)-Reviews on Bioenergetics*, 301(2), 129-154.
- Sonoike, K., & Terashima, I.** (1994). Mechanism of photosystem-I photoinhibition in leaves of *Cucumis sativus* L. *Planta*, 194(2), 287-293.
- Sonoike, K.** (1996). Degradation of psaB gene product, the reaction center subunit of photosystem I, is caused during photoinhibition of photosystem I: possible involvement of active oxygen species. *Plant Science*, 115(2), 157-164.
- Sonoike, K.** (2011). Photoinhibition of photosystem I. *Physiologia Plantarum*, 142(1), 56-64.
- Sonoike, K., Terashima, I., Iwaki, M., Itoh, S.** (1995). Destruction of photosystem I iron-sulfur centers in leaves of *Cucumis sativus* L. by weak illumination at chilling temperatures. *FEBS letters*, 362(2), 235-238.
- Stark, J.** (1914). Beobachtungen über den Effekt des elektrischen Feldes auf Spektrallinien. I. Quereffekt. *Annalen der Physik*, 348(7), 965-982.
- Stirbet, A., Riznichenko, G. Y., & Rubin, A. B.** (2014). Modeling chlorophyll a fluorescence transient: relation to photosynthesis. *Biochemistry (Moscow)*, 79(4), 291-323.
- Suzuki, K., Ohmori, Y., Ratel, E.** (2011). High root temperature blocks both linear and cyclic electron transport in the dark during chilling of the leaves of rice seedlings. *Plant and Cell Physiology*, 52(9), 1697-1707.
- Tagawa, K., Tsujimoto, H. Y., & Arnon, D. I.** (1963). Role of chloroplast ferredoxin in the energy conversion process of photosynthesis. *Proceedings of the National Academy of Sciences of the United States of America*, 49(4), 567.
- Talts, E., Oja, V., Rämme, H., Rasulov, B., Anijalg, A., Laisk, A.** (2007). Dark inactivation of ferredoxin-NADP reductase and cyclic electron flow under far-red light in sunflower leaves. *Photosynthesis research*, 94(1), 109-120.
- Terashima, I., Funayama, S., Sonoike, K.** (1994). The site of photoinhibition in leaves of *Cucumis sativus* L. at low temperatures is photosystem I, not photosystem II. *Planta*, 193(2), 300-306.
- Viola, S., Bailleul, B., Yu, J., Nixon, P., Sellés, J., Joliot, P., & Wollman, F. A.** (2019). Probing the electric field across thylakoid membranes in cyanobacteria. *Proceedings of the National Academy of Sciences*, 116(43), 21900-21906.

- Voss, I., Koelmann, M., Wojtera, J., Holtgreffe, S., Kitzmann, C., Backhausen, J. E., Scheibe, R.** (2008). Knockout of major leaf ferredoxin reveals new redox-regulatory adaptations in *Arabidopsis thaliana*. *Physiologia plantarum*, 133(3), 584-598.
- Wang, J. H., Li, S. C., Sun, M., Huang, W., Cao, H., Xu, F., Zhou, N. N., Zhang, S. B.** (2013). Differences in the stimulation of cyclic electron flow in two tropical ferns under water stress are related to leaf anatomy. *Physiologia plantarum*, 147(3), 283-295.
- Warren, P. V., Parrett, K. G., Warden, J. T., & Golbeck, J. H.** (1990). Characterization of a photosystem I core containing P₇₀₀ and intermediate electron acceptor A1. *Biochemistry*, 29(28), 6545-6550.
- Webber, A. N., Su, H., Bingham, S. E., Käss, H., Krabben, L., Kuhn, M., ... & Lubitz, W.** (1996). Site-directed mutations affecting the spectroscopic characteristics and midpoint potential of the primary donor in photosystem I. *Biochemistry*, 35(39), 12857-12863.
- Weis, E., Ball, J. T., Berry, J.** (1987). Photosynthetic control of electron transport in leaves of *Phaseolus vulgaris*: evidence for regulation of photosystem 2 by the proton gradient. In *Progress in photosynthesis research* (pp. 553-556). Springer, Dordrecht.
- Witt, H. T.** (1979). Energy conversion in the functional membrane of photosynthesis. Analysis by light pulse and electric pulse methods: The central role of the electric field. *Biochimica et Biophysica Acta (BBA)-Reviews on Bioenergetics*, 505(3-4), 355-427.
- Zivcak, M., Brestic, M., Kunderlikova, K., Sytar, O., Allakhverdiev, S. I.** (2015). Repetitive light pulse-induced photoinhibition of photosystem I severely affects CO₂ assimilation and photoprotection in wheat leaves. *Photosynthesis research*, 126(2-3), 449-463.

Chapter 3: Diversity of cyclic electron flow in microalgae

Summary

3.1 Introduction: CEF, a still mysterious alternative pathway	158
3.1.1. Role of CEF in ATP/NADPH adjustment and photo-protection	158
3.1.2. Regulation of CEF rate	161
3.1.3. Measuring CEF is a methodological challenge.....	163
3.1.4. Chapter outlines	165
3.2 Material and methods	167
3.2.1 Strains, growth and sampling	167
3.2.2 Chemicals.....	168
3.2.3 In vivo spectroscopy	168
3.2.4 ECS spectra and linearity with electric field	169
3.2.5 Absorption cross section assessment	170
3.3 Results (I): Exploring CEF diversity	172
3.3.1 DCMU titration reveals CEF behavior	172
3.3.2 Which observables?.....	174
3.3.3 CEF is not essential to photosynthesis in the dinoflagellate <i>Amphidinium carterae</i>	176
3.3.4 CEF is independent on LEF photosynthesis in the dinoflagellate <i>Symbiodinium sp.</i>	177
3.3.5 <i>Chlamydomonas reinhardtii</i> displays a CEF which is dependent on LEF	179
3.3.6 Partial conclusion on CEF diversity	181
3.4 Results (II): Evaluating CEF and LEF absolute rates as a function of light irradiance in the green alga <i>Chlamydomonas reinhardtii</i>	182
3.4.1 ECS-based estimations of the PSI and PSII absorption cross sections	183
3.4.2 Validation of the method for measurement of absorption cross sections	186
3.4.3 Evaluating CEF absolute rates from ETR(total) and ETR(II).....	191
3.4.4 Calculations of the ATP/NADPH ratio produced by the photosynthetic chain.....	193
3.5 Discussion and future perspectives	196
3.5.1 A simple and robust protocol to investigate CEF diversity highlights three different behaviors	196
3.5.2 Limitations of the DCMU titration method	203
3.5.3 Despite a complex relationship, CEF and LEF remain proportional at all light intensities in <i>Chlamydomonas reinhardtii</i>	206
3.6 Bibliography	210

3.1 Introduction: CEF, a still mysterious alternative pathway

The existence of cyclic phosphorylation in chloroplasts has first been proposed by Arnon and his collaborators in 1954 (Arnon, Allen and Whatley, 1954). It is now well established that in plants and green algae, a cyclic electron flow (CEF) around PSI can generate ATP. As already mentioned in the Introduction to the thesis (Chapter 1), genetic analyzes have elucidated mainly two independent pathways of CEF in plants, a pathway involving the proteins PGR5 and PGRL1 (Munekage et al, 2002; Hertle et al, 2013), and another one using the chloroplast complex NADPH dehydrogenase, NDH (Munekage et al, 2002). Structures of the cytochrome *b₆f* (Stroebel et al., 2003) have revived a third possibility proposed by Mitchell (Mitchell, 1975) and reiterated afterwards (Joliot, Béal and Joliot, 2004; Nawrocki et al, 2019a) which involves the electron transfer from ferredoxins directly to the Q_i site of the cyt *b₆f* complex. The mechanistic aspects of CEF and LEF, the important question of the proton-to-electron coupling in both LEF and CEF modes and the photo-protection mechanisms have been discussed in the general introduction (chapter 1), and are only briefly recalled in this chapter. In the introduction of this chapter, I will focus on the proposed roles of CEF (3.1.1), on its possible modes of regulation (3.1.2) and on the methodological limitations of its measurement (3.1.3).

3.1.1. Role of CEF in ATP/NADPH adjustment and photo-protection

Two main roles have been proposed for CEF. Hereafter, we present arguments that led to highlight those roles and discuss them.

a) Role of CEF in ATP/NADPH ratio equilibration

It has long been debated whether the ATP/NADPH ratio produced by LEF is equivalent to the ATP/NADPH ratio consumed in the CBB cycle and other metabolic processes. According to the most recent cryo-electron microscopy works on plant chloroplast ATP synthase (CF₁-F₀), it takes 14 H⁺ to synthesize 3 ATP (Hahn et al., 2018). Moreover, 6 H⁺ are moved into the lumen for 2 electrons transferred through the linear chain to reduce 1 NADP⁺ into NADPH. All in all, the linear transport chain produces about 1.3 ATP per NADPH (1.286 from the computation above).

It is well admitted that CBB cycle uses 1.5 ATP per NADPH but this ratio can increase to 1.65 depending on CO₂ concentration (Kramer & Evans, 2011). Another metabolic process that depends on CO₂ concentration and on photosynthetic activity is the carbon concentrating mechanisms (CCM), the active transport of inorganic carbon inside the chloroplast (see chapter 1 - general introduction for more details), which requires additional ATP. All in all, the minimal requirement of carbon assimilation is 1.5 ATP per NADPH but this ratio may increase depending on environmental conditions.

It is therefore widely assumed that in plants and green algae, the ATP/NADPH produced by LEF is insufficient. CEF has been proposed as a complementary pathway to increase ATP production by the photosynthetic chain (Allen, 2002). Indeed, the latter flow induces an electron transfer through the cytochrome *b₆f*, and thus proton pumping and synthesis of ATP, without producing any reducing power. It is therefore a potential route that would balance the ATP/NADPH ratio to reach the metabolic pathways needs. One can then easily calculate the ratio of ATP/NADPH produced by the photosynthetic chain depending on the CEF/LEF ratio, i.e. the fraction rate of PSI turnovers used for CEF divided by the rate of PSI turnovers used for LEF. LEF is translocating 3 H⁺ into the lumen per PSI turnover involved in LEF, i.e. per electron transferred to NADPH (6 H⁺ per NADPH). CEF is translocating 2 H⁺ per PSI turnover involved in CEF. If we assume that the chloroplast ATP synthase (CF₁-F₀) comprises 14 c-subunit and thus requires 14 H⁺ to produce 3 ATP, then LEF produces 9/14 ATP and 0.5 NADPH per PSI turnover. CEF produces 6/14 ATP per PSI turnover.

ATP/NADPH ratio produced by the photosynthetic chain can thus be calculated as:

$$(1) \text{ ATP/NADPH} = (9/14 \text{ LEF} + 6/14 \text{ CEF}) / (0.5 \text{ LEF}) = 18/14 + 12/14 \text{ CEF/LEF}$$

Therefore, one can calculate that the minimal CEF/LEF ratio which allows CEF to fulfill the ATP shortfall. When the minimal value of 1.5 ATP per NADPH in the CBB cycle is considered, equation (1) indicates that a CEF/LEF of 0.25 (20% of PSI turnovers are used for CEF) is enough to fuel CO₂ assimilation.

b) Role of CEF in photoprotection

We have discussed the risk of photo-destruction of both photosystem I and II in conditions of excess light in the general introduction (chapter 1). The CEF can reduce the risk of photodestruction of photosystems by playing a role in two main photo-protection mechanisms. The first is the slowdown of cytochrome *b₆f* via a regulation called “photosynthetic control”: by increasing the I proton gradient (ΔpH), the CEF decreases the turnover of cytochrome *b₆f*, of which kinetically limiting step is the release of protons at the Q_0 site (Tikonov et al., 2014). This moves the limiting step of the electron transfer from downhill PSI to uphill PSI, releasing the reducing pressure on the acceptor side of the PSI.

The second consequence of the ΔpH generated by CEF is to promote non-photochemical quenching of PSII fluorescence, q_E , a mechanism that increases the light energy dissipation as heat (Golding, Finazzi, & Johnson, 2004; Heber & Walker, 1992; Kramer, Avenson, & Edwards, 2004; Li et al., 2000; Müller, Li, & Niyogi, 2001). We should note here that some studies show q_E implementation under high light without the intervention of CEF (Avenson, Cruz, Kanazawa, & Kramer, 2005; Ishikawa, Endo, & Sato, 2008).

c) What about other alternative electron flows?

Several other alternative pathways have been proposed to increase the ATP/NADPH production by the photosynthetic chain and to play a role in photosystems photoprotection. The main ones are grouped as water to water cycles which use electrons from water at the Oxygen evolving complex and reroute them to an oxidase. Several oxidases associated to water to water cycles have been identified, including the flavodiiron proteins (Chaux et al., 2017; Allahverdiyeva et al., 2013), and the Mehler reaction, or superoxide dismutase pathway (Asada, Allen, Foyer, & Matthijs, 2000), which both transfer electrons to O_2 downhill PSI (Nawrocki et al., 2019). The plastoquinone terminal oxidase (PTOX) reroutes the electrons from plastoquinol towards molecular oxygen, but seems to play a role only in some very specific cases, like in iron deprived algae (Bailey et al., 2008; Cardol et al., 2008; Zehr & Kudela, 2009, Nawrocki et al., 2019b) or in alpine plants (Streb et al., 2005, Lareau et al., 2013). Last, the rerouting of reducing power from the stroma towards the mitochondrion, which can take place in green algae (Lemaire, Wollman, Bennoun, & Plant, 1988), in diatoms (Bailleul et al., 2015) or in plants (Scheibe, 2004) can be considered as a “meta” water to water cycle. There are also alternative pathways that reroute electrons to other molecules than molecular oxygen. This is the case of the hydrogenase pathway which

occurs mostly in anoxia (Ghirardi et al., 2007) and transfers electrons from the acceptor side of the PSI to catalyze the reduction of protons into dihydrogen (see chapter 1 for more information on water to water cycles).

All those alternative electron flows also involve the photosystem II and (except for PTOX) the cytochrome *b₆f*, favoring extra proton pumping (Eberhard, Wollman and Finazzi, 2008). By doing so, they participate to the ΔpH dependent processes, q_E and photosynthetic control. They also promote ATP production, without producing any reducing power, increasing the ATP/NADPH produced by the overall photosynthetic activity. This must be considered when discussing the role of CEF in ATP/NADPH adjustment or in the ΔpH related photo-protective mechanisms. It might be a naïve view to assume that CEF alone regulates those photosynthetic regulations, and a more cautious point of view would be to consider *a priori* that they are ensured by all these alternative electron flows.

3.1.2. Regulation of CEF rate

In the first section, we have discussed the several roles of CEF: adjusting the ATP/NADPH produced by the photosynthetic chain to the metabolic needs, increasing the proton motive force (and especially its osmotic component ΔpH) to protect photosystem II (through the q_E mechanism) and photosystem I (through the photosynthetic control). We have also mentioned in the general discussion (chapter 1) that the main molecular actors involved in the electron transfer step allowing the recycling of electrons from PSI acceptors back to the inter-system chain are not yet fully determined. A third important aspect of CEF that needs to be discussed in order to complete the view about this process is the mode of regulation. What does the rate of CEF depend on? It is clear that CEF rates need to be adjusted to LEF rates to fulfill its roles. It can be involved efficiently in photo-protection if –and only if- its rate modifies significantly the pmf under high light. It can provide the extra ATP/NADPH needed for CO_2 assimilation if –and only if- the rate of its ATP production matches with the CBB associated ATP shortfall. This means its rate must be at least a given fraction (~20%, see 3.1.1) of the LEF rate, regardless of the irradiance. How does the photosynthetic chain regulate the relative rates of LEF and CEF?

Determinants of CEF rate remain unclear and models are still strongly debated. Three major modes have been proposed for CEF-to-LEF regulation that are not mutually exclusive: a modulation of kinetic constants of enzymes involved in CEF, a regulation by substrate

concentration (i.e. the redox state of the PQ pool and the redox state of PSI acceptors, ferredoxin and NADPH) or physical separation of photosystems and other photosynthetic complexes involved in the two processes. The CEF rate could be simply determined passively by the concentrations of its substrates. In a model where electrons are reintroduced in the inter-system chain at the level of the plastoquinone pool, from ferredoxin (the FQR pathway), then the rate of CEF would be determined by the redox state of the PQ pool and the redox state of ferredoxins (Allen, 2003; Alric et al, 2010). The ATP shortfall for CO₂ assimilation in the CBB cycle would lead to an over-reduction of PSI acceptors. The increase in the concentration of the latter, substrates of CEF would in turn favor CEF, increasing ATP production.

However, another mode of regulation is possible, where the kinetic constant of the electron re-injection step is regulated. Kramer and collaborators proposed that the both ferredoxin-quinone reductase (FQR) and the NDH pathway are inhibited by the ATP level itself (Fisher et al., 2019). Again, the ATP shortfall would at the contrary favor the CEF, producing more ATP as a response.

Another mode of regulation of the CEF and LEF rates comes from the segregation of LEF and CEF chains. Several works propose the formation of super-complexes involving cytochrome *b₆f*, PSI and enzymes involved specifically in CEF such as PGRL1 and PGR5 (Iwai et al., 2010, Steinbeck et al., 2018, Kouril et al., 2014). If such super-complexes exist in significant concentration –which has not been demonstrated yet- they would constrain the electron carriers in a cyclic mode by reducing the distance between the intermediates (Steinbeck et al., 2018). It has also been proposed that under certain physiological conditions, the FNR could move from the PSI vicinity towards a docking site on the *b₆f* causing an increase of the affinity of ferredoxins for the CEF pathway (Joliot and Johnson, 2011; Zhang, Whitelegge, & Cramer, 2001). Another mode of structuration has been proposed which involved a fine coupling between CEF/LEF ratio, and state transitions (Finazzi, 2002) but is not considered any more after several works demonstrated that there is no causal link between the two processes (Takahashi et al., 2013).

Another important issue in the regulation of CEF rate is the one of its limiting step. This issue is rarely discussed explicitly but has a tremendous importance regarding the potential role and mode of regulation of CEF. Under high light, the limiting step of the electron transfer from plastoquinols to PSI acceptors, which is common to both LEF and CEF, is the cytochrome *b₆f*. Is the cytochrome *b₆f* also the limiting step of CEF under high light? Or is it

instead the “cycling step”, i.e. the electron transfer step from PSI acceptors to the inter-system chain closing the cycle?

Many studies suggest that CEF rates are low in comparison to maximal LEF rates under non-stressful conditions. Values range from 3% in wild type *Chlamydomonas* to 10% in a FNR mutant of the same green alga (Alric, 2010), whereas it is less than 14% of the maximal LEF rate in plants (Laisk, Eichelmann, Oja, Talts, & Scheibe, 2007; Livingston, Cruz, Kohzuma, Dhingra, & Kramer, 2010; Fan et al., 2007). This has been an argument to propose that the CEF limiting step is slower than the LEF limiting step, most likely because the kinetics of reinjection of the reducing power into the chain would be limiting for CEF (Alric 2010). In that case, the CEF/LEF ratio is expected to decrease with light irradiance, and a role of CEF under high light is doubtful. But many of the measurements in steady state illumination were performed in the presence of DCMU, which might not provide a good measurement of the “physiological” CEF (Fan et al, 2016) (see 3.1.3). On the other hand, measurements of CEF during dark to light transition in the presence of DCMU give a different view. In these conditions, CEF rate reaches 60 electrons.s⁻¹.PSI⁻¹ in *Chlamydomonas reinhardtii* (Nawrocki et al., 2019c) and up to 120 electrons.s⁻¹.PSI⁻¹ in plant leaves (Joliot and Johnson, 2011; Joliot, Béal and Joliot, 2004). The latter value is close to the maximal LEF rate in plant leaves, which would mean that in physiological conditions, CEF might be limited by the turnover of the cytochrome *b₆f*. If CEF and LEF have the same limited step, it is plausible that the CEF/LEF remains constant at all light irradiances, making CEF a likely candidate for ATP/NADPH regulation.

3.1.3. Measuring CEF is a methodological challenge

There are still many doubts as to the physiological significance of CEF, its amplitude in stationary illumination regime, or even its existence in many groups of photosynthetic organisms. The main reason for the remaining doubts and open questions regarding CEF, after half a century of research, is the absence of a definitive method for measuring the CEF *in vivo* under physiological conditions (Shikanai, 2014; Johnson, 2005). In this chapter, I aim to set the basis of an exploration of the diversity of the CEF in phytoplankton, where very little is known. This task is obviously endless and there are numerous traps when one wants to measure CEF, as highlighted in chapter 2. That is the reason I will review here the limitations in CEF measurements.

CEF has no net product. Thus, its rate cannot be probed thanks to the evolution of a product, like LEF with molecular oxygen for example. In addition, there is no clear consensus regarding the pathway of the “cycling step” (through PGRL1/PGR5, through the NDH or directly via the Q_{CO2} site of cytochrome b_6f) and no specific spectroscopic signal associated to them. In order to reduce the complexity of the system, a simple approach is to inhibit the PSII with chemicals like DCMU (Fan et al., 2007; Joliot and Joliot, 2002; Nawrocki et al., 2019c) or to diminish its activity by using PSI specific light quality (far red in plants, Joliot and Joliot, 2005). Then, the PSI activity, and more generally photosynthetic activity, can only be attributed to CEF. However, if LEF and CEF are interacting, in competitions for a substrate for example, then the flux measured when the PSII is inhibited is not representative of the actual flux under physiological conditions (i.e. when the PSII is active) (Fan et al 2007). If one wants to understand the physiological role of the CEF, it seems important to first understand the relationship between CEF and LEF before discussing the results obtained when the PSII is inactive.

The only remaining approach is then to estimate the CEF rate as the difference between the electron transfer rate through PSI, the photosystem involved in both CEF and LEF, and the one through photosystem II, involved in LEF only (Fan et al, 2016). The electron transfer rate (ETR) through a photosystem (PSII or PSI) is the product of the light irradiance I ($\mu\text{mol photons m}^{-2} \text{s}^{-1}$), the absorption cross section σ (m^2) and the quantum yield of the photosystem i.e. the probability that a photon gives rise to a charge separation, Y (without unit). We can write:

ETR(I) (electrons/PSI/s) = $I \cdot \sigma_I \cdot Y(I)$ and ETR(II) (electrons/PSII/s) = $I \cdot \sigma_{II} \cdot Y(II)$, which, once the fractions n_2 and n_1 of PSII and PSI are considered, leads to:

$$(2) \text{ CEF (electrons/PSI/s)} = \text{ETR(I)} - n_2/n_1 \cdot \text{ETR(II)} = I \cdot (\sigma_I \cdot Y(I) - n_2/n_1 \cdot \sigma_{II} \cdot Y(II))$$

From equation (2), it appears that a correct measurement of CEF requires accurate measurements of both PSI and PSII yields and absorption cross-sections, and the photosystems stoichiometry. Each error on the measurement of one of those parameters will sum up in the error on the contribution of CEF to the overall photosynthetic activity. To test whether CEF can represent 20% of LEF, a relative error or noise-to-signal ratio of 10% for each of those parameters would be already prohibitive.

3.1.4. Chapter outlines

CEF capacity is conserved among plants and green algae (Alric and Johnson, 2017), where most of the studies have been conducted. Therefore, our knowledge is mainly based on results obtained in higher plants and green algae. The model systems *Arabidopsis thaliana*, for plants, and *Chlamydomonas reinhardtii*, for green algae, played a major role because genetics approaches are available (Grossman, 2000). The aim of this chapter is to investigate the occurrence and if so, the diversity of CEF characteristics within eukaryotic photosynthetic organisms. Figure 3-1 displays the fraction of publication dedicated to CEF in the different groups of photosynthetic organisms. The proportion of the studies focusing on diatoms, dinoflagellates and haptophytes is very small; only 2.5% of the publications on the subject concern species which are not cyanobacteria or part of the green lineage.

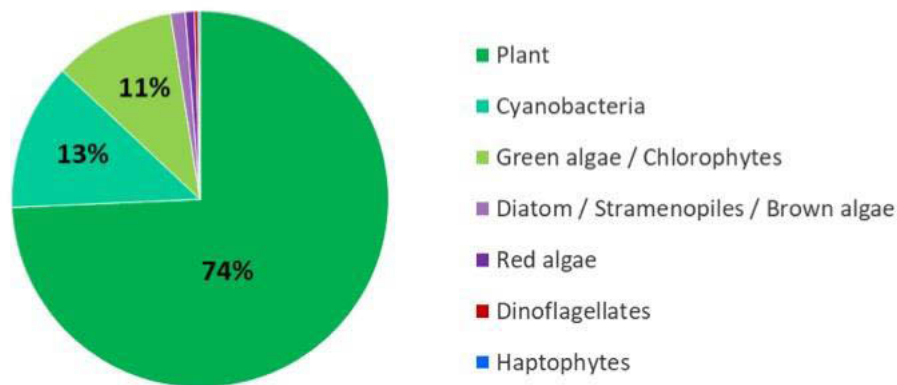


Figure 3-1: Percentage of the publications about cyclic electron flow among the various oxygenic photosynthetic clades

The percentage of publications was estimated by searching on the Pubmed database the number of publications mentioning “Photosynthesis” AND “cyclic electron flow” AND a photosynthetic clade such as “Plant”, “Cyanobacteria”, [“Green algae” OR “Chlorophytes”], [“Diatom” OR “Stramenopiles” OR “Brown algae”], “Red algae”, “Dinoflagellates” and “Haptophytes”.

When considering the amount of work done in the last 50 years to progress on understanding the mechanisms and regulations of the CEF in plants and green algae, one can be pessimistic about the possibility of reaching the same level of knowledge in all the phytoplankton groups before tens of years. Some studies have been performed on phytoplankton groups (e.g. Bailleul et al, 2015; Roberty et al, 2014; Meneghesso et al, 2016), showing low CEF rates and concluding that CEF was not sufficient to regulate the ATP/NADPH ratio. But most of those studies were performed in DCMU conditions and could have under-estimated the CEF rate under physiological (non-treated) conditions. Genetic approaches are not yet developed for most phytoplankton groups (transformation techniques are now routinely used in diatoms only). And we have listed all the

methodological difficulties related to the measurement of CEF. This is why it seems reasonable to take a step back and think about a simple and robust method usable for all species and that still gives basic important information about CEF.

In *Rules for the direction of the mind*, Descartes says : “Sur les objets proposés à notre étude il faut chercher, non ce que d’autres ont pensé ou ce que nous-même nous conjecturons, mais ce dont nous pouvons avoir l’intuition claire et évidente ou ce que nous pouvons déduire avec certitude : car ce n’est pas autrement que la science s’acquiert », traduced in english by “As regards any subject we propose to investigate, we must inquire not what other people have thought, or what we ourselves conjecture, but what we can clearly and manifestly perceive by intuition or deduce with certainty. For there is no other way of acquiring knowledge.” We will follow this advice and spend some time determining what can reasonably be done regarding CEF measurements, before starting a “screening” of CEF in the phytoplankton groups.

The results of this chapter are divided in two parts:

- I first determined a robust and simple protocol to assess CEF *in vivo*, while minimizing sources of errors or noise. With this, we could investigate whether CEF exists or not in several microalgae and, when it is present to determine its relationship with LEF. This approach revealed three different CEF behaviors, provided CEF/LEF ratios for two of the three cases, but failed at giving absolute rates of CEF (3.2. Results (I): Exploring CEF diversity).
- The second part can be seen as a more ambitious attempt to measure absolute rates of CEF and LEF. Here, I estimated the PSII and PSI absorption cross-sections and stoichiometry, and from there I could calculate CEF and LEF absolute rates. A significant fraction of PSI activity is associated to CEF in *Chlamydomonas reinhardtii* and this ratio remains the same at all light intensities. This is consistent with a role in ATP/NADPH regulation, and the extent of CEF seems largely sufficient to provide the extra ATP needed for C assimilation (3.3. Results (II): Measuring absolute rates of LEF and CEF in *Chlamydomonas reinhardtii*).

3.2 Material and methods

3.2.1 Strains, growth and sampling

Chlamydomonas reinhardtii stt7-9 mutant were obtained from the Chlamystation (<http://chlamystation.free.fr/>). The dinoflagellates *Amphidinium carterae* (RCC1522) was obtained from the Roscoff Culture Collection (<http://roscoff-culture-collection.org/>) and *Symbiodinium sp.* strain FIAp1 isolated from *Aiptasia pallida* (clade B1, see Roberty et al, 2014) was obtained from M. A. Coffroth (the BURR Culture Collection, University at Buffalo, NY, USA).

Chlamydomonas cells were grown in Tris/Acetate/Phosphate (TAP) medium (Harris, 1989), at 25°C and under continuous light provided by white LEDs and were harvested between 2 and 6 million cells per mL. The irradiance was 30 $\mu\text{mol photons m}^{-2} \text{s}^{-1}$. *Amphidinium carterae* and *Symbiodinium sp* were grown in ESAW medium (Berges et al, 2001) or ESAW with only 10% if the nitrogen indicated in the recipe (Figure 3-18) at 19°C and under 12h photoperiod at a light irradiance of 30 $\mu\text{mol photons.m}^{-2}.\text{s}^{-1}$ using fluorescent tubes. It was harvested in exponential phase between 80 000 and 200 000 cells per mL.

For photosynthetic measurements, liquid cultures of *Chlamydomonas reinhardtii*, *Amphidinium carterae* and *Symbiodinium sp* were concentrated by centrifugation (4 minutes at 3500 rpm) and resuspended in their supernatant to reach $\sim 10^7$ cells.mL⁻¹. Ficoll® was added to avoid drifts in the absorption measurements due to fast sedimentation of the cells. Concentrated samples were then stirred at 350 rpm under low light (~ 10 $\mu\text{mol photons.m}^{-2}.\text{s}^{-1}$ white light) for at least 30 minutes before starting measurements.

Chaetoceros dominated sample from the field was collected in the Penzé estuary (Roscoff, France). Water was sampled from surface brackish water (salinity: 16.3g.L⁻¹, water temperature: 16 °C) and then kept for 24 hours in a temperature controlled chamber (set at 16°C) with a 14h light/10h dark photoperiod. The sample was then purified and concentrated by filtration with a 20 μm polycarbonate filter and preservation of the retentate, later measured. A fraction of the sample was fixed by addition of iodine and its specific composition was determined later. We sedimented 10 mL of the sample using a combined plate chamber (Utermöhl 1931). The sample was then observed under an inverted light microscope and cells species were identified using a phytoplankton species determination guide provided by Laure Guillou from the “Adaptation and Diversity in

Marine" laboratory of the Roscoff Biological Station. More than 600 cells were counted and the percentage of each species was calculated.

3.2.2 Chemicals

Hydroxylamine (HA) and (3,4-dichlorophenyl)-1,1-dimethylurea (DCMU) and Carbonyl cyanide 4-(trifluoromethoxy)phenylhydrazone (FCCP) were obtained from Sigma Aldrich (Saint Louis, Missouri, USA). DCMU was diluted in ethanol. HA was diluted in distilled water. FCCP was diluted in dimethylsulfoxide. PSII was inhibited with 10 μM DCMU and 100 to 500 μM HA (for each experiment, the minimal concentration to reach maximal fluorescence in the dark was determined and used).

3.2.3 In vivo spectroscopy

All spectroscopic measurements were performed using a Joliot Type Spectrophotometer (JTS10, Biologic, Grenoble, France), which allowed to perform fluorescence and absorption difference measurements on the same sample. The actinic continuous light and the saturating pulse ($5000 \mu\text{mol photons m}^{-2} \text{s}^{-1}$) were provided by orange leds (630 nm) and the saturating laser flash was provided by a dye laser (690 nm) pumped with a Nd:YAG laser (6 ns duration, 532 nm).

For fluorescence, the detecting pulses were provided by a white led filtered by a blue filter (470 nm). The reference and measuring photodiodes were protected from actinic light by a BG39 Schott filter (Mainz, Germany) and a LPF650+RG665 Schott filter, respectively.

PSII quantum yield in the light were measured as $Y(\text{II}) = (F_m' - F')/F_m'$, respectively. F' is the fluorescence level under actinic light illumination, F_m' is the maximal fluorescence level obtained after a saturating light pulse in light-adapted sample. The maximal quantum yield of PSII was measured in dark-adapted cells (at least 1 minutes in the dark) and calculated as $F_v/F_m = (F_m - F_0)/F_m$, where F_m is the maximal value of fluorescence, measured after a saturating light pulse and F_0 is the minimal value of fluorescence in a dark adapted sample.

For Electro-chromic Shift (ECS) measurements, all data shown are the difference between the measurement in the presence of the actinic light (laser flash, background actinic light or saturating pulse) and the one in the absence of actinic light, to correct for artifacts. ECS signals were measured as the difference of the absorbance changes at 520 and 546 nm for *Chlamydomonas reinhardtii* and for the *Chaetoceros* dominated sample from the field; at

563 nm for *Amphidinium carterae* and for *Symbiodinium sp.* Those wavelength or combinations of wavelength were chosen to eliminate absorption changes related to c-type cytochromes. The detecting wavelength were provided by a white led filtered with interferential filters at the wavelength of interest (10 nm full width at half-maximum, Edmund Optics). The measuring and reference photodiodes were protected from scattered and transmitted actinic light by a BG39 Schott filter (Mainz, Germany).

The fraction of open PSI centers, $Y(I)_{ECS}$, was calculated as the ratio between the saturating flash induced ECS increase in the condition of interest and the one in dark-adapted samples. The stoichiometry between photosystems was calculated as n_2/n_1 where n_2 and n_1 ($1-n_2$) are the fraction of photosystem II and photosystem I to the total photosystems, respectively. n_2 was calculated as the ratio between the saturating flash induced ECS in conditions of PSII inhibition (DCMU and HA) and the one in control conditions (Bailleul et al, 2010).

The photochemical rate was calculated as in (Bailleul et al, 2010). In brief, the method uses “dark window” (Joliot and Joliot, 2002) or “dark interval relaxation kinetics” (DIRK, Sacksteder et al., 2000). The principle is the following: the steady state value of the electric field (and ECS) is the sum of the activities of the two photosystems, and other photosynthetic complexes or processes involved in the movement of charges across the thylakoid membrane (cytochrome *b₆f*, ATP synthase, proton pumping NDH, ion channels...). When the light is turned off, only the two photosystems stop instantaneously (they are the only ones using light as substrate) and therefore the initial slope of the ECS decay measures the rate at which the two photosystems were moving charges before the light offset. The slope of the ECS decay was normalized to the flash induced ECS increase in the dark-adapted sample, to express the photochemical rate in charge separations per PS per second.

3.2.4 ECS spectra and linearity with electric field

Symbiodinium sp ECS spectrum was obtained from a previous work published in 2014 (Roberty et al., 2014) and its linearity over the electric field was verified in the same publication. To determine *Amphidinium carterae* ECS spectrum, a concentrated sample was treated with an uncoupler (FCCP) with concentration necessary and sufficient to decrease the electric field in the dark. Under these conditions, the low concentration of uncoupler does not prevent the light-induced establishment of an electric field, but the electric field in the dark is suppressed and the activity of the plastid ATP synthase is slowed down (Joliot and Joliot, 2008). Hence, the long-lived ECS signals are no longer contaminated by other light-

induced absorption changes (e.g. cytochrome oxidation-reduction signals). A strong pulse of light ($\sim 2000 \text{ photons s}^{-1} \text{ PS1}^{-1}$) allowed the generation of electric field and ECS signals were measured from 50 ms after the end of the pulse. The homothetic decay of the ECS spectrum of *Amphidinium carterae* indicates that there cannot be both a linear and a quadratic component of ECS. The fact that the ECS induced by a saturating laser flash does not depend on the pre-existing electric field demonstrates the linearity of the ECS signal as a function of the electric field (data not shown here).

The ECS spectra of *Amphidinium carterae* (A) and *Symbiodinium sp.* (B) are shown in Figure 3-2.

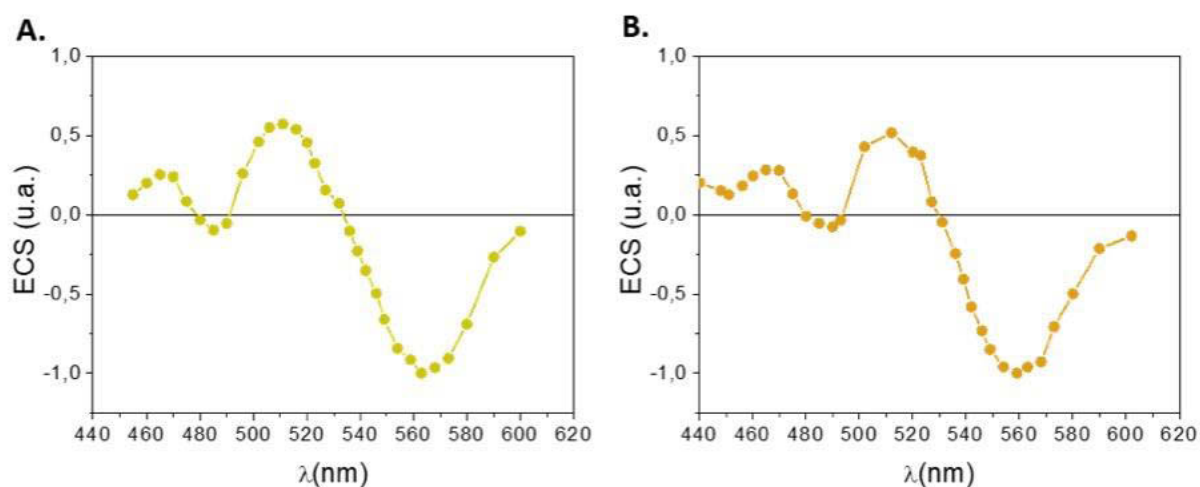


Figure 3-2: ECS spectrum of *Amphidinium carterae* (A.) and *Symbiodinium sp* (B.)

A. *Amphidinium carterae* ECS spectrum was obtained by Benjamin Bailleul before I started my PhD and have been measured as the absorption changes induced by a saturating pulse of light and remaining after 50 ms of dark (see Methods). B. *Symbiodinium sp.* ECS spectrum was obtained from Roberty and co-workers (Roberty et al, 2014) and correspond to the absorption changes induced by a saturating pulse of light in anoxia.

3.2.5 Absorption cross section assessment

The total absorption cross section per PS, σ_{total} , as well as the absorption cross section of PSI, σ_{I} were estimated by a method based on the ECS. σ_{total} and σ_{I} were calculated as the slope of ECS at light onset in the absence and in the presence of DCMU and HA, respectively. The measurement time has been determined so that the ECS creation does not exceed 0.5 charge separation per PS and per PS1, respectively. Figure 3-8A is an exception used to demonstrate the linearity of ECS with time.

The measurements of σ_{total} and σ_{I} were performed at several intensities (56, 135, 340, 800, 1500 $\mu\text{mol photons m}^{-2} \text{ s}^{-1}$). The curves $\sigma_{\text{total}} = f(I)$ and $\sigma_{\text{I}} = f(I)$ were fitted by a linear function forcing the intercept to 0, the slope giving σ_{total} and σ_{I} , respectively. Absorption cross section of PSII, σ_{II} , was estimated by two different methods. It was

calculated from σ_{total} and σ_i thanks to the equation $\sigma_{\text{total}} = n_1 \cdot \sigma_i + n_2 \cdot F_v/F_m$. σ_{II} . σ_{II} was also estimated using the kinetics of fluorescence rise at the onset of light in the presence of saturating DCMU concentration (10 μM). The curves were fitted by an exponential function ($y = y_0 + A_1 \cdot \exp(-t / \tau)$) and $\sigma_{\text{II}} \cdot I$ was estimated as $1 / \tau$. The estimation of $\sigma_{\text{II}} \cdot I$ was carried out at several light irradiances (as was done with ECS for σ_{total} and σ_i) and the curves $\sigma_{\text{II}} \cdot I = f(I)$ were fitted by a linear function, forcing the intercept to 0, the slope giving σ_{II} .

3.3 Results (I): Exploring CEF diversity

In this first part of the results, I will present the work I have done to explore the CEF diversity in freshwater and marine microalgae. For that, the first step consisted in elaborating a robust, simple and accurate protocol to extract basic information about CEF. I first determined the best spectroscopic tools that we possess to assess CEF *in vivo*. In order to get the most reliable measurements, we propose to probe CEF using the less parameters measurement as possible in order to reduce the technical noise and/or errors associated with each parameter measurement. The following two sections will present the reasoning behind the choice of the protocol we used to investigate CEF in different microalgae.

3.3.1 DCMU titration reveals CEF behavior

We have written before that the CEF rate can be calculated as:

$$(2) \text{ CEF} = \text{ETR(I)} - n_2/n_1 \cdot \text{ETR(II)}$$

This equation indicates that calculations of CEF through the comparison of PSII and PSI activities require accurate and non-biased measurement of both PSI and PSII yields and absorption cross-sections. The most widely used method to assess PSI quantum yield is based on P_{700} absorption change (Klughammer & Schreiber, 1994), but we have seen in chapter 2 that this method induces a bias that cannot be perfectly corrected (Ferté et al, unpublished). Based on this, we eliminated P_{700} absorption changes to probe PSI yield, $Y(I)$. We have seen in chapter 2 that the PSI yield can be obtained thanks to ECS if PSII is inhibited. But in conditions where PSII is functioning normally, ECS probes the activity of both photosystems. If we call $\text{ETR}(\text{total})$ the sum of PSI and PSII activities, i.e.

$\text{ETR}(\text{total})$ (electrons per PS per second) = $n_2 \cdot \text{ETR(II)} + n_1 \cdot \text{ETR(I)}$, then equation (2) becomes:

$$(3) \text{ ETR}(\text{total}) = 2 \cdot n_2 \cdot \text{ETR(II)} + n_1 \cdot \text{CEF}$$

The protocol we used is the following: under steady state light, we titrated both the ETR(II) and $\text{ETR}(\text{total})$ with a PSII inhibitor, the DCMU. In order to better understand our approach, I represented the expected DCMU dependence of ETR(II) (blue curve in Figure 3-3A) and simulated the evolution of $\text{ETR}(\text{total})$. Let's start with a situation where CEF is independent of the linear electron flow, i.e. does not change with DCMU concentrations. The activity of PSI involved in LEF should be, by definition equal to the one of PSII. And the contribution of

CEF, constant because independent of LEF, adds a pedestal to the total PSI activity (red curves for different CEF scenarios in Figure 3-3A). The total activity of photosystems, $ETR(\text{total})$, is the sum of PSII activity, $ETR(\text{II})$, and PSI activity, $ETR(\text{I})$ (black curves for the different CEF scenarios in Figure 3-3B).

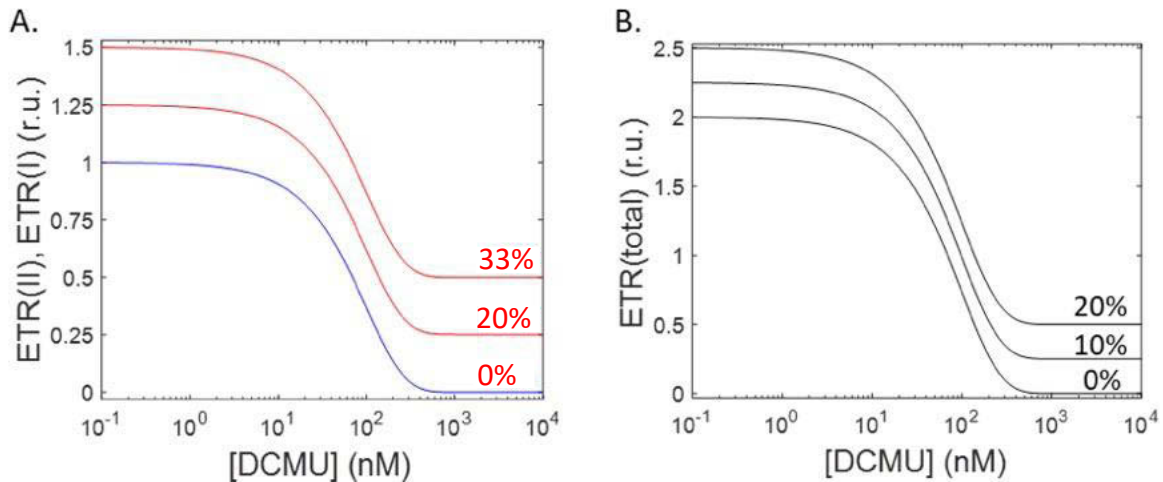


Figure 3-3: Simulation of the change of $ETR(\text{II})$ (blue), $ETR(\text{I})$ (red) and $ETR(\text{total})$ (black) as a function of DCMU concentration in the case of a CEF independent of LEF

A. Simulations of the DCMU titration of $ETR(\text{II})$ and $ETR(\text{I})$ correspond to different proportions of photosystem I initially involved in CEF (0, 20 and 33%); note that when there is no cyclic electron flow, $ETR(\text{I})$ and $ETR(\text{II})$ evolutions are confounded. B. Simulations of the DCMU titration of $ETR(\text{total})$ correspond to different proportions of total photosystems (I and II not differentiated) initially involved in CEF (0, 10 and 20%).

Once normalized to the initial value (untreated situation), the evolutions of $ETR(\text{II})$ (blue curve) and $ETR(\text{total})$ (black curves for different CEF scenarios) as a function of DCMU are shown in Figure 3-4A. If one is plotted against the other (Figure 3-4B), this gives a plot which is easy to interpret. If there is no CEF, we then expect a relationship of proportionality between $ETR(\text{total})$ and $ETR(\text{II})$. If CEF exists but is not dependent of LEF variation, then we expect $ETR(\text{total})$ and $ETR(\text{II})$ to follow an affine relationship. The y-intersect reflects the fraction of total activity corresponding to CEF. And by elimination, if CEF depends on LEF, we expect a more complex relationship between $ETR(\text{total})$ and $ETR(\text{II})$ which depends on the relationship between the two modes of electron flow and is not shown here.

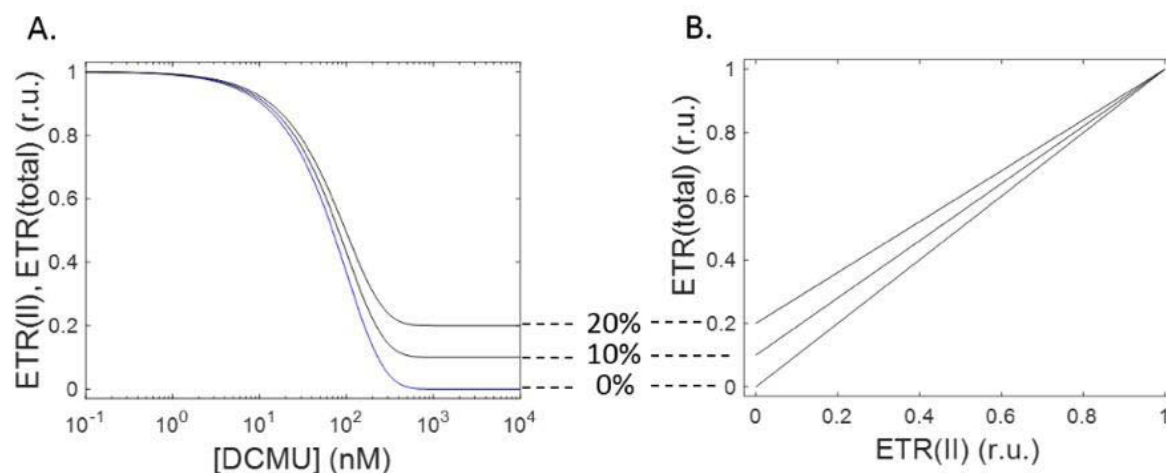


Figure 3-4: Simulations of the relative changes of ETR(II) (blue) and ETR(total) (black) when titrating LEF by DCMU

Simulations correspond to different proportions of total photosystems (I and II not differentiated) initially involved in CEF (0%, 10% and 20%). A. shows evolutions of ETR(II) and ETR(total) as a function of DCMU concentration. Note that when there is no cyclic electron flow, ETR(total) and ETR(II) evolutions are confounded. B. shows the same simulations as in A but ETR(total) is plotted as a function of ETR(II).

3.3.2 Which observables?

At this stage, we still need to explain how ETR(total) can be calculated with ECS. There are two ways to do this. The first one measures the photochemical rate of PSII and PSI by measuring the slope of the ECS at the offset of light (see Methods). The second one postulates that, by analogy with ETR(II) and ETR(I), we can calculate the total electron transfer rate through the fraction of open photosystems (PSI + PSII), that we will call $Y(\text{total})$ hereafter, and the total absorption cross-sections of PSII and PSI, that we will call σ_{total} (m²) from now. This gives:

$$(4) \text{ ETR}(\text{total}) \text{ (electrons per PS per second)} = \sigma_{\text{total}} \cdot Y(\text{total}) \cdot I.$$

Combining equations (3) and (4) gives:

$$(5) Y(\text{total}) = 2 \cdot n_2 \cdot \sigma_{\text{II}} / \sigma_{\text{total}} \cdot Y(\text{II}) + n_1 / (\sigma_{\text{total}} \cdot I) \cdot \text{CEF}$$

With equation (5), measurements of absolute rates of CEF still require accurate measurements of $Y(\text{total})$ and $Y(\text{II})$, absorption cross-sections (σ_{II} and σ_{total}) and photosystems stoichiometry. In this work, in order to increase the robustness of our approach, we don't measure any absolute values of electron flows but only the quantum yield $Y(\text{II})$ and $Y(\text{total})$, of photosystems. If σ_{II} and σ_{total} are constant, relative changes in electron flows, ETR(II) and ETR(total), are proportional to relative changes in $Y(\text{II})$ and

$Y(\text{total})$ respectively. And we can follow the protocol presented in the previous section (3.3.1) to highlight CEF and investigate its dependence upon LEF. It is important to note that equation $Y(\text{total})$ is not a weighted average of the yield of the two photosystems, and that the equation (4) cannot be derived mathematically from the expressions of $ETR(\text{II})$ and $ETR(\text{I})$. We will test experimentally the validity of this calculation of $ETR(\text{total})$ as the sum of activities of the two photosystems in part 3.4.1 and discuss its theoretical validity in the discussion (part 3.5.2). The meaning of σ_{total} will also be discussed later (part 3.4.1).

Finally, the protocol I propose is to follow the relative changes of $Y(\text{total})$ and $Y(\text{II})$ during a DCMU titration. Such a protocol does not require the measurement of PSII an total absorption cross-sections and requires only the measurements of the quantum yield of photosystem II and the $Y(\text{total})$. The PSII quantum yield is routinely assessed through chlorophyll fluorescence measurements (Harbinson, Genty, & Baker, 1989; Kramer et al., 2004). This method has been cross validated with O_2 evolution (Genty et al., 1992) and is well established in the community. Moreover, the PSII quantum yield $Y(\text{II})$ is valid whatever the level of energetic connectivity we consider (i.e. in both extreme “puddle” and “lake” models). $Y(\text{total})$ can be calculated through the “a phase” of the ECS signal generated by a saturating laser flash (see chapter 2). We are working on organisms that do not perform any state transition, i.e. there is no movement of antenna between photosystems. State transitions are absent in diatoms (Owens, 1986), there is no report, to my knowledge of state transitions in dinoflagellates. And we used a mutant of state transitions for *Chlamydomonas reinhardtii* (the *stt7* mutant; Depège et al., 2003). Thus, σ_{II} and σ_{total} are constant throughout the experiment. Yields measured in the initial conditions were not exactly the same between replicates (< 10% variation), but the normalization to the initial values of $Y(\text{total})$ and $Y(\text{II})$ allows to get rid of small biological variation between replicates.

In the introduction, we have shown that most of the questions regarding CEF role, regulation or pathways would benefit from a better understanding of the relationship between CEF and LEF. CEF has mostly been investigated in higher plants and green algae. Thus, all the models regarding CEF mechanisms and regulations have been elaborated from a very small sample of the phylogenetic diversity. With such a protocol, I voluntarily give up the possibility to give absolute rates of CEF. But it allows to test models of CEF behavior, like situations where no CEF is occurring, others where CEF is present but is not influenced by LEF or CEF is occurring and influenced by LEF. We decided to apply this protocol on species from various photosynthetic groups. In this work, we present the results obtained in three species, two

dinoflagellates, *Amphidinium carterae* and *Symbiodinium sp.*, that originates from secondary endosymbiosis and a green alga *Chlamydomonas reinhardtii*, which is used here as a model for the green lineage and where the existence of CEF is well established (e.g. Joliot and Johnson, 2011; Shikanai, 2014; Alric, 2010; Chaux, 2015). Results obtained on natural population of diatoms will be shown also (see 3.5.1.c). I also investigated CEF in a haptophyte, *Isochrysis galbana*, and in *Euglena gracilis*, but those results are not shown (because the ECS signals were too small and giving low signal-to-noise or because independent replicates showed a too high variability to conclude).

3.3.3 CEF is not essential to photosynthesis in the dinoflagellate *Amphidinium carterae*

In the dinoflagellate *Amphidinium carterae*, the $Y(\text{total})$ and the photosystem II quantum yield $Y(\text{II})$ decrease at the same rate when titrating with DCMU (Figure 3-5A). The sum of the activities of the two photosystems follows the activity of PSII alone, whatever the DCMU concentration, suggesting that PSII activity is the only determinant of PSI activity. When plotting $Y(\text{total})$ as a function of $Y(\text{II})$ for three biological replicates, we get a linear relationship: the data was fitted by an affine function, the correlation coefficient is high ($R^2 = 0.997$) and the intercept corresponds to the origin of the axis ($y\text{-intercept} = 0.02 \pm 0.01$) (Figure 3-5B). This behavior is compatible with the model of absence of cyclic electron flow we drew before.

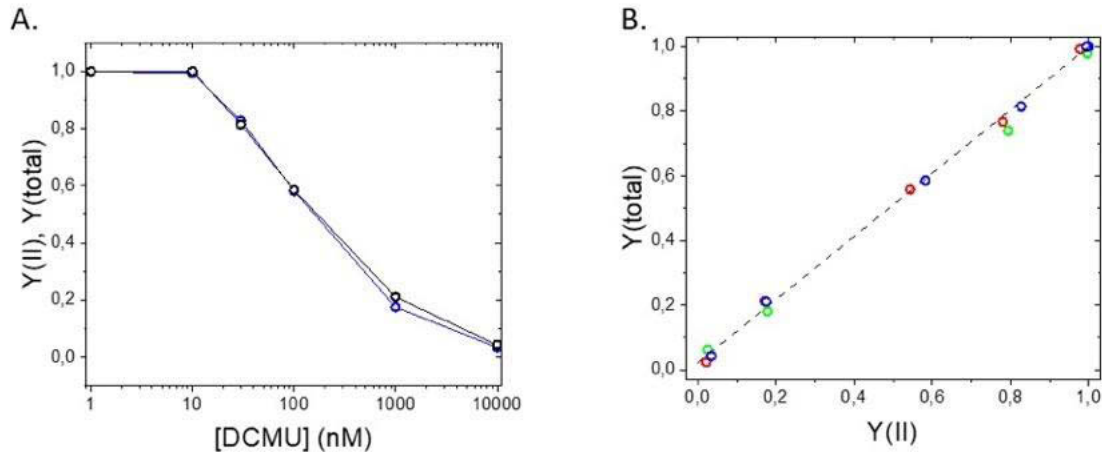


Figure 3-5: Relative changes of the fraction of open PS, $Y(\text{total})$, and the quantum yield of PSII, $Y(\text{II})$, when titrating LEF by DCMU in the dinoflagellate *Amphidinium carterae*

All measurements were performed under steady state illumination at $135 \mu\text{mol photons}\cdot\text{m}^{-2}\cdot\text{s}^{-1}$ and $Y(\text{total})$ and $Y(\text{II})$ were normalized to their initial values, when no DCMU was added. A. $Y(\text{total})$ (black) and $Y(\text{II})$ (blue) as a function of DCMU concentration obtained in one representative biological replicate (blue points in panel B). B. $Y(\text{total})$ as a function of $Y(\text{II})$. Data corresponds to 3 independent biological replicates. The dashed line shows the linear regression of the experimental data ($y = 0.97x + 0.02$ with an adjusted correlation coefficient of 0.997).

The most parsimonious conclusion is that, in the conditions we use here, CEF is not essential to photosynthesis in *Amphidinium carterae*. In plants and green algae, CEF has been proposed to play a crucial role in equilibration of ATP/NADPH production and requirement and in the photo-protection under saturating light. The case of *Amphidinium carterae* shows that it is not absolutely necessary in all photosynthetic species. *Amphidinium carterae* might set up other strategies to fulfill the ATP/NADPH shortfall (see discussion in 3.5.1.a).

3.3.4 CEF is independent on LEF photosynthesis in the dinoflagellate *Symbiodinium sp.*

When titrating photosynthesis with DCMU in *Symbiodinium sp.*, $Y(\text{total})$ decreases more slowly than $Y(\text{II})$ (Figure 3-6A) meaning that total electron flow decreases more slowly than PSII electron flow. It is to note that DCMU concentrations are expressed in arbitrary units because the full inhibitor penetration until the Q_B site is a very long process in this species (~45 minutes) and measurements of total and PSII yields were performed before the effect of the given concentration of DCMU was steady, i.e. during the kinetics of penetration. This does not affect the relationship between $Y(\text{total})$ and $Y(\text{II})$ since both measurements were made at the same time. It is to note that despite its slow penetration kinetics, DCMU inhibited more than 95% of PSII at the end of the experiments. When plotting $Y(\text{total})$ as a

function of $Y(II)$ for three biological replicates, we get an affine relationship: linear regression gives a very good correlation coefficient ($R^2 = 0.995$). Contrary to the case of the previous dinoflagellate, the linear fit of the experimental points does not go through the origin of axes. This data is compatible with our model of cyclic electron flow functionally independent on LEF.

Linear regression estimates a y-intercept of 0.19 ± 0.01 . This means that about 19% of initial photosystems (PSI + PSII) activity in the absence of DCMU was involved in CEF. Before normalization the $Y(\text{total})$ in the absence of DCMU was 0.87 ± 0.11 , meaning that 87% of photosystems were initially open. From there, we can conclude that $\sim 16.5\%$ of the photosystems are involved in CEF in these light conditions. We did not estimate the PSII/PSI ratio because *Symbiodinium sp.* is hardly sensitive to inhibitors. But, assuming that PSII/PSI = 1 (as it is the case in most of the *Symbiodinium* strains, (Roberty et al, 2014), then, we can calculate that about 33% of PSI were initially involved in CEF.

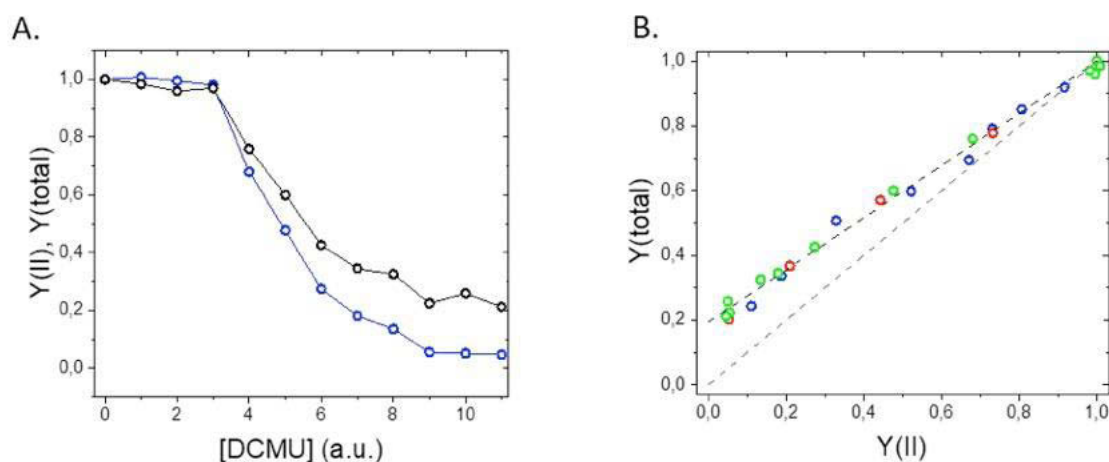


Figure 3-6: Relative changes of the fraction of open PS, $Y(\text{total})$, and the quantum yield of PSII, $Y(II)$, when titrating LEF by DCMU in the dinoflagellate *Symbiodinium sp.*

All measurements were performed under steady state illumination at $26 \mu\text{mol photons m}^{-2} \text{s}^{-1}$. $Y(\text{total})$ and $Y(II)$ were normalized to their initial values, when no DCMU was added. A. $Y(\text{total})$ (black) and $Y(II)$ (blue) as a function of DCMU concentration obtained in one representative biological replicate (green points in panel B). Note that DCMU concentrations are expressed in an arbitrary unit the full inhibitor penetration until the Q_B site is a very long process in this species. B. $Y(\text{total})$ as a function of $Y(II)$. Data corresponds to 3 independent biological replicates. The dashed grey line shows the $y=x$ line, corresponding to the situation where there is no CEF. The dashed black line shows the linear regression of the experimental data ($y = 0.80x + 0.19$ with an adjusted correlation coefficient of 0.995).

According to this result, in *Symbiodinium sp.*, CEF is not disturbed by modifications of LEF when PSII is inhibited: CEF is functionally independent of LEF. Stated otherwise, the LEF and CEF are functionally isolated. One question that rises is what mechanistic model enables an isolation of the chains? The independence of CEF and LEF strongly suggest a physical

separation, which could be due to lateral segregation of the photosystems or to the confinement of some PSI in super-complexes (see discussion, in 3.5.1.b).

3.3.5 *Chlamydomonas reinhardtii* displays a CEF which is dependent on LEF

When titrating $Y(\text{total})$ and $Y(\text{II})$ with DCMU in *Chlamydomonas reinhardtii*, the behavior is a lot more complex than for the two dinoflagellates (Figure 3-7). $Y(\text{total})$ and $Y(\text{II})$ do not follow each other. When plotting $Y(\text{total})$ as a function of $Y(\text{II})$ for seven biological replicates, we obtain a non-affine relationship: the amplitude of CEF is not constant when PSII activity is changing. Hence, CEF is depending on PSII activity, that is to say, on LEF. We see two different phases. At low DCMU concentrations, $Y(\text{total})$ decreases more slowly than $Y(\text{II})$ and, as discussed before, this most probably indicates the increase of CEF. The situation at low DCMU concentration can be better understood by considering an extreme case, where the activity of PSI is constant, i.e. the decrease of LEF with increasing DCMU is compensated by an increase of CEF. In such a situation, the $Y(\text{total})$ would decrease linearly with $Y(\text{II})$ with a y-intercept at 0.5 (the fraction of PS corresponding to PSI given the stoichiometry PSII/PSI close to 1 in *Chlamydomonas reinhardtii*). In the Figure 3-7, the red dashed line represents this extreme case scenario. At low concentrations of DCMU (inhibition of $Y(\text{II})$ lower than 20%), experimental data is compatible with this simulation. We can therefore assume that at low DCMU concentration, the CEF compensates the decrease of LEF at the level of the PSI.

At high concentration of DCMU however, the opposite behavior takes place: $Y(\text{total})$ decreases faster than $Y(\text{II})$. This means that CEF decreases dramatically with decreasing PSII activity. We attribute this effect to the need of electrons from PSII to compensate for the electron loss in the CEF process due to leaks downhill PSI (to CBB or other metabolic sinks). The fact that CEF in saturating DCMU concentration is lower than its maximal value due to those leaks is well documented in *Chlamydomonas reinhardtii* (Nawrocki et al. 2019c; Joliot and Johnson, 2011).

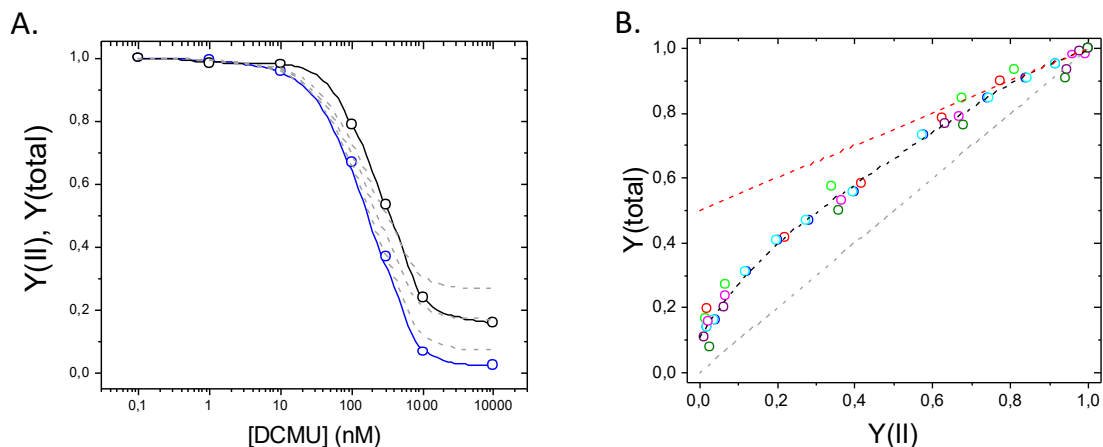


Figure 3-7: Relative changes of the fraction of open PS, $Y(\text{total})$, and the quantum yield of PSII, $Y(\text{II})$, when titrating LEF by DCMU in the green alga *Chlamydomonas reinhardtii*

All measurements were performed under steady state illumination at $135 \mu\text{mol photons}\cdot\text{m}^{-2}\cdot\text{s}^{-1}$. $Y(\text{total})$ and $Y(\text{II})$ were normalized to their initial values, when no DCMU was added. A. $Y(\text{total})$ (black) and $Y(\text{II})$ (blue) as a function of DCMU concentration obtained in one representative biological replicate (pink points in panel B). B. $Y(\text{total})$ as a function of $Y(\text{II})$. Data corresponds to 7 independent biological replicates. The dashed grey line shows the $y=x$ line, corresponding to the situation where there is no CEF. The dashed red line shows the $y=0.5*(1+x)$ line, corresponding to the situation where PSI activity remains constant regardless PSII activity. The dashed black line corresponds to polynomial fit of the experimental data.

In summary, the $Y(\text{total})$ relationship to $Y(\text{II})$ leads us to make three conclusions:

- The observation that $Y(\text{total})$, reflecting activities by both photosystems, and $Y(\text{II})$, reflecting the activity of PSII alone, are not proportional to each other during DCMU titration necessarily implies some activity of CEF in *Chlamydomonas reinhardtii*.
- Under low DCMU concentrations, PSI activity seems to remain constant despite LEF inhibition, which indicates that CEF activity replaces LEF activity in PSI when PSII is inhibited, i.e. a competition between LEF and CEF.
- Under high DCMU conditions, when PSII activity becomes very low, the total activity diminishes faster than PSII activity, which reveals that CEF decreases together with LEF. We propose that such a dependency of CEF on LEF stems from the need for electrons from PSII to compensate the electron leak from CEF.

3.3.6 Partial conclusion on CEF diversity

Despite its proposed crucial role for photosynthesis regulation, the CEF in many photosynthetic groups is hardly investigated. In plants and green algae, although CEF has been investigated for almost 70 years, models of regulation remain unclear. I believe that the approach proposed in this section will make it possible to study further the diversity of CEF and to understand better its relationship with LEF. The approach used here is robust and reliable because: (i) it relies on quantum yield measurements only, whose reliability have been established by cross validation (Genty et al, 1992), (ii) it does not require the assessment of absorption cross-sections, which are prone to bias, and (iii) it can distinguish between the three main possibilities: the absence of CEF, the presence of CEF independent from LEF and the inter-dependent CEF and LEF.

We have shown that several models of relationship between CEF and LEF occurs depending on the species suggesting that CEF regulation models can differ between species. It is important here to highlight that the three behaviors we have identified are not signatures of the species, since the CEF behavior has been investigated only in one specific condition (see discussion, part 3.5.1.d).

This approach allows to highlight CEF and to study its relationship with LEF. But it can also be used to calculate absolute rates of CEF in two of the three cases. When CEF is independent on LEF, we can easily calculate the ratio CEF/LEF since CEF under saturating DCMU is then equal to CEF under physiological conditions (before addition of DCMU, when LEF is occurring). It is the case in the two dinoflagellates, *Amphidinium carterae* and *Symbiodinium sp.* In the case of *A. carterae*, it is an easy situation where one can conclude that there was no CEF in the conditions before DCMU was added. In *Symbiodinium* case, we calculated that one third of the PSI activity was a cyclic activity, assuming a PSII/PSI stoichiometry of 1.

When LEF is dependent on CEF though, physiological rate of CEF is not accessible through this method. The assessment of CEF in saturating DCMU conditions is not an option since by definition CEF is modified by DCMU. Then, a full picture of the CEF when CEF and LEF are inter-dependent cannot be obtained by the robust but simple protocol proposed in this chapter. This is one of the limitations of the method. Then, measurements of absolute rates, ETR(total) and ETR(II), are necessary, which themselves require the measurements of absorption cross-sections (σ_{II} and σ_{total}). This is the task I am going to work on in the next section, on the example of *Chlamydomonas reinhardtii*.

3.4 Results (II): Evaluating CEF and LEF absolute rates as a function of light irradiance in the green alga *Chlamydomonas reinhardtii*

In the previous section (3.3), we proposed a method to test for the presence of CEF and to investigate the relationship between CEF and LEF. We could show that CEF behavior is not conserved among phylogeny suggesting that CEF regulation mechanisms are not universal. The method proposed is sufficient to fully characterize CEF in two of the three types of situations presented. When there is no CEF, no further investigation is needed. If CEF is occurring independently of LEF, then, by nature, CEF rate measured when PSII is fully inhibited (saturating concentration of DCMU) is the same as the one occurring in physiological conditions. This enables easy access to CEF rate and the calculation of the CEF/LEF ratio is straightforward. This was the case in *Symbiodinium sp* in the conditions we used. It was unexpected on the basis of our knowledge on CEF in plants and green algae. When CEF is dependent on LEF, it is not possible to assess CEF rate in physiological conditions with the method proposed in the previous section. We need to measure absolute LEF and CEF rates and this is the aim of this section.

We decided to use *Chlamydomonas reinhardtii* as a working organism. As shown in the previous section (3.3), in this microalga CEF is dependent on LEF and the method we proposed is not sufficient to assess CEF in physiological conditions. In addition, it is a model organism for photosynthesis investigation in the green lineage and many controls have already been carried out on spectroscopic methods for the study of photosynthetic physiology. Moreover, it is the only microalgae for which we have mutants of proteins involved in CEF, PGRL1, PGR5 (Alric 2014), or of the kinase involved in state transitions (stt7, Depège, Bellaïre and Rochaix, 2003). Moreover, it does not perform any q_E when grown under low light (Peers, Nature, 2009). Single mutants can be crossed allowing easy establishment of double mutants.

As you will see, obtaining LEF and CEF absolute values requires many different measurements and controls. It is not a rapid screening protocol like the one developed in the previous section. We divided this work into two parts: the first one is dedicated to testing the reliability of the methods for assessment of absorption cross-sections (3.4.1 and 3.4.2) and the second part aims to estimate absolute values of CEF under different conditions of light irradiance (3.4.3).

3.4.1 ECS-based estimations of the PSI and PSII absorption cross sections

$Y(\text{total})$ is accurately measured by ECS and $Y(\text{II})$ is assessable with fluorescence measurement. The PSII/PSI stoichiometry measured by flash-induced ECS (see Methods) is also a routine measurement. Here, the methodological challenge is to estimate the PSI, PSII and total absorption cross-sections. In a first time, we will expose the method we used to estimate those parameters with ECS measurements (paragraph 3.4.1). The approach is similar to what was used in (Roberty et al, 2014). Then, we will test the results using two cross validation approaches (paragraph 3.4.2).

Measurement of photochemical rate of both photosystems at light onset is assessable thanks to ECS. When the light is switched on, the PS start working immediately while the activation of the b_6f and ATPase, that are non-photochemical steps, is slower. In the first ms after light onset, we assume that the increase of the electric field is only due to the activity of the PS. This activity depends on light irradiance, absorption cross-section and the fraction of open photosystems. If all PS are open, then the slope is proportional to the product of light irradiance and absorption cross-section. Absorption cross-sections should therefore be measured in conditions where the photochemistry is not limited by the availability of photosystems donors and acceptors. It is the case in dark-adapted samples; then, all the complexes of the chain are at the thermodynamic equilibrium with the ambient redox potential: the PSII and PSI primary donors, P_{680} and P_{700} , are reduced and the primary acceptors, Q_A and iron-sulfur proteins, are oxidized.

Let's start with the measurement of PSI absorption cross-section. It is possible to inhibit the participation of PSII to the electric field creation by the addition of two inhibitors, DCMU and hydroxylamine (HA). In these conditions, ECS increase at light onset is only due to PSI charge separation and PSI photochemistry only depends on the light irradiance and the absorption cross-section (and its maximal quantum yield, close to 1 for PSI). The ECS increase at light onset is therefore a good measurement of the product of the light irradiance and the absorption cross-section of PSI, σ_i . The situation is more complex for the measurements in the absence of PSII inhibitors. Of course, the slope of ECS increase then reflects the sum of PSII and PSI photochemistry. But it cannot be considered as the product of light irradiance and the sum of PSI + PSII absorption cross-sections. This is because the maximal quantum yield of PSII, F_v/F_m , is significantly different from 1. Therefore the slope is proportional to $I \cdot \sigma_{\text{total}}$, where σ_{total} is not strictly speaking the sum of PSI and PSII absorption cross-sections. Instead:

$$(6) \sigma_{\text{total}} = \sigma_I + F_v/F_m \sigma_{II}$$

Figure 3-8A/B shows measurements of ECS increase in the presence and absence of PSII inhibitors after light onset at different light intensities and at different time after light onset. As expected, the lowest is the light irradiance, the slowest is the ECS increase. And the slope of ECS increase is proportional to light irradiance. The observation that ECS increases linearly with time in this range indicates that the PS remain open.

The plot of the slopes of the ECS increase as a function of light irradiance directly gives σ_{total} and σ_I in the absence (Figure 3-8D) and presence (Figure 3-8C) of PSII inhibitors, respectively. The photochemical rate of PSII is simply the difference between the total photochemical rate and the PSI photochemical rate. The absorption cross-section of PSII can then be directly calculated from equation (6) as: $\sigma_{II} = (\sigma_{\text{total}} - \sigma_I) / (F_v/F_m)$

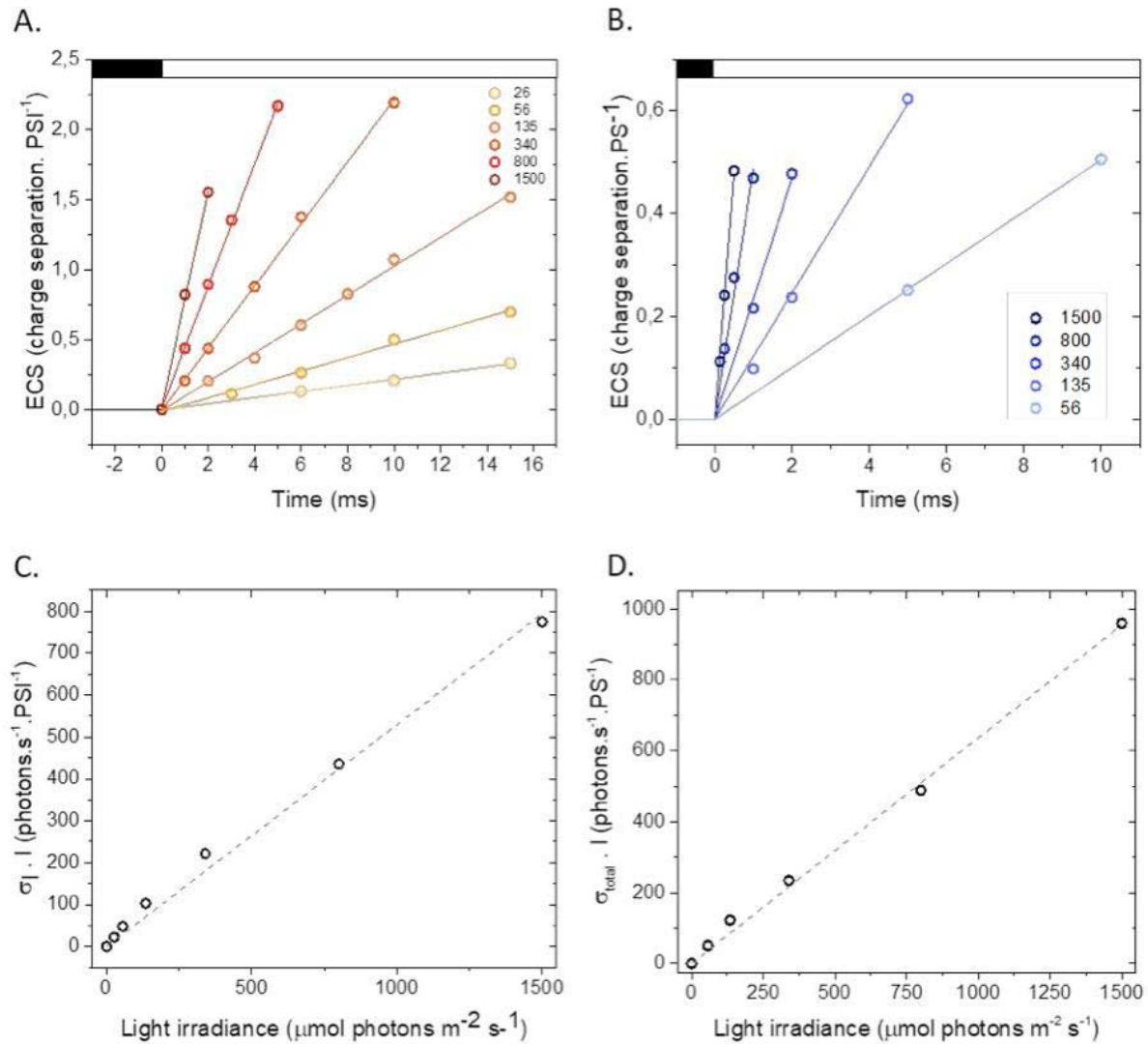


Figure 3-8: Estimation of the fraction of light absorbed by all PS and by PSI with an ECS-based method

A. and B. ECS increase has been measured at different times after light onset and at different light irradiances in the presence (A) and absence (B) of PSII inhibitors. ECS value at time 0 has been set at 0 and the signals were normalized by the amplitude of the ECS increase when all PS perform one charge separation (i.e. after a single turnover laser flash in the dark). Black and white horizontal bars correspond to darkness and light, respectively. The fraction of light absorbed by PSI (C) and by all PS (D) has been calculated as the slope of ECS increase at light onset based on data from A. and B., respectively. Dashed grey lines show linear regression of the experimental points.

Measurements in A and B were done on two different cultures of *stt7-9* mutant.

Absorption cross-section measurement through ECS probe has been scarcely used in the literature (Roberty et al, 2014) and never validated to my knowledge. We thus propose to test its reliability through two cross validation approaches.

3.4.2 Validation of the method for measurement of absorption cross sections

a) Cross-validation of the two ECS-based methods to estimate ETR(total)

In order to test the reliability of absorption cross-section measurements, we propose to compare the values of ETR(total) measured with the two methods mentioned in 3.3.1. Indeed ETR(total) can be calculated as the product of σ_{total} , I and Y(total) but also with an alternative ECS-based method which does not require measurements of absorption cross-sections. The latter is the measurement of the photochemical rate of PSI and PSII through the initial slope of ECS at the offset of light (see Methods). Figure 3-9 shows ECS decay after light offset that were previously set at 135 (A) and 1500 (B) $\mu\text{mol photons m}^{-2} \text{s}^{-1}$. Data has been fitted by an exponential decay in the first 16 ms (that we expect if b_6f and ATPase activity do not change during the time of measurement) and initial slope has been drawn in red. As expected, the initial slope is higher at 1500 $\mu\text{mol photons m}^{-2} \text{s}^{-1}$ than at 135 $\mu\text{mol photons m}^{-2} \text{s}^{-1}$, reflecting a higher photochemical rate at higher irradiance.

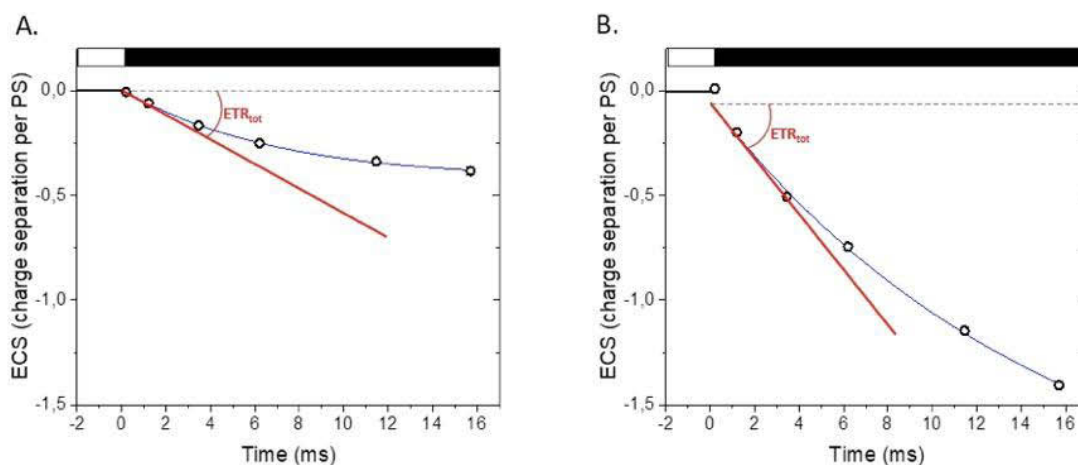


Figure 3-9: Kinetics of ECS decrease after light offset at two different light irradiances

Light was turned off at time 0 and the ECS decrease from 1.3 ms to 16 ms was fitted by an exponential decay function (blue line). The initial slope is calculated from the result of the fit (red line) and estimates the total electron transfer rate, ETR(total). Measurements were performed for two different light intensities: 135 $\mu\text{mol photons m}^{-2} \text{s}^{-1}$ (A) and 1500 $\mu\text{mol photons m}^{-2} \text{s}^{-1}$ (B). White and black horizontal bars correspond to light and darkness, respectively. Each panel corresponds to one representative measurement performed on a same sample of the *Chlamydomonas reinhardtii stt7-9* mutant.

It is to note that when PS are limited by their acceptor side, charge recombination can occur in the first few hundreds of μs following light offset. This artificially increases the initial slope

but does not correspond to the generation of stable charge separations giving rise to LEF or CEF electron transfer. To take this into account, the first point of the ECS decay (time 0) was rejected from the fit, which started only with the first point of the decay (1.2 ms after light offset). The light dependence of photochemical rate is shown in Figure 3-11A.

As presented in the introduction of this chapter, $ETR(\text{total})$ can be calculated as the product of σ_{total} , I and $Y(\text{total})$. $Y(\text{total})$ has been measured in the same way as presented in the first part of the results (3.3) i.e. as the ECS increase after a single turnover laser flash. This amplitude, expressed in charge separation per PS, indicates the fraction of centers that are able to transfer a charge if they receive a photon, i.e. the fraction of open PS. As already discussed in chapter 2 (2.3.1) most charge recombinations can occur in the first hundreds of μs to few ms following a laser flash (Alric, 2010) affecting the estimation of $Y(\text{total})$. With our spectroscopic tools, it is not possible to discriminate charge recombinations occurring faster than the hundreds of microsecond timescale, i.e. between P_{700} and the phylloquinone. The centers giving rise to such unstable charge recombinations will therefore be counted as closed. But we observed that under high light, the ECS decay after the saturating laser flash was biphasic with a first phase taking place in between 0.3 and 1.2 ms. This early phase was attributed to slower charge recombination, i.e. to ECS creation that was not due to a stable charge separation. In order to remove this contribution, we followed a modified protocol. In a background light irradiance, we followed the increase of ECS upon a laser flash and then followed the relaxation of this ECS during a short (22 ms) period of darkness. We fitted the ECS decay after rejecting the first point (300 μs after the flash) by a mono-exponential decay and extrapolated the curve to get the amplitude of ECS increase after the laser flash that was due to stable charge recombination only. Figure 3-10 shows that under low light (135 $\mu\text{mol photons m}^{-2} \text{ s}^{-1}$, Figure 3-10A), ECS increase measured after a single turnover laser flash equals the $Y(\text{total})$ fitted from the dark relaxation. At the contrary, under high light (1500 $\mu\text{mol photons m}^{-2} \text{ s}^{-1}$, Figure 3-10B), ECS decrease after a single turnover laser flash shows a biphasic relaxation, the first phase being attributed to fast charge recombination. Thus, the fitted $Y(\text{total})$ diverged from the flash-induced ECS increase.

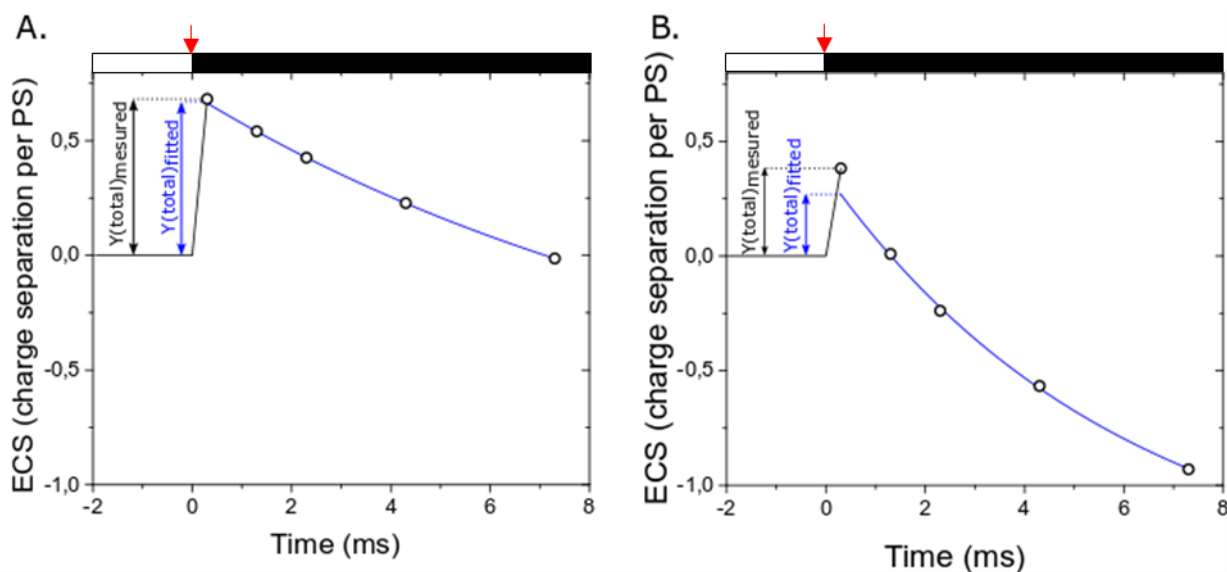


Figure 3-10: ECS decrease after a single turnover laser flash superimposed to two different light irradiances

A single turnover laser flash was superimposed to a beam of actinic light of 135 and 1500 $\mu\text{mol photons m}^{-2} \text{s}^{-1}$ for panels A and B, respectively. The subsequent ECS decrease in the dark was measured and fitted by an exponential function excluding the first point of the kinetics and extrapolated to the time of “a phase” measurement (i.e. 300 μs). White and black horizontal bars correspond to light and darkness, respectively. Red arrows represent the single turnover laser flash that was applied at time 0. Each panel shows one representative measurement performed on a same sample of the *Chlamydomonas reinhardtii stt7-9* mutant.

The $Y(\text{total})$ obtained with this modified protocol is plotted as a function of light irradiance in Figure 3-11B. As expected, $Y(\text{total})$ decreases with light irradiance because PS activity becomes limited by the rate of chemical steps (cytochrome b_6f or CBB cycle). Figure 3-11C shows the $\text{ETR}(\text{total})$ calculated as the product $Y(\text{total})$, I and σ_{total} . The results are very similar to the ones obtained with the DIRK method (Figure 3-11C).

Figure 3-11D shows the relationship between the photochemical rate obtained with the DIRK method as a function of the $\text{ETR}(\text{total})$ based on yield and absorption cross-section. Both methods concord at all light intensities (linear relationship with a factor of proportionality of 1.02 and a correlation coefficient of 0.995). This is very reassuring: the concordance between the two methods, which rely on the same signal (ECS) but very different measurements, strongly suggests that the methods we use for measurements of photochemical rate, yields and absorption cross-sections are correct.

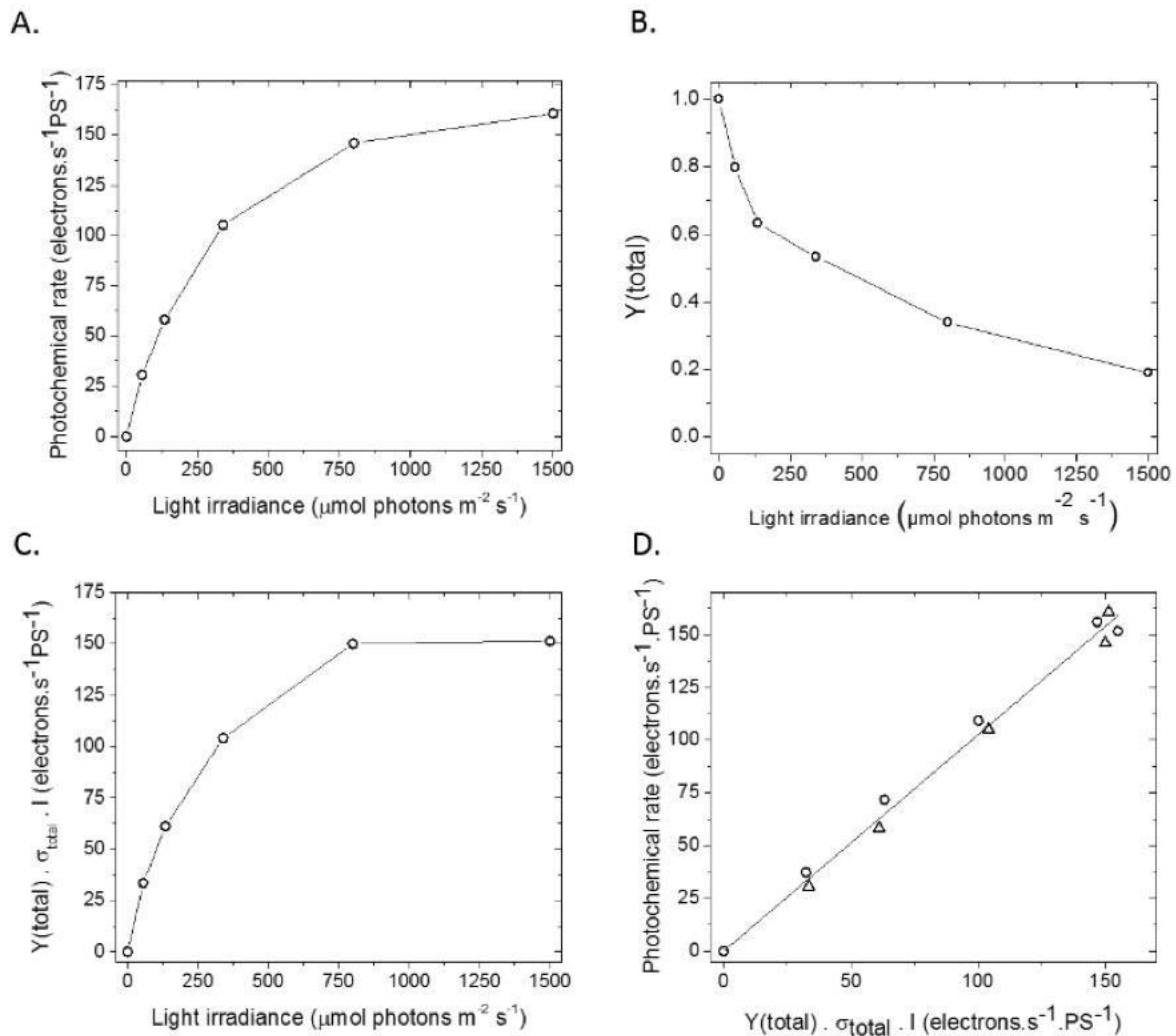


Figure 3-11: Comparison of the total electron transfer rate, ETR(total), estimated by the DIRK method and by the yield method

A: Light irradiance dependency of the photochemical rate (i.e. ETR(total)) that was estimated as the slope of the ECS decay after light offset (DIRK method). B: Light dependency of the fraction of open PS, Y(total), measured with flash-induced ECS. C: Light dependency of ETR(total) estimated as the product of the fraction of open PS and the rate of photon absorption (i.e. Y(total) \cdot σ_{total}). D: Comparison between ETR(total) measured by the two methods. Black line corresponds to the linear regression of the experimental data ($y=1.02x$ with an adjusted correlation coefficient of 0.995). Data corresponds to two biological replicates using the *Chlamydomonas reinhardtii* *st7-9* mutant.

d) Cross-validation of the ECS-based and fluorescence-based estimations of PSII antenna size

If the previous section demonstrated that results based on ECS are self-consistent, one could still wonder if the measurements of absorption cross-sections based on ECS agree with more widespread methods. It is also possible to estimate σ_{II} by chlorophyll fluorescence rise measurements (Lazar and Naus, 1998) and we propose here to compare the results obtained

with the two methods in order to test their reliabilities. The principle of the fluorescence-based measurement of σ_{II} is to estimate the average time required to perform one charge separation per PSII. For this purpose, PSII are inhibited with DCMU, which competes with PQ for the Q_B site, thus preventing electron transfer from Q_A to PQ. Hence, when DCMU is fully saturating, all PSII can perform one and only one charge separation by transferring an electron from the special pair, P_{680} , to Q_A , the primary stable acceptor. The rise from F_0 (open centers) to F_m (closed centers, Q_A reduced) therefore informs on the rate of photon absorption by PSII. As discussed in the introduction (chapter 1), the shape of the fluorescence induction curve depends on the energetic grouping of PSII. If PSII are isolated units, then the curve should follow an exponential shape. It should be sigmoidal if there is connectivity between PSII units (a closed PSII center can share an exciton with a nearby open PSII center). In our hands, the fluorescence rise showed an exponential behavior, as expected in a “puddle” model (Figure 3-12A). And the absorption cross-section can be calculated from the exponential time constant (see Methods). Plotting the PSII absorption cross-section measured by fluorescence or by ECS one against the other reveals a good proportionality between the two methods but fluorescence based estimation is 33% higher than ECS based one. The reason for this discrepancy can be the known underestimation of the PSII absorption cross-section due to the small reduction of Q_A (the fluorescence value in the dark is slightly higher than the true F_0) in the presence of DCMU (Tian et al, 2019).

In the next section and for the sake of clarity, we will present the reasoning steps with the results obtained with ECS-based σ_{II} . But the figures on which the discussion is based will also show the results obtained from σ_{II} estimated by fluorescence.

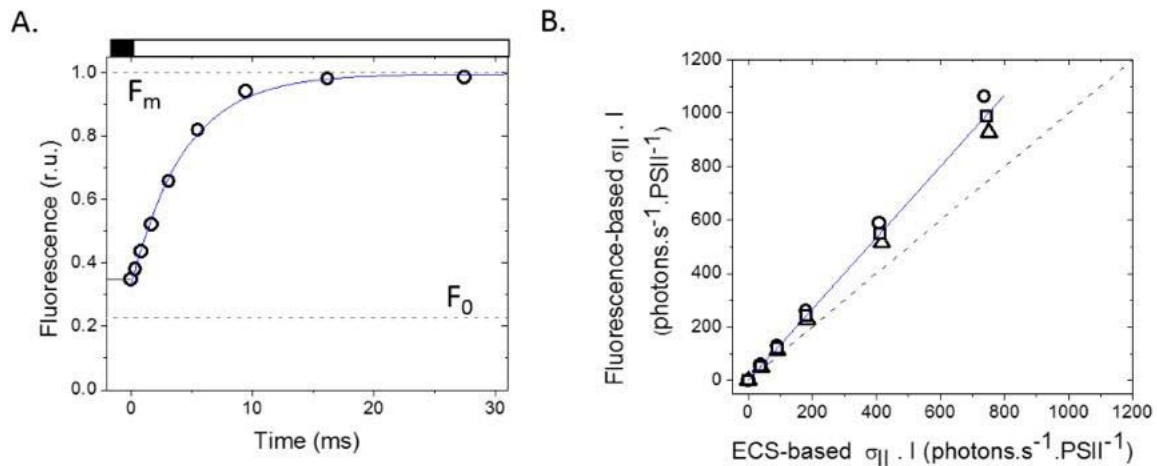


Figure 3-12: Estimation of the PSII photon absorption rate by fluorescence and comparison with the ECS-based method

A. Fluorescence induction curve in the presence of DCMU. Light was turned on at time 0 and fluorescence datapoints were normalized to the maximal fluorescence (i.e. after a 250ms pulse of saturating light). The resulting “fluorescence induction curve” was fitted by an exponential function (blue curve) and the photon absorption rate was estimated as the area between the fitted curve and the $y=F_m$ curve. Data corresponds to one representative experiment at 340 $\mu\text{mol photons m}^{-2} \text{s}^{-1}$. White and black horizontal bars correspond to light and darkness, respectively. B. Comparison between the photon absorption rates, $\sigma_{II} \cdot I$, estimated by the ECS-based and fluorescence-based methods. The blue line shows the linear regression of the experimental data ($y = 1.33x$ with an adjusted correlation coefficient of 0.996). Data was obtained on three independent biological replicates using the *Chlamydomonas reinhardtii stt7-9* mutant.

3.4.3 Evaluating CEF absolute rates from ETR(total) and ETR(II)

In the previous part, I introduced the methods to measure the different parameters to calculate total and PSII yields and absorption cross-sections. In this part, we will use these parameters to calculate CEF.

In this section, we will calculate ETR(II) as:

$\text{ETR(II)} = \sigma_{II} \cdot I \cdot Y(\text{II})$, where σ_{II} is calculated based on the ECS method described in the previous section and $Y(\text{II})$ is the quantum yield of PSII based on variable fluorescence measurements. For ETR(total), we have seen in the previous section that the two ECS-based methods give similar methods. Here we will use the photochemical rate based on DIRK method to calculate ETR(total).

Figure 3-13 shows ETR(total) and ETR(II) measured in three biological replicates. ETR(total) and ETR(II) are expressed per total PS and per PSII, respectively. The 3 biological replicates differ in terms of ETR amplitudes. This will be addressed in the discussion of the results.

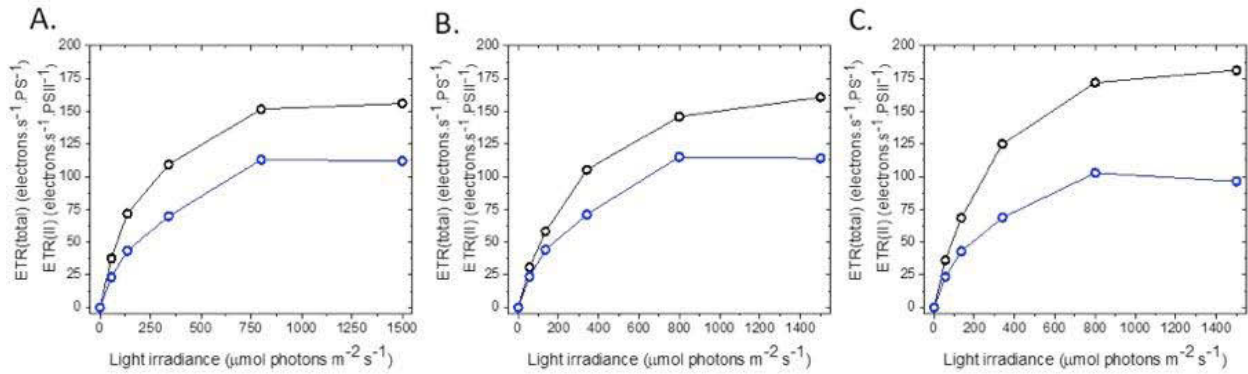


Figure 3-13: ETR(total) (black) and ETR(II) (blue) as a function of light irradiance in three biological replicates (shown in panels A, B and C)

ETR(total) and ETR(II) are normalized per total PS and per PSII, respectively. ETR(total) was assessed with the DIRK method and ETR(II) has been calculated from ECS-based PSII photon absorption rate, $\sigma_{II} \cdot I$. Data was obtained on three independent biological samples of the *Chlamydomonas reinhardtii* *stt7-9* mutant.

It is important to note that here, ETR(total) and ETR(II) are not expressed in the same unit, e.g. ETR(II) is expressed per PSII and ETR(total) is expressed per total PS. If we want to compare those flows and calculate ETR(I) from them, one needs to express them in the same unit. Here, we will normalize all the ETR per total PS. For this purpose, we multiply ETR2 by the ratio n_2 which is the fraction of PSII (number of PSII/number of PS). Figure 3-14 shows ETR(total) and ETR(II) expressed per total PS measured in three biological replicates (same experimental data as in Figure 3-13), with additional calculation of ETR(I), also expressed in electrons per second per PS. The latter value was calculated as: $ETR(I) = ETR(total) - ETR(II)$.

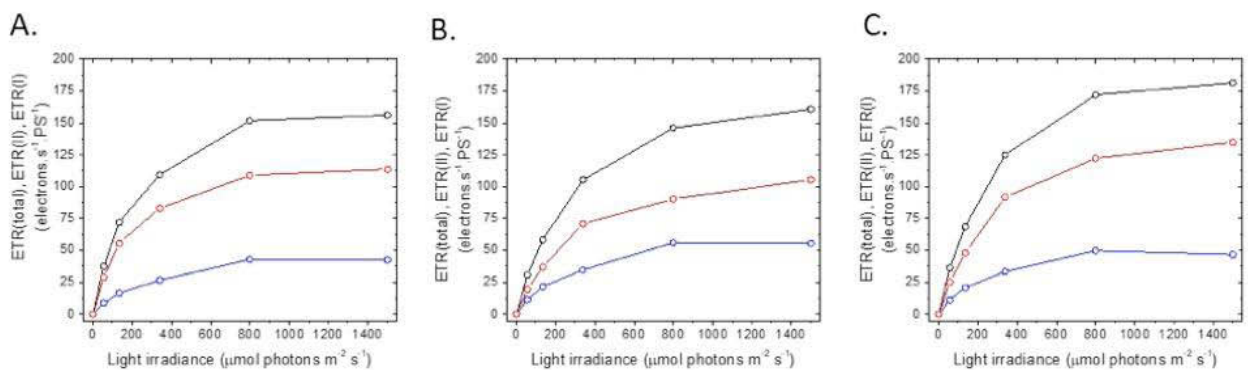


Figure 3-14: ETR(total) (black), ETR(II) (blue) and ETR(I) (red) as a function of light irradiance in three biological replicates (shown in panels A, B and C)

Here, the raw data is the same as in Figure 3-13 but ETR(total) and ETR(II) are both normalized per total PS. ETR(I) was calculated as the difference between ETR(total) and ETR(II) (being normalized per total PS).

ETR(I) being the sum of the cyclic flow and of the linear flow that is given by ETR(II), we can calculate the CEF as:

$CEF = ETR(I) - ETR(II)$. The values of CEF (expressed in electrons/PS/s) are comparable, or even higher in two of three replicates, to the LEF rate (Figure 3-15). Stated otherwise, 50% or more of PSI activity is involved in CEF.

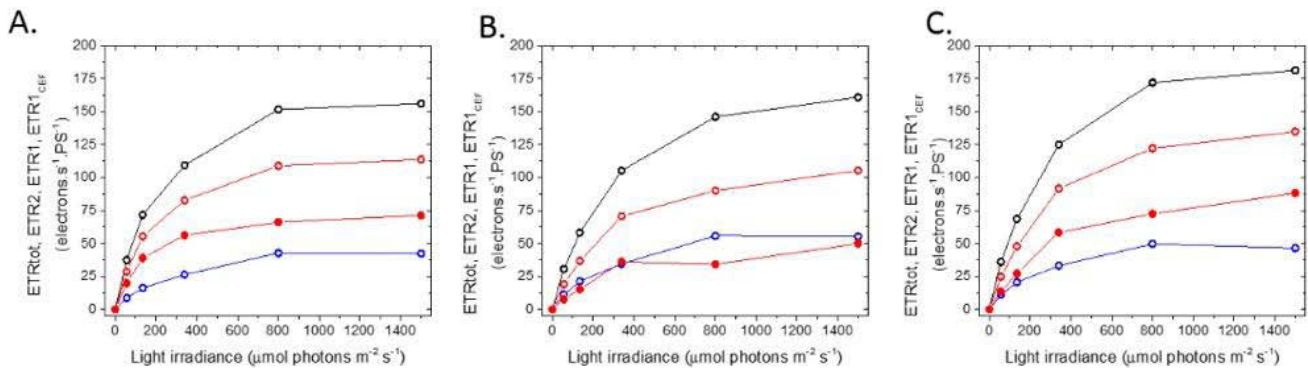


Figure 3-15: ETR(total) (black), ETR(II) (blue), ETR(I) (red, open circles) and ETR(I)_{CEF} (red, closed circles) as a function of light irradiance in three biological replicates (shown in panels A, B and C)

Here, the raw data is the same as in Figure 3-13 and Figure 3-14. ETR(total) and ETR(II) are both normalized per total PS. ETR(I) was calculated as the difference between ETR(total) and ETR(II) and ETR(I)_{CEF} was calculated as the difference between ETR(I) and ETR(II) (being normalized per total PS).

3.4.4 Calculations of the ATP/NADPH ratio produced by the photosynthetic chain

With such high rates of CEF, one can wonder if it is sufficient to provide the missing ATP for carbon assimilation. For CEF to be an efficient APT/NADPH regulator, it should provide extra ATP proportionally to the NADPH generated by LEF, so that the ATP/NADPH provided by the photosynthetic chain (LEF + CEF) is constant, regardless of light irradiance. We can calculate straightforwardly the CEF/LEF ratio at all light intensities by dividing the corresponding values obtained in the Figure 3-15 (indeed, they are expressed in the same unit). The result is shown in Figure 3-16B. The CEF/LEF ratio is ~ 1.5 , independent of the light irradiance (open circles, panel B), which means that almost 60% of the PSI activity is cyclic (panel A).

The calculation of the ATP/NADPH produced by the photosynthetic chain as a function of CEF/LEF was presented in equation (1) (3.1.1). Figure 3-16C show the ATP/NADPH ratio produced by the photosynthetic chain calculated from data presented above (open circles,

panel C). This indicates that the ATP/NADPH ratio produced by the light phase of photosynthesis is ~ 2.25 at all irradiances, significantly higher than the ratio required for carbon assimilation (1.5) even the higher value of 1.65 expected in low CO₂ concentration (Kramer and Evans, 2011). The ATP overage is used for other metabolic pathways such as carbon concentrating mechanisms. Indeed, it is known that CEF is increasing in conditions where inorganic carbon is lowly available (Lucker & Kramer, 2013b), strongly suggesting that CCM are requiring ATP to operate.

Those very high values of CEF providing tremendous amounts of extra ATP should be taken with a lot of care. As discussed before, these CEF values involve the assessment of many parameters, $Y(II)$, σ_{II} and $ETR(\text{total})$, which all can be prone to errors. In my opinion, the most delicate measurement is the one of the absorption cross-section of PSII. It is therefore interesting to check what happens if we use the fluorescence-based value instead of the ECS-based one for the calculations. We present in Figure 3-16 the expected results with this alternative measurement of σ_{II} (closed circles). When CEF/LEF and ATP/NADPH ratio are calculated with fluorescence-based σ_{II} , results show the same trend but different amplitudes. Again, CEF/LEF seems to be independent of light irradiance, as expected in a model where CEF is regulated in order to balance the ATP/NADPH ratio between photosynthetic chain production and metabolic pathways requirements.

However, results obtained with ECS-based σ_{II} show a smaller ratio between CEF and LEF (~ 0.5 , panel B) meaning that about a third of the PSI are involved in CEF (panel A). Calculations of ATP/NADPH ratio produced by the chain (Figure 3-16, closed circles) shows a lower –but still independent of light –between 1.5 and 1.8. This means that the photosynthetic chain ATP production at least equals the CBB cycle even when the highest estimation of the PSII absorption cross-section is used.

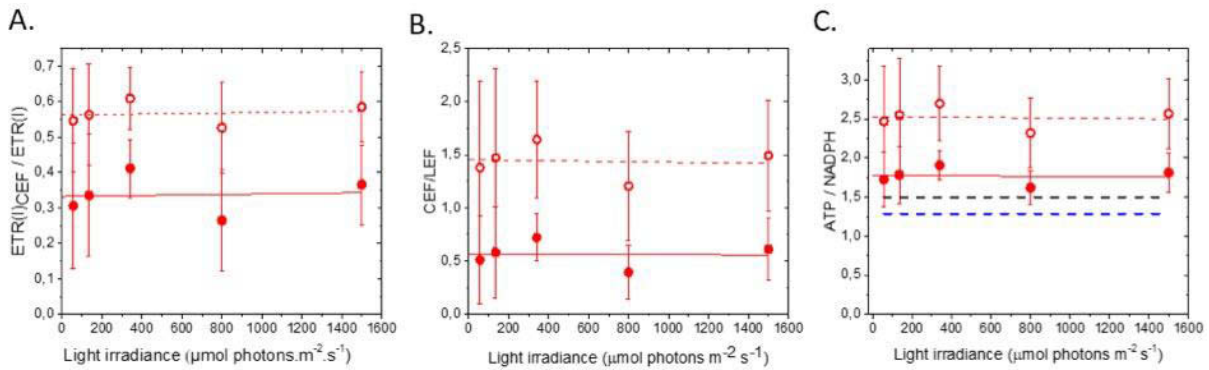


Figure 3-16: Light dependency of the ratios $\text{ETR(I)}_{\text{CEF}}:\text{ETR(I)}$, $\text{CEF}:\text{LEF}$ and ATP/NADPH produced by the photosynthetic chain

A. Proportion of PSI involved in CEF as a function of light irradiance. B. Relative proportion of CEF and LEF as a function of light irradiance. C. Resulting calculation of the ratio ATP/NADPH produced by the photosynthetic reactions.

Here, the raw data is the same as in Figure 3-15. For all graphs, open and closed circles respectively represent the data obtained with ECS-based and fluorescence-based estimation of the photon absorption rate ($\sigma_{\text{II}} \cdot I$), respectively. Dashed and solid red lines are their respective linear fits. In panel C, blue dashed line represent the ratio ATP/NADPH produced by LEF only and black dashed line represents the ATP/NADPH ratio required for the CBB to function.

Data is the mean of three biological replicates ($\pm\text{SD}$).

3.5 Discussion and future perspectives

3.5.1 A simple and robust protocol to investigate CEF diversity highlights three different behaviors

CEF has been proposed as an alternative electron pathway about 70 years ago and, while linear electron flow is now rather well understood, many questions regarding CEF remain unclear, especially: is CEF occurring in all photosynthetic organisms? How are the rates of LEF and CEF regulated?

In this chapter, we first developed a simple and robust method based on the measurements of only two parameters, the quantum yield of PSII by fluorometry, and the “averaged” quantum yield of photosystems probed with ECS. Titrating these parameters with an inhibitor affecting specifically LEF (DCMU) enables (i) to test the existence of CEF in a given species and in a given condition and (ii) in case CEF is occurring, to characterize the relationship between CEF and LEF.

This method seems particularly convenient for screening CEF diversity. Chlorophyll fluorescence is a signal available in all organisms performing oxygenic photosynthesis. ECS is also present in most of the eukaryotic photosynthetic organisms (Bailleul, Cardol, Breyton, & Finazzi, 2010), including diatoms (Bailleul et al, 2015), dinoflagellates (Roberty et al, 2013), eustigmatophytes (Meneghesso et al., 2016) and cyanobacteria (Viola et al., 2019).

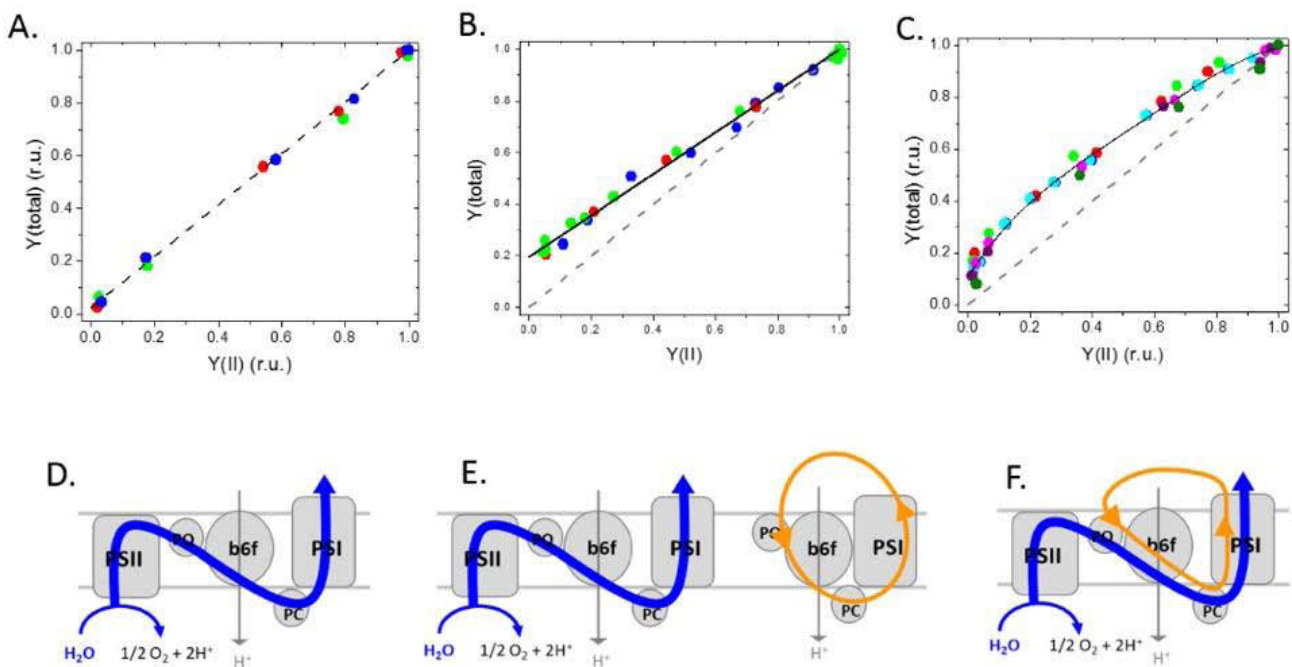


Figure 3-17: Relative changes of $Y(\text{total})$ and $Y(\text{II})$ when titrating LEF by DCMU in (A) *Amphidinium carterae* (dinoflagellate), (B) *Symbiodinium sp.* (dinoflagellate) and (C) *Chlamydomonas reinhardtii* (green alga)

Measurements were performed under steady state light in three different species. A. the dinoflagellate *Amphidinium carterae* at $135 \mu\text{mol photons m}^{-2} \text{s}^{-1}$, B. the dinoflagellate *Symbiodinium sp.* at $26 \mu\text{mol photons m}^{-2} \text{s}^{-1}$ and C. the green alga *Chlamydomonas reinhardtii* at $135 \mu\text{mol photons m}^{-2} \text{s}^{-1}$. Yields were normalized to their values in the initial conditions, when no DCMU were added and under steady state light. Graph A, B and C results from 3, 3 and 7 biological replicates, respectively. D, E and F, show schemes of 3 CEF models. A: pure linear electron flow. B: LEF and CEF are independent. C: CEF and LEF are dependent. Blue and orange arrows represent LEF and CEF, respectively.

a) An absence of CEF in the dinoflagellate *Amphidinium carterae*

We could show that a dinoflagellate, *Amphidinium carterae*, is not displaying CEF under steady state light (Figure 3-17, A and D), indicating that a pure linear electron flow takes place in this species in the conditions we used. This means that CEF is not mandatory for photosynthesis. In plants and green algae, CEF has been proposed to play a crucial role in equilibration of ATP/NADPH production and requirement and in the photoprotection under saturating light. The stromal CO_2 reduction pathway being conserved in all photosynthetic eukaryotes (Hügler & Sievert, 2011), suggesting that the shortfall of ATP for CO_2 assimilation is a common feature for organisms performing oxygenic photosynthesis. The case of *Amphidinium carterae* shows that it is possible to fully depend on other strategies to respond to this common constraint.

Very little is known about *Amphidinium carterae*'s photosynthetic physiology. We can imagine two possible strategies for ATP/NADPH ratio equilibration. The first one is an increase of the ATP/NADPH ratio produced by linear electron flow. It is possible if the

chloroplast ATP synthase in *Amphidinium carterae* possess 12 (or less) c subunits. In that case only 12H^+ would be needed to produce 3 ATP molecules and the ratio of ATP/NADPH produced by LEF would be 3/2, reaching exactly the CBB cycle requirement. Is this a credible hypothesis? Phylogenetic diversity of the chloroplast ATP synthase structure has scarcely been investigated until now but it seems that the number of c subunits of ATP synthases may vary according to genetic or physiological determinants. Structural data show that the stoichiometry of c subunits per (C)F1 in spinach chloroplast CF0-CF1 is 14 (Seelert et al., 2000) while it ranges between 13 and 15 in cyanobacteria (Pogoryelov et al., 2007) but is only 10 yeast mitochondria (Stock et al., 2000). The number of c subunits could also depend on environmental determinants like carbon source as shown in *E. coli* (Schemidt et al., 1998). It is to note that changes in the number of c subunits number induce a change the Gibbs free energy per proton translocation needed to synthesize ATP: if there are less fold, the minimal energy per proton required would increase. The second possibility for *Amphidinium carterae* is to replace the CEF by other alternative pathways, like water to water cycles. By definition, the alternative pathways cause rerouting of high energy electrons produced by the photosynthetic chain to other pathways than carbon reduction. These alternative routes therefore enable to increase the ATP/NADPH ratio available for the CBB cycle. They also generate an extra pmf which would play a role in PSI and PSII photoprotection (Eberhard, Finazzi and Wollman, 2008).

Can we say that *Amphidinium carterae* does never perform CEF? This would be the case if the genes coding for enzymes required for CEF were absent from the genome, or if some structural differences in the structure of the *b₆f* disallowed direct transfer to Q_i site of *b₆f*, for examples. Without surprise, the answer is no. Results obtained with our protocol is valid in one species/ one condition. This is illustrated by the following experiment.

In order to understand better the determinants of CEF and thus to better discriminate between genetic capacity to perform CEF and physiology influence on CEF behavior, I tested CEF behavior in *Amphidinium carterae* in different environmental conditions. *Amphidinium carterae* was cultivated in minimum media with 10% nitrogen concentration. The stationary phase occurred before the one in complete media (Figure 3-18A) indicating that cells were suffering nitrogen limitation which limited their growth. At the beginning of stationary phase, roughly one or two days after cells started experiencing nitrogen limitation, we harvested cells and titrated DCMU while measuring $Y(\text{total})$ and $Y(\text{II})$ evolution (Figure 3-18B). Results are very different from the ones in non-stressful conditions. The relationship

between $Y(\text{total})$ and $Y(\text{II})$ is similar to the one in *Chlamydomonas*, indicating that there is some CEF at play and that there is an interplay between CEF and LEF. This clearly shows that *Amphidinium carterae* is not species which cannot perform CEF. It possesses the ability to perform CEF but does not do it constitutively, in non-stressful conditions. Here, a very striking peculiarity should be further discussed: in these conditions, *Amphidinium carterae* performs CEF but in saturating DCMU conditions, there was absolutely no sign of CEF. This is a very clear evidence that measurements made in saturating DCMU conditions should be interpreted with a lot of care!

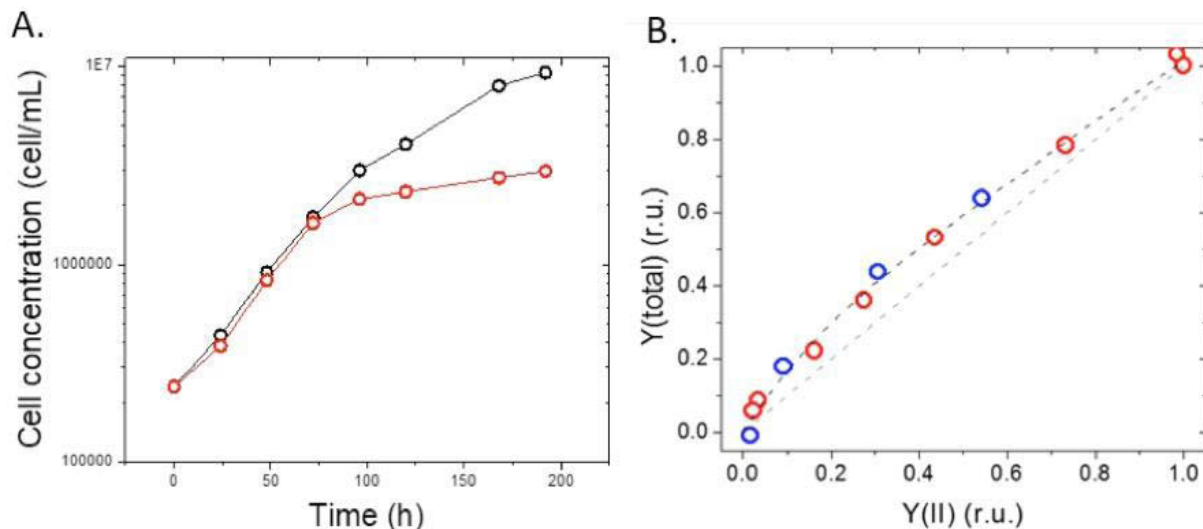


Figure 3-18: Relative changes of $Y(\text{total})$ and $Y(\text{II})$ when titrating LEF by DCMU in nitrogen depleted *Amphidinium carterae* (dinoflagellate)

A. Growth curve of *Amphidinium carterae* in nitrogen replete (black) and nitrogen depleted (red) (10% of the nitrogen concentration of the complete medium) ESAW medium. B. DCMU titration of $Y(\text{total})$ and $Y(\text{II})$ in nitrogen-depleted sample. Measurements were performed between 2 to 3 days after the end of the exponential growth. Measurements were performed under steady state light at $135 \mu\text{mol photons m}^{-2} \text{s}^{-1}$. The normalized values of $Y(\text{total})$ and $Y(\text{II})$ are plotted one against the other. Red and blue datapoints correspond to two biological replicates.

b) A standalone CEF in the dinoflagellate *Symbiodinium sp.*

We also pointed out that another dinoflagellate, *Symbiodinium sp.*, was performing CEF that remained constant as LEF was increasingly inhibited. In this case, physiological and absolute CEF measurement can be extracted from the experiment. First, the CEF/LEF ratio can be obtained straightforwardly by looking at the ratio between the photosystems activity involved in CEF (the y-intercept, at saturating DCMU concentration) to the initial photosystems activity. Since CEF does not depend on LEF, the absolute rate of CEF can be

simply assessed in conditions of saturating DCMU concentration. The y -intercept corresponds here to the yield of PSI which can be multiplied by PSI absorption cross-section and light irradiance to give the CEF rate. But other classical methods are used in routine to measure CEF in saturating DCMU conditions: photochemical rate from ECS or P_{700} rereduction rate (Alric, 2010).

In our case, we calculated that roughly a third of PSI was involved in CEF. From equation (5) this gives an ATP/NADPH ratio of ~ 1.7 , which is largely sufficient to rule out a shortfall of ATP for downhill metabolic processes. These considerations are true for the physiological conditions used in the experiment and the light irradiance that *Symbiodinium* experiences during in the experiment.

The independence between CEF and LEF suggests a functional isolation of the two pathways (Figure 3-17 panels B and E). The first possibility invokes a physical separation of the LEF and CEF chains, i.e. a regionalization of CEF at the plastid scale. This could be a lateral segregation of PSII and PSI. In plants and green algae, PSII and PSI are not homogeneously distributed into the cell (Anderson, 1999). PSII are mostly localized into the grana regions while PSI are mostly concentrated into lamellae (Anderson, 1999). If plastoquinone or plastocyanin diffusion from one region to the other one is limiting, then regions are functionally isolated (at least partly). One can imagine that one third of the PSI are physically separated from PSII, then it would explain the CEF behavior in *Symbiodinium*. However, the ultrastructure of thylakoids in secondary plastids is very homogeneous, showing no grana/lamella structuration (Pyszniak and Gibbs, 1992; Bedoshvili et al., 2009). But this does not mean that segregation between photosystems is absent; for example PSII can be organized in patches in cyanobacteria (Folea et al, 2008). Another possibility would be that CEF are isolated from LEF by protein arrangement. Several works propose that CEF occur in super-complexes containing PSI, cytochrome b_6f and proteins involved in reducing power reintroduction into the chain (Iwai et al, 2010). In supercomplexes, the distance between PSI first acceptors and cytochrome b_6f is reduced, which would contribute to reduce drastically the competition with LEF, thus highly favoring CEF rather than electron leak to other pathway.

What does a model of independence between CEF and LEF mean regarding the putative role of CEF in ATP/NADPH ratio equilibration? To my opinion, there are two possibilities: if the limiting step of the electron transfer process in the physically separated CEF and LEF chains

are the same (e.g. cytochrome *b₆f*) then the light dependence of the CEF and LEF will be the same. Therefore, one can imagine that the ATP/NADPH ratio remains the one we calculated (i.e. ~ 1.7) regardless of light irradiance. But if this is not the case, if the electron flow in CEF chains saturates at lower intensities than the electron flow in LEF chain, then the problem of the ATP shortfall arises again under high light. *Symbiodinium* species have been shown to possess efficient alternative electron flows under high light conditions, which were attributed to Mehler reaction (Roberty et al, 2014). Understanding the photosynthetic regulation in *Symbiodinium* will therefore require a more sophisticated approach to consider both CEF and water to water cycles.

c) The DCMU-titration method in the field?

One question I wanted to address is whether this method can be applied in the field. In June 2017, I had the pleasure of being welcomed by Laure Guillou, within the UMR "Adaptation and Diversity in Marine" of the biological station of Roscoff (France). Near the station, the Penzé River flows into the sea and thanks to the high nutrient content of the water (Maguer et al., 2004), its estuary is the site of massive microalgae development in the spring (Chambouvet et al., 2008). In June 2017, we were able to collect a sample rich in diatoms that we concentrated and purified by filtration on a 20 μ m filter. We kept the retentate and the cytological analysis revealed a composition largely dominated by one species, *Chaetoceros* (more than 94% of the phytoplankton cells, Figure 3-19A). The ECS spectrum of this sample was characteristic of diatoms (data not shown). We applied our method to estimate the relation between CEF and LEF by DCMU titration. When plotting $Y(\text{total})$ as a function of $Y(\text{II})$, we get an affine relationship (Figure 3-19B, linear regression gives a high adjusted correlation coefficient, $R^2 = 0.999$). This data is compatible with our model of cyclic electron flow functionally independent on LEF.

Linear regression estimates a y-intercept of 0.11 ± 0.01 . This means that about 11% of initial photosystems (PSI + PSII) activity in the absence of DCMU was involved in CEF. Before normalization the $Y(\text{total})$ in the absence of DCMU was 0.85, meaning that 85% of photosystems were initially open.

This experience shows that CEF measurement in the field is possible and this paves the way of the study of environmental determinants of CEF, in situ. However, it should be noted that certain conditions are necessary to use this method. First, algae concentrations must be important in order to get a signal-to-noise high enough. This is particularly important for the

ECS absorbance changes measurements. In the laboratory, the minimum concentrations of microalgae required to have a noise of less than 10% of the signal vary between 10^6 and 10^7 cells/mL depending on the species. In the field, microalgae concentrations of 10^5 are reached anecdotally (e.g. Vardi et al., 2004, Lefebvre et al., 2011) and would make it possible to obtain satisfactory concentrations by means of concentration processes. But the average phytoplankton concentration in the ocean are often lower (estimated between 10 and $5 \cdot 10^3$ cells/mL, Pesant et al., 2015). Another major constraint is that monospecific samples are required. Indeed, in a mixture of species, measurements reflect the signal emitted by all the species present in the sample. An average signal is then measured which does not make it possible to determine the specificities of each species.

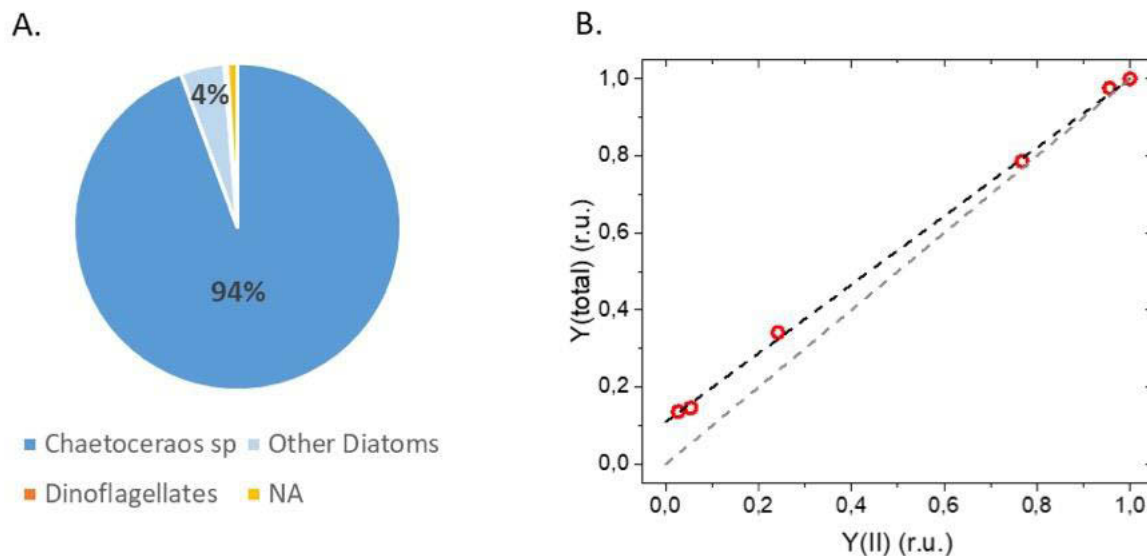


Figure 3-19: Testing CEF behaviour on a *Chaetoceros sp.* dominated sample from the field

A. Water has been sampled in the Penzé River (Roscoff, Brittany, France) and the percentage of *Chaetoceros sp.* (diatom), other diatoms, dinoflagellates and other cells (NA) were determined by morphological identification of more than 600 cells. B. Normalized values of Y_{total} and Y_{II} , measured at different DCMU concentrations in the *Chaetoceros sp.* dominated sample, are plotted one against the other. Measurements were performed under steady state light at $135 \mu\text{mol photons m}^{-2} \text{s}^{-1}$. The dashed grey line shows the $y=x$ line, corresponding to the situation where there is no CEF. The black dashed line shows the linear regression of the experimental data ($y = 0.89x + 0.11$ with an adjusted correlation coefficient of 0.999). Data correspond to one sample measurement.

d) A complex relationship between CEF and LEF in the chlorophyte *Chlamydomonas reinhardtii*

In the last microalga I tested, *Chlamydomonas reinhardtii*, the evolution of $Y(\text{total})$ as a function of $Y(\text{II})$ gave a non-linear function (panel C). CEF is occurring under steady state but is depending on LEF rate. Small perturbations of photosynthesis by adding small amounts of DCMU revealed that CEF increases and compensates for the loss of LEF. This behavior is a signature of a competition between the two processes, which could occur at the PQ pool, at the b_6f level or on the PSI acceptor side (Figure 3-17 panel F). This will be discussed further in part 3.5.3.

3.5.2 Limitations of the DCMU titration method

The protocol used to explore the CEF diversity is based on the hypothesis that throughout the DCMU titration, relative variations of $Y(\text{II})$ and $Y(\text{total})$ are equal to relative variations of $\text{ETR}(\text{total})$ and $\text{ETR}(\text{II})$, respectively. This remains true only if:

- the PSII and total absorption cross-sections, σ_{II} and σ_{total} , remain constant during the experiment. Here, all the strains used do not perform state transitions and this criterion can be considered met.
- the stoichiometry of the two photosystems does not change. It is reasonable to suppose that it is the case given the relatively short duration of the experiment.
- the expression $\text{ETR}(\text{total}) = Y(\text{total}) \cdot \sigma_{\text{total}} \cdot I$ is indeed a good measurement of the total photosystem activity which is the weighted average of $\text{ETR}(\text{I})$ and $\text{ETR}(\text{II})$, i.e. the photochemical rate.

A priori, the expression $\text{ETR}(\text{total}) = Y(\text{total}) \cdot \sigma_{\text{total}} \cdot I$ suffers of several approximations. As stated previously, it cannot be derived mathematically from the sum of $\text{ETR}(\text{II})$ and $\text{ETR}(\text{I})$ (see general discussion). However the comparison between $\text{ETR}(\text{total})$ and the photochemical rate gave a very good agreement (part 3.4.2, Figure 3-11D). It would however be interesting to follow the same protocol using the photochemical rate (measured as the ECS initial slope at light offset) instead of the $\text{ETR}(\text{total})$.

The most important in the DCMU method is that the conclusions of the experiments are not affected by these approximations; the demonstration of the validity of the $Y(\text{total})$ versus $Y(\text{II})$ titration method is demonstrated in the case of a “puddle” model (see appendix 1).

In the case of *Chlamydomonas*, the protocol we used cannot provide a full characterization of the CEF regulation and extent. We cannot provide an absolute rate of CEF or a CEF/LEF ratio; this is one of the limitations of the protocol. Another limitation is that we cannot exclude the occurrence of two concomitant CEF mechanisms in *Chlamydomonas reinhardtii*: one being independent of LEF and another one being dependent. In order to better investigate the relationship between CEF and LEF and to get estimation of the amplitude of CEF, this simple protocol was not sufficient. We developed, tested and applied a method requiring measurements of PSI and PSII absorption cross-sections and monitor CEF and LEF absolute rates as a function of light irradiance. This is the topic of the section (3.5.3). Before that, I would like to list some questions which could be addressed with this simple protocol and to propose variants of the DCMU titration protocol which could help investigating the effect of environmental parameters on the regulation of CEF.

3.5.3 Future directions for CEF investigations

The methods developed in this work pave the way for tackling many questions regarding CEF pathway, role, regulation and diversity. We detail below some research tracks that could be followed in the future. The results we presented above were obtained in one environmental and physiological condition. But we don't know if the different behaviors observed are due to genetic differences between species (presence / absence of enzymes involved in CEF), or to physiological differences (difference in redox state of the photosynthetic intermediates for example). Thus, it is difficult to question our results with a phylogenetic point of view. In order to understand better the determinants of CEF and thus to better discriminate between genetic capacity to perform CEF and physiology influence on CEF behavior, we tested CEF evolution in different environmental conditions. We will discuss this in the section 3.5.3.

Of course, testing the relationship between CEF and LEF with the protocol described in the first part of the chapter on mutants of the proteins potentially involved in CEF could help to progress in the characterization of the mutants. For example, the absence of phenotype regarding CEF relationship with LEF would be a strong argument favoring the non-implication of the putative protein. With the help of Sandrine Bujaldon, our ingeneer-sheriff, I already crossed the *Chlamydomonas reinhardtii* mutants of PGRL1 and PGR5, proteins putatively involved in CEF, with the *stt7-9* mutant. Sieving enabled to select two PGRL1**stt7-9* mutants and one PGR5**stt7-9* mutant. Unfortunately, I did not yet have time to investigate those double mutants yet.

Another possibility would be to use other treatments than DCMU to modify the LEF, and study the modification of the CEF/LEF ratio in these treatments. LEF and CEF share the electron transfer chain from the PQ pool to PSI acceptors, so the two possibilities to affect specifically LEF are (i) using PSII inhibitors, i.e. inhibiting LEF uphill the PQ pool (that is the approach we used here) or (ii) inhibiting the LEF downhill PSI acceptors. We can imagine two ways to achieve the second possibility –there are more.

One would be to play with the substrate of carbon assimilation, CO₂; this is very similar to the approach used by Lucker and Kramer (Lucker and Kramer, 2013), who demonstrated that the CO₂ status modifies the CEF/LEF. The authors conclude that CEF is needed to provide extra ATP for CBB cycle and CCM to operate. In the light of the work of Lucker and Kramer the high level of CEF in our samples suggests that in our conditions *Chlamydomonas reinhardtii* was CO₂ limited; this is likely since our sample was only manually mixed every minute which might be insufficient to replenish the sample with CO₂. We expect the CEF/LEF ratio to decrease if CO₂ is bubbled in the cuvette.

An alternative way to affect the metabolic pathways downhill PSI would be to modify temperature. Temperature modifies the kinetics all physico-chemical processes but will especially affect the fate of electrons downhill PSI, which require diffusion of molecules. Figure 3-20 is not meant to represent robust data but can be useful to illustrate this possibility (it is a very preliminary experiment performed only once). When the temperature of a *Chlamydomonas* (stt7 mutant) sample was decreased (phase 1 in Figure 3-20), the Y(total) decreased less than the Y(II) indicating an activation of CEF. This response was reversible when the temperature was increased again. Developing such a protocol would help understanding how the photosynthetic physiology, in terms of CEF/LEF regulation, responds to temperature changes.

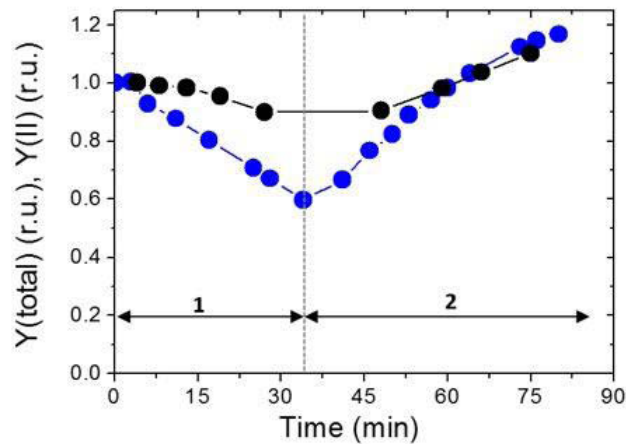


Figure 3-20: Evolution of Y(total) (black) and Y(II) (blue) when temperature is decreasing (phase 1) and increasing (phase 2).

Y(total) and Y(II) were normalized to 1 at the beginning of the experiment (i.e. time 0 and $T^{\circ}\text{C} = 20^{\circ}\text{C}$). Temperature change was induced by a water bath system surrounding the sample cuvette. Temperature within the sample varied from 20°C to approximately 10°C . Data correspond to measurements done in one biological sample.

3.5.3 Despite a complex relationship, CEF and LEF remain proportional at all light intensities in *Chlamydomonas reinhardtii*

The increase of the CEF when LEF is inhibited indicates a competition between these two tracks. Since the two processes share the same components except the "cycling step" the competition most likely takes place at the level of the substrates of this step. If we consider the FQR pathway or the NDH pathway (here NDA2 in *Chlamydomonas reinhardtii*, Peltier and Cournac, 2002), this means that the sites of competition could be the PQ pool or the ferredoxin pool. This is compatible both with the model proposed by Allen in which he states that CEF depends mainly on PQ redox state (Allen, 2003), and with the model proposed by Alric and co-workers of a CEF regulation at the level of the PSI acceptors, ferredoxin or NADPH (Alric, 2010).

The measurement of the absolute rates of CEF and LEF at different light irradiances revealed that the CEF/LEF ratio was very important (0.5 or 1.5 depending on the mode of estimation of the absorption cross-section of PSII). It is not easy to find a model which can explain both the concomitant changes of CEF and LEF with light irradiance, but their inter-dependence during DCMU titration. The parallel increase of CEF and LEF with light is not compatible with

the regulative model proposed by Allen (Allen, 2003) in which PQ redox state would be the main determinant of CEF amplitude. Indeed, from low light to high light, because cytochrome *b₆f* becomes limiting, the plastoquinone pool gets reduced (almost fully). Hence, under this hypothesis, CEF should decrease with light irradiance while LEF is increasing and CEF/LEF would not decline. Regulative process compatible with this behavior will be discussed more deeply in the overall discussion. Another surprising observation which must be taken into account in the building of a model of the CEF-to-LEF regulation is the fact that the LEF saturates at 100-125 electrons per second per PSII, which would often be interpreted as a sign of photosynthetic control. However, the PSI activity saturates at 200-250 electrons per second per PSI, which means that the cytochrome *b₆f*, which is stoichiometric to PSI in *Chlamydomonas*, transfers electrons with a maximal turnover of ~5ms or less, close to the maximal turnover rate of the cytochrome *b₆f* and therefore incompatible compatible with a photosynthetic control.

Finally, one important point to discuss is the difference of ETR amplitudes between the three replicates shown in section 3.4.3 (Figure 3-13, Figure 3-14 and Figure 3-15). In Figure 3-21, we represented the fraction of PSI involved in CEF in the three replicates that is rather stable at all light irradiance. However, its average amplitude varies depending on the replicate. This difference in CEF amplitude can be attributed to difference in physiological conditions, for example the CO₂ availability, which is not well controlled in our set up, and that is known to influence the CEF amplitude (Lucker and Kramer, 2013). But if the biological variability prevents us from giving a precise value of the CEF rate, this variability also has one advantage. Indeed, the rather stable CEF/LEF ratio in all replicates, even if the amplitude is different, is a strong argument in favor of a fine tuning of the CEF/LEF ratio.

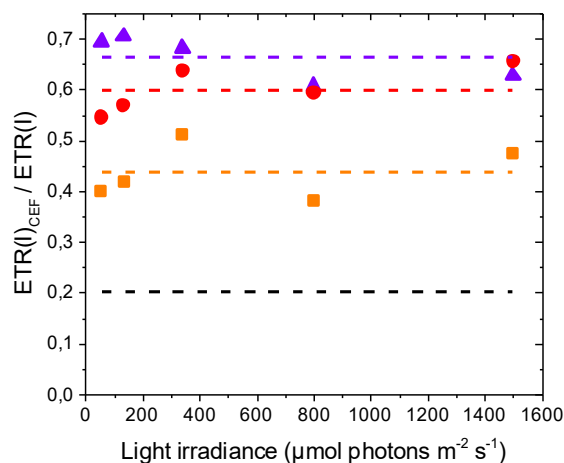


Figure 3-21 : Fraction of PSI involved in CEF as a function of light intensity for the three replicates used in section 3.4.3

The three colors correspond to the three replicates shown in Figure 3-13, Figure 3-14 and Figure 3-15 (purple, orange and red, being the replicate shown in the left, middle and right panels, respectively). Here, only the data obtained with ECS-based estimation of the photon absorption rate ($\sigma_{II} \cdot I$) is shown. Purple, orange and red dashed lines correspond to the average $ETR(I)_{CEF}/ETR(I)$ for each replicate, $ETR(I)$ being the electron transfer rate through the PSI. Black dashed line correspond to the ratio $ETR(I)_{CEF}/ETR(I)$ required for the CBB cycle to function.

The limiting factor in our work aiming at extracting absolute rates of CEF and LEF in *Chlamydomonas* is the accurate measurements of the PSII absorption cross-section. The way we measured the PSII absorption cross-section was by fitting the fluorescence rise as an exponential function. However, Pierre and Anne Joliot first demonstrated the excitonic connectivity from a close PSII reaction center to an adjacent open one (Joliot, 1964), following a similar observation by Vredenberg and Duysens in a purple photosynthetic bacterium (Vredenberg and Duysens, 1963). Because of the connectivity between PSII centers, the fluorescence rise is sigmoidal instead of exponential in plants and *Chlorella* (Strasser et al., 2000). The reason why the sigmoidicity does not always appear clearly is because in DCMU conditions, a fraction of Q_A is reduced in the dark. The area above the fluorescence induction curve corresponds to the average time between two photo absorption, assuming that the initial state is $[P_{680}, Q_A]$ (open PSII reaction centers) and the steady-state is $[P_{680}, Q_A^-]$ (fully closed PSII). We know that at least one of these conditions is not met. This is because the semi quinone Q_B^- is at the equilibrium with Q_A and when DCMU replace Q_B , part of the Q_A remains reduced (Lazár, 1999). It can be seen in Figure 3-12A where the initial value at the beginning of the fluorescence rise is slightly higher than the true F_0 measured in the absence of DCMU. This experimental default may explain the

divergence between the σ_{II} measured with fluorescence or with ECS. A recent work suggests that the underestimation of the area above the curve, and thus the underestimation of the σ_{II} can reach up to 36% when F_0 were increased by a factor 1.5 (Tian et al., 2019). Considering the sigmoidicity of the fluorescence rise in the fluorescence-based estimation of the PSII absorption cross-section might reconcile its estimations by fluorescence and ECS, and strengthen the conclusions we have drawn from the calculations of the light dependence of absolute rates of LEF and CEF.

3.6 Bibliography

- Allahverdiyeva, Y., Mustila, H., Ermakova, M., Bersanini, L., Richaud, P., Ajlani, G., ... & Aro, E. M. (2013).** Flavodiiron proteins Flv1 and Flv3 enable cyanobacterial growth and photosynthesis under fluctuating light. *Proceedings of the National Academy of Sciences*, *110*(10), 4111-4116.
- Allen, J. F. (2002).** Photosynthesis of ATP—electrons, proton pumps, rotors, and poise. *Cell*, *110*(3), 273-276.
- Allen, J. F. (2003).** Cyclic, pseudocyclic and noncyclic photophosphorylation: new links in the chain. *Trends in plant science*, *8*(1), 15-19.
- Alric, J. (2010).** Cyclic electron flow around photosystem I in unicellular green algae. *Photosynthesis research*, *106*(1-2), 47-56.
- Alric, J. (2014).** Redox and ATP control of photosynthetic cyclic electron flow in *Chlamydomonas reinhardtii*:(II) Involvement of the PGR5–PGRL1 pathway under anaerobic conditions. *Biochimica et Biophysica Acta (BBA)-Bioenergetics*, *1837*(6), 825-834.
- Alric, J., & Johnson, X. (2017).** Alternative electron transport pathways in photosynthesis: a confluence of regulation. *Current opinion in plant biology*, *37*, 78-86.
- Anderson, J. M. (1999).** Insights into the consequences of grana stacking of thylakoid membranes in vascular plants: a personal perspective. *Functional Plant Biology*, *26*(7), 625-639.
- Arnon, D. I., Allen, M. B., & Whatley, F. R. (1954).** Photosynthesis by isolated chloroplasts. *Nature*, *174*(4426), 394-396.
- Asada, K. (2000).** The water–water cycle as alternative photon and electron sinks. *Philosophical Transactions of the Royal Society of London. Series B: Biological Sciences*, *355*(1402), 1419-1431.
- Avenson, T. J., Cruz, J. A., Kanazawa, A., & Kramer, D. M. (2005).** Regulating the proton budget of higher plant photosynthesis. *Proceedings of the National Academy of Sciences*, *102*(27), 9709-9713.
- Bailleul, B., Berne, N., Murik, O., Petroutsos, D., Prihoda, J., Tanaka, A., ... & Krieger-Liszkay, A. (2015).** Energetic coupling between plastids and mitochondria drives CO₂ assimilation in diatoms. *Nature*, *524*(7565), 366.
- Bailleul, B., Cardol, P., Breyton, C., & Finazzi, G. (2010).** Electrochromism: a useful probe to study algal photosynthesis. *Photosynthesis research*, *106*(1-2), 179.
- Bedoshvili, Y. D., Popkova, T. P., & Likhoshway, Y. V. (2009).** Chloroplast structure of diatoms of different classes. *Cell and Tissue Biology*, *3*(3), 297-310.
- Bendall, D. S., & Manasse, R. S. (1995).** Cyclic photophosphorylation and electron transport. *Biochimica et Biophysica Acta (BBA)-Bioenergetics*, *1229*(1), 23-38.
- Cardol, P., Bailleul, B., Rappaport, F., Derelle, E., Béal, D., Breyton, C., ... & Finazzi, G. (2008).** An original adaptation of photosynthesis in the marine green alga *Ostreococcus*. *Proceedings of the National Academy of Sciences*, *105*(22), 7881-7886.
- Chambouvet, A., Morin, P., Marie, D., & Guillou, L. (2008).** Control of toxic marine dinoflagellate blooms by serial parasitic killers. *Science*, *322*(5905), 1254-1257.
- Chaux, F., Burlacot, A., Mekhalfi, M., Auroy, P., Blangy, S., Richaud, P., & Peltier, G. (2017).** Flavodiiron proteins promote fast and transient O₂ photoreduction in *Chlamydomonas*. *Plant physiology*, *174*(3), 1825-1836.

- Chaux, F., Peltier, G., & Johnson, X. (2015).** A security network in PSI photoprotection: regulation of photosynthetic control, NPQ and O₂ photoreduction by cyclic electron flow. *Frontiers in plant science*, *6*, 875.
- Depège, N., Bellafiore, S., & Rochaix, J. D. (2003).** Role of chloroplast protein kinase Stt7 in LHCII phosphorylation and state transition in *Chlamydomonas*. *Science*, *299*(5612), 1572-1575.
- Eberhard, S., Finazzi, G., & Wollman, F. A. (2008).** The dynamics of photosynthesis. *Annual review of genetics*, *42*, 463-515.
- Fan, D. Y., Fitzpatrick, D., Oguchi, R., Ma, W., Kou, J., & Chow, W. S. (2016).** Obstacles in the quantification of the cyclic electron flux around Photosystem I in leaves of C₃ plants. *Photosynthesis research*, *129*(3), 239-251.
- Fan, D. Y., Nie, Q., Hope, A. B., Hillier, W., Pogson, B. J., & Chow, W. S. (2007).** Quantification of cyclic electron flow around Photosystem I in spinach leaves during photosynthetic induction. *Photosynthesis Research*, *94*(2-3), 347.
- Finazzi, G., Rappaport, F., Furia, A., Fleischmann, M., Rochaix, J. D., Zito, F., & Forti, G. (2002).** Involvement of state transitions in the switch between linear and cyclic electron flow in *Chlamydomonas reinhardtii*. *EMBO reports*, *3*(3), 280-285.
- Fisher, N., Bricker, T. M., & Kramer, D. M. (2019).** Regulation of photosynthetic cyclic electron flow pathways by adenylate status in higher plant chloroplasts. *Biochimica et Biophysica Acta (BBA)-Bioenergetics*, *1860*(11), 148081.
- Folea, I. M., Zhang, P., Aro, E. M., & Boekema, E. J. (2008).** Domain organization of photosystem II in membranes of the cyanobacterium *Synechocystis* PCC6803 investigated by electron microscopy. *FEBS letters*, *582*(12), 1749-1754.
- Genty B, Goulas Y, Dimon B, Peltier JM, Moya I. (1992).** Modulation of efficiency of primary conversion in leaves, mechanisms involved at PSII. In *Research in Photosynthesis, Volume 4*, ed. N Murata, pp. 603–10. Dordrecht: Kluwer Academic Publishers
- Ghirardi, M. L., Posewitz, M. C., Maness, P. C., Dubini, A., Yu, J., & Seibert, M. (2007).** Hydrogenases and hydrogen photoproduction in oxygenic photosynthetic organisms. *Annu. Rev. Plant Biol.*, *58*, 71-91.
- Golding, A. J., Finazzi, G., & Johnson, G. N. (2004).** Reduction of the thylakoid electron transport chain by stromal reductants—evidence for activation of cyclic electron transport upon dark adaptation or under drought. *Planta*, *220*(2), 356-363.
- Grossman, A. R. (2000).** *Chlamydomonas reinhardtii* and photosynthesis: genetics to genomics. *Current opinion in plant biology*, *3*(2), 132-137.
- Hahn, A., Vonck, J., Mills, D. J., Meier, T., & Kühlbrandt, W. (2018).** Structure, mechanism, and regulation of the chloroplast ATP synthase. *Science*, *360*(6389), eaat4318.
- Harbinson, J., Genty, B., & Baker, N. R. (1989).** Relationship between the quantum efficiencies of photosystems I and II in pea leaves. *Plant Physiology*, *90*(3), 1029-1034.
- Heber, U., & Walker, D. (1992).** Concerning a dual function of coupled cyclic electron transport in leaves. *Plant Physiology*, *100*(4), 1621-1626.
- Hertle, A. P., Blunder, T., Wunder, T., Pesaresi, P., Pribil, M., Armbruster, U., & Leister, D. (2013).** PGRL1 is the elusive ferredoxin-plastoquinone reductase in photosynthetic cyclic electron flow. *Molecular cell*, *49*(3), 511-523.
- Hügler, M., & Sievert, S. M. (2011).** Beyond the Calvin cycle: autotrophic carbon fixation in the ocean. *Annual review of marine science*, *3*, 261-289.

- Ishikawa, N., Endo, T., & Sato, F. (2008).** Electron transport activities of *Arabidopsis thaliana* mutants with impaired chloroplastic NAD (P) H dehydrogenase. *Journal of plant research*, 121(5), 521-526.
- Iwai, M., Takizawa, K., Tokutsu, R., Okamuro, A., Takahashi, Y., & Minagawa, J. (2010).** Isolation of the elusive supercomplex that drives cyclic electron flow in photosynthesis. *Nature*, 464(7292), 1210.
- Johnson, G. N. (2005).** Cyclic electron transport in C3 plants: fact or artefact? *Journal of Experimental Botany*, 56(411), 407-416.
- Johnson, G. N. (2011).** Physiology of PSI cyclic electron transport in higher plants. *Biochimica et Biophysica Acta (BBA)-Bioenergetics*, 1807(3), 384-389.
- Joliot, P. (1964).** Etude cinétique de la réaction photochimique libérant l'oxygène au cours de la photosynthèse. *CR Acad. Sci.*, 258, 4622-4625.
- Joliot, P., & Johnson, G. N. (2011).** Regulation of cyclic and linear electron flow in higher plants. *Proceedings of the National Academy of Sciences*, 108(32), 13317-13322.
- Joliot, P., & Joliot, A. (2002).** Cyclic electron transfer in plant leaf. *Proceedings of the National Academy of Sciences*, 99(15), 10209-10214.
- Joliot, P., & Joliot, A. (2005).** Quantification of cyclic and linear flows in plants. *Proceedings of the National Academy of Sciences*, 102(13), 4913-4918.
- Joliot, P., & Joliot, A. (2008).** Quantification of the electrochemical proton gradient and activation of ATP synthase in leaves. *Biochimica et Biophysica Acta (BBA)-Bioenergetics*, 1777(7-8), 676-683.
- Joliot, P., Béal, D., & Joliot, A. (2004).** Cyclic electron flow under saturating excitation of dark-adapted *Arabidopsis* leaves. *Biochimica et Biophysica Acta (BBA)-Bioenergetics*, 1656(2-3), 166-176.
- Klughammer, C., & Schreiber, U. (1994).** Saturation pulse method for assessment of energy conversion in PS I. *Planta*, 192, 261-268.
- Kouřil, R., Strouhal, O., Nosek, L., Lenobel, R., Chamrád, I., Boekema, E. J., ... & Ilík, P. (2014).** Structural characterization of a plant photosystem I and NAD (P) H dehydrogenase supercomplex. *The Plant Journal*, 77(4), 568-576.
- Kramer, D. M., & Evans, J. R. (2011).** The importance of energy balance in improving photosynthetic productivity. *Plant Physiology*, 155(1), 70-78.
- Kramer, D. M., Avenson, T. J., & Edwards, G. E. (2004).** Dynamic flexibility in the light reactions of photosynthesis governed by both electron and proton transfer reactions. *Trends in plant science*, 9(7), 349-357.
- Kramer, D. M., Johnson, G., Kiirats, O., & Edwards, G. E. (2004).** New fluorescence parameters for the determination of Q_A redox state and excitation energy fluxes. *Photosynthesis research*, 79(2), 209.
- Laisk, A., Eichelmann, H., Oja, V., Talts, E., & Scheibe, R. (2007).** Rates and roles of cyclic and alternative electron flow in potato leaves. *Plant and Cell Physiology*, 48(11), 1575-1588.
- Laureau, C., De Paepe, R., Latouche, G., Moreno-Chacón, M., Finazzi, G., Kuntz, M., ... & Streb, P. (2013).** Plastid terminal oxidase (PTOX) has the potential to act as a safety valve for excess excitation energy in the alpine plant species *R. anunculus glacialis* L. *Plant, cell & environment*, 36(7), 1296-1310.
- Lazár, D., & Nauš, J. (1998).** Statistical properties of chlorophyll fluorescence induction parameters. *Photosynthetica*, 35(1), 121-127.

- Lefebvre, A., Guiselin, N., Barbet, F., & Artigas, F. L. (2011). Long-term hydrological and phytoplankton monitoring (1992–2007) of three potentially eutrophic systems in the eastern English Channel and the Southern Bight of the North Sea. *ICES Journal of marine science*, 68(10), 2029-2043.
- Lemaire, C., Wollman, F. A., & Bennoun, P. (1988). Restoration of phototrophic growth in a mutant of *Chlamydomonas reinhardtii* in which the chloroplast atpB gene of the ATP synthase has a deletion: an example of mitochondria-dependent photosynthesis. *Proceedings of the National Academy of Sciences*, 85(5), 1344-1348.
- Li, X. P., BjoÈrkman, O., Shih, C., Grossman, A. R., Rosenquist, M., Jansson, S., & Niyogi, K. K. (2000). A pigment-binding protein essential for regulation of photosynthetic light harvesting. *Nature*, 403(6768), 391.
- Livingston, A. K., Cruz, J. A., Kohzuma, K., Dhingra, A., & Kramer, D. M. (2010). An *Arabidopsis* mutant with high cyclic electron flow around photosystem I (hcef) involving the NADPH dehydrogenase complex. *The Plant Cell*, 22(1), 221-233.
- Lucker, B., & Kramer, D. M. (2013). Regulation of cyclic electron flow in *Chlamydomonas reinhardtii* under fluctuating carbon availability. *Photosynthesis research*, 117(1-3), 449-459.
- Maguer, J. F., Wafar, M., Madec, C., Morin, P., & Denn, E. E. L. (2004). Nitrogen and phosphorus requirements of an *Alexandrium minutum* bloom in the Penzé Estuary, France. *Limnology and Oceanography*, 49(4), 1108-1114.
- Meneghesso, A., Simionato, D., Gerotto, C., La Rocca, N., Finazzi, G., & Morosinotto, T. (2016). Photoacclimation of photosynthesis in the Eustigmatophycean *Nannochloropsis gaditana*. *Photosynthesis research*, 129(3), 291-305.
- Mitchell, P. (1975). The protonmotive Q cycle: a general formulation. *FEBS letters*, 59(2), 137-139.
- Müller, P., Li, X. P., & Niyogi, K. K. (2001). Non-photochemical quenching. A response to excess light energy. *Plant physiology*, 125(4), 1558-1566.
- Munekage, Y., Hashimoto, M., Miyake, C., Tomizawa, K. I., Endo, T., Tasaka, M., & Shikanai, T. (2004). Cyclic electron flow around photosystem I is essential for photosynthesis. *Nature*, 429(6991), 579.
- Munekage, Y., Hojo, M., Meurer, J., Endo, T., Tasaka, M., & Shikanai, T. (2002). PGR5 is involved in cyclic electron flow around photosystem I and is essential for photoprotection in *Arabidopsis*. *Cell*, 110(3), 361-371.
- Nawrocki W, Bailleul B, Picot D, Cardol P, Rappaport F, Wollman F-A and Joliot P (2019a) The mechanism of cyclic electron flow. *Biochim Biophys Acta*, 1860(5):433 – 438
- Nawrocki, W. J., Bailleul, B., Cardol, P., Rappaport, F., Wollman, F. A., & Joliot, P. (2019c). Maximal cyclic electron flow rate is independent of PGRL1 in *Chlamydomonas*. *Biochimica et Biophysica Acta (BBA)-Bioenergetics*, 1860(5), 425-432.
- Nawrocki, W. J., Buchert, F., Joliot, P., Rappaport, F., Bailleul, B., & Wollman, F. A. (2019b). Chlororespiration controls growth under intermittent light. *Plant physiology*, 179(2), 630-639.
- Owens, T. G. (1986). Light-harvesting function in the diatom *Phaeodactylum tricoratum*: II. Distribution of excitation energy between the photosystems. *Plant Physiology*, 80(3), 739-746.
- Peers, G., Truong, T. B., Ostendorf, E., Busch, A., Elrad, D., Grossman, A. R., ... & Niyogi, K. K. (2009). An ancient light-harvesting protein is critical for the regulation of algal photosynthesis. *Nature*, 462(7272), 518.
- Peltier, G., & Cournac, L. (2002). Chlororespiration. *Annual review of plant biology*, 53(1), 523-550.

- Pesant, S., Not, F., Picheral, M., Kandels-Lewis, S., Le Bescot, N., Gorsky, G., ... & Dimier, C. (2015).** Open science resources for the discovery and analysis of Tara Oceans data. *Scientific data*, 2, 150023.
- Pogoryelov, D., Reichen, C., Klyszejko, A. L., Brunisholz, R., Muller, D. J., Dimroth, P., & Meier, T. (2007).** The oligomeric state of c rings from cyanobacterial F-ATP synthases varies from 13 to 15. *Journal of bacteriology*, 189(16), 5895-5902.
- Pysznik, A. M., & Gibbs, S. P. (1992).** Immunocytochemical localization of photosystem I and the fucoxanthin-chlorophylla/c light-harvesting complex in the diatom *Phaeodactylum tricornutum*. *Protoplasma*, 166(3-4), 208-217.
- Roberty, S., Bailleul, B., Berne, N., Franck, F., & Cardol, P. (2014).** PSI Mehler reaction is the main alternative photosynthetic electron pathway in *Symbiodinium sp.*, symbiotic dinoflagellates of cnidarians. *New Phytologist*, 204(1), 81-91.
- Sacksteder, C. A., Kanazawa, A., Jacoby, M. E., & Kramer, D. M. (2000).** The proton to electron stoichiometry of steady-state photosynthesis in living plants: a proton-pumping Q cycle is continuously engaged. *Proceedings of the National Academy of Sciences*, 97(26), 14283-14288.
- Scheibe, R. (2004).** Malate valves to balance cellular energy supply. *Physiologia plantarum*, 120(1), 21-26.
- Schmidt, R. A., Qu, J., Williams, J. R., & Brusilow, W. S. (1998).** Effects of carbon source on expression of Fo genes and on the stoichiometry of the c subunit in the F1Fo ATPase of *Escherichia coli*. *Journal of bacteriology*, 180(12), 3205-3208.
- Seelert, H., Poetsch, A., Dencher, N. A., Engel, A., Stahlberg, H., & Müller, D. J. (2000).** Structural biology: proton-powered turbine of a plant motor. *Nature*, 405(6785), 418.
- Shikanai, T. (2014).** Central role of cyclic electron transport around photosystem I in the regulation of photosynthesis. *Current opinion in biotechnology*, 26, 25-30.
- Steinbeck, J., Ross, I. L., Rothnagel, R., Gäbelein, P., Schulze, S., Giles, N., ... & Stahlberg, H. (2018).** Structure of a PSI-LHCI-cyt *b₆f* supercomplex in *Chlamydomonas reinhardtii* promoting cyclic electron flow under anaerobic conditions. *Proceedings of the National Academy of Sciences*, 115(41), 10517-10522.
- Stirbet, A. (2013).** Excitonic connectivity between photosystem II units: what is it, and how to measure it? *Photosynthesis research*, 116(2-3), 189-214.
- Stock, D., Gibbons, C., Arechaga, I., Leslie, A. G., & Walker, J. E. (2000).** The rotary mechanism of ATP synthase. *Current opinion in structural biology*, 10(6), 672-679.
- Strasser, R. J., Srivastava, A., & Tsimilli-Michael, M. (2000).** The fluorescence transient as a tool to characterize and screen photosynthetic samples. Probing photosynthesis: mechanisms, regulation and adaptation, 445-483.
- Streb, P., JOSSE, E. M., Gallouet, E., Baptist, F., Kuntz, M., & Cornic, G. (2005).** Evidence for alternative electron sinks to photosynthetic carbon assimilation in the high mountain plant species *Ranunculus glacialis*. *Plant, Cell & Environment*, 28(9), 1123-1135.
- Stroebel, D., Choquet, Y., Popot, J. L., & Picot, D. (2003).** An atypical haem in the cytochrome *b₆f* complex. *Nature*, 426(6965), 413.
- Takahashi, H., Clowez, S., Wollman, F. A., Vallon, O., & Rappaport, F. (2013).** Cyclic electron flow is redox-controlled but independent of state transition. *Nature communications*, 4, 1954.
- Tian, L., Nawrocki, W. J., Liu, X., Polukhina, I., Van Stokkum, I. H., & Croce, R. (2019).** pH dependence, kinetics and light-harvesting regulation of nonphotochemical quenching in *Chlamydomonas*. *Proceedings of the National Academy of Sciences*, 116(17), 8320-8325.

Tikhonov, A. N. (2014). The cytochrome b_6f complex at the crossroad of photosynthetic electron transport pathways. *Plant Physiology and Biochemistry*, 81, 163-183.

Utermöhl, V. H. (1931). Neue Wege in der quantitativen Erfassung des Plankton.(Mit besonderer Berücksichtigung des Ultraplanktons.) Mit 4 Abbildungen im Text. *Internationale Vereinigung für theoretische und angewandte Limnologie: Verhandlungen*, 5(2), 567-596.

Viola, S., Bailleul, B., Yu, J., Nixon, P., Sellés, J., Joliot, P., & Wollman, F. A. (2019). Probing the electric field across thylakoid membranes in cyanobacteria. *Proceedings of the National Academy of Sciences*, 116(43), 21900-21906.

Vredenberg, W. J., & Duysens, L. N. (1963). Transfer of energy from bacteriochlorophyll to a reaction center during bacterial photosynthesis. *Nature*, 197(4865), 355-357.

Whatley, F. R. (1995). Photosynthesis by isolated chloroplasts: the early work in Berkeley. *Photosynthesis research*, 46(1), 17-26.

Zehr, J. P., & Kudela, R. M. (2009). Photosynthesis in the open ocean. *Science*, 326(5955), 945-946.

Zhang, H., Whitelegge, J. P., & Cramer, W. A. (2001). Ferredoxin: NADP⁺ Oxidoreductase Is a Subunit of the Chloroplast Cytochrome b_6f Complex. *Journal of Biological Chemistry*, 276(41), 38159-38165.

Chapter 4: Photosynthetic physiology of the coccolithophore *Emiliana huxleyi*

Major environmental determinants and signature of viral infection in the field

Summary

4.1	Introduction	217
4.2	Material and methods	219
	4.2.1 Mesocosm setup, treatments and sampling.....	219
	4.2.2 Flow cytometry/ qPCR.....	220
	4.2.3 Measurement of environmental (abiotic) parameters	221
	4.2.4 Photophysiology by Fast Induction and Relaxation fluorometry (FIRe).....	222
	4.2.5 Statistical analyses	225
4.3	Results	227
	4.3.1 A two phases phytoplankton bloom occurred	228
	4.3.2 Photosynthetic physiology	232
	4.3.3 Fluorescence signals were mainly due to <i>Emiliana huxleyi</i> from day 9 to 24th of the experiment	237
	4.3.4 Evolution of environmental parameters during the experiment	240
	4.3.5 Environmental determinants of <i>E. huxleyi</i> photosynthesis.....	242
	4.3.6 A photosynthetic signature of viral infection?	249
4.4	Conclusion and discussion	252
4.5	Bibliography	255

After studying CEF in the laboratory, where conditions are well controlled, I wanted to investigate this process in the field and had two opportunities to do so. The first one was the study of the phytoplankton community sampled in Penzé estuary (Brittany, France) which allowed me to perform a study of the dependency of CEF on LEF in a natural population of diatoms (presented in 3.5.1). The second attempt to do so was in two field campaigns that took place in the Bergen marine station (Norway), the goals of which were to study the rapid development (i.e. bloom) and demise of a population of the coccolithophore *Emiliana huxleyi*. At the risk of spoiling the suspense too rapidly, this second attempt failed. This chapter will therefore seem a little aside of the main topic of my thesis at first sight: it aims to understand the determinants of the photosynthetic physiology of the coccolithophore during the course of the bloom. We thus attempted to determine the major environmental (biotic and abiotic) factors influencing photosynthesis and more specifically the linear electron transfer. However, questions about the CEF amplitude will emerge from this study.

4.1 Introduction

The coccolithophore *Emiliana huxleyi* is one of the species that forms the largest ocean blooms (Tyrrell and Merico, 2004). Reaching areas of several square kilometers, these bodies of water containing up to tens of thousands of cells per milliliter are visible from space as whitish areas in the ocean (Tyrrell and Merico, 2004). *Emiliana huxleyi* blooms, which develop in time scales of the order of the week, then collapse in a few days giving rise to a massive release of organic matter feeding the trophic chain, and calcitic shells that surround them can sediment and give rise to carbon storage in the form of calcareous sediments (Bramlette, 1958; Milliman, 1993; Westbroek et al., 1993). The parameters determining the birth and death of a bloom are still an unresolved research topic. The causes of *Emiliana huxleyi*'s bloom demise are most often attributed to a specific virus of this species, *Emiliana huxleyi* virus (Ehv), that is part of the DNA double stranded nucleocytoplasmic, viruses family of *Phycodnaviridae* (Wilson et al., 2009). However, it has recently been shown that some strains of *Emiliana huxleyi* are resistant to viruses and that bacteria could also be involved in bloom demise (Barak-Gavish et al., 2018).

In order to study the dynamics of the birth and death of a bloom, an intermediate solution between the laboratory reductionism and the open sea oceanography surveys, more random because of the difficulty of predicting blooms, is the use of mesocosm (Odum, 1984). During

my thesis, I had the pleasure of participating in two field on the coast of Raunefjorden near Bergen in Norway, in the spring of 2017 and 2018. In 2017, the Mesohux campaign was organized by Bidle and Thamatrakoln labs (Rutgers, USA). In this chapter, I present the results from the most spectacular and verified bloom of *Emiliana huxleyi*, obtained in 2018 as part of a scientific campaign organized by the Vardi group (Weizmann Institute, Israel). This campaign was part of a collaboration with several international laboratories, each of them bringing a particular expertise (see material and methods of this chapter, section 4.2.1) for a better understanding of the ecological determinants of an *Emiliana huxleyi* bloom and demise. Within this consortium, we were responsible for following the evolution of photosynthetic physiology. *Emiliana huxleyi* is a photosynthetic species and the vast majority of its anabolic pathways are provided by the products of photosynthesis. When investigating the reasons of its growth, measuring the efficiency of its photosynthesis is crucial. Moreover, in such organisms, the study of photosynthesis is a unique tool to address the physiological state of whole cells and to investigate the result of abiotic stresses such as nutrient deficiency (e.g. Cullen et al., 1992; Kolber et al., 1988; Berges et al., 1996; ; Jiang et al. 2012), iron deficiency (Muggli et al., 1996), light or temperature stress (Loebl et al., 2010; Trimborn et al., 2007; Teoh et al., 2013).

We had several objectives, some more ambitious than others. The first one was to follow the photosynthetic physiology of *Emiliana huxleyi* and to identify the environmental parameters which determine the efficiency of photosynthesis. We had two other objectives whose attainment were more uncertain. The first one was directly related to CEF: we hoped that the cell concentration reached at the top of the bloom would be high enough to test our CEF methods in the field, on *Emiliana huxleyi* dominated samples. But even at the top of the bloom and with gentle cell concentration, signals-to-noise of the absorption difference spectroscopy approaches were too low and this objective was abandoned. The other one was to identify a photosynthetic signature of the viral infection (if a viral infection happened), which seems to be successful as we will see in the following.

4.2 Material and methods

4.2.1 Mesocosm setup, treatments and sampling

The mesocosm experiment, Aquacosm-viral induced microbial succession (Aquacosm-VIMS), was carried out over 24 days (May 24 – June 17, 2018) in Raunefjorden at the University of Bergen's Marine Biological Station Espegrend, Norway (60.27° N; 5.22° E). Enclosures consisted of seven transparent polyethylene bags made (11 m³, 4 m deep and 2 m wide, 90% photosynthetically active radiation) mounted on floating frames and moored to a raft in the middle of the bay. Four of them were uncovered (bags number 1 to 4) and three of them were covered by a polyethylene plastic sheeting (bags number 5 to 7) in order to collect the aerosols emitted along the days. Each bag was filled with surrounding fjord water in several times to ensure homogeneous initial water masses in all bags on day 0. Mesocosms were supplemented with nutrients at days 0-7 and 13-17 at a nitrogen:phosphorus ratio of 16:1 (1.6 μM NaNO₃, 0.1 μM KH₂PO₄, as previously described in (Vardi *et al.*, 2012) with some modification. In days 6, 7 and 13 only NaNO₃ was added because nitrogen was at that moment clearly the growth limiting nutrient. No silicate was added. The water in each bag was continuously mixed by pumping air to the bottom of the bag.

Every day, "core measurements", i.e. routine measurements in oceanography were made in the morning, starting at 07.00 am. This includes measurements of:

- Chlorophyll *a*, dissolved and particulate Nitrogen, Carbon and Sulfur, (Marasé, Cabrera, Masdeu & Simó, Institut de Ciències del Mar, Spain),
- Nutrients (NO₃⁻, NO₂⁻, NH₄⁺, PO₄³⁻, SiO₄⁴⁻) (Schleyer, Egge & Vardi, Weizmann Institute, Israël),
- Measurements performed by Conductivity Temperature Depth (CTD) device (temperature, salinity and turbidity in the bags) (Schleyer, Egge & Vardi, Weizmann Institute, Israël),
- Determination of the structure of the phytoplankton composition by flow cytometry (Vincent & Vardi, Weizmann Institute, Israël)

On top of these usual measurements, other analysis were performed:

- Evolution of photosynthetic physiology (Ferté & Bailleul, IBPC, Paris)
- Image recognition of microorganisms by FlowCAM (high throughput of phytoplankton imaging) (Mayers, Bergen University, Norway)

- qPCR of proxi genes for *E. huxleyi* (cox gene) and *E. huxleyi* virus (mcp gene) (Schleyer, Schatz, Kuhlisch, Vincent, Lang-Yona & Vardi, Weizmann Institute, Israël)
- Carbohydrate forms and concentration (Hehemann, Max Planck Institute for Marine Microbiology, Germany)
- Estimation of the extent of grazing and viral lysis (Mayers, Bergen University, Norway)
- Metabolomics (Schleyer, Kuhlisch & Vardi, Weizmann Institute, Israël)
- Aerosols composition extracted from the covered bags (Trainic, Flores and Koren, Weizmann Institute, Israël)
- Metagenomics (18S, 16S) (Vardi lab, Weizmann Institute, Israël)

Strains from the mesocosms were also isolated at some critical stages of the population evolution (Gachenot & Probert, Roscoff biological Station, France).

Hereafter, only material and methods of the data that we used will be described.

4.2.2 Flow cytometry/ qPCR

Phytoplankton composition and abundance were assessed by analyses of fresh samples on an Eclipse (iCyt) FACS flow cytometer. Samples for flow cytometric counts were taken twice a day, morning (7 am) and evening (8-9 pm) using 50 mL centrifugal tubes and following filtration using a 50 µm cell strainer to remove chains of diatoms.

Flow cytometry is a technique that measures cells characteristics in liquid suspension. Cells are aligned hydrodynamically by an entrainment fluid into a very narrow stream (10 to 20 mm wide) onto which one or several powerful light sources are focused. Each time a particle passes through the beam, it scatters light and measurements of angular intensity gives information on the refractive index, size, and shape of the particle. Moreover, phytoplankton species contains fluorescent pigments such as chlorophyll that emits fluorescence at a higher wavelength than what it absorbs (e.g., red light for chlorophyll). They can thus be easily differentiated from other heterotrophs microorganisms (Veldhuis and Kraay, 2000; Marie et al 2005). The different populations were discriminated as explained in the Figure 4-1 and gates used for population discrimination are explained in Figure 4-1. Nanoeukaryotes were identified by their high chlorophyll signal (excitation: 488nm and emission: 663-737nm). Among nanoeukaryotes, calcified *E. huxleyi* cells were identified by high side scatter. Low chlorophyll cells with no phycoerythrin fluorescence (FL3) signal were annotated as picoeukaryotes. Synechococcus cells were identified by their low chlorophyll content and high phycoerythrin fluorescence signal.

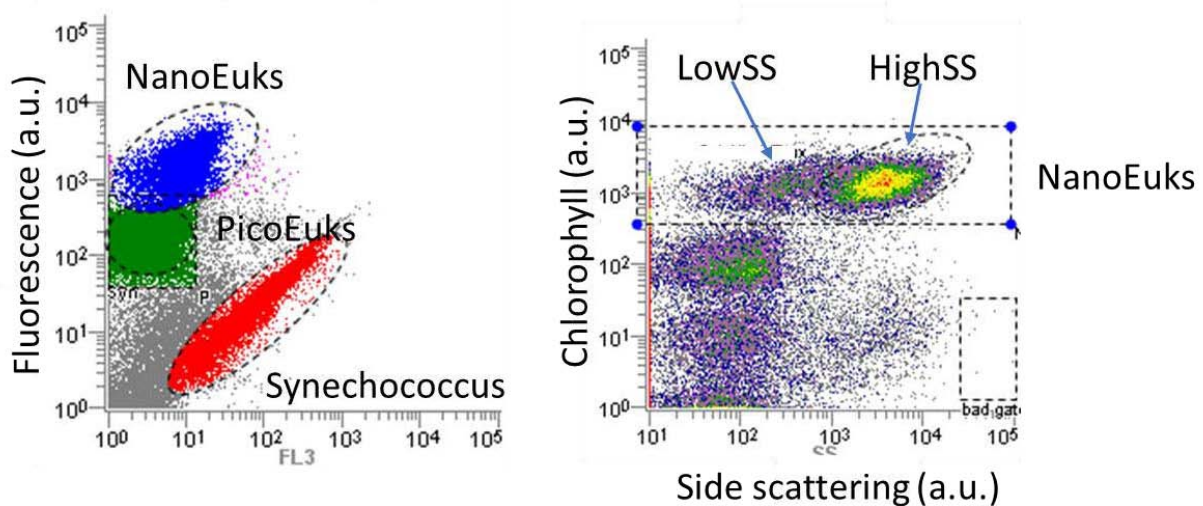


Figure 4-1: Gates used for flow cytometry measurements

Left: representation of the three populations based on red (chlorophyll) fluorescence (channel FL4, y axis) and green-yellow (phycoerythrin) fluorescence (channel FL3, x axis). Right: calcified and non-calcified nanoeukaryotes are discriminated based on their red (chlorophyll) fluorescence (channel FL4, y axis) and side-scattering (SS). NanoEuks: nanoeukaryotes; PicoEuks: picoeukaryotes; LowSS and HighSS: nanoeukaryotes displaying low and high side-scattering of light, respectively. Courtesy of F. Vincent and A. Vardi (Weizmann Institute, Israël)

4.2.3 Measurement of environmental (abiotic) parameters

a) Light intensity, air and water temperature

Light intensity and air temperature were obtained from the Ytrebygda weather station (<https://www.bergensveret.no/stasjon/?vis=download&id=18>) which measures those parameters every 10 minutes. In order to determine the influence of these parameters on the photosynthetic physiology, we used the value at 9 am (we measured photosynthetic physiology from 8 to 10). Water temperature was measured daily with a Conductivity Temperature Depth (CTD) device during sampling, between 8 and 10 am. The average of data points from depth 1-3 m was used. Data for all bags for day 14 of the campaign were missing. Some datapoints were removed because they were obviously outliers: bag 1, days 0, 4, 15; bag 7, day 15.

b) Chlorophyll *a* concentration

Seawater aliquots were filtered on glass fiber filters (GF/F), which were stored frozen at -20°C . After extraction with 90% acetone at 4°C in the dark for 24 hours, the chlorophyll *a* concentration in the extract was measured with a calibrated Turner Designs fluorometer.

c) Nutrient concentrations

Unfiltered seawater samples were stored in 15 mL acid-cleaned polyethylene tubes at -20°C until analysis. Concentrations of inorganic nutrients (nitrate, nitrite, ammonium, orthophosphate and silicate) were measured by continuous flow analysis with colorimetric detection using a SEAL ANALYTICAL autoanalyzer.

4.2.4 Photophysiology by Fast Induction and Relaxation fluorometry (FIRE)

Photosynthesis physiology was measured for each bag independently every day between 8 am and 10 am. The photosynthetic physiology was measured directly after sampling, the fluorometer being installed on the raft adjacent to the mesocosms. We used a miniFIRE (Miniaturized Fluorescence Induction and Relaxation System, Figure 4-2A). Our MiniFire was built by Maxim Gorbunov, from Paul Falkowski's laboratory (Department of Marine Sciences, Rutgers University, NJ, USA). MiniFIRE records fluorescence induced by a series of subsaturating flashes that cumulatively saturate PSII within 100-200 μs (Kolber et al. 1998). A background actinic light could be added (blue LED). A typical induction curve is presented in Figure 4-2B. MiniFIRE analysis program fits induction curve with a mathematical model that estimate 4 parameters:

- the initial fluorescence level in the conditions of interest (extrapolated at time 0). This level is called F' if measured in the presence of background light, and F_0 if measured on dark adapted sample,
- the maximal fluorescence yield at the end of the induction. It is called F_m or F_m' in dark adapted or illuminated samples, respectively
- the absorption cross section, σ_{II} , that depends on the kinetics of F_0 (or F') to F_m (or F_m') fluorescence rise. We only use this value from dark-adapted samples.
- the connectivity between PSII, p , that explains the shape of the induction curve (sigmoidal versus exponential).

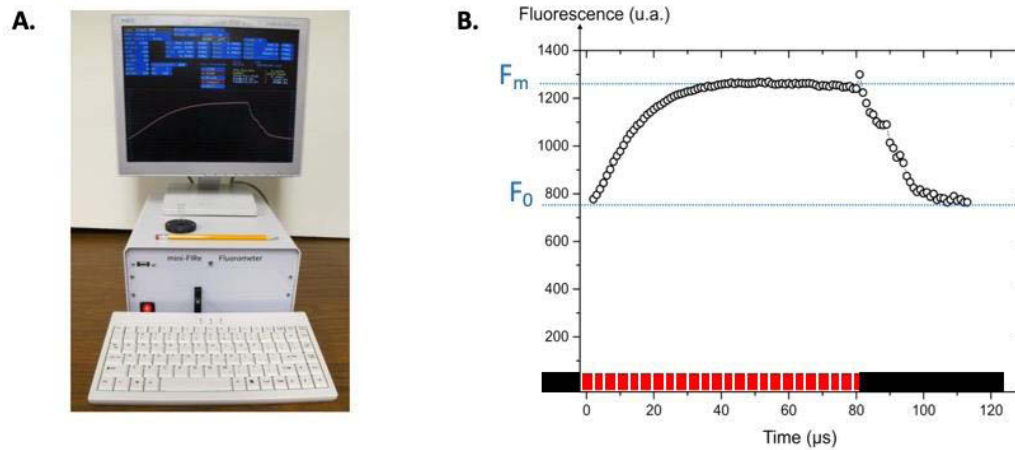


Figure 4-2: MiniFIRE is a hand luggage transportable device that measures chlorophyll fluorescence

A. Picture of a Miniaturized Fluorescence Induction and Relaxation System (miniFIRE); B. Typical fluorescence induction curve measured in a sample from bag 3 day 14 with a miniFIRE under the single turnover mode. F_0 and F_m correspond to fluorescence in dark-adapted sample and after a series of subsaturating flashes, respectively. Black and red horizontal bars correspond to darkness and series of subsaturating flashes, respectively.

The 4 parameters produced by the miniFIRE were automatically analyzed using a Matlab script. The maximum quantum yield of PSII was determined in dark adapted samples as the ratio $F_v/F_m = (F_m - F_0)/F_m$ (e.g. Butler 1972). The reference maximal fluorescence, F_m , the absorption cross section, σ_{II} , and the connectivity between PSII, p , were also assessed in dark adapted samples. The quantum yield of PSII in the light, $Y(II)$, was assessed thanks to Genty parameter calculation: $Y(II) = (F_m' - F')/F_m'$ (Genty et al. 1989). Electron transfer rate through PSII, $ETR(II)$, was calculated as the product: $ETR(II) = Y(II) \cdot \sigma_{II} \cdot I$ (where I is light irradiance). The magnitude of non-photochemical quenching was calculated from the light-induced decrease in the maximum fluorescence yield (F_m) and characterized by the NPQ parameter (Bilger and Björkman 1990): $NPQ = (F_m - F_m')/F_m'$. The contributions of high energy state quenching (q_E) and photoinhibition (q_I) to NPQ were estimated from the relaxation of F_m' for several minutes till a steady state was reached. NPQ relaxation was allowed under low light ($25 \mu\text{mol photons m}^{-2} \text{s}^{-1}$) because it was faster than in dark conditions (data not shown) and therefore allowed a better discrimination between q_E and q_I . State transitions were not considered since genes coding for the kinase involved in this process has not been found in other clades than the green lineage (Grouneva et al., 2013).

$ETR(II)$ was measured under 25, 50, 100, 200, 300, 400 and 500 $\mu\text{mol photons m}^{-2} \text{s}^{-1}$ (blue light). $ETR(II)$ vs I curves were fitted by an exponential function: $ETR(II) = ETR_{\text{max}} (1 - \exp(-I/E_k))$ (Platt et al, 1980) using non-linear least square method. Three parameters were estimated: the maximal electron transport rate, ETR_{max} , the light saturation parameter, E_k , and the initial slope, $\alpha = ETR_{\text{max}}/E_k$ (see Figure 4-3).

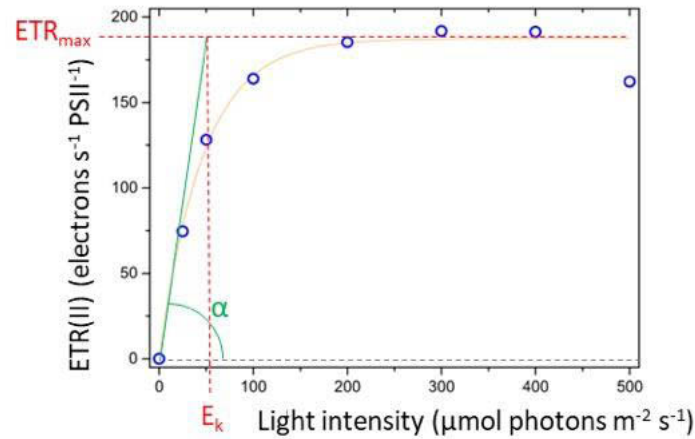


Figure 4-3: Three parameters are estimated out of the ETR(II) versus intensity curves

ETR(II) was measured under steady state at different light irradiances (blue points). Data was fitted by the exponential function: $ETR(II) = ETR_{max} * \exp(-I/E_k)$ (orange line) where ETR_{max} is the maximal PSII electron transfer rate when light is saturating, E_k is the light saturation parameter. In order to exclude light intensity that were much higher than the saturating light (for which the measurement noises are important), two consecutive fits were performed. The first one enabled a preliminary estimation of E_k from the whole dataset and the second one used only data below $3 * E_k$ intensities. ETR_{max} and E_k were taken from the second fit and the initial slope of the fitted curve was noted α and was calculated as $\alpha = ETR_{max} / E_k$. Data presented in this graph were measured on day 14 and on bag 3.

The complete measurement protocol for photosynthetic physiology assessment consisted of a first measurement right after sampling that measured the maximal fluorescence in situ, F_m' . A second fluorescence induction was performed after one minute of dark adaptation to estimate F_v/F_m in situ. Then, an incubation of 15 minutes at low light intensity (10 to $20 \mu\text{mol photons m}^{-2} \text{s}^{-1}$) allowed a relaxation of the mechanisms of dissipation of excess light in place in situ (q_E , fast reversible NPQ). The time required for this relaxation to be complete was tested daily around 10 am and never exceeded 10 minutes (data not shown). The samples were then subjected to a series of increasing light intensities and a fluorescence induction measurement was performed after acclimation to each light step. The time required for full acclimation to each light step was tested at the beginning of the experiment (and checked every day) and a measurement program was written specifically for our project by the miniFIRE designer, Max Gubernov (FPRO-ut for FIRE Programme - Utile Time) and was calibrated to ensure that steady state photosynthesis was reached at each light intensity.

4.2.5 Statistical analyses

All statistical analyses were performed using R version 3.5.2 in collaboration with Pascal Campagne, research engineer in the group STATS of the Institut Pasteur, Paris. He helped also in the preparation of the plots related to the statistical analyses.

a) RS: function repeatability

Variance observed in each photosynthetic and environmental variable was partitioned to assess the proportion of variance observed within each bag across days (RS, a repeatability score) and the proportion of variance ($1 - RS$) that could be attributed to differences among bags (within a day). Note that any arbitrary distribution of observations into groups (bags, days) results in a non-null amount of variance among groups, due to random sampling fluctuation. We used *ad hoc* functions (R package *heritability*) that correct for such a random noise so that effects due to contrasts across days only (*RS*) are properly estimated.

b) Correlation matrix

Pairwise Pearson's correlation coefficients were computed and plotted using both packages *psych* and *corrplot*. The corresponding *p* values were further adjusted to account for multiple testing using the Benjamini-Yekutieli procedure.

c) Between-Class Analysis (BCA)

Between-Class Analyses (BCA) were performed using the package *ade4*.

Principal Component Analysis (PCA) is a mathematical algorithm that reduces the number of dimensions of a dataset while retaining most of its variation. It achieves this reduction by identifying directions, called principal components, along which the data variation is maximum. Samples can then be plotted, along those axes allowing a visual assessment of similarities and differences between samples and whether samples can be grouped together (Hotelling 1933; Abdi and Williams 2010). Here, based on a first PCA applied to a numerical matrix of variables, we applied a BCA that operates another set of rotations to maximize contrasts among previously defined groups. Instead of maximizing the projection of variance bound to individual observations such as done with a PCA, the BCA maximizes the projected variance of group barycentres.

d) Partial least square regression (PLS)

Partial Least Square regression is generally used to explain or predict a response variable Y as a function of a set of predictors (dependent variables, X). It is generally used (i) when the number of predictors is high as compared to the number of observations and (ii) when the predictors are intercorrelated (multicollinearity) as it is often the case in environmental variables. More usual statistical approaches such as the multiple regression may not estimate correctly variable coefficients when the predictors are multicollinear. Here we use PLS regression of type I (or PLS1), that is a mode of PLS regression where the response is univariate.

Instead of directly relating the Y variable to the predictors X , PLS regression makes use of latent variables (i.e., multivariate axes) to relate those. More precisely, PLS regression determines orthogonal components in the matrix X of predictors that maximize their correlation with the Y variable. The analysis then reconstitutes the regression coefficients of the original predictors based on their association with the multivariate components. It may therefore be interpreted in a similar manner to multiple regression: (i) a coefficient of determination R^2 represents the amount of variation in Y explained by X , (ii) the sign and values of the regression coefficients provide information on the effect of a predictor on the response variable. Note that predictors which are not well represented on the multivariate axes will tend to be characterized by coefficients close to 0.

We performed the PLS regression using the R package (pls). The optimal number of components used in the analysis was determined based on a cross validation procedure ("leave-one-out"): it estimates the number of components minimizing prediction error while avoiding over-fitting, an issue that may arise when the model fits too closely to specificities of a given sample. The significance of PLS regression coefficients was assessed with a standard Jackknife method (i.e., a re-sampling procedure close to Bootstrap) that is provided in the pls package: 95% confidence intervals were calculated to test whether the regression coefficients significantly differed from 0.

4.3 Results

Emiliana huxleyi is a model microalga for the study of the establishment and collapse of blooms, and especially for the virus-induced ending of blooms (Bidle and Vardi, 2011). As with all photosynthetic organisms, one of the determining parameters of its growth is the efficiency of its photosynthesis. The collapse of *Emiliana huxleyi*'s blooms is often attributed to infection of cells by its specific coccolithovirus, Ehv, and laboratory studies show that the infection may have an influence on photosynthetic physiology (Evans et al., 2006, Bidle et al. 2007, Gilg et al., 2016; Thamatrakoln et al., 2018). From lab experiments, we know that photosynthetic physiology is influenced by environmental parameters like light, nitrogen, iron, phosphorus or temperature (Loebl et al., 2010; Trimborn et al., 2007; Muggli et al., 1996; Paasche and Brubak, 1994; Feng et al., 2008). A particularity of *Emiliana huxleyi* is to be highly sensitive to pH, CO₂, and calcium since it possesses coccoliths, which are cell walls made of carbonate (Bach et al., 2013; Trimborn et al., 2007; Balch et al., 1992; Feng et al., 2008). The questions we addressed in this project were the following: can we identify the relative influence of each environmental parameters on *E. huxleyi* photosynthesis in the field? If so, can we “subtract” the effects of those abiotic parameters to highlight abnormalities? Can we relate those abnormalities to the more subtle influence of other factors like biotic interactions (allelopathy, viral infection)?

In order to tackle those issues, we used University of Bergen mesocosm facilities that are part of the Aquacoscum european network of mesocosms and that are particularly adapted for the study of *Emiliana huxleyi*. This biological station is located in the Raunefjorden, near Bergen (Figure 4-4A), a region where *Emiliana huxleyi* blooms sometimes naturally (Bratbak et al. 1993, Figure 4-4B). Previous experiences have shown that when adding nutrients in mesocosms during late spring (May or June) *Emiliana huxleyi* often blooms (Rochelle-Newall 2004; Martínez-Martínez 2006; Engel 2007; Vardi et al., 2012; Segovia 2017). During our campaign, we installed seven mesocosms filled with surrounding sea water and moored to a raft in the middle of the bay (Figure 4-4C) between May 24th and June 16th, 2018. Among these seven bags, three (bags 5, 6 and 7; Figure 4-4E) were covered with a plastic film to allow the collection of aerosols -fine particles suspended in the air, four remained uncovered (bags 1, 2, 3 and 4; Figure 4-4D). Nutrients were added on days 1 to 7 and 13 to 17 (see Methods).

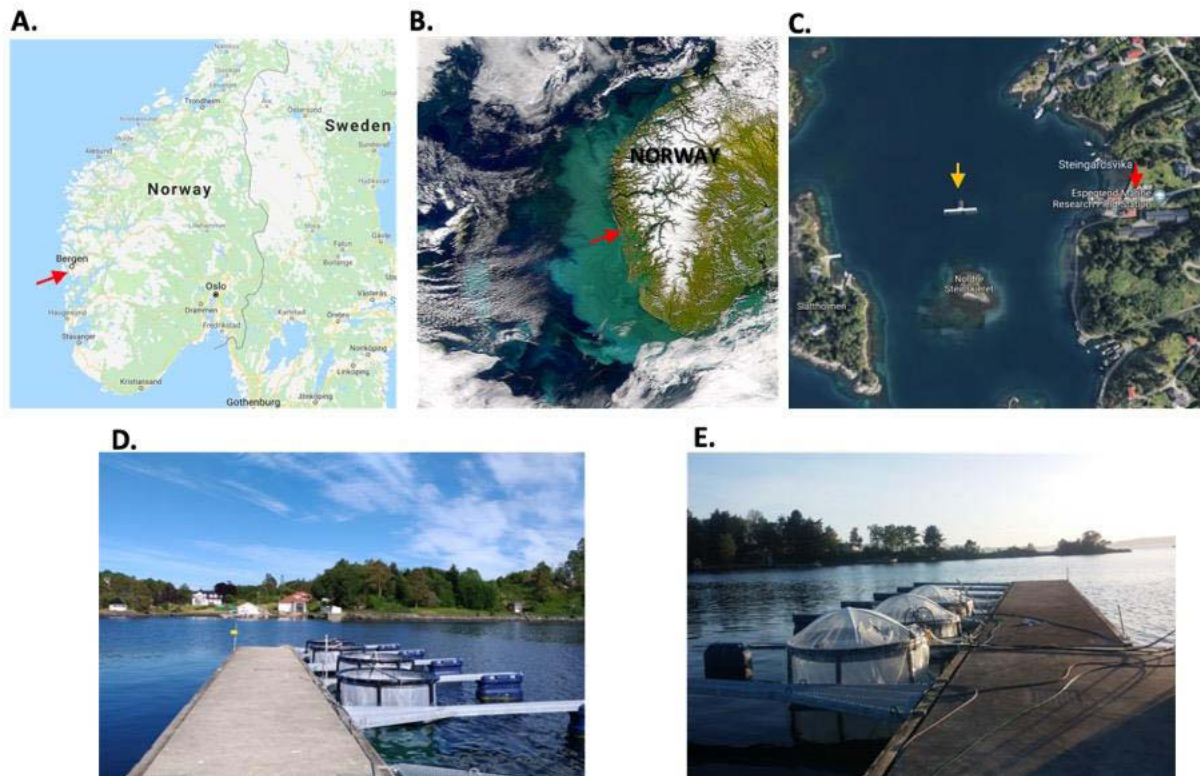


Figure 4-4: Location of the experiment and mesocosms setting

A. Map of Norway. Red arrow points to the location of the University of Bergen mesocosm center (Googlemaps).

B. *Emiliana huxleyi* is naturally blooming on the Norwegian coast nearby Bergen. Picture was taken from satellite. Red arrow points to the location the University of Bergen mesocosm center. Image provided by the SeaWiFS Project, NASA/Goddard Space Flight Center and GeoEye.

C. Satellite view of the Bergen's Marine Biological Station (Googlemaps). Yellow arrow points to the raft where the mesocosms were set and red arrow points to the laboratory.

D. and E. Set up consisted in four uncovered mesocosms (D.) and 3 covered ones with a polyethylene plastic sheeting (E.) (Courtesy of Vardi lab)

4.3.1 A two phases phytoplankton bloom occurred

During the course of the mesocosm, titration of chlorophyll *a* (chl *a*) in water by chemical measurement shows an increase by at least 15000 fold in two phases: a first rise from day 0 to day 9 and a second one from 14 to day 19 indicating that photosynthetic organisms have developed (Figure 4-5A). Those two rises are correlated with nutrient addition periods: from day 0 to 7 and from day 13 to 17. The chl *a* concentration went as high as 20-25 $\mu\text{g/L}$ in most bags at the peak of the bloom. The concentration of chlorophyll then decreases from day 19 to the end of the campaign indicating a decrease of the concentration of photosynthetic organisms: this is the bloom demise. These measurements are well correlated with the in vivo maximum chlorophyll fluorescence data that we obtained (F_m , see Methods) (Figure 4-5B and C).

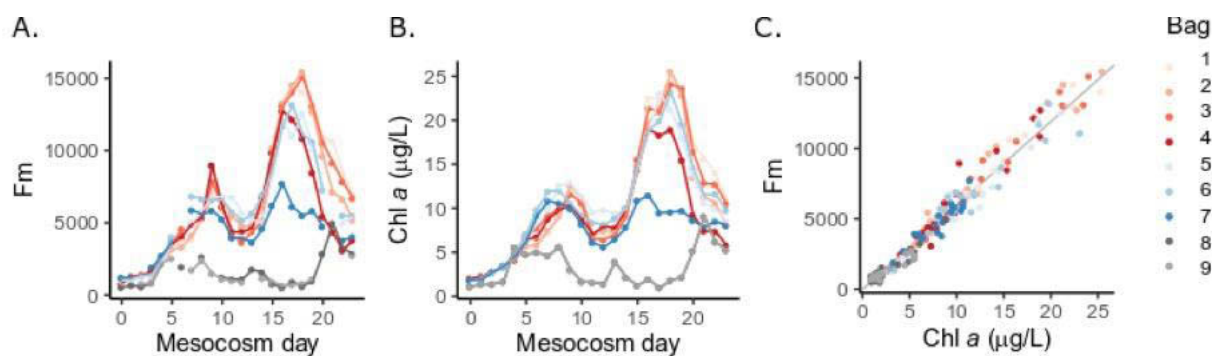


Figure 4-5: Estimation of the chlorophyll concentration in the mesocosms water along the campaign

A. Maximal fluorescence, F_m , was measured in vivo each day of the campaign; B. Evolution of chlorophyll *a* concentration along the campaign (Marrasé and Simó, see methods). C. Correlation between maximal fluorescence, F_m , and chlorophyll *a* concentration in the water. Grey line corresponds to the linear fit of the data (correlation coefficient = 0.96). Colors of each points and curves correspond to samples from different bags (see right hand side): bags 1 to 4 were uncovered, bags 5 to 7 were covered by a polyethylene plastic sheeting and bags 8 and 9 refer to sampling directly in the open water. In the panel A, the light and dark grey points correspond to 2 independent measurements on the control sample (open water), before and after the measurements of all the bags, respectively.

The structure of the populations of microorganisms present in the mesocosms as well as their dynamics of growth could be followed more precisely thanks to flow cytometry. Here, phytoplankton was divided into three classes, nanoeucaryotes (Neuks) that display high chlorophyll signal, picoeucaryotes (Peuks) cells that show lower chlorophyll signal and a group corresponding to the cyanobacterium *Synechococcus* that is easily distinguishable by its high phycoerythrin content and was by far the most abundant cyanobacterium (based on 16S, data not shown). Neuks have been divided into two subclasses: those that scatter the light in a particularly important way, they are called high side scattering nanoeukaryotes (Neuks HSS) while the the others, which scatter less the light are called low side scattering nanoeukaryotes (Neuks LSS) (see Methods for discrimination of populations). *Emiliana huxleyi* displays two life forms, a diploid calcified one which participates to the high-scattering population and a haploid non-calcified one which participates to the low scattering population (Frada et al., 2008; Green et al., 1996). The composition of the phytoplankton population was measured every day of the campaign and the results are presented in Figure 4-6. At day 0, the composition of the bags and the fjord are similar but from day 2, the populations diverge with a significant growth of phytoplankton in the mesocosms.

The evolution of the calcified *Emiliana huxleyi* population follows a similar evolution in all bags. Their concentration becomes detectable on day 9, after a lag phase. It then develops and reaches a peak of growth rate between days 14 and 17 (almost a doubling per day) reaching a maximum concentration of 4 to $9 \cdot 10^4$ cells per mL for bags 1 to 6. Note nevertheless

that the maximum growth phase is not observed in the bag 7 and that the maximum concentration reached in the bag 4 is lower than those reached in the other uncovered replicates. From day 18 to the end of the campaign, the population collapses. Waves of demise and growths are observed on flow cytometry data but could be due to artifacts (Flora Vincent, Assaf Vardi, personal communication). Indeed, those waves are not detected in chlorophyll or F_m measurements. It is important to note that from day 10 to the end of the campaign, the phytoplankton population was dominated by nanoeukaryotes in terms of biomass volume.

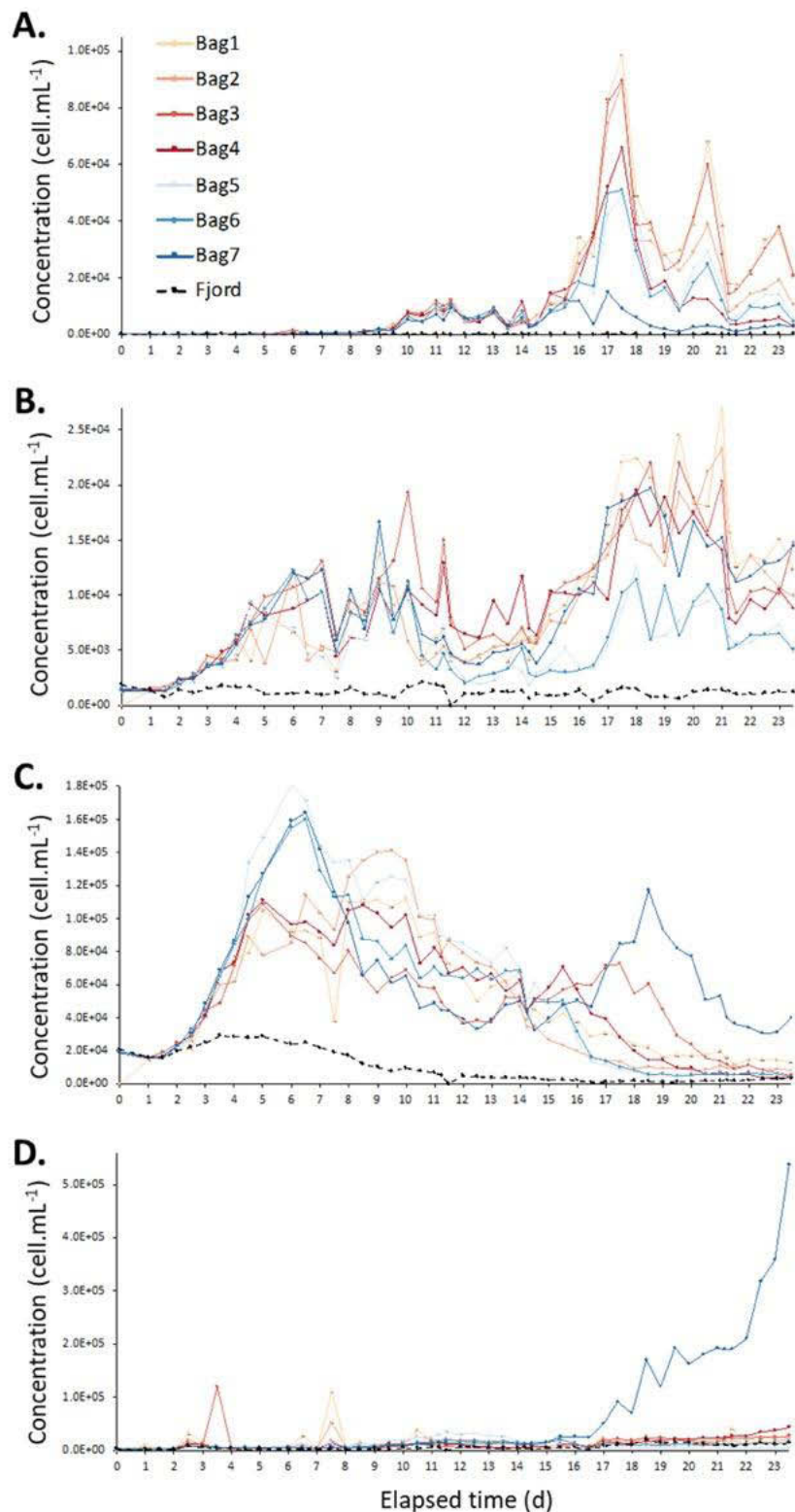


Figure 4-6: Evolution of the concentration of the different groups of phytoplankton from day 0 to day 24 of the campaign

A. High side scattering nanoeukaryotes, B. Low side scattering nanoeukaryotes, C. Picoeukaryotes, D. Synechococcus. Colors of curves and data points correspond to distinct bags: bags 1 to 4 were uncovered, bags 5 to 7 were covered by a polyethylene plastic sheeting and fjord refers to sampling directly in the open water. (Vincent and Vardi, personal communication)

4.3.2 Photosynthetic physiology

a) Nine parameters to describe photosynthesis

One of the main objectives of our study was to evaluate the effect of abiotic environmental parameters on the photosynthetic physiology of microalgae (hoping that the population would be dominated by *Emiliana huxleyi*). One of the major constraints in the field is the fact that the environmental parameters, and in particular those having a circadian rhythm such as the light intensity and the temperature, vary rapidly over time. In order to minimize the drift between bags, we have developed a protocol to collect as much information as possible in the shortest possible time, i.e. not more than 2 hours between the first and the last measurement. We controlled that the photosynthetic parameters were not changing significantly during those 2 hours by measuring the photosynthetic physiology of samples from open water (water sampled from the fjord, outside the bags) at the beginning and the end of the set of measurements. The photosynthetic parameters were similar for the two measurements (see one example for F_m in Figure 4-8A) indicating that the physiology was quite constant during the two hours of measurement.

In order to measure physiology in situ, we installed our fluorometer directly on the raft, which allowed the first measurement to be performed ~ 10 s after sampling. The principle of our protocol is based on three steps.

First, we measured photosynthetic parameters in situ, just after sampling:

- The maximum efficiency of the PSII, in situ F_v/F_m (Figure 4-8H). In situ F_v/F_m is clearly lower in bags 1 to 4 than in bags 5 to 7 for days 9 to 14. These days were marked by a particularly high intensity of light and follow the stop of nutrient addition (Figure 4-8C).
- The in situ NPQ, mechanism of dissipation of excess light energy in the form of heat, that is occurring in situ and that is reversible in the minute time scale, (Figure 4-8I).

Then, after a relaxation period under low light to dissipate any fast reversible photoprotection mechanisms, we measured dark-adapted PSII parameters. We have initially tested that a low light incubation for 15 min was sufficient, whatever the intensity of light in situ (data not shown). We measured:

- The PSII maximal efficiency, F_v/F_m , i.e. its capacity to use light energy to perform photochemistry when the photosystem II is open (Figure 4-8A),
- The PSII absorption cross section, σ_{II} , which provides information on the ability of PSII to capture light energy (Figure 4-8B)

- And the connectivity, p , which characterizes the probability of exciton transfer between a closed PSII and an open adjacent PSII (Figure 4-8C).

Finally, four parameters tell us about the overall photosynthesis efficiency. The measurement of fluorescence induction on cells subjected to different light intensities allowed to draw a photosynthesis vs intensity curve (see Material and methods, Figure 4-3). This curve provides three parameters informing about the characteristics of the whole photosynthetic chain:

- The maximum rate of photosynthesis, ETR_{max} (Figure 4-8D) gives information on the rate of the (non-photochemical) limiting step (i.e. in general the cytochrome b_6/f electron transfer or the Calvin Benson Bassham cycle).
- A second parameter is the characteristic saturation intensity of photosynthesis, E_k (Figure 4-8E) which gives information on the optimal intensity of operation of the photosynthetic chain.
- Thirdly, the α parameter (Figure 4-8F) measured as the initial slope of the photosynthesis versus intensity curve, informs about the efficiency of photosynthesis under low light.

A last parameter concerns the capacity of the chain to set up mechanisms for the dissipation of light energy in the form of heat, NPQ (Figure 4-8G). The level of NPQ depends on the light irradiance in a non-linear manner; here, we used the amplitude of the NPQ at the maximum intensity tested ($500 \mu\text{mol photons m}^{-2} \text{s}^{-1}$). The daily measurement of the relaxation of this NPQ under low light intensity on pooled samples from bags 1 to 4 made it possible to demonstrate that the measured NPQ was mainly reversible after 2-3 minutes of low light (Figure 4-7). It can therefore be attributed to regulative mechanisms (q_E) and not to photoinhibition of PSII (q_I).

This protocol was carried out every day of the campaign.

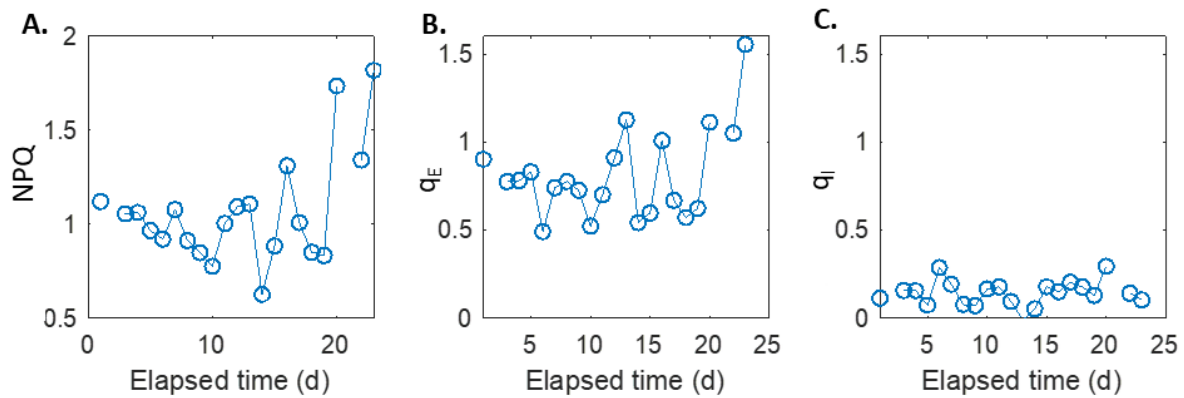


Figure 4-7: Measurement of Non Photochemical quenching (NPQ) measured in steady state at 500 $\mu\text{mol photons m}^{-2} \text{s}^{-1}$. (A) and its reversible (q_E , fully reversed in 2-3 minutes) and irreversible (q_I) components (B and C, respectively)

Measurements were performed around 10.30 am on a sample pooled from bags 1 to 4. Non photochemical quenching, NPQ, was measured under steady state at 500 $\mu\text{mol photons m}^{-2} \text{s}^{-1}$ each day of the campaign (A). NPQ relaxation was monitored until reaching a pseudo steady state (from 1 to 5 minutes of relaxation) and the reversible NPQ was noted q_E (B) while the remaining NPQ was noted q_I (C).

b) Evolution of photosynthetic physiology during the experiment

One first observation (Figure 4-8) is that photosynthetic physiology changes over the course of the mesocosm. The maximum variation factor ranges from 0.3 for the σ_{II} to 10 for the ETR_{max} . And there is no clear phenotype related to the phases of the phytoplankton bloom. We hypothesized that environmental parameters play a role in photosynthetic physiology but how to evaluate the contributions of environmental parameters and stochastic effects on the variation of the photosynthetic parameters?

By a statistical approach, we can assess the relative contribution to the variance of the photosynthetic parameters due to environmental parameters (which should be the same for all bags) and the variability between bags (which reflect technical noise, bias in the bag filling at day 0, stochastic effects). The fraction of common variability between the bags (repeatability score) estimates the amount of variability between days in the total variability of photosynthetic physiology. Overall, it appears that much of the variability in photosynthetic physiology is explained by external control (environmental parameters) as evidenced by high RS values (greater than 0.6 for all except in situ parameters and α , up to at 0.86 for ETR_{max}). In situ data have lower RS. We can propose two explanations: covered bags received slightly less light than open bags because of the plastic cover covering them, causing different light stress. Secondly, we have to highlight that those measurements were subjected to more technical

noise since the measurement was done "as quickly as possible after sampling" which does not exclude differences depending on the efficiency of the sampler.

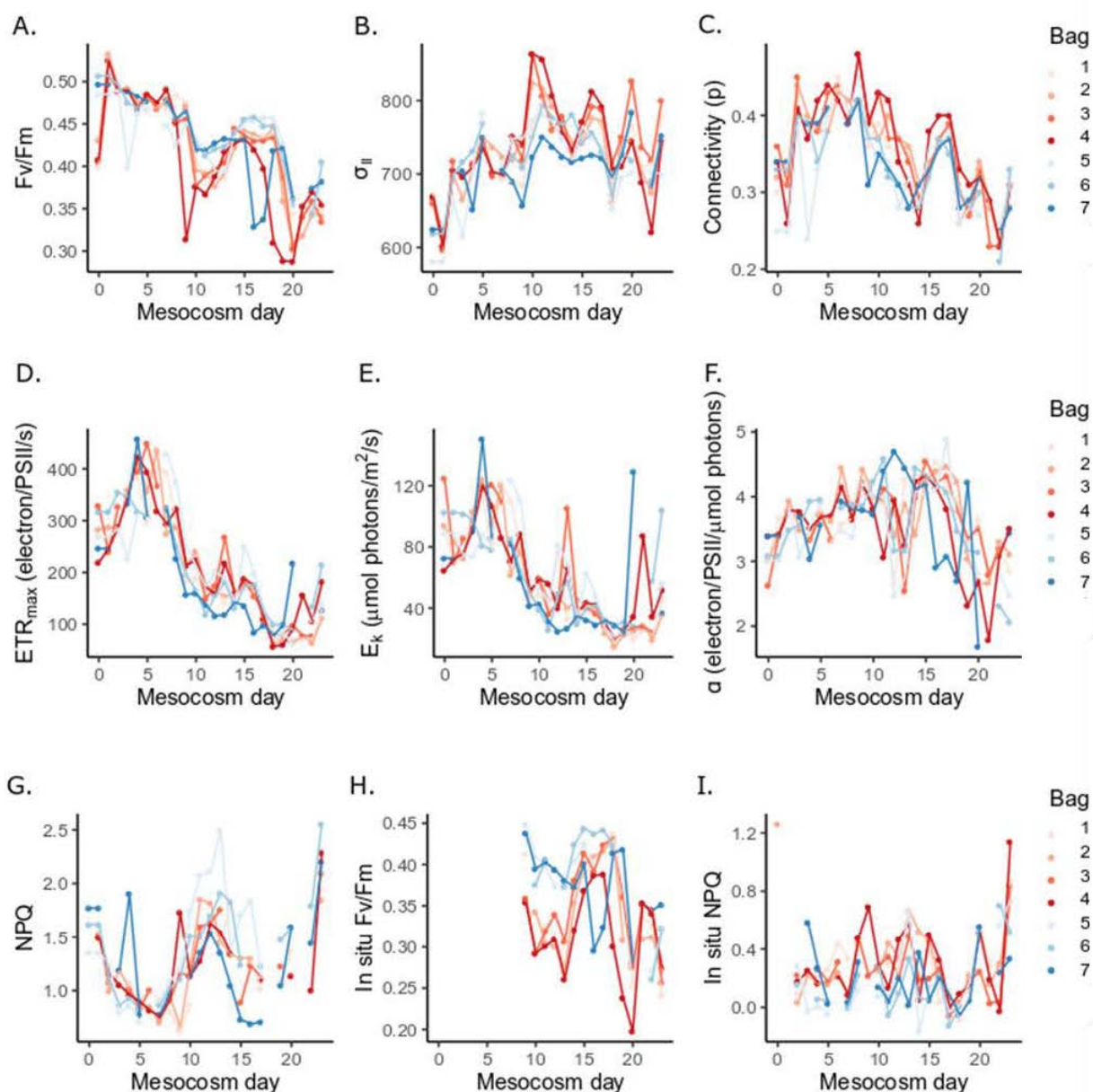


Figure 4-8: Evolution of fluorescence parameters indicative of photosynthetic physiology from day 0 to day 23 of the campaign

Each day of the campaign, 9 parameters were estimated from fluorescence measurement data: the maximal PSII quantum yield, F_v/F_m (A), the absorption cross section, σ_{II} (B), the connectivity between PSII (C), the maximal PSII electron transfer rate, ETR_{max} (D), the light saturation parameter, E_k (E), the initial slope of the photosynthesis versus intensity curve, α (F), the non-photochemical quenching, NPQ (G), the maximal PSII quantum yield measured directly after sampling, In situ F_v/F_m (H) and the non-photochemical quenching in place in the bags (before sampling), In situ NPQ (I). The repeatability score, RS, that is the fraction of common variability between the bags was estimated for all variables. For F_v/F_m , σ_{II} , and p , RS values are 0.707, 0.712 and 0.77, respectively. For ETR_{max} , E_k and α , RS values are 0.864, 0.695 and 0.474, respectively. For NPQ, in situ F_v/F_m and in situ NPQ, RS values are 0.626, 0.485 and 0.551, respectively. Bags 1 to 4 were uncovered, bags 5 to 7 were covered by a polyethylene plastic sheeting.

In order to describe the evolution of the photosynthetic parameters in a more global way, and to highlight possible correlation between them, we carried out a between class analyses (BCA), a variant of principal component analysis. Figure 4-9B shows the correlation circle of the variables obtained with the BCA. The understanding of the mathematical detail to obtain a BCA is complex but the interpretation of the results is quite simple: the positively correlated variables are group together and negatively correlated variables are positioned on opposite sides of the chart origin (opposite quadrants). Finally, the distance between the variables and the origin measures the quality of representation of the variables: variables that are far from origin are well represented by the BCA (Abdi and Williams 2010).

Here, the BCA explains more than 77% of the variance with two axes, which means that little variance is not represented by these two axes. Figure 4-9B shows an anti-correlation between parameters measuring photosynthetic efficiency, e.g. ETR_{max} or F_v/F_m , and NPQ measured at $500 \mu\text{mol photons m}^{-2} \text{s}^{-1}$, indicating a saturation of the photosynthetic chain. Moreover, in situ F_v/F_m and in situ NPQ are highly anticorrelated and this is expectable: in the PSII antenna, the light energy dissipation pathways by photochemistry (measured by F_v/F_m) and by heat (estimated by the NPQ) are in competition. It therefore seems coherent that when one increases, the other decreases. The anticorrelation between ETR_{max} and σ_{II} can be discussed by invoking mechanisms of acclimation. High ETR_{max} and low antenna size can be mechanisms of acclimation to high light intensity.

Now, can we highlight a trend in the changes of photosynthetic physiology during the experiment? Figure 4-9A presents the projection of photosynthetic parameters on the axes of the BCA day after day. We can highlight 3 successive phases in the evolution of the photosynthetic parameters. Days 0, 1 and 2 show a transition in the direction of an increase in ETR_{max} , E_k and a decrease in NPQ and in situ NPQ highlighting an increase of photosynthesis efficiency that might be attributed to the acclimation to the nutrient depleted conditions. From day 2 to day 8, the parameters remain relatively stable and correlated with a strong ETR_{max} , F_v/F_m , in situ F_v/F_m and a low NPQ. The third phase, from day 10 to day 23, shows globally a decrease in ETR_{max} , F_v/F_m and an increase in NPQ. These last two phases correspond to the pre-bloom and bloom phases of *Emiliana huxleyi* defined based on flow cytometry data. We can hypothesize that the microalgae species that developed before *Emiliana huxleyi* (mainly nanoeukaryotes) had greater photosynthetic efficiency than the latter.

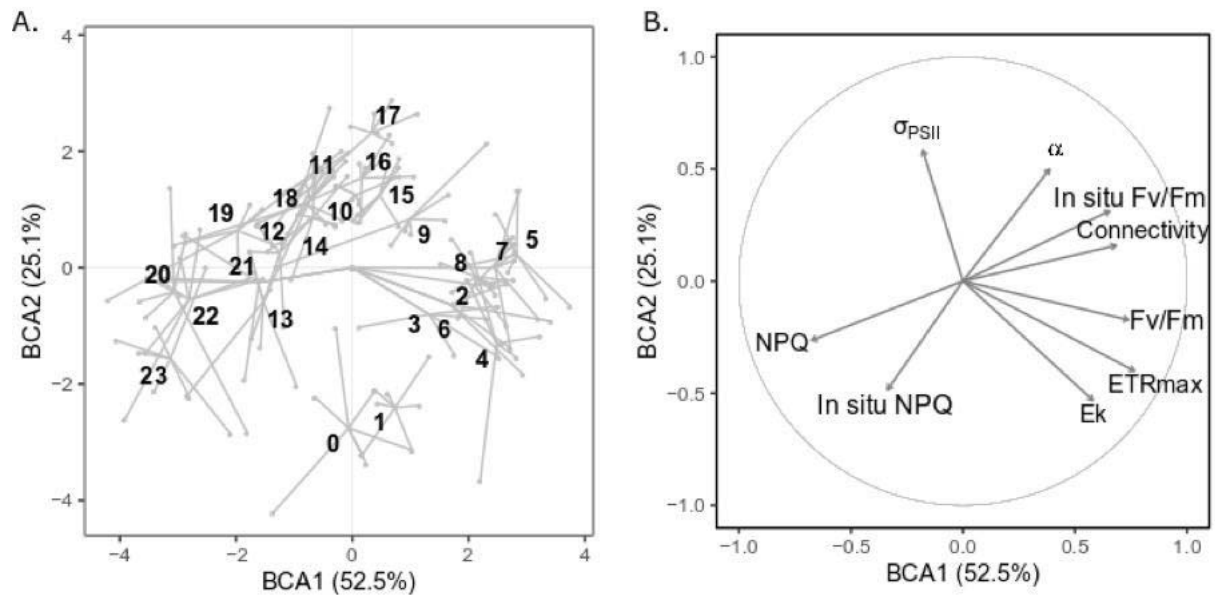


Figure 4-9: Between Class Analysis (BCA) on the photosynthetic parameters

BCA analysis was performed on the photosynthetic dataset from the whole campaign. A. For each day of the campaign, the barycenter of the 7 bags was projected on the plan made of the two first axes of the BCA (BCA1 and BCA2) and is denoted by a number (the mesocosm day). Data from each bag has also been projected on the plan and are represented by a grey point connected to the barycenter with a grey line. B. correlation circle of the photosynthetic parameters. Variables whose arrows are close to the correlation circle of radius 1 tend to be fully represented on the two first axes.

4.3.3 Fluorescence signals were mainly due to *Emiliana huxleyi* from day 9 to 24th of the experiment

We could show that the evolution of photosynthetic physiology was similar between the bags, which raises the question of the cause of these changes. Is it due to changes in abiotic parameters or does it reflect a succession of phytoplankton populations with different physiological characteristics? When measuring chlorophyll fluorescence in a mixture, a major constraint is that we measure the signal emitted by many species. Which phytoplankton group is the main fluorescence emitter? Here we have evidence showing that fluorescence signals are mainly emitted by nanoeukaryotes, and principally from *Emiliana huxleyi* from day 9 of the campaign. The maximum fluorescence, F_m , measured in a sample depends on the number of photosynthetic cells. If only one phytoplankton group is involved in the fluorescence emission, then F_m will be well correlated the concentration of this group. Figure 4-10A shows that the maximum fluorescence, F_m , measured in the samples is well correlated with the concentration of nanoeukaryotes (coefficient of correlation, R^2 , of 0.84) and cannot be correlated with the concentration of picoeukaryotes ($R^2 = 0$) or with *Synechococcus* ($R^2 =$

0.23). It is to note here that, given the low concentrations of cells (less than 10^5 cells per mL, see Figure 4-10), the reabsorption of fluorescence by neighboring cells is negligible.

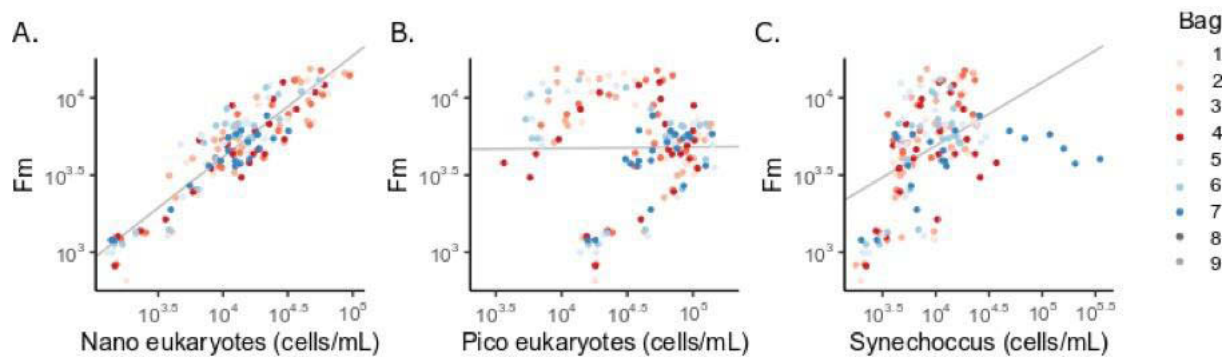


Figure 4-10: Maximal fluorescence, F_m , as a function of the concentration of nanoeukaryotes (A), picoeukaryotes (B) and *Synechococcus* cells (C)

Each datapoint corresponds to one bag (color code on the right) and one day of the campaign. The relation was fitted by a linear function (grey line) and the correlation coefficient was 0.84, 0 and 0.23 for F_m as a function of Neuks, Peuks and *Synechococcus*, respectively.

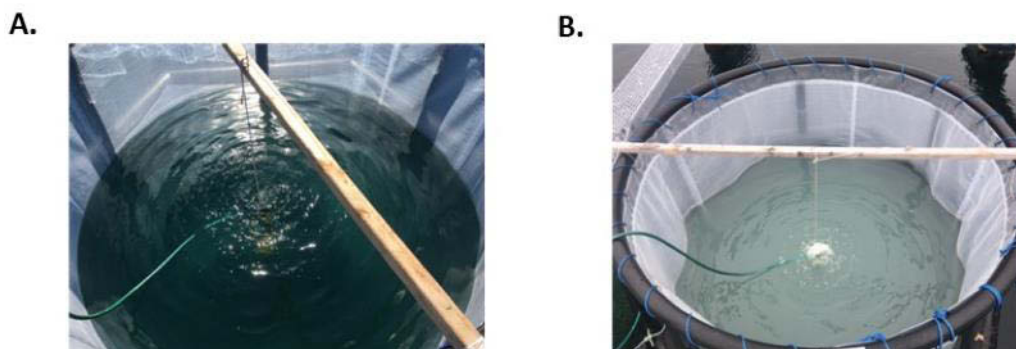


Figure 4-11: Comparison of the water color between day 0 (A) and day 21 of the campaign (B) for the bag 3. Pictures were taken from the top of the bag. Courtesy of Vardi lab.

But we can go even further and demonstrate that during the bloom, the photosynthetic signals were mainly emitted by *Emiliana huxleyi*. Firstly, the water turbidity observed with the naked eye. During the campaign, the water contained in the mesocosms took a milky appearance (Figure 4-11), which became obvious from day 10, indicating the development of microorganisms having the property of diffusing the light as it is the case for *Emiliana huxleyi* of which the calcic shell deviates the trajectory of the luminous rays. Secondly, electron microscopy data on samples from the peak of the bloom, most of the cells were *Emiliana huxleyi*, easily recognizable by the shape of its wall composed of calcitic coccoliths (Figure 4-12).

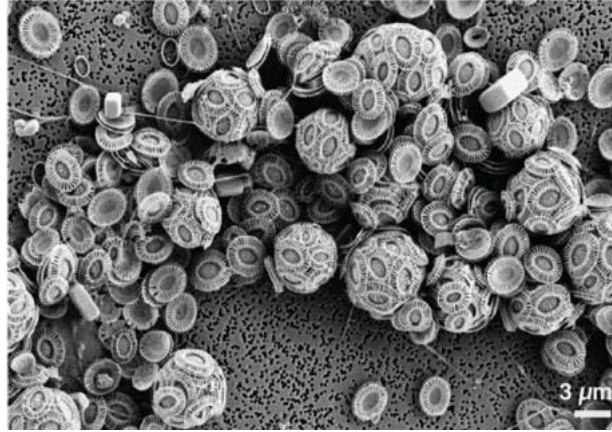


Figure 4-12: Electron microscopy observation of a sample harvested in bag 4, day 16 of the campaign
Courtesy of Vardi lab

Finally, the measurement of the fluorescence signals measured on filtrates of the bags makes it possible to affirm that we mainly measured the fluorescence signals of *E. huxleyi* from day 9 marking the beginning of the bloom. We regularly filtered the water samples on a 3 μm polycarbonate filter in order to separate the cells smaller than 3 μm (in theory mainly the picoeukaryotes and *Synechococcus*) and the cells larger than 3 μm (in theory mainly nanoeukaryotes including *E. huxleyi*). We then measured the maximum fluorescence in the initial sample and in the fraction greater than 3 μm and calculated a percentage of the signal emitted by the fraction greater than 3 μm (Figure 4-13A). From day 9, the signal emitted by this fraction is greater than 60% and reaches 90% of the signal between days 15 and 21. We also estimated the composition of the population in the fraction higher than 3 μm by flow cytometry and it shows that from day 15, the Neuks HSS (most probably *E. huxleyi*) dominate the fraction higher than 3 μm. It should also be noted that this estimation is probably an underestimation for two reasons. First, a fraction of the low scattering nanoeukaryotes may be non-calcified *E. huxleyi*, and some *E. huxleyi* cells have been found in the fraction less than 3 μm (some cells might be also lost on the filter). A more complete view of the contribution of *E. huxleyi* will be available soon (sequencing of ribosomal genes and analysis of photosynthetic pigments from our samples are planned). In the following, we will therefore assume that the fluorescence signals measured from to the end day 9 mainly informs mostly the photosynthetic physiology of *Emiliana huxleyi*.

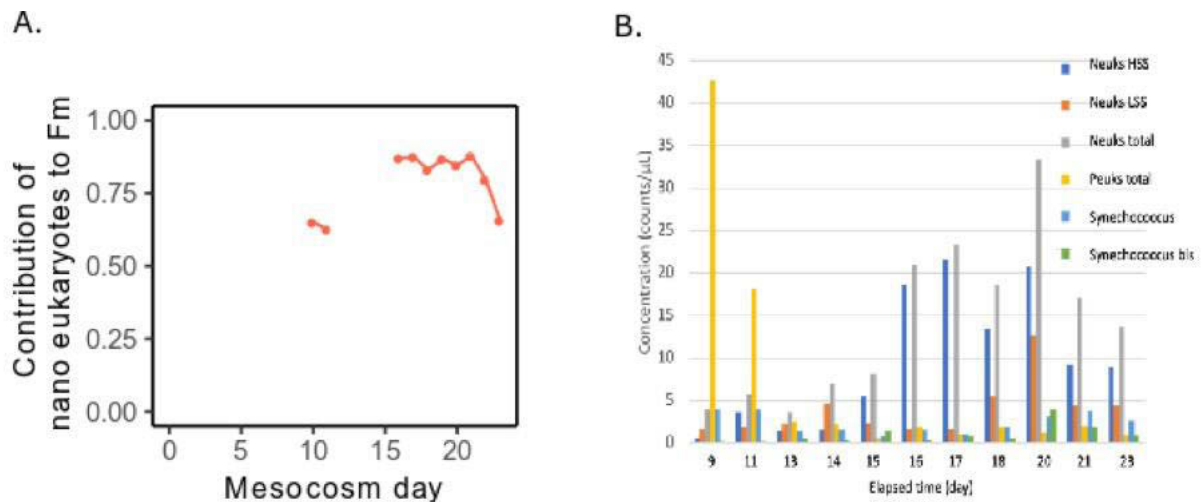


Figure 4-13: Estimation of the fraction of the fluorescence signal emitted by *Emiliana huxleyi*

From day 9 of the campaign, a sample pooled from bags 1 to 4 was filtrated on a 3 μ m filter and the retentate was resuspended in the same volume of sea water filtrated on a 22 μ m. A. The maximal fluorescence emitted by the retentate (> 3 μ m fraction) is expressed as a proportion of the maximal fluorescence emitted by the initial sample (before filtration). B. The relative abundance of the 4 groups of phytoplankton was measured by flow cytometry in the retentate (> 3 μ m fraction) (color code of the species on the right).

Analysis of panel B was performed by F. Vincent and A. Vardi.

4.3.4 Evolution of environmental parameters during the experiment

We have shown above that the variation of photosynthetic physiology appeared mainly due to environmental and / or population evolution parameters. The signals being mainly emitted by the nanoeukaryotes and mainly coming from *Emiliana huxleyi* from day 9 indicates that physiology is rather dictated by the environmental parameters.

Here we made the initial bet that abiotic factors would be the most important. Is that the case? What are the most important parameters? The principle of our approach is based on statistical model design explaining the variance of photosynthetic physiology using environmental parameters. In order to optimize our model, we used all the available environmental parameters that are known to influence the photosynthetic physiology in the laboratory: the temperature of air and water, the concentration of nutrients in their most abundant dissolved form such as nitrogen (NO_3^- , NO_2^- , NH_4^+) phosphorus (PO_4^{3-}) and silica (SiO_4^{4-}) and the light intensity at the time of measurement. The evolution of these parameters over time are presented in Figure 4-14.

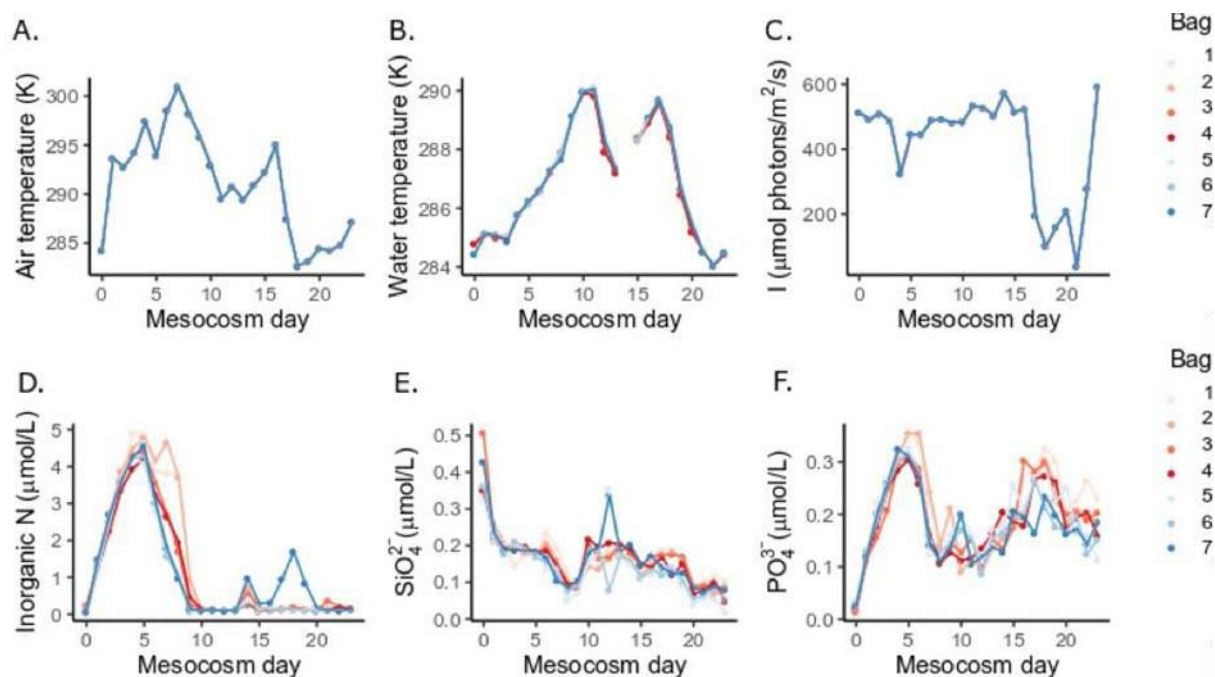


Figure 4-14: Evolution of abiotic parameters as a function of time

A. and B. air and water temperature, respectively, C. Light intensity at 9 am, D. concentration of dissolved inorganic nitrogen (i.e. NO_3^- and NO_2^-), E. concentration of dissolved silicate (SiO_4^{4-}) and F. concentration of dissolved phosphorous (PO_4^{3-}). A. and C. data come from Ytrebygda weather station (see material and methods), B. were obtained from Schleyer, Egge and Vardi and D. to F. were obtained from Marrasé and Simó. Color codes of the bags shown on the right-hand side. The repeatability score, RS, which is the fraction of common variability between the bags was estimated for each parameter. RS values are 1 for air temperature and light intensity because those are the only two parameters which were not individually measured for each bag. RS values are 0.998, 0.928, 0.806 and 0.839 for water temperature, inorganic nitrogen, SiO_4^{4-} , and PO_4^{3-} , respectively.

We performed the same BCA analysis used for photosynthetic parameters, on the environmental parameters. The first two dimensions resume about 65% of the total variance of the dataset meaning that most of the variations are represented by these two axes. Some variables are partially correlated as it is the case for air temperature and inorganic nitrogen (mostly due to the increase of air temperature during the period of nutrient enrichment from day 0 to day 5), air temperature and light intensity (mostly due to cloudy and cold days from day 17 to 22) or dissolved inorganic nitrogen and phosphorus (mostly because they were added in a joint way from day 0 to day 7). Without surprise, the temperature of the air and water seem to be only slightly correlated. Right panel of Figure 4-15 shows that the temperature of the water follows the evolutions of the temperature of the air with a delay of 3 days. This is easily explained by the high thermal capacity of a 10 000 L water body: it takes time to heat up such a volume.

Left panel of Figure 4-15 shows the projection of environmental data day by day on the axes of the BCA. Several phases can be described: the evolution from day 0 to day 4-5 mostly

reflects the fact that inorganic nitrogen and phosphorous are increasing due to enrichment; from day 4-5 to 10, the evolution reflects mostly the decrease of inorganic nitrogen and phosphorous. From day 10 to 16, environmental parameters are rather stable. The evolution from day 16 to 21 indicate mostly that air temperature, water temperature and light decrease; finally, from day 21 to 23, the same parameters increase again.

It can be noted that several non-consecutive days cluster together (indicating that they are characterized by similar environmental parameters): days 1, 8, 14, 16; days 0, 10, 11, 12; days 9, 13 and 15 and days 17, 22, 23. These observations will be important for the robustness of the statistical model. Indeed, if the environmental parameters actually determine the photosynthetic physiology, then these days should have similar phenotypes.

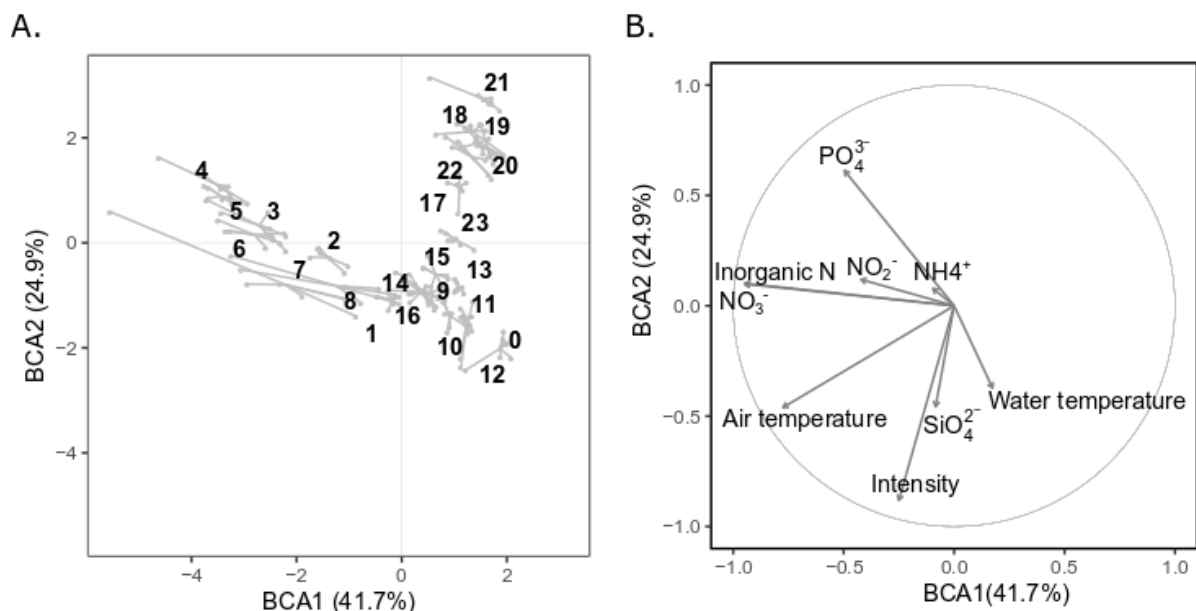


Figure 4-15: Between Class Analysis (BCA) on environmental parameters

BCA analysis was performed on the environmental parameters dataset from the whole campaign. A. For each day of the campaign, the barycenter of the 7 bags was projected on the plan made of the two first axes of the BCA (BCA1 and BCA2) and is denoted by a number. Data from each bag has also been projected on the plan and are represented by a grey point connected to the barycenter with a grey line. B. correlation circle of the environmental parameters. Variables whose arrows are close to the correlation circle of radius 1 tend to be fully represented on the two first axes.

4.3.5 Environmental determinants of *E. huxleyi* photosynthesis

a) Pairwise correlations

How to highlight correlations between environmental variables, taxonomic distributions and photosynthetic physiology parameters? The simplest approach that I initially applied is to test for pairwise correlations between all those parameters. Correlation matrix is presented in

Figure 4-16 where the correlation coefficient is indicated by a color from dark red (-1) to dark blue (+1). The level of significance is represented by the size of the disk and the crosses indicate non-significant correlations. Strong correlations can be highlighted such as between air temperature and F_v/F_m , ETR_{max} and connectivity or between inorganic nitrogen concentration and F_v/F_m , ETR_{max} , E_k and NPQ. The in situ F_v/F_m and in situ NPQ are strongly anti-correlated, which makes sense: the development of heat dissipation mechanisms in PSII should decrease its maximal efficiency. However, this type of approach seems limited since only pairwise correlations are tested and this could not highlight correlations if a photosynthetic variable depends on several environmental factors. To illustrate this, air temperature and light intensity are positively correlated, which is just a random effect (cloudy days from day 16 to 21 were also cold days). Then, is the positive correlation between ETR_{max} and light irradiance meaningful, or just an artifact due to the random correlation between air temperature and light irradiance?

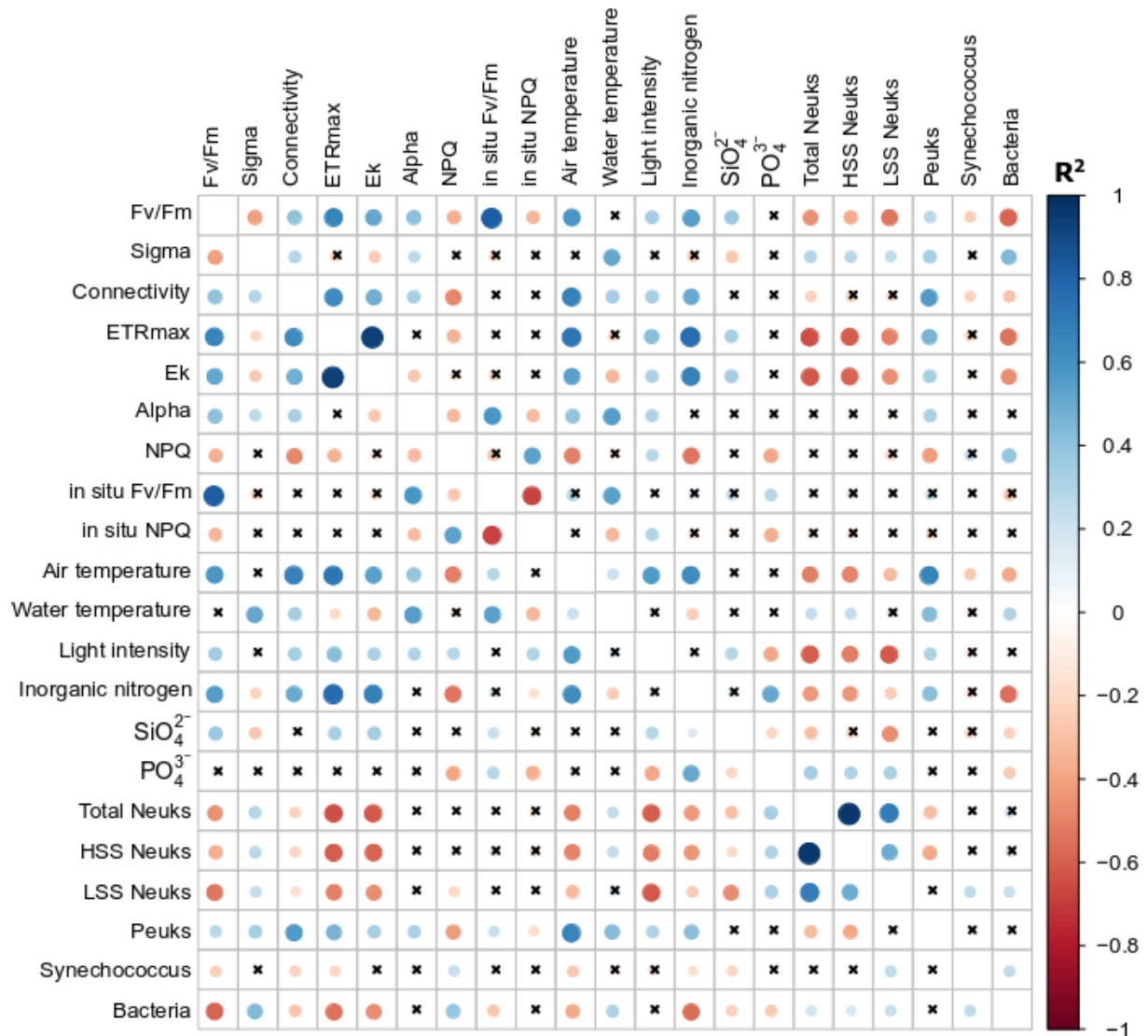


Figure 4-16: Correlation matrix containing photosynthetic variables and abiotic environmental parameters
Data from all bags and all days of the campaign were used to calculate pairwise correlations. The correlation coefficient, R^2 , is presented as a color code (legend on the right). Crosses represent correlations that are not significant ($p < 0.5$).

b) Multivariate model

When several explanatory variables can be involved in the variations of a parameter, a multivariate approach is necessary. In order to understand better the mathematical concepts of this approach, I followed a multivariate modeling course organized by Agroparitech (National School of Agronomy) and the University of Paris Saclay and received a great support from Pascal Campagne, research engineer in the Institut Pasteur Institute (Paris), an expert in statistics applied to experimental results in biology. Because the explanatory variables of the model (i.e. the environmental parameters) are partially correlated, the regression-based approaches cannot be used (one of its fundamental hypotheses is the independence of the

explanatory variables). With the help of Pascal, we followed a different approach based on Partial Least Square (PLS) regression, which is generally used to explain or predict a response variable as a function of a set of predictors (dependent variables).

At first, we decided to focus our analyses on the three most descriptive parameters of the photosynthetic physiology: the maximum efficiency of PSII (F_v/F_m) which is an indicator of the “physiological state” of photosystem II, the maximum electron transfer rate of the photosynthetic chain (ETR_{max}) and the ability to set up mechanisms for the dissipation of excess light energy by heat dissipation (NPQ). The results of the PLS analysis are presented in Figure 4-17. For each environmental parameter, the amplitude of the bar represents the regression coefficient of this predictor. Negative, positive, and non-significant coefficients are colored in orange, blue, and grey, respectively. The analysis gave very satisfying outputs, the PLS models explaining a significant part of the variance of the photosynthetic parameters. For ETR_{max} , 2 orthogonal components in the environment parameters matrix explain 75% of the variance (Figure 4-17B). We have seen previously that ~14% of the ETR_{max} variance was due to noise and/or stochastic effects (calculated as 1-RS). This means that most of the remaining variance is “captured” by the 2 orthogonal components used. For F_v/F_m and NPQ, for which the contribution of stochastic effects and noise was higher (29 and 37% of the variance respectively), one component could still explain 47 and 37% of the variance, respectively.

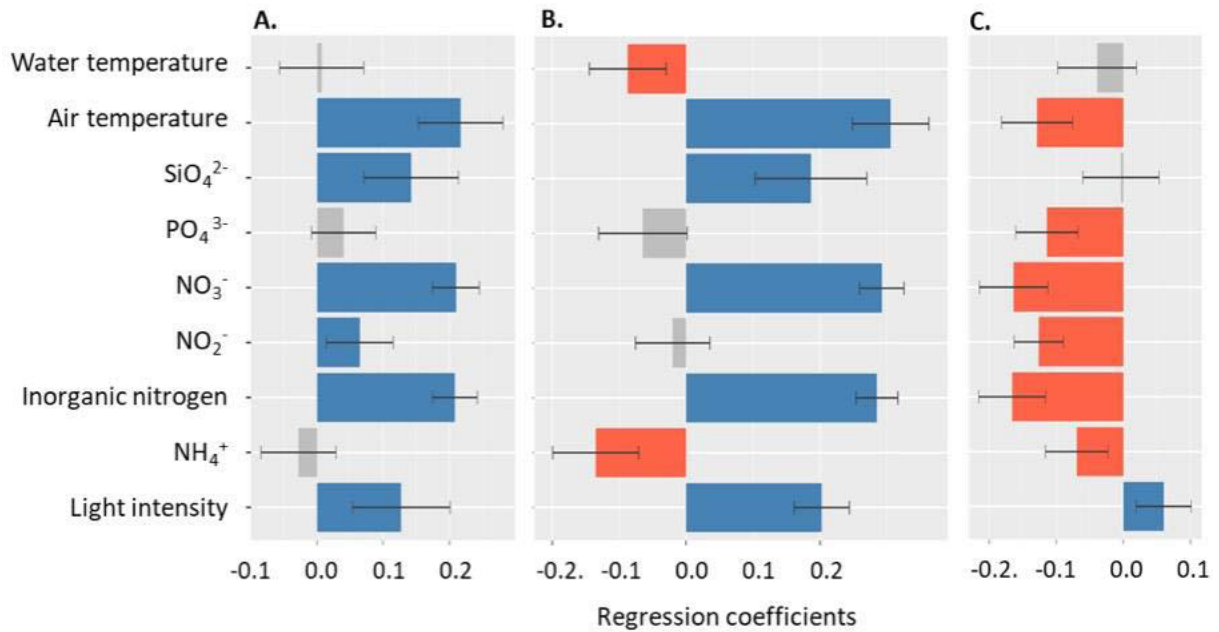


Figure 4-17: Contribution of environmental variables to the explanatory model for maximal PSII efficiency, F_v/F_m (A), maximal PSII electron transfer rate, ETR_{max} (B) and non-photochemical quenching, NPQ (C)

Partial least square analysis was performed on F_v/F_m , ETR_{max} and NPQ using 9 abiotic parameters (water and air temperature, SiO_4^{2-} , PO_4^{3-} , NO_3^- , NO_2^- , total inorganic nitrogen, NH_4^+ and light intensity). The percentage of the variance explained by the model is 75, 47 and 37% for F_v/F_m , ETR_{max} and NPQ, respectively. Value of the regression coefficients for each of the environmental variables are indicated in the horizontal axis. Error bars delimit 95% confidence intervals. In grey, blue and orange, the non-significant, positive and negative standardized coefficients, respectively.

Influence of nutrients on photosynthesis

The concentration of dissolved silica seems to be significantly correlated with F_v/F_m and ETR_{max} . This could be due to an artifact. The main variations of the silica concentration concerns a decrease during the first 3 days of the experiment (due to the development of diatoms in the samples seen by flow cam data, not shown), and is concomitant with an increase of F_v/F_m and ETR_{max} that might be related to the initial addition of nutrients.

Four parameters related to N availability are used in the model. The two most significant ones are the total dissolved inorganic nitrogen and nitrate concentration, whereas nitrite and ammonium show less clear behaviors. Moreover, nitrate and total nitrogen concentrations have the virtually the same influence on the three photosynthetic parameters considered here. This can be explained easily: nitrate is the most abundant form, and contributes to >90% of dissolved nitrogen. NH_4^+ represented a negligible fraction of the total nitrogen in the first 10 days, and only after day 10, its contribution to total nitrogen became significant and rather constant. Its apparent effect on ETR_{max} and NPQ could therefore be biased since the first 10

days also correspond to high temperature and presence of NO_3^- in the water, parameters that are correlated to high ETR_{max} and low NPQ. The analysis did not catch any significant influence of phosphate concentration on photosynthesis, except for a negative correlation with NPQ. The nutrient data show that from day 10, the dissolved nitrogen is close to 0 whereas there is a significant amount of phosphate (and silicate) throughout the mesocosm. The N/P ratio is way below the Redfield ratio, which is the consistent nitrogen to phosphorus ratio found in marine phytoplankton (Redfield, 1934). This simply means that the growth of phytoplankton is nitrogen-limited.

Influence of temperature on photosynthesis

The relative influences of water and air temperatures on photosynthesis are strikingly different. There is no significant effect of water temperature on F_v/F_m or NPQ and only a small negative correlation with ETR_{max} . In contrast, the influence of air temperature seems to be very significant on those three parameters. The PLS analysis suggests that ETR_{max} and F_v/F_m are positively correlated with air temperature. It is important to remember here that the average temperature phytoplankton cells experience is the one of the water; however, they were sampled at the surface where the strong mixing due to pumping allows fast equilibration of air and surface water temperatures. Moreover, the measurement was made at air temperature. Those results might imply that (i) photosynthetic rate and PSII maximal quantum yield are dependent on the immediate temperature at the moment of sampling/measurement, and (ii) there is no significant long-term acclimation of the photosynthetic physiology to the temperature in the range of temperature experiences in this mesocosm.

The correlation between air temperature and ETR_{max} can easily be explained using the Arrhenius law, which describes the relationship between the kinetic constant of a chemical reaction, k , and the temperature, T : $k = A \cdot \exp\left(\frac{-E_a}{RT}\right)$, where A is a constant, E_a is the activation energy of the reaction and R is the universal constant of the perfect gases. As previously explained, the ETR_{max} depends on the speed of a chemical step and the measurements were made directly on the raft, at the temperature of the air; such a relation between the ETR_{max} and the air temperature is therefore expected. The very strong influence of temperature on F_v/F_m could reflect the temperature-dependent process of PSII repairment (see general introduction, chapter 1).

Influence of light intensity

Light irradiance is the only environmental parameter which correlates positively and significantly with the three photosynthetic parameters considered here. This is probably due to light acclimation processes. Indeed, it is known that some proteins involved in the establishment of NPQ (i.e. LHCX, Bailleul et al, 2010; Zhu and Green 2010; or LHCSR3 in green algae, Peers et al, 2009) can be induced by high light and give rise to a greater capacity to set up NPQ mechanisms. Note that the PLS model is best adapted to catch linear relationships between variables while the expected relationship between NPQ and acclimation light intensity is not linear (Serôdio et al., 2013). If we plot the NPQ according to the intensity of light from our dataset, we get a non-linear relationship (Figure 4-18). For low intensities, the implementation of NPQ is weak and increases from a threshold intensity (here $\sim 450 \mu\text{mol photons m}^{-2} \text{s}^{-1}$ of solar light). It can be proposed that the induction of the proteins involved in the NPQ only takes place when the acclimation intensities exceed this threshold.

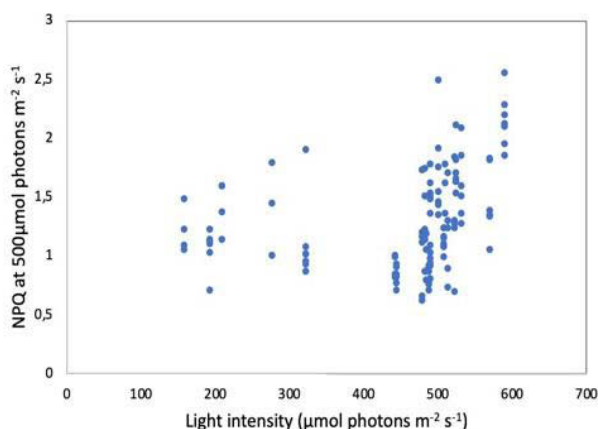


Figure 4-18: NPQ at 500 $\mu\text{mol photons m}^{-2} \text{s}^{-1}$ as a function of light intensity

Each point represents the NPQ vs light intensity for one bag and one day. Data corresponds to bags 1 to 7 for all days of the campaign.

Let's focus on the three parameters which appear to be significant in all explanatory models: the air temperature, the light intensity at the time of sampling and the concentration of inorganic nitrogen (which follows nitrate concentration, see correlation matrix, Figure 4-16). The trend is here very clear: low nitrogen availability or low temperature decrease the photosynthetic efficiency (F_v/F_m , ETR_{max}), and light intensity is positively correlated to those parameters. Since the NPQ is a process which takes place when light absorption exceeds the capacity of the photosynthetic chain, it is not surprising that it positively correlates with light intensity and negatively correlates to the environmental factors that favour high photosynthetic activity, i.e. temperature and nitrogen availability.

4.3.6 A photosynthetic signature of viral infection?

In the previous section, we have seen that an important part of the variance of our photosynthetic parameters can be explained by environmental parameters. This is especially true for ETR_{max} (75%), and to a lesser extent for F_v/F_m (47%). In this section, we will focus on the fraction of the variance which is not explained by the environmental parameters considered. Part of this unexplained variance comes from noise and stochastic effects, all the more important as the field experiments are subject to the vagaries of an outdoor laboratory. Some of it can stem from the fact that some of the environmental parameters are not well chosen; for example, we considered the light intensity at the time of sampling but maybe a most relevant parameter is the average intensity experienced over the last 24h, as it was shown for the green alga *Chlamydomonas reinhardtii* (Nawrocki et al., 2020). Also, the parameters used for the nitrogen status are the concentration of dissolved nitrogen in the water at the moment of sampling. The dissolved inorganic nitrogen concentration is virtually null in the bags at days 10 to 12 and at days 15 to 17 (except for bag 7), even though for the second period, nutrient addition were performed daily. Therefore, it is possible that considering the concentration of dissolved nitrogen at the moment of the addition would be more relevant to assess the nutrient status of phytoplankton.

But it is also possible that some of the unexplained variance comes from a factor which has not been taken into consideration, which could correspond to biotic interactions for example. This possibility can be addressed by studying the remaining variance of a photosynthetic parameter, i.e. the residuals of the PSL model. The residuals correspond to the difference between the value predicted by the PSL model and the experimental value. If their distribution is stochastic, then it suggests that most of the unexplained variance stems from technical noise. If, on the contrary, a significant abnormality has a good chance to reveal a relevant predictor of the considered photosynthetic parameter. The residues calculated on the F_v/F_m are presented in Figure 4-19A. A generally similar residual variance is observed between the bags ($RS = 0.71$), and residues are small, except for four events: day 3 for bag 5, day 9 for bag 4, days 16-17 for bag 7 and days 18-19 for bag 4. The first event will not be considered here; it occurs before *Emiliana huxleyi* dominates the signal and therefore is difficult to attribute. Those deviations can be highlighted by another means –less satisfactory from the point of view of statistics- which is to calculate, for each day, the difference between the F_v/F_m of a given bag and the median of all bags. The results are presented in Figure 4-19C and show that the decrease in F_v/F_m observed for the above-mentioned abnormalities correspond to a

deviation of 25-30% from the median value. The same analysis was carried out on the ETR_{max} (Figure 4-19B and D) and does not display significant residues for the days concerned by the fall of F_v/F_m (note that overall ETR_{max} variance is much more important than F_v/F_m variance, see Figure 4-8). The same analysis will be done in the near future on the other parameters of photosynthetic physiology. From the evolution of photosynthetic parameters (see Figure 4-8) the days concerned by the decrease of F_v/F_m do not show any particular phenotype concerning non-photochemical quenching (NPQ). But a drop appears for the two parameters which are expected to depend on the efficiency of PSII, the α parameter that characterizes the efficiency of photosynthesis at low light intensity and the in situ F_v/F_m on the particular days concerned by the negative residues of F_v/F_m (Figure 4-8).

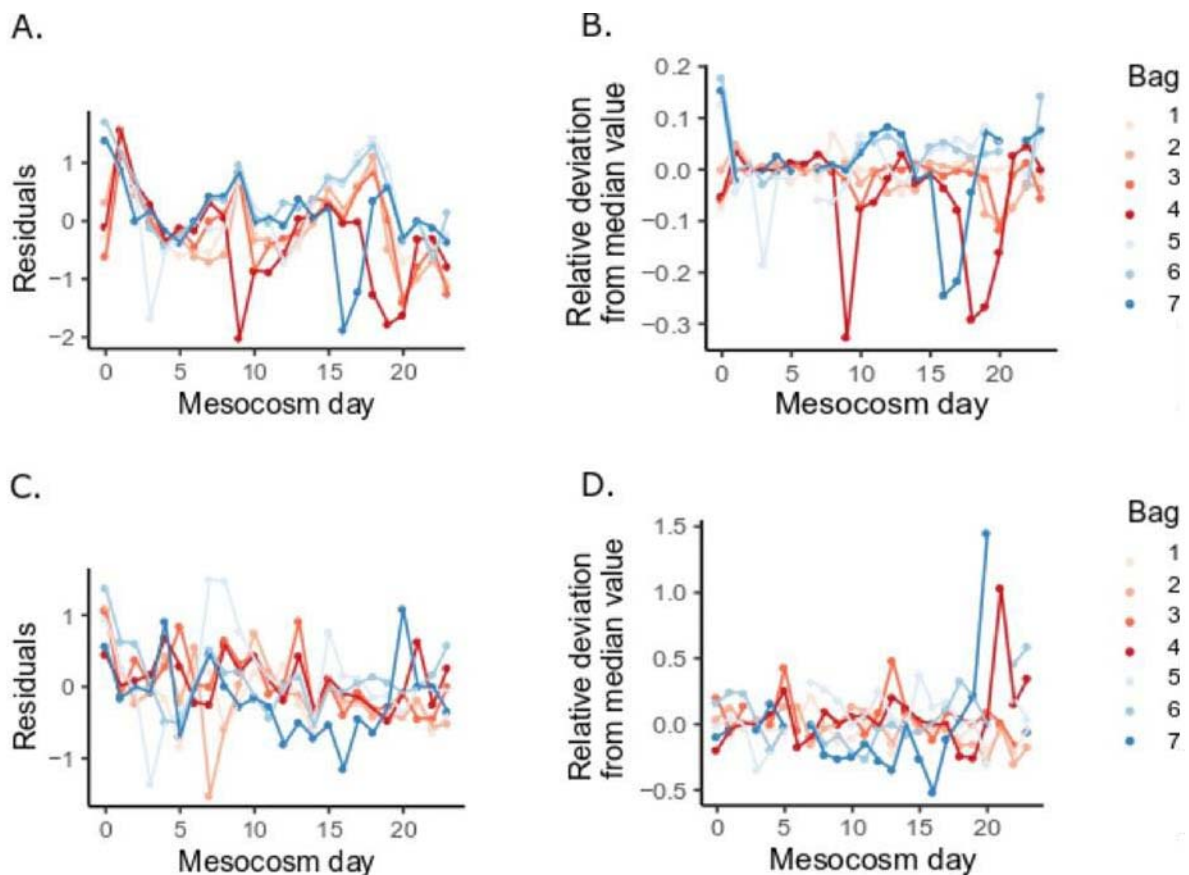


Figure 4-19: Estimation of the deviation to the model of the maximal PSII efficiency, F_v/F_m (A, B) and the maximal electron transfer rate, ETR_{max} (C, D).

A. and C. Data from bag 1 to 7 was fitted to a partial least square model (see results in Figure 4-17) and the residual variance was calculated for each bag and each day for F_v/F_m and ETR_{max} , respectively. B. and D. represent the relative deviation to the daily median value of all bags for F_v/F_m and ETR_{max} . Color codes correspond to different bags as shown on the right-hand side of figure.

What do those events – a specific decrease of F_v/F_m - reflect? What happened on those days in those bags?

The evolution of chlorophyll concentration and concentration of *Emiliana huxleyi* cells (high scatter nanoeukaryotes in the flow cytometry data) start to diverge around day 15 in bag 7, and around day 17 in bag 4, compared to other bags. Figure 4-20 shows the evolution of the abundance of the EhV, *Emiliana huxleyi* virus, measured by qPCR for the MCP (Major Capsid Protein) gene. EhV abundance increases very rapidly from day 17 in bag 4 and from day 15 in bag 7. Taken together, those data draw a possible scenario: viral infection occurred around day 15 in bag 7 and around day 17 in bag 4, leading to the replication and accumulation of coccolithovirus, a specific decrease of the maximal quantum efficiency of PSII and growth arrest in those bags. A significant part of the samples from the 2018 campaign are not yet analyzed by the different groups, but all preliminary data from Vardi's group comfort this scenario: (i) the detection of viral DNA in *E. huxleyi* single cells around days 18-19 in bag 4 and around days 17-18 in bag 7, but not in bag 3, used as a negative control, and (ii) the detection of a sphingolipid encoded in the genome of the virus, (Ziv et al., 2016) in those bags starting approximatively at the same dates (not shown).

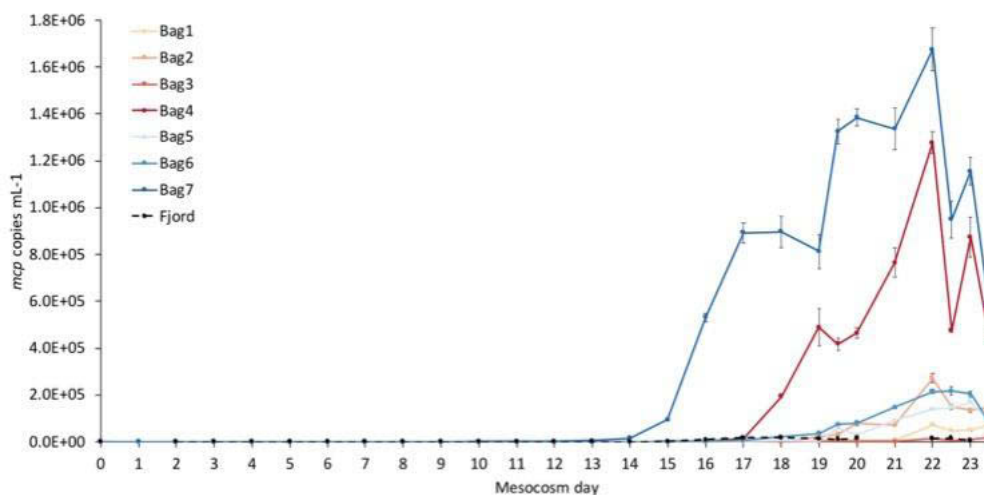


Figure 4-20: Evolution of the number of mcp gene copies per mL along the experiment in each bag.

Color codes for each bag shown on the left-hand side of figure: bags 1 to 4 were uncovered, bags 5 to 7 were covered by a polyethylene plastic sheeting and fjord refers to sampling directly in the open water. Data obtained by Schleyer, Schatz, Kuhlisch, Vincent, Lang-Yona and Vardi.

4.4 Conclusion and discussion

In this chapter, we followed the evolution of the photosynthetic physiology during a bloom of *Emiliana huxleyi* followed in seven mesocosms. The fluorescence measurements used to describe the photosynthetic physiology of the phytoplankton mainly reflected the signals emitted by the nanoeukaryotes and in particular by *E. huxleyi*, except during its growth lag phase from day 0 to day 9. A multivariate statistical approach allowed us to develop a model correlating the environmental parameters and the photosynthetic physiology of *E. huxleyi* explaining almost half of the total variance. This approach allowed us to highlight the main determinants of *E. huxleyi* photosynthesis. Most of the variations stems from the availability of nitrogen, air temperature and light intensity. Dissolved nitrogen and air temperature influence positively the maximal efficiency of PSII and the maximal rate of photosynthesis, and negatively the photoprotection mechanisms. Light intensity correlates positively with the three photosynthetic parameters. The statistical analysis did not reveal a significant influence of water temperature on photosynthesis of the coccolithophore, which suggests that there is no clear photosynthetic long-term acclimation to the temperature experienced in the mesocosm.

Once the contribution of the environmental parameters was “subtracted” from the experimental values of PSII maximal efficiency and maximal photosynthetic rate, some abnormalities appeared. Around day 16-17 in bag 7 and day 18-19 in bag 4, a specific decrease of the PSII efficiency appeared (without significant modification of the maximal rate of photosynthesis). Those transitory drops strongly correlate to a bundle of evidences for a viral infection, in those bags only: an increase of viral genes, the detection of intra-cellular viruses in *E. huxleyi* single cells, the apparition of specific sphingolipids whose biosynthesis pathway is encoded in the viral genome, and finally growth arrest. A question immediately arises: has this specific photosynthesis phenotype already been described as a response of viral infection in the laboratory?

Several laboratory studies described such a decrease in F_v/F_m , concomitant with the increase in the concentration of viral particles and the decrease in the concentration of *Emiliana huxleyi* cells (Evans et al., 2006, Bidle et al. 2007, Gilg et al., 2016). In a mesocosm, a decrease of less than 10% of F_v/F_m was observed, which occurred both during the bloom of *Emiliana huxleyi* and its demise (Kimmance and 2014). In this work, the possible environmental

parameters variation has not been considered. Thamtracoln and coworkers showed recently that the maximum rate of photosynthetic electron transfer was maintained during the viral infection in the laboratory (Thamtracoln et al, 2018). However, the mechanisms underlying the specific decrease of F_v/F_m during infection is not yet explored.

I would like to propose a model to explain such a phenotype during viral infection, which is based on recent studies in the laboratory of Assaf Vardi (Rosenwasser 2014, Gilg 2016, Ku et al, 2019). The analysis of the single-cell transcriptome of *Emiliana huxleyi* during its infection by its specific coccolithovirus reveals that the expression of nuclear genome of the host is arrested at the early stage of the infection, while plastid and mitochondrial transcriptomes were completely arrested at later stages (Ku et al, 2019).

It is well known that the D1 protein, a subunit of PSII, has a faster turnover than the other proteins involved in the photosynthetic chain (Lindahl et al., 2000; Aro et al., 1993). For example, the turnover of the D1 pool is ~20 min in high light stressed *Dunaliella salina* (Kim et al., 1993a). D1 being encoded by the PsbA gene in the plastid genome, blocking protein expression from the chloroplast genome by specific inhibitors, like chloramphenicol or lincomycin, therefore leads to a decrease in the D1 protein of photosystem II in plants, as well as in *Emiliana huxleyi* (Tyystjärvi and Aro, 1996; Loebel et al., 2010). However, this treatment affects the abundance of other proteins of the photosynthetic machinery only at later stages. During early stages, one therefore expects the repair of PSII to be hampered, whereas the other photosynthetic protein complexes remain unaffected. This would explain why viral infection leads to a specific decrease of the maximal PSII quantum efficiency without modifying the maximal rate of photosynthesis, as measured when light (and thus PSII efficiency) is not limiting electron transfer.

Such a specific drop of F_v/F_m has energetic consequences for the efficiency of viral infection. Viral replication requires the production of new viral particles from energy and organic matter (Ku et al, 2019). In photosynthetic cells, the vast majority of anabolic pathways are provided by the activity of the photosynthetic chain. Maintaining, at least initially, a photosynthetic activity of the host cell thus seems particularly important for the effectiveness of the viral multiplication. Some cyanophages are known to carry in their genome homologues of genes encoding the D1 protein (Mann et al 2003, Dammeyer et al., 2008) to maintain maximum efficiency of the PSII. In addition, some viruses such as *Micromonas pusilla* virus SP1 may even increase the maximum efficiency of PSII at certain critical stages of infection (Brown et al.,

2007). During the infection of *Emiliania huxleyi* by its coccolithovirus, the activity of PSII decreases. One could imagine that the maintenance of an active mitochondria throughout the infection progression (Ku et al, 2019) is sufficient to provide the high demand in reducing power and energy required for the viral replication. However, the number of viral particles released at the moment of the cell lysis phase depends on the light irradiance during the infection (Tamatrakoln, 2018). Such a light dependency of the production of viral particles in conditions of PSII inhibition suggests that a light-dependent PSII-independent process might be involved, making it plausible that cyclic electron flow around PSI plays a role during *Emiliania huxleyi* infection. Interestingly, what we suggest here corresponds to the behavior observed in *Chlamydomonas*: when PSII is inhibited, PSI can compensate the loss of activity related to linear electron flow by increasing CEF. Such a response during *E. huxleyi* infection would provide a precious supplementary source of ATP. With the protocol developed in the chapter 3 (part 3.3), one could test such a model where the inhibition of PSII (due to the arrest of plastid genome expression and of PSII repair) is compensated by PSI-driven CEF, supplying the high energy demanding virus infection process with ATP.

4.5 Bibliography

- Abdi, H., & Williams, L. J. (2010). Principal component analysis. *Wiley interdisciplinary reviews: computational statistics*, 2(4), 433-459.
- Aro, E. M., Virgin, I., & Andersson, B. (1993). Photoinhibition of photosystem II. Inactivation, protein damage and turnover. *Biochimica et Biophysica Acta (BBA)-Bioenergetics*, 1143(2), 113-134.
- Bach, L. T., Mackinder, L. C., Schulz, K. G., Wheeler, G., Schroeder, D. C., Brownlee, C., & Riebesell, U. (2013). Dissecting the impact of CO₂ and pH on the mechanisms of photosynthesis and calcification in the coccolithophore *Emiliana huxleyi*. *New Phytologist*, 199(1), 121-134.
- Bailleul, B., Rogato, A., De Martino, A., Coesel, S., Cardol, P., Bowler, C., ... & Finazzi, G. (2010). An atypical member of the light-harvesting complex stress-related protein family modulates diatom responses to light. *Proceedings of the National Academy of Sciences*, 107(42), 18214-18219.
- Balch, W. M., Holligan, P. M., & Kilpatrick, K. A. (1992). Calcification, photosynthesis and growth of the bloom-forming coccolithophore, *Emiliana huxleyi*. *Continental Shelf Research*, 12(12), 1353-1374.
- Barak-Gavish, N., Frada, M. J., Ku, C., Lee, P. A., DiTullio, G. R., Malitsky, S., ... & Sheyn, U. (2018). Bacterial virulence against an oceanic bloom-forming phytoplankter is mediated by algal DMSP. *Science advances*, 4(10), eaau5716.
- Berges, J. A., Charlebois, D. O., Mauzerall, D. C., & Falkowski, P. G. (1996). Differential effects of nitrogen limitation on photosynthetic efficiency of photosystems I and II in microalgae. *Plant Physiology*, 110(2), 689-696.
- Bidle, K. D., & Vardi, A. (2011). A chemical arms race at sea mediates algal host-virus interactions. *Current opinion in microbiology*, 14(4), 449-457.
- Bidle, K. D., Haramaty, L., e Ramos, J. B., & Falkowski, P. (2007). Viral activation and recruitment of metacaspases in the unicellular coccolithophore, *Emiliana huxleyi*. *Proceedings of the National Academy of Sciences*, 104(14), 6049-6054.
- Bilger, W., & Björkman, O. (1990). Role of the xanthophyll cycle in photoprotection elucidated by measurements of light-induced absorbance changes, fluorescence and photosynthesis in leaves of *Hedera canariensis*. *Photosynthesis research*, 25(3), 173-185
- Bramlette, M. N. (1958). Significance of coccolithophorids in calcium-carbonate deposition. *Geological Society of America Bulletin*, 69(1), 121-126.
- Butler, W. L. (1972). On the primary nature of fluorescence yield changes associated with photosynthesis. *Proceedings of the National Academy of Sciences*, 69(11), 3420-3422.
- Castberg, T., Larsen, A., Sandaa, R. A., Brussaard, C. P. D., Egge, J. K., Heldal, M., ... & Bratbak, G. (2001). Microbial population dynamics and diversity during a bloom of the marine coccolithophorid *Emiliana huxleyi* (Haptophyta). *Marine Ecology Progress Series*, 221, 39-46.
- Cermeño, P., Lee, J. B., Wyman, K., Schofield, O., & Falkowski, P. G. (2011). Competitive dynamics in two species of marine phytoplankton under non-equilibrium conditions. *Marine Ecology Progress Series*, 429, 19-28.

- Cullen, J. J., Yang, X., & MacIntyre, H. L. (1992).** Nutrient limitation of marine photosynthesis. In *Primary productivity and biogeochemical cycles in the sea* (pp. 69-88). Springer, Boston, MA.
- Dammeyer, T., Bagby, S. C., Sullivan, M. B., Chisholm, S. W., & Frankenberg-Dinkel, N. (2008).** Efficient phage-mediated pigment biosynthesis in oceanic cyanobacteria. *Current Biology*, *18*(6), 442-448.
- Engel, G. S., Calhoun, T. R., Read, E. L., Ahn, T. K., Mančal, T., Cheng, Y. C., ... & Fleming, G. R. (2007).** Evidence for wavelike energy transfer through quantum coherence in photosynthetic systems. *Nature*, *446*(7137), 782.
- Evans, C., Malin, G., Mills, G. P., & Wilson, W. H. (2006).** Viral infection of *Emiliana huxleyi* (Prymnesiophyceae) leads to elevated production of reactive oxygen species 1. *Journal of phycology*, *42*(5), 1040-1047.
- Feng, Y., Warner, M. E., Zhang, Y., Sun, J., Fu, F. X., Rose, J. M., & Hutchins, D. A. (2008).** Interactive effects of increased pCO₂, temperature and irradiance on the marine coccolithophore *Emiliana huxleyi* (Prymnesiophyceae). *European Journal of Phycology*, *43*(1), 87-98.
- Frada, M., Probert, I., Allen, M. J., Wilson, W. H., & de Vargas, C. (2008).** The “Cheshire Cat” escape strategy of the coccolithophore *Emiliana huxleyi* in response to viral infection. *Proceedings of the National Academy of Sciences*, *105*(41), 15944-15949.
- Genty, B., Briantais, J. M., & Baker, N. R. (1989).** The relationship between the quantum yield of photosynthetic electron transport and quenching of chlorophyll fluorescence. *Biochimica et Biophysica Acta (BBA)-General Subjects*, *990*(1), 87-92.
- Gilg, I. C., Archer, S. D., Flöge, S. A., Fields, D. M., Vermont, A. I., Leavitt, A. H., ... & Martínez, J. M. (2016).** Differential gene expression is tied to photochemical efficiency reduction in virally infected *Emiliana huxleyi*. *Marine Ecology Progress Series*, *555*, 13-27.
- Green, J. C., Course, P. A., & Tarran, G. A. (1996).** The life-cycle of *Emiliana huxleyi*: A brief review and a study of relative ploidy levels analysed by flow cytometry. *Journal of marine systems*, *9*(1-2), 33-44.
- Grouneva, I., Gollan, P. J., Kangasjärvi, S., Suorsa, M., Tikkanen, M., & Aro, E. M. (2013).** Phylogenetic viewpoints on regulation of light harvesting and electron transport in eukaryotic photosynthetic organisms. *Planta*, *237*(2), 399-412.
- Haenlein, M., & Kaplan, A. M. (2004).** A beginner's guide to partial least squares analysis. *Understanding statistics*, *3*(4), 283-297.
- Hansen, H. P., and Grasshoff, K. (1983).** “Automatic chemical analysis,” in *Methods of Seawater Analysis*, 2nd Edn., eds K. Grasshoff, M. Ehrhardt, and K. Kremling (Weinheim: Verlag Chemie), 368–376
- Hotelling, H. (1933).** Analysis of a complex of statistical variables into principal components. *Journal of educational psychology*, *24*(6), 417.
- Jiang, Y., Yoshida, T., & Quigg, A. (2012).** Photosynthetic performance, lipid production and biomass composition in response to nitrogen limitation in marine microalgae. *Plant Physiology and Biochemistry*, *54*, 70-77.

- Kimance, S. A., Allen, M. J., Pagarete, A., Martínez, J. M., & Wilson, W. H. (2014).** Reduction in photosystem II efficiency during a virus-controlled *Emiliana huxleyi* bloom. *Marine Ecology Progress Series*, 495, 65-76.
- Kolber, Z., Zehr, J., & Falkowski, P. (1988).** Effects of growth irradiance and nitrogen limitation on photosynthetic energy conversion in photosystem II. *Plant physiology*, 88(3), 923-929.
- Ku, C., Sheyn, U., Sebé-Pedrós, A., Ben-Dor, S., Schatz, D., Tanay, A., ... & Vardi, A. (2019).** Tracking infection dynamics at single-cell level reveals highly resolved expression programs of a large virus infecting algal blooms. *bioRxiv*, 757542
- Lindahl, M., Spetea, C., Hundal, T., Oppenheim, A. B., Adam, Z., & Andersson, B. (2000).** The thylakoid FtsH protease plays a role in the light-induced turnover of the photosystem II D1 protein. *The Plant Cell*, 12(3), 419-431.
- Loebl, M., Cockshutt, A. M., Campbell, D. A., & Finkel, A. Z. V. (2010).** Physiological basis for high resistance to photoinhibition under nitrogen depletion in *Emiliana huxleyi*. *Limnology and Oceanography*, 55(5), 2150-2160.
- Mann, N. H. (2003).** Phages of the marine cyanobacterial picophytoplankton. *FEMS microbiology reviews*, 27(1), 17-34.
- Marie, D., Simon, N., & Vaulot, D. (2005).** Phytoplankton cell counting by flow cytometry. *Algal culturing techniques*, 1, 253-267
- Martínez-Martínez, J., Norland, S., Thingstad, T. F., Schroeder, D. C., Bratbak, G., Wilson, W. H., & Larsen, A. (2006).** Variability in microbial population dynamics between similarly perturbed mesocosms. *Journal of plankton research*, 28(8), 783-791.
- Milliman, J. D. (1993).** Production and accumulation of calcium carbonate in the ocean: budget of a nonsteady state. *Global Biogeochemical Cycles*, 7(4), 927-957.
- Muggli, D. L., & Harrison, P. J. (1996).** Effects of nitrogen source on the physiology and metal nutrition of *Emiliana huxleyi* grown under different iron and light conditions. *Marine Ecology Progress Series*, 130, 255-267.
- Nawrocki, W. J., Liu, X., & Croce, R. (2020).** *Chlamydomonas reinhardtii* exhibits de facto constitutive NPQ capacity in physiologically relevant conditions. *Plant physiology*, pp-00658.
- Odum, E. P. (1984).** The mesocosm. *BioScience*, 34(9), 558-562.
- Paasche, E., & Brubak, S. (1994).** Enhanced calcification in the coccolithophorid *Emiliana huxleyi* (Haptophyceae) under phosphorus limitation. *Phycologia*, 33(5), 324-330.
- Peers, G., Truong, T. B., Ostendorf, E., Busch, A., Elrad, D., Grossman, A. R., ... & Niyogi, K. K. (2009).** An ancient light-harvesting protein is critical for the regulation of algal photosynthesis. *Nature*, 462(7272), 518.
- Platt, T., Gallegos, C. L., Harrison, W. G. (1980).** Photoinhibition of photosynthesis in natural assemblages of marine phytoplankton. *J. mar Res.* 38: 687-701.
- Redfield, A. C. (1934).** On the proportions of organic derivatives in sea water and their relation to the composition of plankton. *James Johnstone memorial volume*, 176-192.

- Rochelle-Newall, E., Delille, B., Frankignoulle, M., Gattuso, J. P., Jacquet, S., Riebesell, U., ... & Zondervan, I. (2004).** Chromophoric dissolved organic matter in experimental mesocosms maintained under different pCO₂ levels. *Marine Ecology Progress Series*, 272, 25-31.
- Rosenwasser, S., Mausz, M. A., Schatz, D., Sheyn, U., Malitsky, S., Aharoni, A., ... & Pohnert, G. (2014).** Rewiring host lipid metabolism by large viruses determines the fate of *Emiliana huxleyi*, a bloom-forming alga in the ocean. *The Plant Cell*, 26(6), 2689-2707.
- Rosipal, R., & Krämer, N. (2005).** Overview and recent advances in partial least squares. In *International Statistical and Optimization Perspectives Workshop "Subspace, Latent Structure and Feature Selection"* (pp. 34-51). Springer, Berlin, Heidelberg.
- Segovia, M., Lorenzo, M. R., Maldonado, M. T., Larsen, A., Berger, S. A., Tsagaraki, T. M., ... & Mausz, M. A. (2017).** Iron availability modulates the effects of future CO₂ levels within the marine planktonic food web. *Marine Ecology Progress Series*, 565, 17-33.
- Serôdio, J., Ezequiel, J., Frommlet, J., Laviale, M., & Lavaud, J. (2013).** A method for the rapid generation of nonsequential light-response curves of chlorophyll fluorescence. *Plant physiology*, 163(3), 1089-1102.
- Teoh, M. L., Phang, S. M., & Chu, W. L. (2013).** Response of Antarctic, temperate, and tropical microalgae to temperature stress. *Journal of Applied Phycology*, 25(1), 285-297.
- Thamatrakoln, K., Talmy, D., Haramaty, L., Maniscalco, C., Latham, J. R., Knowles, B., ... & Bidle, K. D. (2019).** Light regulation of coccolithophore host-virus interactions. *New Phytologist*, 221(3), 1289-1302.
- Trimborn, S., Langer, G., & Rost, B. R. (2007).** Effect of varying calcium concentrations and light intensities on calcification and photosynthesis in *Emiliana huxleyi*. *Limnology and Oceanography*, 52(5), 2285-2293.
- Tyrrell, T., & Merico, A. (2004).** *Emiliana huxleyi*: bloom observations and the conditions that induce them. In *Coccolithophores* (pp. 75-97). Springer, Berlin, Heidelberg.
- Tyystjärvi, E., & Aro, E. M. (1996).** The rate constant of photoinhibition, measured in lincomycin-treated leaves, is directly proportional to light intensity. *Proceedings of the National Academy of Sciences*, 93(5), 2213-2218.
- Vardi, A., Haramaty, L., Van Mooy, B. A., Fredricks, H. F., Kimmance, S. A., Larsen, A., & Bidle, K. D. (2012).** Host-virus dynamics and subcellular controls of cell fate in a natural coccolithophore population. *Proceedings of the National Academy of Sciences*, 109(47), 19327-19332.
- Veldhuis, M. J., & Kraay, G. W. (2000).** Application of flow cytometry in marine phytoplankton research: current applications and future perspectives. *Scientia Marina*, 64(2), 121-134.
- Westbroek, P., Young, J. R., & Linschooten, K. (1989).** Coccolith production (biomineralization) in the marine alga *Emiliana huxleyi*. *The Journal of protozoology*, 36(4), 368-373.
- Wilson, W. H., Van Etten, J. L., & Allen, M. J. (2009).** The Phycodnaviridae: the story of how tiny giants rule the world. In *Lesser Known Large dsDNA Viruses* (pp. 1-42). Springer, Berlin, Heidelberg.
- Zhu, S. H., & Green, B. R. (2010).** Photoprotection in the diatom *Thalassiosira pseudonana*: role of L1818-like proteins in response to high light stress. *Biochimica et Biophysica Acta (BBA)-Bioenergetics*, 1797(8), 1449-1457.

Ziv, C., Malitsky, S., Othman, A., Ben-Dor, S., Wei, Y., Zheng, S., ... & Vardi, A. (2016). Viral serine palmitoyltransferase induces metabolic switch in sphingolipid biosynthesis and is required for infection of a marine alga. *Proceedings of the National Academy of Sciences*, 113(13), E1907-E1916.

Chapter 5: General discussion

Summary

5. 1. Methodological overview	261
5. 1. 1. The importance of cross validations of methods	261
5. 1. 2. Using the flash-induced ECS to estimate the photochemical rate: a good choice?	263
5. 1. 3. Studying CEF and its abiotic and biotic determinants in the field: an accessible project?.....	266
5. 2. Roles of CEF and mechanisms of the regulation of the CEF and LEF	271
5. 2. 1. ATP:NADPH ratio equilibration.....	271
5. 2. 2. A role of CEF when PSII is inhibited?	274
5. 2. 3. CEF and LEF regulation	275
5. 3. Three years were too short for.....	277
5. 3. 1. Revisiting literature using P ₇₀₀ method	277
5. 3. 2. Exploring cyclic electron flow using our methods	277
5. 3. 3. Harness all data collected in the field.....	278
5. 4. Bibliography.....	280

This thesis work has two main axes: the exploration of CEF in microalgae and the study of determinants of photosynthesis in the field. In this discussion, I first suggest some methodological conclusions in a more general context and some research tracks that could be developed to enable CEF measurement in situ. In a second time, I discuss the putative roles of CEF and propose an additional function related to the response to specific inhibition of PSII that occurs in several conditions in the field. I also discuss the CEF regulation mechanisms compatible with our results. Finally, I present some lines of research that I would have liked to continue if the PhD thesis was lasting more than three years.

5. 1. Methodological overview

The work I have presented partly consists in a methodological exploration around two central themes: the CEF and the study of photosynthesis in the field. I would first like to take a step back on the methodological approaches used in my work before proposing some methodological tracks to progress in the study of CEF in the field.

5. 1. 1. The importance of cross validations of methods

Are we measuring what we believe we are measuring? Of course, this question is fundamental when trying to answer a biological question. In this thesis, a systematic verification of the methods used has been performed, often relying on cross-validations. This approach allowed to (i) show that the P_{700} method, commonly used for 25 years to estimate the activity of PSI, is unreliable under many particularly interesting physiological conditions (chapter 2), but also (ii) to question and refine protocols (chapter 2 and 3).

The interest of cross-validations for refining methods was mentioned in several places along this manuscript but I would like to come back to it through few examples. When we compared the ETR(total) values measured with the DIRK method or with the flash-induced method, we initially measured discrepancies at high light irradiances (Figure 5-1). By questioning the possible causes of this discrepancy, we were able to highlight that this was the consequences of charge recombination: the “a phase” measured in ECS that is thought to estimate stable charge separations (Bailleul et al., 2010) wrongly counted unstable charge separations. Those unstable charge separations lead to charge recombination in the time

range of a few hundreds of μs which affects the ECS decay at light offset and affects the DIRK measurements of photochemical rate as well. Realizing the disagreement between the two methods allowed me to identify an unanticipated problem and to correct it. After correction (we eliminated the contribution of charge recombination by extrapolating the decay kinetics in the first 1.2 ms where charge recombination occurs), the two methods agreed (Figure 5-1).

Another example relates to the measurement of P_m , the maximum variation of P_{700} absorbance between its completely reduced and completely oxidized state. In the presence of MV, when we expect the P_{700} pulse method to be reliable, we initially obtained a linear relationship between $Y(I)P_{700}$ and $Y(I)_{ECS}$. However, the slope of the relationship was not 1 but ~ 1.15 , indicating an overestimation of $Y(I)P_{700}$. This discrepancy led us to understand that we underestimated P_m , the normalization factor in the calculation of $Y(I)P_{700}$. Indeed, under saturating concentration of DCMU and in strong light, we did not reach 100% of oxidized P_{700} because the reduction of P_{700} by the CEF became significant. We then modified the way we measured P_m by adding DBMIB which inhibits most of the CEF.

These changes in experimental procedures, however minor they may look at first sight, are of paramount importance since they radically change the results. When, as it is the case for the CEF investigation, several measurement methods are used while we try to measure potentially small values or variations, these details are particularly important. I have learned from my thesis to be cautious about the way one measures the CEF and LEF in *Chlamydomonas*. Indeed, one cross-validation attempt failed during my thesis and remains to be solved: the discrepancy between the measurements of PSII absorption cross-section by the method based on ECS and on fluorescence measurements. As we have seen, this might stem from not considering correctly energetic connectivity between PSII centers, drawing the path for the next step of improvement.

Figure 5-1: Importance of considering charge recombinations when measuring the fraction of PS open centers.

ETR(total) measured with the method based on $Y(\text{total})$ with and without correction for charge recombinations (black and red points, respectively) was plotted as a function of ETR(total) measured with the DIRK method. Dashed grey line represents the expected $y=x$ relation curve. Squares and circles represent data from two different biological samples.

5. 1. 2. Using the flash-induced ECS to estimate the photochemical rate: a good choice?

The principle of the method we proposed in chapter 3 (section 3.3) for the screening of CEF behaviors in different microalgae is to compare the changes of electron flow through PSII (i.e. the LEF) and the sum of PSI and PSII activities and to test the relationship models between LEF and CEF. In chapter 3 section 3.4, we showed that, when light intensity is varied, the DIRK method, and the method based on the estimation of $Y(\text{total})$, and the total absorption cross section, σ_{total} agreed with each other. However, the choice I have made to use the second method instead of the DIRK one is a priori questionable because the DIRK method is easy to use and does not require any strong assumptions. At the contrary, the validity of the ETR(total) as a measurement of the sum of PSII and PSI activities is not mathematically correct and it is necessary to question its window of validity. I will come back to this, but first I would like to insist on the importance of the work performed in chapter 1 to invalidate P_{700} based methods for the use of CEF.

a) Questioning the choice of ECS versus P700 to investigate CEF

At the beginning of my PhD, we used a different protocol to investigate CEF. We used the P₇₀₀ method to estimate the evolution of the flow through PSI and fluorescence for the one through PSII, as suggested in a recent review (Fan et al, 2016). The results obtained on a representative sample of *Chlamydomonas reinhardtii* are presented in Figure 5-2. When adding DCMU, Y(II) (blue line) decreases as expected. But the evolution of Y(I)_{P700} (red line) is spectacular. When Y(II) decreases by 30% (4th point of the titration), Y(I) is almost multiplied by 3 which, when interpreted blindly, would indicate that the CEF has increased tremendously. The electron transfer rate through PSI would have increased by almost a factor 3, which is at least difficult to explain. In addition, the activity of the PSI when all PSII are inhibited (i.e. when there is only CEF) appears to be equal to the initial activity. This would suggest that the CEF in conditions when the PSII is inhibited is equivalent to or higher than LEF under initial conditions, against all the literature on CEF in *Chlamydomonas* under saturating DCMU. The fluxes measured in saturating DCMU are much lower than untreated LEF flows measured through the PSII (e.g. Alric 2010; Theis et al., 2019).

These observations led us to question the P₇₀₀ method, which gave birth to chapter 2 of my thesis. At the beginning, we compared the results obtained with ECS and P₇₀₀ method, Y(I)_{P700} and Y(I)_{ECS} respectively in order to understand better the conditions when P₇₀₀ was not reliable. Thus, when we understood that Y(I)_{P700} was not reliable, we decided to study the CEF and LEF relationship by comparing the evolutions of Y(II) and Y(total) calculated from ECS signals (see Figure 5-2, black line). We therefore continued with the same single turnover flash method and did not consider other methods to estimate the total electron flow changes such as the photochemical rate. The choice of the ECS-based method we used in chapter 3 comes from this and deserves critical thinking.

Figure 5-2: DCMU titration of Y(total), Y(II) and Y(I)_{P700} in *Chlamydomonas reinhardtii* stt7 mutant. Measurements were performed under steady state light at 135 μmol photons.m⁻².s⁻¹. Y(total) (black), Y(II) (blue) and Y(I)_{P700} (red) were normalized to their initial values, when no DCMU was added and under steady state light. Data were obtained in one representative biological replicate

b) Questioning the choice of using the fraction of open centers for measuring ETR(total)

We made the assumption that the sum of PSII and PSI activities (ETR(total)) could be calculated as the product of light irradiance, I, total absorption cross-section, σ_{total} , and the fraction of open centers, Y(total) : $\text{ETR}(\text{total}) = I \cdot \sigma_{\text{total}} \cdot Y(\text{total})$.

Even though the agreement between this measurement and the one of photochemical rate by the DIRK method is reassuring, it is worth discussing what are the required assumptions for the validity of this calculation. What is actually calculated with ETR(total) is:

$$(1) \quad \text{ETR}(\text{total}) = \sigma_{\text{total}} \cdot Y(\text{total}) \cdot I = \sigma_{\text{total}} \cdot (n_1 \cdot \text{FOC}(\text{I}) \cdot I + n_2 \cdot \text{FOC}(\text{II}) \cdot I)$$

where FOC(I) and FOC(II) are the fractions of open centers (FOC) for PSI and PSII, respectively. As assumed in chapter 2, the quantum yield of PSI, Y(I), is equal to the fraction of open PSI, since the maximal quantum yield of PSI is close to 1. If we consider the “puddle” model then $\text{FOC}(\text{II}) = q_p = Y(\text{II}) / (F_v/F_m)$. Therefore equation (1) can be rewritten:

$$(2) \quad \text{ETR}(\text{total}) = \sigma_{\text{total}} \cdot (n_1 \cdot \text{ETR}(\text{I}) / \sigma_1 + n_2 \cdot \text{ETR}(\text{II}) / (F_v/F_m \cdot \sigma_{\text{II}}))$$

Since $n_1 \cdot \text{ETR(I)} = n_2 \cdot \text{ETR(II)} + n_1 \cdot \text{CEF}$, and $\sigma_{\text{total}} = (n_1 \cdot \sigma_1 + n_2 \cdot \text{Fv/Fm} \cdot \sigma_{\text{II}})$ equation (2) can be rewritten to express $\text{ETR}(\text{total})$ as a function of $\text{ETR}(\text{II})$ and CEF :

$$\begin{aligned} (3) \quad \text{ETR}(\text{total}) &= \sigma_{\text{total}} \cdot (n_2 \cdot (1/\sigma_1 + 1/(\text{Fv/Fm} \cdot \sigma_{\text{II}})) \text{ETR}(\text{II}) + n_1 \cdot \text{CEF}/\sigma_1) \\ &= \alpha \cdot \text{ETR}(\text{II}) + \beta \cdot \text{CEF} \end{aligned}$$

where $\alpha = n_2 \cdot \sigma_{\text{total}}^2 / (\sigma_1 \cdot (\text{Fv/Fm} \cdot \sigma_{\text{II}}))$ and $\beta = n_1 \cdot \sigma_{\text{total}} / \sigma_1$.

Note that when the maximal photochemical rates of PSI (σ_1) and PSII ($\text{Fv/Fm} \cdot \sigma_{\text{II}}$) are equal, which means that $\sigma_{\text{total}} = \sigma_1 = \text{Fv/Fm} \cdot \sigma_{\text{II}}$, then $\text{ETR}(\text{total}) = n_2 \cdot \text{ETR}(\text{II}) + n_1 \cdot \text{CEF}$, i.e. the correct expression. In all other cases, $\text{ETR}(\text{total})$ is not a proper expression of the total PS activity.

In part 3.4, in order to calculate the absolute values of $\text{ETR}(\text{total})$, using this expression would have not been correct, despite the good agreement between the absolute values of $\text{ETR}(\text{total})$ and the photochemical rates obtained with the DIRK method. Instead, we used the latter method for this part of the chapter 3. Regarding the part 3.3, where we titrated the $Y(\text{total})$ and $Y(\text{II})$ to investigate the behavior of CEF , the use of $\text{ETR}(\text{total})$ is correct, assuming a “puddle” model. The demonstration of the validity of this approach is demonstrated in Appendix 1.

5. 1. 3. Studying CEF and its abiotic and biotic determinants in the field: an accessible project?

In the field, the complexity of the systems studied is much greater than in the laboratory: for example, there are mixtures of several species, microalgae are generally present in low concentrations and most of the time, several environmental parameters vary concomitantly. This is the interest of the field approach: we study the microalgae in their real life, which is the platform for new discoveries. But it has a price: the interpretation of the experimental results is much more complex than in the lab. When going into the field, one of my dreams was to measure CEF in situ and to study the biotic and abiotic determinants of its amplitude in the field. In this section, I would like to come back to the three constraints that we were able to identify concerning the study of CEF in situ and to discuss the ways we could overcome them in the future. If one wants to understand the biotic and abiotic determinants of CEF in the field, some conditions are required:

- samples need to be concentrated enough to obtain an appropriate signal-to-noise ratio;
- the signals emitted by the species of interest need to be distinguished from other signals;
- the photosynthetic physiology should be carefully assessed in order to determine a statistical model that allows one to highlight the influence of each environmental parameter.

a) Measuring absorption changes on field samples

In the field, most of the studies of photosynthetic physiology are based on the analysis of fluorescence parameters as a means to study the electron flow through PSII. Fluorescence signals are high enough to be measured in a single cell. However, as we pointed out in Chapter 3, the methods used to investigate CEF are based on the measurement of absorption changes that are signals of much lower amplitude. For example in the laboratory, we generally work at cell concentrations of the order of 10^7 cells/mL (which measure 3 to 20 μm in diameter). In the field, the concentrations of algae are always much lower. For example, in mesocosms experiments and after adding nutrients, the concentrations of *Emiliana huxleyi* can reach 10^5 cells/mL (data from Chapter 4; Catsberg et al., 2001) but are generally lower than 10^3 cells/mL (e.g. Rochelle-Newall et al., 2004; Martinez-Martinez et al., 2006). During blooms in the open sea, the concentration of *Emiliana huxleyi* varies between 10^3 and 10^5 cells/mL (reviewed in Tyrell and Merico, 2004) and the picoeukaryote blooms reach similar cell densities (e.g. Not et al., 2005; Thyssen et al., 2014; Zhao et al., 2016). From our own experience, it is difficult to concentrate without modifying the physiology. In the current state of biophysical devices, it therefore seems difficult to measure CEF in situ in field experiments.

A way to overcome this constraint would be to increase the amplitude of the absorption spectroscopy signals. This is presently on its way in the laboratory where a prototype sample cuvette which is based on an integrating sphere principle has recently been produced. It aims at increasing the optical path, and thus the absorption signals. It consists in a hollow spherical cavity with its interior covered with a diffuse white reflective coating, with small holes for optical paths. Its relevant property is a uniform scattering or diffusing effect. Light rays incident on any point on the inner surface are, by multiple scattering reflections, distributed equally to all other points. The first tests on this prototype are highly promising with an optical path increased by 10-100 fold.

b) Tackling the issue of the species mixture in the field

In the field, we measured photosynthetic activity resulting from a mix of several species. It is thus difficult – if not impossible- to study the physiology of each microalga independently. This constraint can be alleviated when we are faced with rather monospecific samples as for the *Chaetoceros* dominated sample from the Penzé (Roscoff, France) on which we have shown the existence of a CEF independent of LEF (chapter 3) or for photosynthetic physiology measurements on a population dominated by *Emiliana huxleyi* (chapter 4). Still in most in situ situations the study of photosynthetic physiology is hampered by this constraint.

I worked together with Alexandra Peltekis, another PhD student, and Benjamin Bailleul on the development of an innovative method to deconvolute the ECS signals emitted by each species in a mixture. The principle of the method is based on the differences in ECS spectrum between species of different clades (see some ECS spectrum examples in Bailleul et al., 2010). Within this project, I developed a Matlab script for the deconvolution of ECS signals and participated to the proof of methods. Figure 5-3 shows the ECS spectra obtained 300 μ s after a single turnover laser flash in a homogenous sample of the haptophyte *Isochrysis galbana* (panel A), in a homogenous sample of the dictiophyte *Pseudopedinella sp* (panel B) and in the mixture of these two species (1/1 ratio, volume-to-volume) (panel C, black curve). The expected spectrum of the mixture (average of the spectra obtained in isolated samples, panels A and B) is shown in blue in panel C and is almost superimposed to the experimental spectrum of the mixture. Here, the ECS signal of the mixture is equal to the sum of the signals emitted by each species.

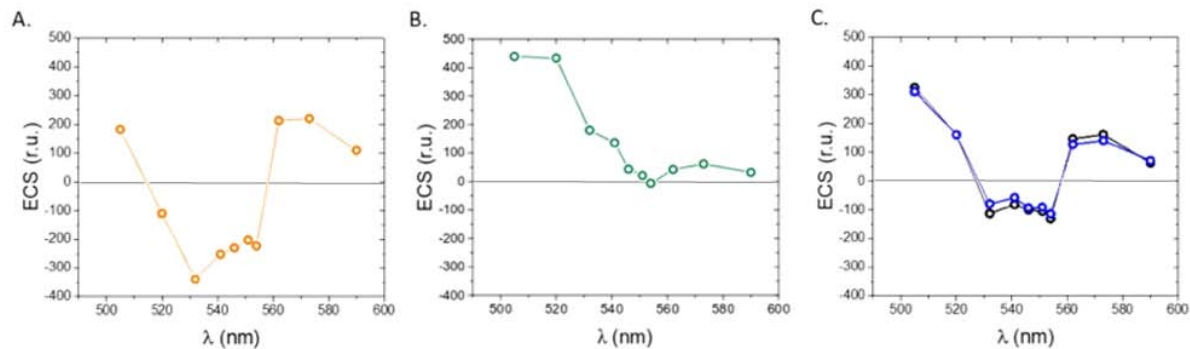


Figure 5-3: Example of ECS spectra measured in mono-cultures and in co-culture.

ECS spectra were measured in a monoculture of the haptophyte *Isochrysis galbana* (panel A.) and of the dictiophyte *Pseudopedinella sp.* (panel B.) and in their co-culture (C, black curve). In C, the blue curve represents the expected ECS spectrum based on the sum of the ECS spectra from the two mono-cultures. The concentration of each microalgae in the mixture was half the one in the mono-culture. Data correspond to measurements obtained in one representative experiment.

We then checked the relationship between the expected and measured ECS in this mixture and other mixtures of different species (Figure 5-4). We used the ECS kinetics at the light offset at different wavelengths to explore this relationship. The expected and measured ECS values show a linear relationship aligned on the line $y = x$ (grey curve) for three pairs of algae that are: the dinoflagellate *Amphidinium caterae* with the eustigmatophyte *Nannochloropsis salina* (panel A), *Amphidinium caterae* with the haptophyte *Isochrysis galbana* (panel B) and the dictiophyte *Pseudopedinella sp.* with *Isochrysis galbana* (panel C).

This approach could be used to measure CEF amplitude of each species in a mixture. Indeed, by inhibiting PSII, we could use ECS signals to measure PSI activity for each species, that would only be due to CEF.

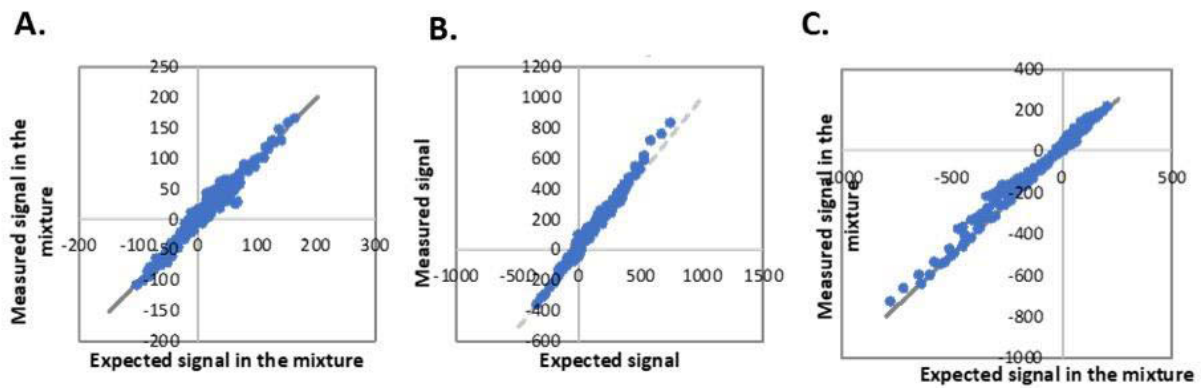


Figure 5-4: Expected versus measured ECS signals in 3 mixtures of microalgae.

ECS signals were measured during the ECS decay after light offset in isolated samples and mixed samples of the dinoflagellate *Amphidinium carterae* and the eustigmatophyte *Nannochloropsis salina* (A), *Amphidinium carterae* and the haptophyte *Isochrysis galbana* (B) and the dictyophyte *Pseudopedinella sp* and *Isochrysis galbana* (C). The ECS signal in the mixture was plotted as a function of the expected ECS signal based on the sum of the signals emitted in isolated samples in the same conditions. Grey line represents the expected $y=x$ line. Data correspond to measurements obtained in one representative experiment in each panel.

c) Determining biotic and abiotic determinants of CEF in the field

In the laboratory, we can show the effect of a biotic or abiotic parameter on photosynthetic physiology using a reductionist approach: we modify this parameter everything else being equal and we measure possible phenotypic changes. For example, the CEF amplitude is known to depend on light irradiance and CO_2 availability. Is it so in the field as well? Are some parameters more important than others? Can we highlight signatures of a particular environmental parameter? Very few studies deal with photosynthetic physiology in situ by taking into account all the environmental parameters known to influence photosynthetic activity.

This was the aim of our study depicted in Chapter 4. We could show that during a 24-days campaign, the parameters describing photosynthetic physiology varied significantly. In order to explain their variance, we measured abiotic parameters such as dissolved nutrient concentrations, temperature, and light intensity and could build a statistical model explaining most of the photo-physiology variance (75%, 47% and 37% of the variance explained by the model for ETR_{max} , F_v/F_m and NPQ, respectively). We have shown that because of the inevitable partial correlation between abiotic parameters, a correct statistical treatment requires a multivariate approach and that the PLS (partial least square) regression is particularly suitable under conditions where abiotic parameters are partially correlated

(e.g. temperature and intensity). This approach makes it possible to highlight potential causal relationships between an abiotic parameter and photosynthetic physiology. If we had been able to measure CEF in the field (which was not feasible) on the same population and to follow its evolution overtime, we would have been able to discuss the major environmental parameters that determine CEF in situ.

Despite these present limitations in the study of photosynthetic physiology, we could show that the residues of the PLS model (remaining variance) could be used as a powerful tool for determining the influence of other parameters, such as biotic interactions. If the residuals to the model are not stochastically distributed along time, then we can highlight “abnormalities”, i.e. the effect of a parameter which is not considered by the model. In our study, we were able to show anecdotal strong deviations from the model explaining the maximum efficiency of PSII, F_v/F_m . And those deviations seem to correlate with viral infection of cells. More generally, this approach could be used to highlight anecdotal effects of biotic parameters leading to a deviation from the model, such as the effects of pollutants or the allelopathic effects of a minority species on an algal population. Provided that a high frequency coverage is used, it could be also applied to disentangle light responses from circadian rhythms for example.

5. 2. Roles of CEF and mechanisms of the regulation of the CEF and LEF

5. 2. 1. ATP:NADPH ratio equilibration

In Chapter 3, we calculated ATP/NADPH ratios produced by the photosynthetic chain using the formula:

$$(1) \text{ ATP/NADPH} = 18/14 + 12/14 \text{ CEF/LEF}$$

We estimated that the photosynthetic chain produced ATP and NADPH in ratios of ~ 1.3 in *Amphidinium carterae*, ~ 1.8 in *Symbiodinium sp* and ~ 1.8 or ~ 2.5 in *Chlamydomonas reinhardtii* (depending on the method used to calculate the photon fluxes at PSII). We then used the estimated ratio of ATP per NADPH produced by the photosynthetic chain to discuss

the possible ways of utilization of those compounds (CBB cycle, CCM, other pathways). But these calculations are based on strong assumptions such as:

1. the conservation of the structure of the chloroplast ATP synthase within the phylogeny;
2. the conservation of the Q-cycle mechanism;
3. the absence of alternative electron flows other than CEF.

Hereafter, I propose to discuss those hypotheses and to estimate the possible estimation errors we did.

- *About variation of the number of c-subunits composing ATP synthases*

If the number of ATP synthase c subunits was greater than 14, as counted in plants, then the number of ATP produced per proton transferred would be lower than what we estimated and we would have overestimated the ATP/NADPH ratio produced by the chain. The highest number of c subunits mentioned in the literature is 15 in cyanobacteria (Pogoryelov et al., 2007). If this was the case in the organisms studied, then the ATP/NADPH ratios would be overestimated by 7%.

If the number of c subunits of ATPase was less than 14, then the number of ATP produced per proton transferred would be greater and we would have underestimated the ATP/NADPH ratio produced by the chain. In other cyanobacteria, down to 13 c subunits were counted in F-ATP synthase (Pogoryelov et al., 2007) and the mitochondrial ATP synthase of *Saccharomyces cerevisiae* counts only 10 c subunits (Stock et al., 2000). If there was only 13 c subunits per chloroplastic ATP synthase in the organisms studied, then the ATP/NADPH ratios would be underestimated by 8%.

- *Occurrence of the Q-cycle*

We can show that the Q-cycle is occurring in the organisms studied in chapter 3. Indeed, after a single turnover laser flash in the dark, we observe a first phase of ECS increase in time scales of the order of 100 μ s which is attributed to the activity of PS and then a second phase of ECS increase in the time scales of the order of ms and which is attributed to the activity of cyt. *b₆f* which is therefore electrogenic (data not shown). If the Q-cycle did not take place, the cyt. *b₆f* activity would not modify the electric field across the thylakoid membrane: *b₆f* turnovers would result in 1 electron (negative charge) transferred from the membrane PQ to the lumen per proton (positive charge) transferred from the stroma to the lumen.

- *Presence of alternative electron flows (AEF)*

AEF are electron transfer that are not using the canonical pathway from water to CO₂. In the General introduction of this manuscript, we reviewed the AEF pathways proposed in the literature (section 1.3.3). They induce either PSII activity only (e.g. PTOX catalyzed water to water cycle) either both PS activity (other water to water cycles such as Mehler reactions or O₂ reduction mediated by flavodiiron proteins, nitrite reduction or hydrogenase pathways). Therefore, they participate to the establishment of an electrochemical proton gradient and thus produce ATP. But none of them participate in reducing NADP⁺. Therefore, their occurrence participates to ATP/NAPH ratio increase. In chapter 3, we used PSII activity to estimate the LEF, i.e. the electron transfer from water to NADP⁺. But if part of PSII activity is due to alternative electron flows (AEF), we have underestimated the ATP/NADPH ratio production by the photosynthetic chain.

Can we estimate the extent of AEF in the three species we studied in chapter 3?

In the literature, there is no work aiming at measuring AEF in *Amphidinium carterae*. In *Symbiodinium sp*, the amplitude of Mehler reactions were studied by Roberty and collaborators (Roberty et al., 2014) and they estimated that up to 50% of the electrons transferred through PSII ultimately reduce molecular oxygen which means that the ATP/NADPH ratios calculated could be largely underestimated. In *Chlamydomonas reinhardtii*, AEF would be negligible under steady state light. Flavodiiron protein pathway would be mainly active at light onset (Chaux et al., 2017), super oxide dismutase involved in Mehler reaction would be down regulated in light (Shao et al., 2008) and PTOX pathway would be negligible under steady state light regarding the LEF amplitude with a maximal rate of about 6 electrons s⁻¹ PSII⁻¹ (Houille-Vernes et al., 2011).

All in all, it is more likely that we underestimated rather than overestimated the ATP/NADPH ratios produced by the photosynthetic electron transport chain. It would be particularly interesting to quantify AEF and in particular the water to water cycle reactions in order to discuss more significantly the ATP/NADPH ratios produced by the photosynthetic chain. For example, we could couple spectroscopic measurements as we performed in chapter 3 and oxygen exchange measurement using [¹⁸O]-labeled O₂ and a membrane inlet mass spectrometer (as used for example in Chaux et al., 2017).

5. 2. 2. A role of CEF when PSII is inhibited?

In Chapter 3, we used DCMU as a means of specifically inhibiting LEF, thereby testing the dependence of CEF on LEF. But we can also consider the DCMU titration as mimicking conditions encountered in situ when PSII is poorly active and to propose an additional role for the CEF: that of allowing the production of ATP when PSII is specifically inhibited. Indeed, in Chapter 3, we have shown that certain organisms such as *Symbiodinium sp.*, *Chlamydomonas reinhardtii* or *Chaetoceros sp.*, exhibit a cyclic flow of electron even in the absence of PSII activity. This generates an electron transfer through the cyt. *b₆f*, and therefore the establishment of a proton gradient and finally the synthesis of ATP.

In nature, many biotic and abiotic stresses target PSII. For example, the first consequence of an excess of light energy is the specific destruction of PSII in time scales which can be of the order of a minute and can lead to a full inhibition of PSII (Powles, 1984; Aro et al., 1993; Andersson and Aro, 2001). Excess in light energy is reached under different conditions for which the intensity of light received is much higher than its use by photosynthesis. This is the case under high light, for example in the middle of the day in surface waters (e.g. Gorbunov et al., 2001; Mackey et al., 2008; Kimmance et al., 2014). Certain conditions also lead to a decrease in the intensity at which light saturation is reached, such as when the availability of CO₂ is low or under nutrient deprivation (Thomas and Dodson, 1972; Osborne and Geider, 1986; Philipps et al., 2012).

In addition, certain biotic interactions also specifically target PSII. The freshwater macrophyte *Myriophyllum spicatum* (Haloragaceae) (Leu et al., 2002), or the cyanobacteria *Fischerella muscicola* (Gross et al., 1991; Gantar et al., 2008) inhibit the growth of green algae and other cyanobacteria by producing molecules specifically targeting PSII. Moreover, infection of *E. huxleyi* with its specific virus is known to decrease the quantum yield of PSII and we proposed in Chapter 4 that the rest of the chain remains intact (at least during the first phase of infection).

Is there an evolutionary interest in being able to produce ATP when the PSII is inhibited? A first role that has already been proposed is to provide the energy needed for PSII repair. Indeed, after photoinhibition, the repair of PSII involves replacement of photodamaged D₁ subunit by newly synthesized D₁ protein. This process is ATP-dependent (Kuroda et al., 1992; Allakhverdiev et al., 2005). D₁ protein production requires ample supply of energy in the form of ATP, for the *psbA* gene transcription, and for amino-acid synthesis and assembly (reviewed in Murata and Nishiyama, 2018). The CEF seems to play an important role in

repairing PSII. Indeed, the total inhibition of the linear flow by DCMU only decreases the speed of repair of the PSII while the addition of DCMU and a membrane uncoupler (preventing the establishment of an electrochemical gradient of protons on either side of the membrane) almost completely inhibits repair mechanisms (Allakhverdiev et al., 2005).

In the case of PSII destruction induced by allelopathic molecules or viral infection, the role of CEF has never been explored.

We have seen that other AEF than CEF can fulfill the roles of photoprotection in high light or adjustment of the ATP/NADPH ratio proposed for the CEF. But only the CEF enables the production of ATP in the absence of PSII activity. It thus seems particularly interesting to explore the role of CEF in these conditions in order to better understand the evolutionary advantages linked to the ability to perform a CEF.

5. 2. 3. CEF and LEF regulation

There is no consensus regarding the regulation of the relative extent of CEF and LEF in the photosynthesis community even in plants and green algae, where the role of CEF is established and where CEF has been investigated for decades. Several mechanisms have been proposed to adjust CEF and LEF:

(1) a regulation by the concentration of CEF substrates that are reduced Fd and oxidized PQ (e.g. Allen, 2003; Alric, 2010; Alric 2014);

(2) a regulation by changing the kinetic constants of the enzymes involved in the cycling step (i.e. the NDH/Nda2 or the PGRL1/PGR5). Propositions include the thioredoxin-mediated redox activation/inactivation of those enzymes putatively involved in the cycling step (Strand et al., 2016) or competitive inhibition by ATP (Fisher et al., 2019);

(3) the segregation of CEF and LEF chains and the regulation of the fraction of PSI involved in each of them. This separation could be related to establishment of supercomplexes associating the intermediates involved in the CEF (Joliot and Joliot, 2002; Iwai et al., 2010), or structural segregation of the PSII and PSI centers in the appressed and nonappressed regions, respectively, and by restricted diffusion of the PQ (Joliot and Joliot, 2002).

The results I obtained on *Chlamydomonas reinhardtii* in Chapter 3 allow me to discuss some of these models. In *Chlamydomonas reinhardtii*, when we increased light irradiance, CEF was always proportional to LEF. This behavior is compatible with most of the regulatory modes presented above. For example, in model (2) when the light intensity is raised, the increase in

LEF would induce a transient lack of ATP and therefore (i) the suppression of competitive inhibition of the cycling step enzymes and the increase in CEF until reaching the amplitude of CEF for which the ATP/NADPH ratio is adjusted to the needs of the CBB cycle or (ii) a limitation of the CBB cycle and the reduction of PSI acceptors and thioredoxin system that would activate the cycling step enzymes. Here again the CEF would increase until reaching an amplitude for which the ATP/NADPH ratio would be adjusted to the needs of the CBB cycle. In these 2 models, the CEF would follow changes of the LEF and the models are compatible with a CEF always proportional to the LEF. However, the results obtained by DCMU titration show that when the LEF is decreased by inhibition of the PSII, the CEF does not decrease in proportion to the LEF (instead, it increases or remains constant). For the same reasons, model (2) is not compatible with the results obtained in *Symbiodinium sp* and *Chaetoceros sp*.

Another regulatory model compatible with the results obtained in *Chlamydomonas* as a function of light intensity is model (3), that is to say the segregation of linear and cyclic electron transfer chains. In this case, we expect a proportional increase in CEF and LEF activity depending on the light intensity (at constant antenna size, as was the case in our experiments). But the supercomplex model is not compatible with the amplitude of CEF measured in *Chlamydomonas reinhardtii*. I could estimate an average of 35% or 55% of PSI involved in CEF, (results obtained with the antenna sizes measured by ECS or by fluorescence, respectively). If the amount of CEF was determined by the amount of PSI/cyt. *b₆f* supercomplexes, then at least 35% of PSI should be included in such supercomplexes. And this is not what is suggested by studies aimed at purifying supercomplexes. The latter either do not succeed (Buchert et al., 2018) either isolate only a few percent of PSI involved in supercomplexes (Iwai et al., 2010). There is no work aiming at isolating supercomplexes in *Symbiodinium sp*. or *Chaetoceros sp.*, we thus cannot discuss their results. In addition, the model of segregation of the chains is also difficult to reconcile with the results obtained when titrating the LEF with DCMU. The specific inhibition of PSII (and therefore of the linear chains) should not affect the amplitude of the CEF. However, the results in *Chlamydomonas reinhardtii* are compatible with a CEF which increases when LEF is inhibited. It is to note that in a model of segregated linear and cyclic chains, the proportionality of LEF and CEF at all light irradiances is not automatic: this requires that the limiting step of photosynthesis under high light is the same in the two types of chains. This would strongly suggest that the limiting step of the cyclic chains is the cytochrome *b₆f*.

Model (1) is more difficult to discuss because two parameters are to be considered (the redox state of PQ and Fd) and because these parameters are difficult to measure by direct methods. After eliminating the first two models, this one remains our favorite but it is difficult to go further for the moment.

Finally, the differences in CEF behavior observed in the different organisms studied in Chapter 3 seem particularly interesting for discussing the diversity of regulatory modes of CEF. Are there different modes of regulation between species? Are those results related to differences in enzymes involved in the cycling step(s)? Are the differences only due to differences in physiological state? To answer these questions, it seems interesting to test more experimental conditions in these three organisms.

5. 3. Three years were too short for...

5. 3. 1. Revisiting literature using P₇₀₀ method

In Chapter 2, we have shown that the P₇₀₀ method is not reliable under conditions where the PSI acceptor side is reduced during the pulse, which corresponds to conditions where the PSI acceptor pool is small compared to the PSI donor pool. The induced errors result in underestimation of the flux through PSI by a factor up to 10 (in the dataset gathered. This method was proposed in 1994, 25 years ago, and has been used in many articles (cited 175 times according to Google scholar). It therefore seems important to revisit the literature. This task will benefit from the correction to the P₇₀₀ method we proposed which is applicable without requiring new measurements. I started doing so in the discussion of Chapter 2 but it might be interesting to continue this work.

5. 3. 2. Exploring cyclic electron flow using our methods

In Chapter 3, Section 3.3, I presented a robust method to:

- highlight the presence or absence of CEF in a given species and given experimental conditions.
- test the relationship between CEF and LEF (if CEF is present)
- but also test the evolution of CEF according to the conditions applied to the sample.

The development and testing of the method has been long. It now seems reliable and ready

to be used to answer to more biological questions. I did not have time to go further during my thesis but I would like to propose here some tracks for complementary investigations. One idea could be to test the presence of CEF and its relation with LEF in the different clades of photosynthetic species. I started this screen but preferred not to show the results which were too preliminary. However, they suggest that the presence of CEF and its relation with LEF is not preserved within the same clade (e.g. the two species of dinoflagellates, *Amphidinium carterae* and *Symbiodinium sp.*).

Another way is to test the evolution of the CEF according to environmental conditions such as the availability of nutrients, gas, the effect of temperature, or of biotic interactions. Thirdly, we have shown that the method we propose may be used in the field, provided the presence of monospecific samples and sufficient concentrations to obtain significant signals. In Chapter 4, we have shown that a statistical approach enables to highlight abiotic and biotic factors potentially involved in the changes of photosynthetic physiology. Following the same approach, we could propose to study the determinants of CEF in the field. And finally, in Chapter 4, we were able to show that the viral infection of *Emiliana huxleyi* induces the loss of activity of a significant fraction of PSII. The consequences of such changes in the structure of the photosynthetic chain remains unexplored. Viral multiplication requires a significant energy input. In addition, a recent study shows that the dynamics of viral lysis is light dependent (Thamatrakoln et al., 2019) suggesting the dependence of the efficiency of viral infection on photosynthetic activity. It would be interesting to test the presence of CEF during the viral infection and, if necessary, the evolution of its amplitude with time of infection and loss of PSII efficiency (like what was done in chapter 3 with DCMU titration).

5. 3. 3. Harness all data collected in the field

Chapter 4 shows some preliminary conclusions on the effect of viral infection on photosynthesis, which require the support of data from other teams with whom we collaborated. Not all the analyses have been performed yet, and the multivariate analysis will soon benefit from data from meta-genomics, meta-transcriptomics and metabolomics. In addition, our dataset could be further exploited. For example, we could study deviations from the explanatory model for all the parameters of photosynthetic physiology to look for

signs of exceptional events such as population changes, allelopathic effects, or other surprises.

In addition, we have collected other data that have not been shown in this thesis but that could be further developed. For example, in collaboration with the Vardi lab, we tested the allelopathic effect of species present in mesocosms on a lab strain of *Emiliana huxleyi*. For this, we sampled water in the bags at different times of the campaign and put them in co-culture with a strain of *Emiliana huxleyi* in an apparatus allowing to separate the two populations while making possible the diffusion of the chemical molecules. The Vardi lab team followed the evolution of the concentration of *Emiliana huxleyi* in co-culture and monoculture while we were comparing the photosynthetic activity of these two populations. We have been able to highlight potential allelopathic interactions targeting photosynthesis. Strains were isolated on site from the bags by collaborators from Station Biologique de Roscoff (France) and their effect on the growth of *Emiliana huxleyi* has been tested by the Vardi lab team and appears to show allelopathic effects. It might be interesting to test the allelopathic effect of these strains on the photosynthesis of *Emiliana huxleyi*.

In addition, we followed the photosynthetic physiology of a diatom population present in the Fjord during a diel cycle and a collaborative team measured the storage of carbohydrates in the cells. The results show a high consumption of carbohydrate reserves in the morning, while photosynthesis was activated. The exploration of these data seems promising but is very preliminary for the moment.

5.4. Bibliography

- Allakhverdiev, S. I., Nishiyama, Y., Takahashi, S., Miyairi, S., Suzuki, I., & Murata, N. (2005).** Systematic analysis of the relation of electron transport and ATP synthesis to the photodamage and repair of photosystem II in *Synechocystis*. *Plant physiology*, *137*(1), 263-273.
- Alric, J. (2010).** Cyclic electron flow around photosystem I in unicellular green algae. *Photosynthesis research*, *106*(1-2), 47-56.
- Alric, J. (2014).** Redox and ATP control of photosynthetic cyclic electron flow in *Chlamydomonas reinhardtii*:(II) Involvement of the PGR5–PGRL1 pathway under anaerobic conditions. *Biochimica et Biophysica Acta (BBA)-Bioenergetics*, *1837*(6), 825-834.
- Andersson, B., & Aro, E. M. (2001).** Photodamage and D1 protein turnover in photosystem II. In Regulation of photosynthesis (pp. 377-393). Springer, Dordrecht.
- Aro, E. M., Virgin, I., & Andersson, B. (1993).** Photoinhibition of photosystem II. Inactivation, protein damage and turnover. *Biochimica et Biophysica Acta (BBA)-Bioenergetics*, *1143*(2), 113-134.
- Bailleul, B., Cardol, P., Breyton, C., & Finazzi, G. (2010).** Electrochromism: a useful probe to study algal photosynthesis. *Photosynthesis research*, *106*(1-2), 179.
- Becker, S., Scheffel, A., Polz, M. F., & Hehemann, J. H. (2017).** Accurate quantification of laminarin in marine organic matter with enzymes from marine microbes. *Appl. Environ. Microbiol.*, *83*(9), e03389-16.
- Buchert, F., Hamon, M., Gäbelein, P., Scholz, M., Hippler, M., & Wollman, F. A. (2018).** The labile interactions of cyclic electron flow effector proteins. *Journal of Biological Chemistry*, *293*(45), 17559-17573.
- Castberg, T., Larsen, A., Sandaa, R. A., Brussaard, C. P. D., Egge, J. K., Heldal, M., ... & Bratbak, G. (2001).** Microbial population dynamics and diversity during a bloom of the marine coccolithophorid *Emiliania huxleyi* (Haptophyta). *Marine Ecology Progress Series*, *221*, 39-46.
- Cermeño, P., Lee, J. B., Wyman, K., Schofield, O., & Falkowski, P. G. (2011).** Competitive dynamics in two species of marine phytoplankton under non-equilibrium conditions. *Marine Ecology Progress Series*, *429*, 19-28.
- Chaux, F., Burlacot, A., Mekhalfi, M., Auroy, P., Blangy, S., Richaud, P., & Peltier, G. (2017).** Flavodiiron proteins promote fast and transient O₂ photoreduction in *Chlamydomonas*. *Plant physiology*, *174*(3), 1825-1836.
- De Vargas, C., Audic, S., Henry, N., Decelle, J., Mahé, F., Logares, R., ... & Carmichael, M. (2015).** Eukaryotic plankton diversity in the sunlit ocean. *Science*, *348*(6237), 1261605.
- Fan, D. Y., Fitzpatrick, D., Oguchi, R., Ma, W., Kou, J., & Chow, W. S. (2016).** Obstacles in the quantification of the cyclic electron flux around Photosystem I in leaves of C3 plants. *Photosynthesis research*, *129*(3), 239-251.
- Field, C. B., Behrenfeld, M. J., Randerson, J. T., & Falkowski, P. (1998).** Primary production of the biosphere: integrating terrestrial and oceanic components. *Science*, *281*(5374), 237-240.

- Fisher, N., Bricker, T. M., & Kramer, D. M.** (2019). Regulation of photosynthetic cyclic electron flow pathways by adenylate status in higher plant chloroplasts. *Biochimica et Biophysica Acta (BBA)-Bioenergetics*, 1860(11), 148081.
- Gantar, M., Berry, J. P., Thomas, S., Wang, M., Perez, R., & Rein, K. S.** (2008). Allelopathic activity among cyanobacteria and microalgae isolated from Florida freshwater habitats. *FEMS microbiology ecology*, 64(1), 55-64.
- Gorbunov, M. Y., Kolber, Z. S., Lesser, M. P., & Falkowski, P. G.** (2001). Photosynthesis and photoprotection in symbiotic corals. *Limnology and Oceanography*, 46(1), 75-85.
- Gross, E. M., Wolk, C. P., & Jüttner, F.** (1991). Fischerellin, a new allelochemical from the freshwater cyanobacterium *fischerella muscicola*. *Journal of Phycology*, 27(6), 686-692.
- Houille-Vernes, L., Rappaport, F., Wollman, F. A., Alric, J., & Johnson, X.** (2011). Plastid terminal oxidase 2 (PTOX2) is the major oxidase involved in chlororespiration in *Chlamydomonas*. *Proceedings of the National Academy of Sciences*, 108(51), 20820-20825.
- Iwai, M., Takizawa, K., Tokutsu, R., Okamuro, A., Takahashi, Y., & Minagawa, J.** (2010). Isolation of the elusive supercomplex that drives cyclic electron flow in photosynthesis. *Nature*, 464(7292), 1210.
- Joliot, P., & Joliot, A.** (2002). Cyclic electron transfer in plant leaf. *Proceedings of the National Academy of Sciences*, 99(15), 10209-10214.
- Juergens, M. T., Deshpande, R. R., Lucker, B. F., Park, J. J., Wang, H., Gargouri, M., ... & Kramer, D. M.** (2015). The regulation of photosynthetic structure and function during nitrogen deprivation in *Chlamydomonas reinhardtii*. *Plant physiology*, 167(2), 558-573.
- Kimmance, S. A., Allen, M. J., Pagarete, A., Martínez, J. M., & Wilson, W. H.** (2014). Reduction in photosystem II efficiency during a virus-controlled *Emiliania huxleyi* bloom. *Marine Ecology Progress Series*, 495, 65-76.
- Kyle, D. J., Ohad, I., & Arntzen, C. J.** (1984). Membrane protein damage and repair: Selective loss of a quinone-protein function in chloroplast membranes. *Proceedings of the National Academy of Sciences*, 81(13), 4070-4074.
- Leu, E., Krieger-Liszkay, A., Goussias, C., & Gross, E. M.** (2002). Polyphenolic allelochemicals from the aquatic angiosperm *Myriophyllum spicatum* inhibit photosystem II. *Plant physiology*, 130(4), 2011-2018.
- Mackey, K. R., Paytan, A., Grossman, A. R., & Bailey, S.** (2008). A photosynthetic strategy for coping in a high-light, low-nutrient environment. *Limnology and Oceanography*, 53(3), 900-913.
- Martínez-Martínez, J., Norland, S., Thingstad, T. F., Schroeder, D. C., Bratbak, G., Wilson, W. H., & Larsen, A.** (2006). Variability in microbial population dynamics between similarly perturbed mesocosms. *Journal of plankton research*, 28(8), 783-791.
- Moore, C. M., Mills, M. M., Arrigo, K. R., Berman-Frank, I., Bopp, L., Boyd, P. W., ... & Jickells, T. D.** (2013). Processes and patterns of oceanic nutrient limitation. *Nature geoscience*, 6(9), 701-710.
- Murata, N., & Nishiyama, Y.** (2018). ATP is a driving force in the repair of photosystem II during photoinhibition. *Plant, cell & environment*, 41(2), 285-299.

- Not, F., Massana, R., Latasa, M., Marie, D., Colson, C., Eikrem, W., ... & Simon, N.** (2005). Late summer community composition and abundance of photosynthetic picoeukaryotes in Norwegian and Barents Seas. *Limnology and Oceanography*, *50*(5), 1677-1686.
- Ohad, I., Kyle, D. J., & Arntzen, C. J.** (1984). Membrane protein damage and repair: removal and replacement of inactivated 32-kilodalton polypeptides in chloroplast membranes. *The Journal of Cell Biology*, *99*(2), 481-485.
- Osborne, B. A., & Geider, R. J.** (1986). Effect of nitrate-nitrogen limitation on photosynthesis of the diatom *Phaeodactylum tricornutum* Bohlin (Bacillariophyceae). *Plant, Cell & Environment*, *9*(8), 617-625.
- Papanikolopoulou, L. A., de Vargas, C., Speck, F., Probert, I., & Pohnert, G.** (2018). Survey of allelopathic interactions amongst phytoplankton species. *In 2018 Ocean Sciences Meeting*. AGU.
- Philipps, G., Happe, T., & Hemschemeier, A.** (2012). Nitrogen deprivation results in photosynthetic hydrogen production in *Chlamydomonas reinhardtii*. *Planta*, *235*(4), 729-745.
- Pogoryelov, D., Reichen, C., Klyszejko, A. L., Brunisholz, R., Muller, D. J., Dimroth, P., & Meier, T.** (2007). The oligomeric state of c rings from cyanobacterial F-ATP synthases varies from 13 to 15. *Journal of bacteriology*, *189*(16), 5895-5902.
- Powles, S. B.** (1984). Photoinhibition of photosynthesis induced by visible light. *Annual review of plant physiology*, *35*(1), 15-44.
- Rahoutei, J., García-Luque, I., & Barón, M.** (2000). Inhibition of photosynthesis by viral infection: effect on PSII structure and function. *Physiologia Plantarum*, *110*(2), 286-292.
- Roberty, S., Bailleul, B., Berne, N., Franck, F., & Cardol, P.** (2014). PSI Mehler reaction is the main alternative photosynthetic electron pathway in *Symbiodinium sp.*, symbiotic dinoflagellates of cnidarians. *New Phytologist*, *204*(1), 81-91.
- Rochelle-Newall, E., Delille, B., Frankignoulle, M., Gattuso, J. P., Jacquet, S., Riebesell, U., ... & Zondervan, I.** (2004). Chromophoric dissolved organic matter in experimental mesocosms maintained under different pCO₂ levels. *Marine Ecology Progress Series*, *272*, 25-31.
- Shao, N., Beck, C. F., Lemaire, S. D., & Krieger-Liszka, A.** (2008). Photosynthetic electron flow affects H₂O₂ signaling by inactivation of catalase in *Chlamydomonas reinhardtii*. *Planta*, *228*(6), 1055-1066.
- Strand, D. D., Fisher, N., Davis, G. A., & Kramer, D. M.** (2016). Redox regulation of the antimycin A sensitive pathway of cyclic electron flow around photosystem I in higher plant thylakoids. *Biochimica et Biophysica Acta (BBA)-Bioenergetics*, *1857*(1), 1-6.
- Thamatrakoln, K., Talmy, D., Haramaty, L., Maniscalco, C., Latham, J. R., Knowles, B., ... & Bidle, K. D.** (2019). Light regulation of coccolithophore host–virus interactions. *New Phytologist*, *221*(3), 1289-1302.
- Thomas, W. H., & Dodson, A. N.** (1972). On nitrogen deficiency in tropical pacific oceanic phytoplankton. II. Photosynthetic and cellular characteristics of a chemostat-grown diatom 1. *Limnology and Oceanography*, *17*(4), 515-523.
- Thyssen, M., Grégori, G. J., Grisoni, J. M., Pedrotti, M. L., Mousseau, L., Artigas, L. F., ... & Denis, M. J.** (2014). Onset of the spring bloom in the northwestern Mediterranean Sea: influence of

environmental pulse events on the in situ hourly-scale dynamics of the phytoplankton community structure. *Frontiers in microbiology*, 5, 387

Tyrrell, T., & Merico, A. (2004). *Emiliania huxleyi*: bloom observations and the conditions that induce them. In *Coccolithophores* (pp. 75-97). Springer, Berlin, Heidelberg.

Van Kooten, O., Meurs, C., & Van Loon, L. C. (1990). Photosynthetic electron transport in tobacco leaves infected with tobacco mosaic virus. *Physiologia Plantarum*, 80(3), 446-452.

Witt, H. T. (1979). Energy conversion in the functional membrane of photosynthesis. Analysis by light pulse and electric pulse methods: The central role of the electric field. *Biochimica et Biophysica Acta (BBA)-Reviews on Bioenergetics*, 505(3-4), 355-427.

Wolfram, S., Wielsch, N., Hupfer, Y., Mönch, B., Lu-Walther, H. W., Heintzmann, R., ... & Pohnert, G. (2015). A Metabolic Probe-Enabled Strategy Reveals Uptake and Protein Targets of Polyunsaturated Aldehydes in the Diatom *Phaeodactylum tricornutum*. *PLoS one*, 10(10), e0140927.

Wykoff, D. D., Davies, J. P., Melis, A., & Grossman, A. R. (1998). The regulation of photosynthetic electron transport during nutrient deprivation in *Chlamydomonas reinhardtii*. *Plant physiology*, 117(1), 129-139.

Zhao, Y., Zhao, L., Zhang, W., Sun, J., Huang, L., Li, J., ... & Xiao, T. (2016). Variations of picoplankton abundances during blooms in the East China Sea. *Deep Sea Research Part II: Topical Studies in Oceanography*, 124, 100-108.

Appendix 1: Theoretical considerations about the DCMU titration method

In chapter 3, section 3.3.1, we explained the principle of the DCMU titration method “with hands” by simulating how the total activity of PSI and PSII would evolve as a function of PSII activity in 3 different scenarios. In the rest of section 3, we measured the evolution of the fraction of open photosystems, $Y(\text{total})$, and the one of the quantum yield of PSII, $Y(\text{II})$, as a function of DCMU concentration. Here, we aim at demonstrating that the two approaches are equivalent, provided that a model with isolated PSII units, i.e. the “puddle” model, is used.

The fraction of open centers (y axis) depends on the fraction of open PSII and PSI centers, $\text{FOC}(\text{II})$ and $\text{FOC}(\text{I})$. The equation we used in chapter 3 is: $Y(\text{total}) = n_1 \cdot \text{FOC}(\text{I}) + n_2 \cdot \text{FOC}(\text{II})$

Let's divide this equation by the initial fraction of open PS, before DCMU is added: $Y(\text{total})_i$. And let's call $\text{FOC}(\text{I})_{\text{CEF}}$ the initial fraction of PS involved in CEF, that we consider constant (not dependent on DCMU). This gives:

$$(1) Y(\text{total})/Y(\text{total})_i = 1/Y(\text{total})_i \cdot (n_1 \cdot \text{FOC}(\text{I}) + n_2 \cdot \text{FOC}(\text{II}))$$

In a « puddle » model, $n_1 \cdot \text{FOC}(\text{I}) = n_2 \cdot \text{FOC}(\text{II}) \cdot F_v/F_m \cdot \sigma_{\text{II}}/\sigma_{\text{I}} + \text{FOC}(\text{I})_{\text{CEF}}$. Equation (3) becomes

$$\begin{aligned} (2) Y(\text{total})/Y(\text{total})_i &= n_2 \cdot \text{FOC}(\text{II}) \cdot (1 + F_v/F_m \cdot \sigma_{\text{II}}/\sigma_{\text{I}}) / Y(\text{total})_i + \text{FOC}(\text{I})_{\text{CEF}} / Y(\text{total})_i \\ &= n_2 \cdot \sigma_{\text{total}}/\sigma_{\text{I}} \cdot (\text{FOC}(\text{II})_i / Y(\text{total})_i) \cdot (\text{FOC}(\text{II})/\text{FOC}(\text{II})_i) + \text{FOC}(\text{I})_{\text{CEF}} / Y(\text{total})_i \\ &= n_2 \cdot \sigma_{\text{total}}/\sigma_{\text{I}} \cdot (\text{FOC}(\text{II})_i / Y(\text{total})_i) \cdot (Y(\text{II})/Y(\text{II})_i) + \text{FOC}(\text{I})_{\text{CEF}} / Y(\text{total})_i \end{aligned}$$

If we note $y = Y(\text{total})/Y(\text{total})_i$, $X = Y(\text{II})/Y(\text{II})_i$, it gives:

$$(3) Y = (Y(\text{total})_i - \text{FOC}(\text{I})_{\text{CEF}}) / Y(\text{total})_i \cdot X + \text{FOC}(\text{I})_{\text{CEF}} / Y(\text{total})_i$$

When $X = 1$, $Y = 1$ and when $X = 0$, $Y = \text{FOC}(\text{I})_{\text{CEF}} / Y(\text{total})_i$. Our interpretation of the relative $Y(\text{total})$ versus the relative $Y(\text{II})$ was correct: if CEF does not change during DCMU addition, then the relation between $Y(\text{total})$ and $Y(\text{II})$ is linear and the y-intercept is equal to $\text{FOC}(\text{I})_{\text{CEF}} / Y(\text{total})_i$, i.e the fraction of PS which was initially involved in CEF. When there is no CEF, the relationship passes through the origin of the axis. And by elimination, other behaviors imply a CEF which depends on LEF.